PhD degree in Molecular Medicine (curriculum in Molecular Oncology)

European School of Molecular Medicine (SEMM),

University of Milan and University of Naples "Federico II"

Settore disciplinare: BIO/11

Interplay between the DNA helicases Pif1 and Rrm3, the nuclease Dna2 and the checkpoint pathways in the maintenance of the DNA replication fork integrity

Silvia Emma Rossi

IFOM, Milan

Matricola n.R10311

Supervisor: Prof. Marco Foiani

IFOM, Milan

Added Supervisor: Dr. Michele Giannattasio

IFOM, Milan

Anno accademico 2015/2016

Table of Contents

List of abbreviations

WT	Wild-type
DNA	deoxy-ribonucleic acid
dsDNA	double-stranded DNA
ssDNA	single-stranded DNA
ARS	Autonomously Replicating Sequence
ORF	Open Reading Frame
RFB	Replication Fork Barrier
SCJs	Sister Chromatid Junctions
DSB	Double Strand Break
dNTP	deoxynucleoside triphosphate
mRNA	messenger RNA
TER	Termination zone
IP	Immunoprecipitation
SUP	Supernatant
ChIP on chip	Chromatin Immunoprecipitation on chip
BrdU	5-bromo-2'-deoxyuridine
ssDNA BrdU-IP on chip	ssDNA-BrdU Immunoprecipitation on chip
PFGE	Pulse Field Gel Electrophoresis
FACS	Fluorescence-Activated Cell Sorting
2D gel	Two Dimensional Agarose Gel Electrophoresis
CTAB	cetyltrimethylammonium bromide
HU	Hydroxyurea
MMS	Methyl metansulfonate
Gal	Galactose
Glu	Glucose
YPD	Yeast Extract Peptone Dextrose

nt	nucleotides
bp	base pairs
Kb/Kbps	Kilo base pairs
kDa	kiloDalton
O/N	Overnight
Rcf	relative centrifugal force
Rpm	revolutions per minute
RT	Room Temperature
SDS	Sodium Dodecyl Sulfate
SDS-PAGE	SDS-Poly-Acrylamide Gel Electrophoresis
SSC	Saline-Sodium Citrate

Figures index

1.Introduction

2.Material and Methods

3.Results

Tables index

Abstract

Eukaryotic cells have evolved the *ATR/hCHK1, MEC1/RAD53* kinase-mediated signal transduction pathway, known as replication checkpoint, to protect and stabilize stalled replication forks in human cells and budding yeasts, respectively.

rad53 mutants, exposed to high doses of the DNA replication inhibitor hydroxyurea (HU), accumulate hemireplicated, gapped and reversed forks, while treatments of the same cells with low doses of HU induce massive chromosome fragmentation.

The aim of the present work was to better understand the molecular mechanisms through which Rad53 prevents unusual alterations of the architecture of the stalled replication forks and chromosome fragility, under DNA replication stress.

We revealed that Rrm3 and Pif1, DNA helicases assisting fork progression across pausing sites in unperturbed conditions, are detrimental in *rad53* mutants experiencing HU-induced replication stress. Rrm3 and Pif1 ablations synergistically rescue cell lethality, chromosome fragmentation, replisome-fork dissociation, fork reversal and ssDNA gaps formation at the forks of *rad53* cells exposed to replication stress. We provide evidence that Pif1 and Rrm3 associate with stalled DNA replication forks and are regulated through Rad53 mediated phosphorylation.

Our findings uncover a new replication stress induced regulative loop in which Rad53 down regulates the Pif1 DNA helicases at the stalled replication forks preventing genome instability.

In the second part of this PhD thesis we examined the crosstalk between Rrm3, Pif1, the mediator of the DNA damage checkpoint Rad9 and the nuclease Dna2, during unperturbed DNA replication. The experimental evidence collected in this second part of the project, together with pioneering work previously reported from other laboratories, strongly suggest that Dna2, Pif1 and Rrm3 cooperate to finalize late stages of DNA replication, which likely occur during mitosis.

1. Introduction

1.1 *Saccharomyces cerevisiae* DNA replication

Eukaryotic cells proliferation depends on a process called cell cycle, which consists in a series of events that allow the cell to grow and divide into two new daughter cells. The eukaryotic cell cycle is divided in four phases. The replication of the genetic material occurs during S-phase and is followed by the mitosis (M-phase), in which duplicated chromosomes and subcellular components are segregated to the two daughter cells. These two phases are separated by two gap phases, called G1 and G2, during which cells grow and duplicate proteins and organelles. G1, G2 and S-phases are overall called interphase.

In the budding yeast *Saccharomyces cerevisiae,* the cell cycle phases are coupled with morphological changes (Zhang and Siede, 2004): the bud emission is associated with the replication initiation in S-phase, while G1 cells are unbudded, and cells that complete replication and enter into mitosis progressively increase the bud size until the large-budded cells undergo mitotic division (Figure 1.1).

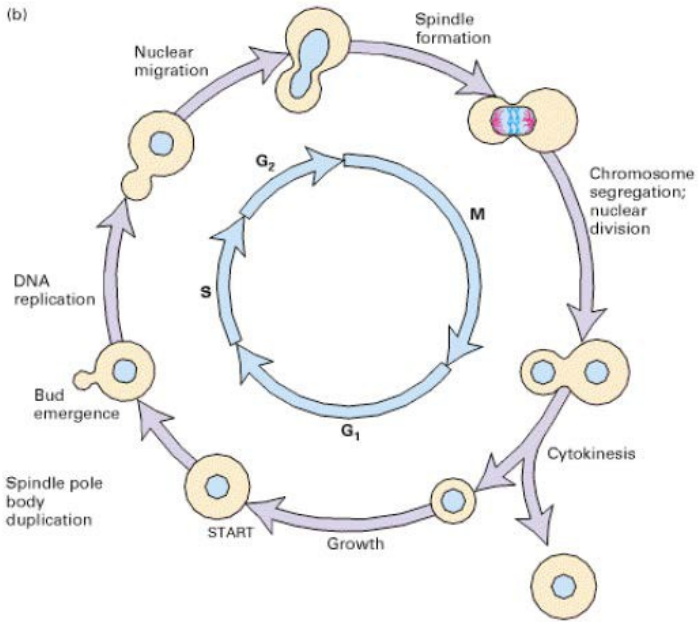

Figure 1.1. Cell cycle phases in *S. cerevisiae* (da Lodish et al., Molecular Cell Biology, 4th ed., 2000).

DNA replication has to be completed before the beginning of mitosis and has to occur only once per cell cycle. DNA replication is tightly regulated to ensure a rapid and faithful

replication of genomic information and to preserve genome stability. Eukaryotic cells have evolved a surveillance mechanism, called DNA replication checkpoint or intra-S-phase checkpoint, to prevent genomic instability and chromosomal rearrangements, which are typical hallmarks of cancer cells (Branzei and Foiani, 2009).

In optimal growth conditions, *S. cerevisiae* completes the semi-conservative replication of its 14 Mbs genome in less than 30 minutes (Poli et al., 2012). DNA replication starts from multiple replication origins, called *autonomously replicating sequences* (ARSs) for their ability to support plasmid replication. ARSs are sequences of around 200 bp that contain the ARS consensus sequences (ACS) of ~11 bp, which are bound by the replication initiation proteins, and secondary B domains (Bell and Stillman, 1992). More than 400 ARSs have been identified in *S.cerevisiae*. ARSs are temporally regulated, can be activated at the beginning or at the end of S-phase and are consequently grouped into *early origins* and *late origins*. A third class of origins, fired only in specific contests, has been identified and these origins are called *dormant origins* (Raghuraman et al., 2001; Raveendranathan et al., 2006; Wyrick et al., 2001).

ARSs are bound throughout the entire cell cycle by the *origin recognition complex* (ORC), formed by six subunits (Orc1-6) (Aparicio et al., 1997). In G1 the *pre-replicative complex* (pre-RC) is assembled, in a process known as *origin licensing*: the recruitment of the replicative factors Cdc6 (*cell division cycle 6*) and Cdt1 (*chromatin licensing and DNA replication factor 1*) allows the binding of MCM (*mini-chromosome maintenance*) helicase complex (Masai et al., 2010; Siddiqui et al., 2013). Mcm10 is required for the chromatin association of MCM complex in S-phase (Homesley et al., 2000). The MCM complex, formed by six subunits (Mcm2-Mcm7), is the replicative helicase, essential for both DNA replication initiation and elongation in all the genome (Labib et al., 2000).

The activation of the replication origins (*firing*) is strictly regulated by the cyclin-dependent kinase Cdc28 (CDK) to ensure only one replication round every cell cycle; pre-RC can be assembled only in G1 phase, when the kinase is not active, while in S-phase,

after the origin activation or the passive replication of that region, CDK impedes DNA re-replication inhibiting ORC and Cdc6 through phosphorylation and causing Cdc6 degradation and the nuclear export of Cdt1 (Blow and Dutta, 2005).

In early S-phase, thanks to the activity of CDK and DDK (Cdc7-Dbf4) kinases, the pre-RC is activated and converted into the *pre-initiation complex* (pre-IC); this allows the recruitment of several replication factors such as Cdc45 and GINS (that, together with MCM, form the CMG helicase complex), Sld3, DNA polymerases, the topoisomerases Top1 and Top2, the checkpoint protein Mrc1 (*mediator of replication checkpoint 1*), Tof1 (*Top1-associated factor 1*), Csm3 (*chrmosome segregation in meiosis protein 3*), the Rrm3 helicase and the heterotrimeric ssDNA binding protein RPA (*replication protein A*). Moreover, Cdc28 phosphorylates Sld3 and Sld2 that mediate the recruitment of Dpb11, an essential factor for the loading of DNA polymerase ε. This complex is comprehensively called *replisome* (Masai et al., 2010; Siddiqui et al., 2013).

The Tof1/Csm3/Mrc1 checkpoint complex moves with the replisome and interacts with the MCM helicase, both in unperturbed conditions and under replication stress (Nedelcheva et al., 2005). Mrc1 in unperturbed conditions is needed for the normal fork progression and for promoting replication in the presence of inverted repeats, which generates hairpin-like structures (Voineagu et al., 2008).

The MCM complex, probably travelling with the leading strand (Fu et al., 2011; Yu et al., 2014), unwinds the DNA duplex and the single-stranded DNA (ssDNA) generated is stabilized by cooperative binding of the heterotrimeric complex RPA. This generates the replication bubble with two replication apparatus that proceed bi-directionally from the replication origin; the two Y-shaped molecules, formed by the unreplicated DNA and the newly-synthesized strands, are the two *replication forks*. DNA replication is a semi-conservative process: each strand of the parental double-stranded DNA (dsDNA) is the template for the synthesis of a complementary strand. Since parental dsDNA is formed by two filaments with an antiparallel orientation and since DNA polymerase can synthetize

DNA exclusively in the 5' to 3' direction starting from a primer, DNA replication is semi-discontinuous; the leading strand is extended continuously, while the lagging strand synthesis is discontinuous and generates short DNA-RNA stretches, called Okazaki fragments (Okazaki et al., 1968).

The DNA polymerase α-primase complex is a low fidelity polymerase that is able to initiate the *de novo* DNA synthesis, both at the replication origins to start the leading strand synthesis and on the lagging strand. Thanks to its primase activity, DNA Pol α synthesizes RNA primers of 7-10 nucleotides, that are used by the subunit with polymerase activity to synthesize short DNA tracts of about 20 nt. The DNA polymerase α-primase complex is formed by four subunits that are essential for the cell viability: the p180 subunit, coded by *POL1* gene, has the polymerase activity; the p48 subunit is the smaller one, it is coded by the *PRI1* gene and has the primase activity; the p58 subunit, coded by the *PRI2* gene, is the accessory subunit of the DNA primase; p86, the B subunit of the complex, coded by *POL12*, does not have an enzymatic activity but could have a regulatory role since it shows a cell cycle-dependent phosphorylation (Muzi-Falconi et al., 2003). Indeed, the p86 subunit, newly-synthetized in early S-phase, is phosphorylated in M phase by the M-CDK forming the p91 B subunit; which is then dephosphorylated when cells exit from mitosis (Foiani et al., 1995; Palou et al., 2015).

The *replication factor C* (RFC) binds the primer-template junctions and loads the sliding clamp PCNA (*proliferating cell nuclear antigen*), which promotes the binding of DNA polymerase δ (for the lagging strand synthesis) and DNA polymerase ε (for the leading strand synthesis) (Nick McElhinny et al., 2008; Pursell et al., 2007; Yu et al., 2014), a phenomenon known as *polymerases switching*. Recently, it has been proposed that DNA polymerase δ replicates both strands, while DNA polymerase ε has a proofreading activity and removes Pol δ errors on the leading strand (Johnson et al., 2015).

DNA polymerase δ and ε have a 5' to 3' polarity and a 3' to 5' proofreading activity, which is able to correct incorporation errors, and are highly processive enzymes thanks to the presence of the homotrimer PCNA (Chilkova et al., 2007; Johansson et al., 2004).

DNA polymerase δ extends the short RNA-DNA fragments on the lagging strand, generating ~150-nt fragments. RNA-DNA primers, synthetized by the error-prone DNA Polymerase α, are then removed and the fragments are ligated to obtain a continuous filament, in a process known as *Okazaki fragments maturation* (Zheng and Shen, 2011). DNA polymerase δ reaches the 5' end of the downstream Okazaki fragment, displaces the RNA primer, generally generating short ssDNA flaps (8-12 nt). The short flaps are cut by the 5' to 3' flap exo/endonuclease 1 Fen1 (encoded by *RAD27*) and the nicks are sealed by DNA ligase I (Garg et al., 2004; Liu et al., 2004; Rossi and Bambara, 2006). The Exo1 exonuclease can act redundantly with Fen1 in the Okazaki fragments processing (Tishkoff et al., 1997).

A small fraction of flaps that is not immediately cleaved by Fen1 can be further lengthened by DNA polymerase δ/Pif1 mediated strand displacement events (see following paragraphs); if flaps longer than 25-30 nt are generated, the single stranded DNA is bound by RPA which inhibits the cleavage by Fen1, while stimulates the activity of another nuclease, Dna2 (Pike et al., 2009). Based on genetic data and *in vitro* studies (Budd et al., 2006; Pike et al., 2009; Rossi and Bambara, 2006), Dna2 is thought to cleave these long single stranded flaps formed at the 5' ends of Okazaki fragments. Dna2 shortens the 5' flap, displaces RPA and the remaining short flap is processed by Fen1 in the so called "two-nuclease processing pathway" (Pike et al., 2009; Rossi et al., 2008), otherwise Dna2 alone can cleave completely the single stranded flaps and the nicked intermediates can directly be ligated (Levikova and Cejka, 2015).

1.1.1 Dna2 roles in replication

Dna2 is an essential ss-DNA-specific exo/endonuclease (both 5' to 3' and 3' to 5'), a DNA dependent ATPase and a 5' to 3' DNA helicase; the presence of the single stranded binding protein RPA stimulates the 5'-3' nuclease activity of Dna2, that preferentially acts on 5'-flap substrates (Budd and Campbell, 1995; Budd et al., 1995; Thangavel et al., 2015). Dna2 plays an important role in Okazaki fragments maturation, telomere stability and DNA repair and its nuclease activity is essential for cell survival (Budd and Campbell, 1997; Budd et al., 2000; Lee et al., 2000).

Temperature sensitive *dna2* mutants, at restrictive temperatures, arrest irreversibly at the G2/M phase of the cell cycle, in a checkpoint-dependent manner, with a 2C DNA content (Fiorentino and Crabtree, 1997).

Similarly, Dna2 depletion in human cells causes a G2/M arrest and leads to the formation of aneuploid cells and internuclear chromatin bridges (Duxin et al., 2009).

1.1.1.1 Okazaki fragment processing

Temperature-sensitive mutations of Dna2 are synthetic lethal with the deletion of *RAD27*, the gene that encodes the flap endonuclease Fen1, while the overexpression of Fen1 rescues some phenotypes of *dna2-ts* mutants (Budd and Campbell, 1997).

Interestingly, the deletion of the nuclear isoform of the Pif1 helicase rescues the lethality of *dna2Δ* cells and the further deletion of *POL32*, which encodes the Pol δ subunit responsible for the strand displacement activity, completely suppresses the residual replication and repair defects of *dna2Δ pif1Δ* double mutant (Budd et al., 2006).

Moreover, *in vitro* experiments have shown that RPA-coated flaps stimulate Dna2 and inhibit Fen1, while Pif1 promotes this inhibitory reaction accelerating the flap elongation. Pif1 is indeed able to stimulate the strand displacement activity of Pol δ *in vitro* and promotes the formation of long 5' flaps (Pike et al., 2009; Rossi et al., 2008; Wilson et al., 2013).

Based on genetic interactions and *in vitro* studies, it has been proposed that Pif1 and Dna2 act in the same pathway of Okazaki fragment processing and that, during the Okazaki fragment maturation, the exceeded unwinding activity of Pif1, together with the strand displacement activity of Pol δ, generate long 5' flaps bound by RPA, which cannot be cleaved by the Fen1 endonuclease, and Dna2 counteracts this phenomena cutting the resulting 5' flaps (Budd et al., 2006; Levikova and Cejka, 2015; Pike et al., 2009; Pike et al., 2010; Rossi et al., 2008).

The combined deletion of *PIF1* and *POL32* is thought to abolish the formation of long flaps, overcoming the need for Dna2 flap processing activity and allowing the viability of the cells in the absence of *DNA2* (Budd et al., 2006).

Deletion of checkpoint genes partially suppresses *dna2* mutants inviability, presumably because cell lethality, in the absence of *DNA2,* is due to accumulation of unprocessed long ssDNA flaps on the lagging strand, which activate the DNA damage checkpoint, leading to permanent cell cycle arrest (Budd et al., 2011).

1.1.1.2 Telomere replication

Dna2 is also involved in the telomere maintenance. Dna2 localizes to telomeres in G1, associates with internal chromosome sites in S-phase and relocalizes to telomeres in late S/G2 (Choe et al., 2002). Also mammalian Dna2 localizes to telomeres and is essential for proper telomere maintenance (Lin et al., 2013).

Dna2 is required for *de novo* telomere synthesis and is involved in telomere lengthening in telomerase-deficient mutants (Choe et al., 2002). *dna2* mutants have slightly longer telomeres compared to wild type cells and slightly shortened telomeric single stranded G-rich tails, due to defects in the resection of the C-rich strand, and accumulate small tracts of newly synthetized telomeric lagging strand DNA (Budd and Campbell, 2013).

1.1.1.3 Ribosomal DNA replication

Dna2 associates with ribosomal DNA in S-phase (Choe et al., 2002; Hoopes et al., 2002). *dna2-2* mutant, carrying a point mutation in the helicase domain, has a reduced life span (Hoopes et al., 2002) and shows fork stalling and breakages at the *replication fork barrier* (RFB) of the ribosomal DNA (Weitao et al., 2003b).

Moreover, recently it has been reported that Dna2, through an N-terminus CIP-box motif, interacts with the homotrimeric adaptor Ctf4, which connects the DNA polymerase α with the CMG helicase complex and this interaction is important for the maintenance of the ribosomal DNA repeats (Villa et al., 2016). Indeed the mutation of the CIP-box motif of Dna2, in the *dna2-4A* allele, does not induce cell lethality but causes a strong reduction in the number of rDNA repeats and the consequently shortening of the chromosome XII (Villa et al., 2016).

1.1.1.4 Additional roles of Dna2

Dna2 acts, together with the Sgs1 helicase and redundantly with the Exo1 exonuclease, in the 5'-end resection of double-strand breaks (DSBs) during homologous recombination (Zhu et al., 2008). It has been shown that the CDK kinase regulates the 5' strand resection activity of Dna2 (Chen et al., 2011).

Dna2 has also a role in mitochondrial DNA maintenance (Budd et al., 2006; Duxin et al., 2009).

1.1.2 Natural impediments to DNA replication

An accurate completion of DNA replication is required for the faithful transmission of the genetic materials to daughter cells. The S-phase is a critical step of the cell cycle, since DNA molecules are dissociated from the chromatin fiber and the DNA duplexes are unwound to be used as templates by the replication machinery (Branzei and Foiani, 2010). Furthermore, replication fork progression is continuously challenged by endogenous and exogenous factors that can interfere with replication fork progression, generating

replication stress. DNA lesions, natural pausing sites and low levels of dNTPs, that induce fork pausing, are causes of replication stress (Branzei and Foiani, 2010). Eukaryotic genome contains natural impediments to replication forks progression, which include stable non-nucleosomal protein-DNA complexes, transcriptional units, RNA-DNA hybrids (which could be formed at the level of pausing elements containing transcribed regions) and DNA secondary structures such as G-quadruplexes, Z- DNA and S-DNA (*slipped-strand DNA*) (Azvolinsky et al., 2009; Brewer and Fangman, 1988; Deshpande and Newlon, 1996; Mirkin and Mirkin, 2007). Replication forks slow down also at the level of specific genomic loci, called *fragile sites,* which exhibit increased chromosome breakages (Cha and Kleckner, 2002; Hashash et al., 2011).

Accessory helicases, such as Rrm3, Pif1 and Sen1, promote replication fork progression at the level of these hard-to-replicate sites (Alzu et al., 2012; Bochman et al., 2010).

Furthermore, it has been reported that in human cells, oncogene overexpression induces replication stress (Bartkova et al., 2005; Di Micco et al., 2006; Dominguez-Sola et al., 2007; Mailand et al., 2000).

1.2 The checkpoint response to replication stress

1.2.1 The checkpoints

To ensure the maintenance of genome integrity, the faithful transmission of the genetic material and the fidelity of cell division, eukaryotic cells have evolved sophisticated surveillance mechanisms called checkpoints, that monitor the completion of the cell cycle events and coordinate the DNA repair mechanisms with the cell cycle transitions.

Many genetic syndromes characterized by an increased cancer predisposition are caused by mutations in genes that protect the genome integrity during DNA replication (Kastan and Bartek, 2004; Vogelstein and Kinzler, 2004).

Cells are constantly exposed to endogenous and exogenous events that challenge genome

integrity. In the presence of DNA lesions, cells activate the DNA damage checkpoint that leads to the activation of DNA repair pathways and delays the cell cycle transitions to allow DNA repair. DNA damage checkpoints are divided in three categories, depending on the cell cycle phase in which the lesions occur: the G1 phase checkpoint arrests the cell cycle before replication initiation (Siede et al., 1993; Weinert and Hartwell, 1988), the intra-S-phase checkpoint works during replication (Paulovich and Hartwell, 1995), and the G2/M phase checkpoint prevents chromosomes segregation, blocking the cell cycle at the metaphase/anaphase transition (Weinert and Hartwell, 1988).

In response to replication stress cells activate the DNA replication checkpoint (Allen et al., 1994; Weinert et al., 1994). Furthermore cells have evolved mitotic spindle checkpoints, activated in case of problems in the assembly or the orientations of the mitotic spindle (Lara-Gonzalez et al., 2012), and the morphogenesis checkpoint, activated by alterations of the cells shape (Lew, 2003).

Checkpoints are signal transduction cascades, evolutionary conserved in all eukaryotes, which amplify the signal to obtain a global cellular response. Key players of the DNA damage and replication checkpoints are the phosphatidylinositol 3-kinase (PI3K)-like kinases Mec1 (the homolog of human ataxia-telangiectasia and Rad3-related kinase (ATR)), and Tel1 (the homolog of human ataxia telangiectasia mutated kinase (ATM)), that work as sensors and initiate the signaling cascade. Mec1 responds to replication stress and DNA damage signals that cause the formation of ssDNA coated by RPA, whereas Tel1 is recruited to DSBs sites through the MRX complex and transduces mainly DSB signaling. The apical kinases transmit the checkpoint signal to mediator proteins, which amplify the signal and activate other downstream kinases working as effector proteins phosphorylating target proteins (Branzei and Foiani, 2009; Putnam et al., 2009).

1.2.2 Replication checkpoint

In the presence of replication stress, the DNA replication checkpoint pathway stabilizes paused or stalled replication forks preventing replisome disassembly, fork resection and unwinding, fork reversal and fork breakage (Branzei and Foiani, 2009; Elledge, 1996; Hartwell and Weinert, 1989). Eukaryotic cells have evolved this surveillance mechanism to prevent genomic instability and chromosomal rearrangements, which are typical hallmarks of cancer cells (Kastan and Bartek, 2004; Lengauer et al., 1998).

In the budding yeast *S. cerevisiae* the key regulators of the replication checkpoint are the apical kinase Mec1 and the effector kinase Rad53, which are, respectively, the ATR homologous and the *h*CHK1 functional orthologue (Branzei and Foiani, 2009).

Replication stress can be induced by treating cells with hydroxyurea (HU), a reversible inhibitor of the ribonucleotide reductase (RNR), that causes a sudden deprivation of the deoxynucleosides triphosphate (dNTPs) leading to fork stalling (Krakoff et al., 1968).

Checkpoint-defective mutants are highly sensitive to HU treatment and are not able to resume DNA synthesis after a transient HU exposure (Allen et al., 1994; Desany et al., 1998; Lopes et al., 2001; Tercero et al., 2003). Treatment of *mec1* and *rad53* mutants with low HU doses, or down regulation of the Mec1 activity, leads to cell lethality and chromosome fragmentation when the replication forks reach specific genomic loci, called replication slow zones (RSZs) (Admire et al., 2006; Cha and Kleckner, 2002; Hashash et al., 2011; Raveendranathan et al., 2006).

In the absence of *RAD53* irreversible DNA transitions happen at the level of the stalled replication forks in the presence of high levels of hydroxyurea; *rad53* mutants undergo fork collapse and accumulate damaged DNA replication forks with long ssDNA tracks at the fork branching points (called hemi-replicated bubbles) and reversed forks, which are further resected by the 5' to 3' directed exonuclease Exo1 (Cotta-Ramusino et al., 2005; Lopes et al., 2001; Lucca et al., 2004; Sogo et al., 2002) (see following paragraphs).

In human cells, down regulation of *ATR* in presence of replication stress causes cell death, increased origins firing, fork collapse and also ssDNA accumulation, fragile site expression and chromosome fragmentation through a CtIP- and SLX4-dependent process (Casper et al., 2002; Couch et al., 2013). Under replication stress human CHK1 prevents unscheduled origins firing, apoptosis, fork remodeling and chromosome breakages caused by the Mus81/Eme1 nuclease (Forment et al., 2011; Syljuasen et al., 2005).

1.2.3 Replication checkpoint signal transduction cascade

Electron microscopy analysis revealed that wild type cells, in untreated conditions, have ssDNA regions of ~200 nucleotides at the fork branching points and that, in the presence of hydroxyurea, additionally accumulate asymmetric ssDNA stretches on the replicated strands of 100 nucleotides (Sogo et al., 2002). These stretches of ssDNA at the stalled forks are likely recognized by RPA. RPA-coated ssDNA, above a certain threshold, constitutes the activation signal of the Mec1-dependent checkpoint (Sogo et al., 2002; Zou and Elledge, 2003). It has been proposed that, in the presence of HU, ssDNA stretches at fork branching points could be induced by the functional uncoupling of DNA polymerases and MCM helicase activities (Byun et al., 2005), or by the uncoupling between leading and lagging strand synthesis (Sogo et al., 2002); while internal ssDNA stretches could be generated on the newly synthesized strands by re-priming activities, both on the leading and on the lagging strand, with a mechanism similar to the one proposed to act in in S-phase in the presence of UV-induced DNA lesions, which are irreparable in the excision repair-deficient *rad14* cells (Lopes et al., 2006).

The apical checkpoint kinase Mec1 is recruited at stalled replication forks, thanks to the interaction of its regulatory subunit Ddc2 with RPA, and initiates the checkpoint signal transduction cascade (Figure 1.2). The ssDNA-RPA complex recruits also the clamp loader Rad24-Rfc2-5, required for the loading of the PCNA-related 9-1-1 complex (Rad17-Mec3-

Ddc1) on the ssDNA. The 9-1-1 complex is phosphorylated by Mec1 and is bound by the replication initiator factor Dpb11 (Branzei and Foiani, 2009).

Both the 9-1-1 complex and Dpb11 are crucial for the activation of Mec1 (Kumar and Burgers, 2013; Majka et al., 2006; Mordes et al., 2008; Navadgi-Patil and Burgers, 2009; Navadgi-Patil et al., 2011).

It is has been recently proposed that also Dna2 is an activator of the checkpoint in replication stress conditions and acts in partial redundancy with the 9-1-1 complex and Dpb11; Dna2 indeed stimulates the Mec1 kinase activity *in vitro* and *in vivo* specifically in S-phase through its unstructured N-terminal domain (Kumar and Burgers, 2013). However, quantitative mass-spectrometry analysis of phospho-substrates (QMAPS), performed by another group, contradicts this idea and shows that Dna2 and Ddc1 are not essential for checkpoint activation in replication stress conditions, but for the activation of Mec1 during normal DNA replication since Mec1 seems to play an important role in unperturbed conditions, redundantly with Tel1 (Bastos de Oliveira et al., 2015). Indeed during a normal S-phase, in the absence of replication stress, Mec1 phosphorylates a series of downstream targets and *mec1Δ* cells exhibit high levels of gross chromosomal rearrangements in unperturbed conditions (Bastos de Oliveira et al., 2015; Myung et al., 2001).

Following the localization of the sensor kinase Mec1 at stalled forks, mediator proteins are recruited to amplify the checkpoint signal. Mec1 phosphorylates multiple residues of the checkpoint mediator protein Mrc1, leading to the formation of a stable replication-pausing complex, formed by Mrc1 and Tof1, that prevents the detachment of Mec1 and of the replisome from DNA and activates the checkpoint cascade (Katou et al., 2003; Naylor et al., 2009). The following recruitment of the effector kinase Rad53 and the Rad53-dependent Mrc1 phosphorylation allow the maintenance of the pausing complex (Naylor et al., 2009). Moreover, Mrc1 phosphorylation arrests the MCM-mediated unwinding of the DNA duplex, impeding the uncoupling between DNA polymerases and the helicase and

the detachment of Cdc45 from the replisome, allowing the resumption of DNA synthesis after a transient exposure to HU (Katou et al., 2003; Nedelcheva et al., 2005).

Finally, Mrc1 is considered a checkpoint mediator factor since it is involved in the activation of the effector kinase Rad53 through a mechanism that is not yet completely understood (Alcasabas et al., 2001; Paulovich and Hartwell, 1995; Pellicioli et al., 1999). In *Xenopus* extracts, Claspin (the Mrc1 orthologous) physically interacts with the effector kinase Chk1 (the Rad53 functional orthologue) and is essential for Chk1 phosphorylation (Kumagai and Dunphy, 2003). In *S. cerevisiae, mrc1*Δ mutants are sensitive to hydroxyurea; HU-treated *mrc1*Δ cells show a delay in Rad53 hyperphosphorylation and accumulate ssDNA regions at stalled replication forks (Alcasabas et al., 2001; Naylor et al., 2009). In the absence of Mrc1, the DNA damage checkpoint mediator Rad9 can partially contribute to Rad53 phosphorylation, probably because *mrc1*Δ cells accumulate breakages at stalled forks (Alcasabas et al., 2001), generating a signal for the DNA damage checkpoint which requires Rad9, but not Mrc1, for Rad53 activation (Harrison and Haber, 2006; Weinert, 1998).

Rad53 has been identified in 1991 in a biochemical screen as a serine/threonine/tyrosine kinase (Stern et al., 1991); Rad53 has two FHA (*forkhead-associated*) domains that bind threonine residues (and maybe serine residues) previously phosphorylated by Mec1 or Tel1 (Durocher et al., 2000; Pike et al., 2003). The typical consensus motifs for the apical kinases Mec1 and Tel1 are indeed SQ/TQ clusters, while Rad53 preferentially phosphorylates serine and threonine residues followed by hydrophobic amino acids (Smolka et al., 2007).

Under replication stress, the Mec1-dependent Rad53 phosphorylation is followed by *in trans* autophosphorylation events, which generate the active form of Rad53; the Rad53 hyperphosphorylated status is indeed associated with an increase in its kinase activity (Pellicioli and Foiani, 2005). To be noticed, a *RAD53* hypomorphic allele*, rad53-K227A,* uncouples the Mec1-phosphorylation from the autophosphorylation process; indeed it is

not able to perform *in trans* autophosphorylation or to phosphorylate target proteins, since it retains only the 10% of the kinase activity, which is sufficient for cell viability in unperturbed conditions but not in the presence of HU; this means that this mutant lacks the checkpoint functions (Fay et al., 1997; Zheng et al., 1993).

The Mec1-mediated Rad53 hyperphosphorylation occurs in response to both DNA damage and DNA synthesis inhibition and can be used as a biochemical marker to monitor the checkpoint activation (Pellicioli et al., 1999).

Once hydroxyurea is removed or DNA lesion is repaired, the Rad53 kinase is switched off and cells can complete DNA replication (Lopes et al., 2001; Pellicioli et al., 1999). Glc7, the catalytic subunit of the PP1 phosphatase, dephosphorylates Rad53 after the removal of replication stress-inducing agents (Bazzi et al., 2010), while the phosphatases Pph3-Psy2 (O'Neill et al., 2007), Ptc2 and Ptc3 (Leroy et al., 2003) that dephosphorylate Rad53 after DNA damage repair or bypass, only partially contribute to Rad53 dephosphorylation after HU removal (Travesa et al., 2008).

Another commonly used marker to detect the checkpoint activation is the phosphorylation of the histone H2A. The histone H2A is phosphorylated on the serine 129 by Mec1 in replication stress and by both Mec1 and Tel1 in the presence of DSBs, to recruit DNA repair and chromatin remodeling factors (Cobb et al., 2005; Downs et al., 2000).

Under replication stress Rad53, thanks to its kinase activity, increases the cellular dNTPs pool (Huang et al., 1998; Zhao and Rothstein, 2002), inhibits late origins firing (Zegerman and Diffley, 2010), stabilizes stalled replication forks (Lopes et al., 2001; Tercero and Diffley, 2001), releases the transcribed chromatin from nuclear envelope (Bermejo et al., 2011) and inhibits chromosomes segregation and mitosis before the completion of DNA replication, preventing spindle extension (Allen et al., 1994).

Three pathways act redundantly to prevent mitosis and therefore the segregation of not completely replicated chromosomes under replication stress: Mec1 downregulates the activity of the mitotic cyclin dependent kinase (M-CDK) through Rad53 and also

phosphorylating and activating Swe1, the M-CDK inhibitor kinase; moreover in *rad53 swe1* mutants chromosome segregation is prevented by the Mec1-dependent stabilization of the securin/Pds1, which inhibits the metaphase-anaphase transition, maintaining the sister-chromatid cohesion (Palou et al., 2015).

In the presence of DNA damage, Mec1 activates, through the Rad9 mediator, not only Rad53 but also a second checkpoint effector kinase, Chk1, which causes the DNA damage checkpoint-dependent preanaphase arrest acting on Pds1 (Cohen-Fix and Koshland, 1997; Sanchez et al., 1999). Chk1, in the absence of Rad53, has also a role in stabilizing stalled replication forks, generated by the presence of intra-S DNA damage (Segurado and Diffley, 2008).

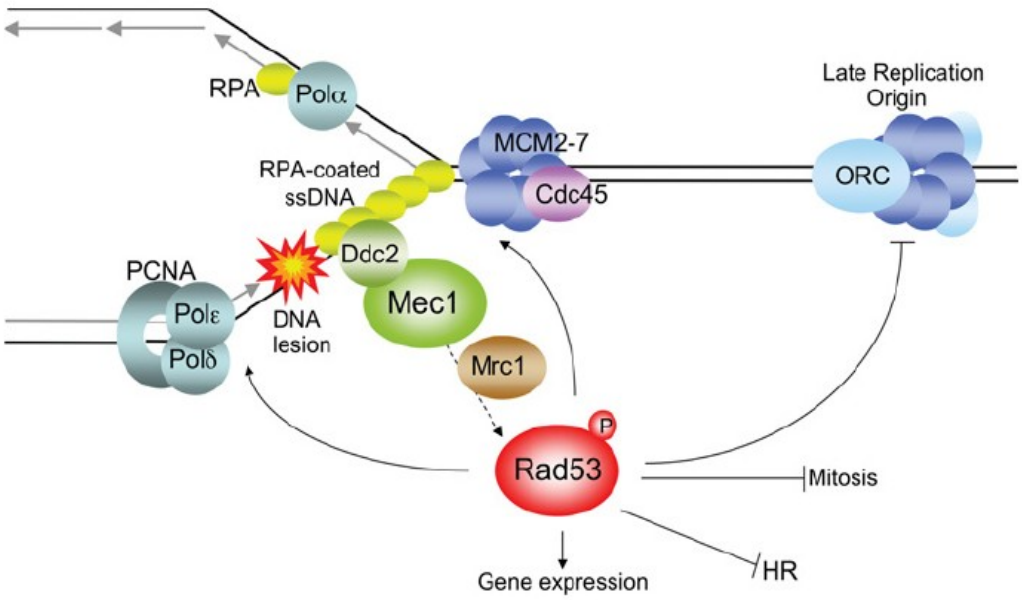

Figure 1.2. Replication checkpoint signal transduction cascade (from (Segurado and Tercero, 2009)).

1.2.4 dNTPs pool regulation

The intracellular level of dNTPs has to be strictly regulated to preserve genome integrity; an imbalanced dNTPs pool increases recombination, mutagenesis, chromosome abnormalities and cell death (Bester et al., 2011; Chabes and Stillman, 2007; Kumar et al., 2011; Kumar et al., 2010; Kunz et al., 1994; Reichard, 1988).

The ribonucleotide reductase (RNR) is the enzyme that catalyzes the rate-limiting step in dNTP synthesis: the reduction of ribonucleotides (NDPs) to deoxyribonucleotides (dNDPs) (Chabes et al., 1999). RNR is a tetrameric complex, composed by two small catalytic subunits, Rnr2 and Rnr4, and two Rnr1 regulatory subunits. DNA lesions induce the transcription of an additional regulatory subunit, Rnr3. The protein levels of the RNR inhibitor, Sml1, fluctuate during the cell cycle; in S-phase, Sml1 levels are reduced in a Mec1 and Rad53-dependent manner (Zhao et al., 2001) leading to an increase of the activity of RNR enzyme and of the levels of dNTPs, which are 3 fold higher than in G1 phase (Kumar et al., 2010). Interestingly, the lethality of *mec1Δ* and *rad53Δ* cells, but not the high HU sensitivity of *mec1* and *rad53* mutants (Desany et al., 1998), can be rescued deleting the *SML1* gene or overexpressing the Rnr1 subunit, which cause an increase in the dNTPs level, respectively of 2.5 fold (Zhao et al., 1998), and 10 fold (Chabes and Stillman, 2007; Desany et al., 1998). The fact that the upregulation of dNTPs pool suppresses the lethality of *mec1* and *rad53* cells demonstrates that, in an unperturbed cell cycle, Mec1 and Rad53 are essential to maintain the proper dNTPs level, which is crucial to complete the DNA replication (Zhao et al., 2001; Zhao et al., 1998).

Low dNTPs levels impede replication fork progression. Treatment with 200 mM hydroxyurea, an RNR inhibitor, induces a rapid transition from a normal replication-speed (0.6-1 Kb/min) to a slow-replication mode (0.1 Kb/min) when the dNTPs goes below a critical level (Alvino et al., 2007; Poli et al., 2012). G1 synchronized cells, released in S-phase in the presence of 200 mM of HU, start the DNA replication using the G1 dNTPs pool, but, after the firing of the 40% of the replication origins and the replication of the 10-15% of the genome, the low level of dNTPs reduces the fork speed, the replication checkpoint is activated and cells shift to a slow-replication mode to complete the replication in about 8 hours (Poli et al., 2012).

In the presence of DNA damage and in replication stress conditions the checkpoint increases the activity of the RNR enzyme through several mechanisms, inducing the

upregulation of dNTPs pool and favoring the progression of the DNA synthesis (Poli et al., 2012). The same checkpoint-dependent regulatory mechanisms are used to increase the dNTPs levels during normal cell growth in S-phase but, in the presence of DNA damage, the dNTPs levels are 3 to 5 fold higher than in an unperturbed S-phase (Chabes et al., 2003).

Replication checkpoint regulates RNR activity acting on Sml1. In unperturbed conditions, Sml1 binds the Rnr1 subunits, inhibiting the RNR enzyme (Chabes et al., 1999; Zhao et al., 2001). In replication stress conditions Mec1 and Rad53 phosphorylate and activate the Dun1 kinase, which subsequently phosphorylates Sml1 and induces its degradation, increasing dNTPs production (Zhao and Rothstein, 2002).

Moreover, the phosphorylated and activated Dun1 kinase inhibits the transcriptional repressor Crt1 through phosphorylation, inducing the transcription of several DNA damage-inducible genes, including the *RNR* genes (Elledge et al., 1993; Zhao and Rothstein, 2002). In an unperturbed cell cycle, Crt1 is associated with the X-box sequences in the promoters of damage-inducible genes and recruits the co-repressor complex Ssn6-Tup1 (Huang et al., 1998). In replication stress conditions, Crt1 is phosphorylated in a Mec1-, Rad53- and Dun1-dependent manner and is no longer able to bind DNA; this results in the transcriptional induction of *RNR2*, *RNR3* and *RNR4* genes (Huang et al., 1998). Interestingly, a negative feedback mechanism regulates this process; even the *CRT1* promoter contains an X-box domain that is bound and repressed by Crt1. In this way also Crt1 expression is induced by the presence of DNA lesions (Huang et al., 1998).

However, the fact that wild type cells, in the absence of protein synthesis, efficiently resume the replication after a transient HU treatment, suggests that the checkpoint-mediated transcriptional induction is not the only contribution in the response to DNA replication stress (Tercero et al., 2003).

A third checkpoint-mediated regulatory mechanism is the control of the subcellular localization of the RNR subunits (Lee and Elledge, 2006; Yao et al., 2003). During normal

cell growth, Rnr1 is mainly localized to the cytoplasm, while, outside the S-phase, Rnr2 and Rnr4 are localized in the nucleus through the action of Dif1 (*Damage regulated import facilitator*). In replication stress conditions Dun1 phosphorylates Dif1 and promotes its degradation, releasing Rnr2 and Rnr4 in the cytoplasm to form an active RNR enzyme with Rnr1 (Lee and Elledge, 2006; Lee et al., 2008; Yao et al., 2003).

Furthermore, the large Rnr1 subunit contains two allosteric sites that regulate both the balance among the four dNTPs and the total dNTPs level, monitoring the dATP/ATP ratio. The dATP feedback inhibition mechanism, which shuts off the RNR enzyme at certain levels of dATP, is released by the checkpoint to increase the dNTPs level in replication stress (Chabes et al., 2003).

1.2.5 Inhibition of late origins firing

In the presence of HU-induced replication stress, the checkpoint slows down the replication timing program, inhibiting the activation of late and dormant origins, while it does not affect the early origins firing (Santocanale and Diffley, 1998; Shirahige et al., 1998; Tercero and Diffley, 2001) (Alvino et al., 2007; Crabbe et al., 2010).

Indeed, late origins are massively derepressed in checkpoint mutants in replication stress conditions and *mec1* and *rad53* mutants exhibit a similar patter of origin activation, indicating that the two checkpoint kinases act in a linear pathway to repress late origins (Crabbe et al., 2010).

The checkpoint-mediated control of origin firing is a genetically distinct mechanism from the stabilization of stalled forks and only modestly contributes to cell viability in replication stress; indeed the hypomorphic *mec1-100* mutant, which is not able to suppress the activation of late and dormant origins in HU but prevents fork collapse, is less HU-sensitive compared to *mec1Δ* cells (Paciotti et al., 2001; Tercero et al., 2003) (Crabbe et al., 2010).

The replication checkpoint inhibits origin firing through the phosphorylation of Sld3 and Dbf4, which affect the CDK- and DDK-mediated origins activation (Zegerman and Diffley, 2010). Sld3 is an essential protein for the replication initiation (but not for the elongation phase) and the interactions with Cdc45 and Dpb11 are essential for its function. In an unperturbed cell cycle, in early S-phase, CDK phosphorylates two residues in the C-terminus of Sld3, allowing the interaction with the BRCT domain of Dpb11; under replication stress Rad53 phosphorylates multiple C-terminus residues of Sld3, impeding both the CDK-dependent Sld3-Dpb11 interaction and the binding of Sld3 and Cdc45 (Zegerman and Diffley, 2010)

Dbf4, the regulatory subunit of the DDK kinase, seems to recruit Cdc7 at the replication origins through its interactions with ORC (Duncker et al., 2002). In the presence of hydroxyurea, Rad53, through the two FHA domains, binds and phosphorylates multiple sites of Dbf4, reducing the kinase activity of the DDK and inducing the detachment of Dbf4 from the origins (Duncker et al., 2002; Zegerman and Diffley, 2010).

The mutation of Rad53-dependent phosphorylation sites to alanine residues in the *sld3-38A dbf4-19A* mutant results in the activation of late replication origins in replication stress, even in the presence of active Rad53 (Zegerman and Diffley, 2010).

Also Mrc1 is involved in the suppression of origin firing under replication stress (Alcasabas et al., 2001; Shirahige et al., 1998). *mrc1Δ* mutan§ts are not able to suppress the activation of the late origins under replication stress, but nevertheless cell viability is rather high if compared to null *rad53* and *mec1* mutant in HU (Alcasabas et al., 2001).

1.2.6 Stabilization of stalled replication forks

The essential function of the replication checkpoint, is to preserve the integrity of stalled replication forks, while the regulation of late origin firing, mitosis and genes expression only partially contributes to the viability of HU-treated cells (Branzei and Foiani, 2009; Tercero et al., 2003). When the replication forks stall, the checkpoint prevents the

dissociation of the replisome from the DNA and the unscheduled activity of nucleases, helicases, or recombination enzymes to avoid the formation of breakages and recombination intermediates (Sogo et al., 2002) (Cotta-Ramusino et al., 2005; Lopes et al., 2001; Lucca et al., 2004).

mec1Δ mutants have an higher HU sensitivity and more chromosome breakages than *rad53Δ* mutants, suggesting that Mec1 ensures the stabilization of stalled forks also by Rad53-independent mechanisms (Desany et al., 1998; Tercero and Diffley, 2001).

1.2.6.1 Stabilization of replisome-fork association

The stabilization of stalled replication forks and the recovery of the DNA synthesis after HU removal depend on the capability to maintain the association of the replisome with the DNA. Chromatin immunoprecipitation (ChIP) experiments reveal that the replisome-fork association in HU-treated cells depends on a functional checkpoint; indeed, in checkpoint-defective cells treated with HU, DNA polymerases (Polα, Polδ e Polε), Mcm10 and MCM helicase dissociate from the template, in a process defined as *fork collapse* (Cobb et al., 2003; Cobb et al., 2005; Lucca et al., 2004; Raveendranathan et al., 2006). In *rad53* mutants, synchronized in G1 and released into S-phase in the presence of high doses of hydroxyurea, Polα and Polε are less associated to the early replication origins compared to wild type cells and their binding decreases with time; at later time points, also Polδ binding is rapidly lost in *rad53* mutants (Lucca et al., 2004).

Moreover, in the presence of high HU doses, in *rad53* mutants replication forks do not proceed in the flanking regions of the replication origins, but remain stacked close to the origin points, suggesting that in the absence of *RAD53* the fork progression is impaired in HU (Lopes et al., 2001; Lucca et al., 2004; Rossi et al., 2015).

In HU-treated checkpoint-defective cells, stalled forks deprived of DNA polymerases are converted into abnormal intermediates that are highly recombinogenic and impede the resumption of DNA synthesis after HU removal (Lopes et al., 2001). These abnormal replication intermediates have been visualized using the neutral/neutral 2D gel

electrophoresis technique in *rad53* cells treated with high HU doses and migrate like four-branched molecules (*reversed forks*), generating a signal called "spike-cone signal". Reversed forks are processed by the Exo1 exonuclease (Cotta-Ramusino et al., 2005). The exonucleolytic processing of bubbles and/or reversed forks causes also the formation of "small Y" structures (Lopes et al., 2001).

Reversed forks are "chicken foot" like structures, characterized by a fourth dsDNA regressed arm, generated by annealing of the newly synthetized strands and re-annealing of the parental strands. According to two different hypotheses, that are not mutually exclusive, reversed forks in HU-treated checkpoint mutants are generated by topological transitions, such as the formation of positive supercoilings induced by the tethering of the transcribed gene to nuclear envelope, not properly counteracted by the checkpoint (Bermejo et al., 2011; Postow et al., 2001a; Postow et al., 2001b) and/or by the stabilization and collision of the sister chromatid junctions (SCJs) with stalled replication forks deprived of the replisomes (Lopes et al., 2003).

SCJs resemble hemicatenanes, which are X-molecules in which the newly synthesized filaments of the sister chromatids are inter-locked at the level of non-homologous sequences hooked connected (Lopes et al., 2003). SCJs are formed in S-phase after origins firing and do not depend upon homologous recombination for their formation. SCJs could have a role in sister chromatids cohesion and their formation could be induced by the discontinuous synthesis of the lagging strand associated with the catenation of the sister chromatids (Lopes et al., 2003). It has been proposed that in checkpoint mutants in HU, SCJs reach collapsed replication forks and promote the annealing of the newly synthesized strands, contributing to the formation of the reversed forks (Lopes et al., 2003).

These abnormal replication intermediates have been also visualized using electron microscopy (Sogo et al., 2002). HU-treated wild type cells accumulate, at the stalled replication forks, small stretches of single-stranded DNA fragments (Sogo et al., 2002), while in *rad53* mutants stalled forks undergo fork collapse, the replisomes dissociate from

the forks and cells accumulate broken forks, reversed forks (Figure 1.3C) and extensive single-stranded DNA regions (~870 nt) at the fork branching points (Figure 1.3A) and hemi-replicated bubbles (Figure 1.3B). These abnormal replication intermediates can induce uncontrolled recombination events and can cause genome instability (Admire et al., 2006). Moreover, in the presence of 200 mM of hydroxyurea, in wild type cells the replication proceeds slowly and bubbles size increases with time, while, in *rad53* mutants, the collapse of the replication fork impedes the progression of DNA synthesis, the bubbles size modestly increases and their number decreases over time, while the percentage of Y-shaped intermediates increases (Sogo et al., 2002).

The extensive single-stranded DNA regions, in HU-treated *rad53* mutants, could result from lagging strand synthesis defects, caused by the uncoupling between leading and lagging strands synthesis (Sogo et al., 2002) and from exonucleolitic processing of the newly synthesized strands by Exo1 or other exo/endonucleases or DNA helicases (Cotta-Ramusino et al., 2005).

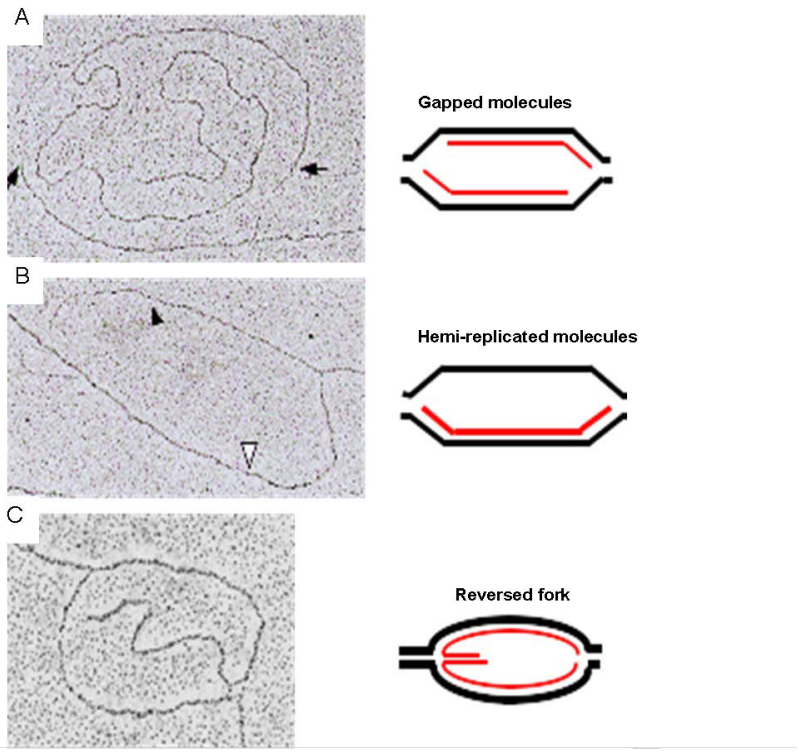

Figure 1.3. Transmission electron microscopy images of abnormal replication intermediates accumulated in HU-treated *rad53* mutants. *rad53-K227A* mutants treated with 200 mM HU accumulate gapped forks (A), hemi-replicated forks (B) and reversed forks (C) (adapted from Sogo et al., 2002).

1.2.6.2 Inhibition of endo/exonuclease activities at stalled forks

Stalled replication forks, if not properly stabilized, can become the substrates of endo/exonucleases, leading to chromosome breakages. The checkpoint stabilizes stalled replication forks inhibiting the activity of recombination enzymes (Branzei and Foiani, 2009). Indeed Rad52 repair foci have been found in checkpoint defective cells after HU treatment, but not in wild type cells (Lisby and Rothstein, 2004).

Following HU treatments, in the absence of hCHK1 the endonuclease complex Mus81/Eme1 generates breakages at stalled replication forks (Forment et al., 2011).

In *S. pombe,* the effector checkpoint kinase Cds1 prevents unscheduled fork processing in replication stress conditions, negatively regulating the recombination proteins Mus81 and Rad60; Cds1-mediated phosphorylations reduce the chromatin association of the Mus81-Eme1 endonuclease and induce localization of Rad60 outside the nucleus (Boddy et al., 2003; Froget et al., 2008; Kai et al., 2005).

In the presence of hydroxyurea, the 5' to 3' exonuclease Exo1 is phosphorylated in a Mec1-dependent manner (Engels et al., 2011), it is recruited at the stalled forks both in wild type and *rad53Δ* cells and processes stalled replication forks in checkpoint defective mutants, generating extensive single-stranded DNA regions (Figure 1.3A,B) and counteracting fork reversal (Cotta-Ramusino et al., 2005; Lopes et al., 2001; Sogo et al., 2002). 2D gels and EM analysis demonstrate that *EXO1* deletion suppresses the formation of gapped-molecules and hemi-replicated bubbles in HU-treated *rad53* mutants, while the number of reversed forks increases in the double mutant *rad53Δexo1Δ* compared to *rad53Δ* cells (Cotta-Ramusino et al., 2005). These data suggest that Exo1 directly processes reversed forks and stalled forks (Cotta-Ramusino et al., 2005). However, *EXO1* deletion fails to rescue cell lethality and replisome-fork dissociation detectable in HU-treated *rad53* mutants, suggesting that the Exo1-mediated processing of stalled forks is downstream of the key event that causes the commitment of stalled forks to inviability (Cotta-Ramusino et al., 2005).

1.2.6.3 Inhibition of replication fork breakage at the replication slow zones (RSZs)

Chromosome breakages can occur even during an unpertubed cell cycle and are preferentially generated at the level of specific late-replicating genomic *loci*, referred to as replication slow zones (RSZs) (Cha and Kleckner, 2002; Hashash et al., 2011). Fragile site breakage, a process known as *fragile site expression*, is associated with increased genome instability (Admire et al., 2006). It has been observed that the checkpoint proteins Mec1 and Rad53 suppress fragile sites expression, probably by stabilizing stalled replication forks (Cha and Kleckner, 2002; Hashash et al., 2011; Raveendranathan et al., 2006).

In *rad53* and *mec1* mutants a series of early origins, termed compromised early origins (CEOs), are prone to breakages both in unperturbed conditions and in the presence of high HU concentrations. In replication stress conditions in checkpoint mutants, CEOs fire efficiently, but are not proficient in replication elongation due to fork stalling and fork collapse (Raveendranathan et al., 2006).

The thermal inactivation of the *mec1-4* temperature sensitive allele causes the arrest of the replication forks when they reach the RSZs; at these genomic *loci* replication fork arrest is followed by chromosome breakages (Hashash et al., 2011). These chromosome breakages occur before anaphase and do not depend on homologous recombination proteins, Sgs1-Top3 complex, Srs2 helicase, and Mus81-Mms4 endonuclease or on the spindle assembly checkpoint. However, RSZs breakages in the absence of *MEC1* require the type II topoisomerase, Top2, and the condensin complex (Hashash et al., 2012). Top2 generates transient nicks in both DNA strands to transfer one DNA double helix through another and is required for the disentanglement of sister chromatids, allowing their separation in mitosis (Baxter et al., 2011). Top2 is also required, together with condensins, for chromosome compaction during mitosis (Vas et al., 2007). Therefore, it has been proposed that the chromosome tensions generated during mitotic chromosome condensation are involved in the formation of breaks at the stalled forks at RSZs; otherwise Top2 could directly generate the DSBs at the RSZs (Hashash et al., 2012).

It has been suggested that RSZs are sensitive to low dNTPs levels and that *mec1* mutants accumulate breakages at these sites since they fail to increase the dNTPs pool during S-phase; indeed, deletion of *SML1,* that increases the dNTPs level, reduces the RSZs expression in temperature sensitive *mec1* mutant and rescues the lethality of *mec1Δ* cells (Cha and Kleckner, 2002; Hashash et al., 2011; Zhao et al., 1998). Also the ablation of the DNA helicase Rrm3 mildly suppresses DSBs formation at the RSZs, and it has been proposed that this happens since *rrm3Δ* cells have a slightly higher level of dNTPs due to a mild and constant activation of the intra-S phase checkpoint (Hashash et al., 2011; Poli et al., 2012).

Treatment of *mec1* and *rad53* mutants with low HU doses leads to cell lethality and causes chromosome fragmentation when replication forks reach the RSZs (Cha and Kleckner, 2002; Hashash et al., 2011). On the contrary, high doses of hydroxyurea are able to suppress fragile site expression in *mec1* and *rad53* mutants (Hashash et al., 2011), probably because high HU doses strongly impair the replication fork progression and, in the absence of a functional checkpoint, replication forks collapse close to the replication origins, without reaching the RSZs.

1.2.6.4 Gene gating inhibition

Chromosomes are complex structures associated with the nuclear membrane and with protein structures that constitute chromosome scaffolds; these cellular structures generate topological barriers which impede the rotation of the DNA molecule. The unwinding of the DNA duplex during DNA replication induces the formation of positive supercoilings ahead of the replication fork, that can be solved by type I and type II topoisomerases, such as Top1 or Top2 respectively, or converted into precatenanes if the replisome is free to rotate around the double helix (Postow et al., 2001a; Wang, 1996). Positive supercoilings, if not properly solved, can induce fork stalling and DNA breakages(Bermejo et al., 2007). The topological tension, created by positive supercoilings ahead of the fork, can also cause the disassemblement of the replisome, the unwinding of the newly-synthesized filaments from

the template and their pairing, generating reversed forks (Postow et al., 2001a; Postow et al., 2001b). The rotation of the replisome around the double helix during replication leads to the catenation of sister chromatids, which can cause DNA breakages during the chromosomes segregation if precatenanes are not properly solved by type II topoisomerases (Top2) (Postow et al., 2001a; Wang, 1996).

One physiological obstacle to DNA replication is transcription; DNA and RNA polymerases compete for the same DNA template and replication and transcription have to be tightly coordinated in order to maintain genome integrity (Aguilera, 2005; Bermejo et al., 2012b). The synthesis of RNA polymerase II-transcribed genes is coupled with mRNA processing, assembling of the messenger ribonucleoparticle (mRNP) and exporting into the cytoplasm (Aguilera, 2005; Kohler and Hurt, 2007). The association of the transcribed chromatin with the nuclear pore complex (NPC), known as gene gating, constitutes a topological barrier to DNA replication and is mediated by protein complexes, such as THO/TREX and TREX-2 (Bermejo et al., 2012a; Cabal et al., 2006). THO moves with the RNA polymerase 2, it is formed by four subunits Tho2, Hpr1, Mft1 and Tph2 (Luna et al., 2008) and associates with the TREX-2 complex composed by Sac3, Thp1, Sus1 and Cdc31 (Kohler and Hurt, 2007). Sac3 mediates the association of the complex with the nuclear membrane, thanks to the binding with the nucleoporin Nup1. Mutations in the THO and TREX-2 complexes cause transcriptional elongation and mRNA nuclear export defects and cells accumulate DNA:RNA hybrids (R-loop) (Aguilera, 2005). It has been proposed that the replication checkpoint stabilizes stalled replication forks through the inhibition of the gene gating and the subsequent release of the transcriptional units from the nuclear pore eliminating the topological barriers and counteracting the torsional energy that would otherwise cause replisome-fork dissociation and fork reversal (Bermejo et al., 2011). In line with this model, several nucleoporins are phosphorylated by the checkpoint kinases under replication stress (Smolka et al., 2007). In replication stress conditions, Rad53 releases the transcribed genes from the nuclear envelope, phosphorylating the nucleoporin

Mlp1; mutations in the THO or THREX-2 complexes, such as *tho2Δ* and *sac3Δ*, or the *mlp1* mutation mimicking the checkpoint-dependent phosphorylation rescue the HU sensitivity, the unscheduled firing of late origins and the formation of reversed forks in *rad53* mutants (Bermejo et al., 2011).

1.2.6.5 Regulation of replisome-associated factors

The molecular mechanisms through which Rad53 protects stalled DNA replication forks are not yet completely understood, but recent findings support the idea that the checkpoint kinases could control the stability of the stalled forks through the regulation of replisome-associated factors (Couch et al., 2013; De Piccoli et al., 2012; Hu et al., 2012; Lossaint et al., 2013).

In replication stress conditions, Psf1, a subunit of the GINS complex associated with stalled replication forks, is phosphorylated by Mec1, but the physiological role of this phosphorylation has to be further investigated (De Piccoli et al., 2012).

In human cells, experiencing replication stress, ATR phosphorylates SMARCAL1 DNA translocase to control its activity at stalled replication forks, preventing replication fork collapse. When ATR is inactivated, the uncontrolled fork regression activity of SMARCAL1 generates substrates that undergo to SLX4-scaffolded endonucleases dependent cleavage and CtIP-dependent resection, leading to DNA breakages and ssDNA accumulation (Couch et al., 2013).

An additional effector of the checkpoint signaling, in replication stress, is the FANCD2 protein (Lossaint et al., 2013). FANCD2 associates with the replisome under replication stress in an ATR-dependent and CHK1-independent manner, thanks to the interaction with the MCM complex and is required to create a stable replication pausing complex (Lossaint et al., 2013).

Moreover, both in mammalian cells and in *S.pombe,* the MCM helicase complex is phosphorylated in replication stress conditions, respectively by ATR and Cds1 (Bailis et al., 2008; Cortez et al., 2004).

In *S.pombe*, the Cds1 effector kinase targets another replisome component, the nuclease Dna2, to prevent stalled replication forks from reversing (Hu et al., 2012). Following HU treatment Dna2 phosphorylation prevents its dissociation from stalled replication forks, where its 5' flap endonuclease activity prevents fork reversal, probably by cleaving regressed leading or lagging strand (Hu et al., 2012). Even human Dna2 has been recently implicated in the processing of reversed replication forks but in the context of DNA replication fork restart mechanisms (Thangavel et al., 2015).

Moreover in *S.cerevisiae,* RPA is phosphorylated in a Mec1-dependent manner and it is involved in the stabilization of stalled forks (Brush et al., 1996). Also the lagging strand apparatus is a checkpoint target; in the presence of intra-S DNA damage, the Rad53 checkpoint kinase, probably by modulating the CDK activity, inhibits the phosphorylation of DNA polymerase α-primase (Pellicioli et al., 1999), which has been proposed to negatively regulate the primase activity of the complex (Marini et al., 1997).

Interestingly, it has been reported that the Pif1 DNA helicase becomes phosphorylated in replication stress conditions (Makovets and Blackburn, 2009) and in this thesis novel data will be presented about the role of this replication stress-induced phosphorylation of Pif1.

1.3 Roles of Pif1 family helicases in promoting replication fork progression

*Sc*Pif1 is the prototype member of the highly conserved Pif1 DNA helicase family, found in nearly all eukaryotes (Bochman et al., 2010). The Pif1 helicases are ssDNA-dependent ATPases and 5' to 3' directed DNA helicases which act as accessory helicases to the replication machinery (Ivessa et al., 2002; Lahaye et al., 1993). They belong to the SFI superfamily of helicases and are characterized by an ATPase/helicase domain of 300-500 amino acids that contains seven helicase motifs conserved within the Pif1 subfamily, while N-terminus and C-terminus domains are evolutionarily divergent (Bochman et al., 2010).

The human genome encodes a single Pif1-like protein (*h*PIF1), like *S.pombe* (Pfh1), while the genome of *S.cerevisiae* encodes two members of this family, Pif1 and Rrm3. Human PIF1 shows equal sequence homology to both ScPif1 and ScRrm3 (Mateyak and Zakian, 2006).

Human PIF1, like *S.cerevisiae* Pif1 and Rrm3, is not essential and recently the mutation of a conserved residue in its ATPase domain has been linked to inherited breast cancer (Chisholm et al., 2012). On the contrary, *S.pombe* Pfh1-deficient cells are not viable (Tanaka et al., 2002); probably because, in the absence of Pfh1, cells rapidly lose the mitochondrial DNA and *S.pombe* cells are not able to survive without mitochondria (Pinter et al., 2008).

In budding yeast, Rrm3 and Pif1 localize in both nucleus and mitochondria and have a key role in the maintenance of nuclear and mitochondrial genome stability.

Rrm3 and Pif1 facilitate replication fork progression through genome sites containing replication pausing elements, acting as DNA replication fork accelerators in unperturbed conditions (Bochman et al., 2010). Rrm3 is thought to remove bulky non-nucleosomal DNA-protein complexes ahead of the replication fork through its translocase like activity, while Pif1 appears more dedicated to the unwinding of problematic DNA structures that can delay replication fork progression. In the absence of Rrm3 and Pif1 replication forks pause at the Rrm3/Pif1 dependent pausing sites (Azvolinsky et al., 2009), leading to checkpoint activation, histone H2A hyperphosphorylation (Ivessa et al., 2003) and chromosome breakages (Ribeyre et al., 2009; Szilard et al., 2010).

1.3.1 Pif1

PIF1 (*Petite Integration Frequency*) gene was identified in 1983 in a genetic screen for mutations which reduced the recombination frequency between mitochondrial DNA of rho^+ (respiratory proficient) and rho^- (respiratory deficient) strains (Foury and Kolodynski,

1983) and was then rediscovered in a screening to identify mutations that affected telomeres (Schulz and Zakian, 1994).

Pif1 has a nuclear isoform and a mitochondrial isoform, expressed from the same open reading frame using two different translational start sites. The Pif1 isoform, translated from the first start site is targeted to mitochondria by a mitochondrial targeting signal (MTS) and, after the cleavage of the MTS, it generates the faster migrating band detectable by Western blotting, while the larger isoform is the nuclear Pif1, translated from the second translational start site. The mutations of the first methionine (*pif1-m1*), or the second AUG codon (*pif1-m2*), allow to separate the Pif1 functions, expressing respectively only the nuclear isoform or the mitochondrial isoform (Lahaye et al., 1991; Schulz and Zakian, 1994; Zhou et al., 2000).

1.3.1.1 Mitochondrial function

Pif1 physically associates with mitochondrial DNA (Cheng et al., 2007) and seems to be involved in mtDNA replication and recombination (Foury and Dyck, 1985; Foury and Kolodynski, 1983). The helicase activity of Pif1 is required for mtDNA maintenance and *pif1Δ* and *pif1-m1* cells exhibit high levels of loss and breakages of mitochondrial DNA and *petite* cells (Lahaye et al., 1991; Van Dyck et al., 1992).

The accelerated loss of mtDNA in *pif1* mutants is partially suppressed by *RRM3* deletion or high dNTPs levels (O'Rourke et al., 2002).

1.3.1.2 Inhibition of telomerase

In the absence of Pif1 telomeres are about 160 nucleotides longer than in wild type cells, while Pif1 overexpression induces telomeres shortening (Schulz and Zakian, 1994; Zhou et al., 2000).

PIF1 deletion cannot alter telomere length in the absence of the *TLC1* gene, which encodes for the RNA subunit of telomerase, indicating that the telomere lengthening in *pif1* mutants is telomerase-dependent and not a recombination-dependent elongation (Zhou et al., 2000).

Cells expressing the *pif1-m2* allele or the helicase defective allele *pif1-K264A* have the same telomere defect of *pif1Δ* cells (Zhou et al., 2000), meaning that the helicase activity of the nuclear isoform of Pif1 is required to inhibit telomerase.

Since the levels of nuclear Pif1 are cell cycle regulated and peak in late S/G2, when telomerase acts (Vega et al., 2007) and Pif1 localizes at telomeres, it probably directly inhibits the telomerase (Zhou et al., 2000). Biochemical data have also demonstrated that Pif1, throughout its helicase activity, reduces the processivity of the telomerase *in vitro*, while in the absence of Pif1 the level of telomere-bound telomerase subunit Est1 increases *in vivo* (Boule et al., 2005). Since Pif1 preferentially unwinds RNA-DNA hybrids, it could negatively regulate the telomere length releasing the RNA component of the telomerase, TLC1, from the single-stranded G-rich tail (Boule and Zakian, 2007).

Interestingly, the Pif1 unwinding activity at telomeres becomes toxic in the absence of the essential telomere capping protein Cdc13 (Dewar and Lydall, 2010). *PIF1* and *EXO1* deletions rescue cell lethality, telomeric ssDNA generation and checkpoint activation in the absence of *CDC13* (Dewar and Lydall, 2010). Therefore it has been proposed that Pif1 binds exposed 5' C-rich ssDNA tails at uncapped telomeres and, together with the Exo1 exonuclease, degrades the 5' strands, generating extensive ssDNA that stimulates the DNA damage checkpoint activation (Dewar and Lydall, 2010).

Also human PIF1 seems to play a role at telomeres: it interacts with the catalytic subunit of telomerase (hTERT) (Mateyak and Zakian, 2006), its overexpression reduces telomere length and it reduces the processivity of telomerase *in vitro* (Zhang et al., 2006). On the contrary, in *S.pombe*, in the absence of Pfh1, telomeres are modestly shorter (Zhou et al., 2002). Moreover, human PIF1, but not *S.pombe* Pfh1, is able to restore the telomere length when expressed in *pif1-m2* mutants (Paeschke et al., 2011).

In yeast, Pif1 inhibits both telomere elongation and *de novo* telomeres formation (Schulz and Zakian, 1994; Zhou et al., 2000). In wild type cells telomeres are rarely added to DSBs but, in the absence of the nuclear isoform of Pif1 in *pif1Δ* or *pif1-m2* cells, the telomerase-

dependent telomeres additions to DSBs increase of up to 1000-fold, causing an high frequency of gross chromosomal rearrangements (GCRs) (Schulz and Zakian, 1994). Deletion of *DNA2* restores the normal telomere length in *pif1Δ* cells and partially suppresses the elevated telomerase-dependent GCRs in *pif1* mutants (Budd et al., 2006).

In the presence of DNA damage, Pif1 is recruited to double strand breaks (DSBs) sites and it is phosphorylated at the C-terminus in a checkpoint-dependent manner, to prevent deleterious telomeres addition at DNA ends of DSBs (Makovets and Blackburn, 2009). The Mec1-, Rad53- and Dun1-dependent phosphorylation of Pif1 inhibits the activity of telomerase at intrachromosomal break sites but not at telomeres (Makovets and Blackburn, 2009).

1.3.1.3 Resolution of G-quadruplexes

Telomeres are made of tandem copies of short DNA repeats rich in guanines that can form secondary structures called *G-quadruplexes*. G-quadruplexes are non-canonical four stranded-DNA structures, formed by at least three quartets of guanine bases, held together by Hoogsteen hydrogen bonds in a planar conformation, and are very stable structures which can impede replication fork progression (Bochman et al., 2012). Sequences that are able to form these structures *in vitro* have been found in telomeres, ribosomal DNA, transcriptional start sites and at the level of spontaneous genomic DSBs sites (Capra et al., 2010; Hershman et al., 2008).

Pif1 is able to bind and unwind G-quadruplex structures *in vitro* thanks to its helicase activity, with an affinity 500-fold higher than for Y-shaped DNA structures (Paeschke et al., 2013; Ribeyre et al., 2009; Sanders, 2010). Genomic sites, that according to a bioinformatics analysis, should assemble into G-quadruplexes *in vivo,* are bound by Pif1 and become replication pausing elements and fragile sites in the absence of the helicase (Paeschke et al., 2011). Accordingly, Pif1 prevents chromosome rearrangements at the level of the G-rich human minisatellite CEB1 sequence, inserted in the genome of *S.cerevisiae* (Ribeyre et al., 2009). Insertion of the CEB1 sequence in the two different

orientations and analysis of the replication fork progression through neutral/neutral 2D gel electrophoresis, have revealed that genetic instability occurs specifically when the G-rich strand is the template of the leading strand replication in the absence of Pif1 (Lopes et al., 2011).

Also Rrm3, Pfh1 and hPIF1 are potent G4 unwinders *in vitro* (Paeschke et al., 2013). Monitoring gross-chromosomal rearrangements (GCRs) in regions proximal to genomic sequences that have been predicted to form G4 structures *in vivo* has revealed that Rrm3 and Pif1 work synergistically in preventing genome instability at G4 sequences (Paeschke et al., 2013). Moreover, bacterial, human and viral Pif1 helicases can suppress the high levels of GCRs of *pif1 rrm3* mutants showing that Pif1 functions are highly conserved among the organisms (Paeschke et al., 2013).

1.3.1.4 Okazaki fragment maturation

Pif1 plays a role in Okazaki fragment processing during the semi-conservative DNA replication (see Introduction, section 1.1.1). *DNA2* is an essential gene involved in the alternative pathway of Okazaki fragment processing (Budd and Campbell, 1997) and *PIF1* deletion was shown to suppress the lethality of *dna2Δ* cells (Budd et al., 2006). This genetic interaction has been interpreted suggesting that Dna2 counteracts toxic and long 5' flaps created by Pif1 on the lagging strand (Budd et al., 2006; Levikova and Cejka, 2015; Pike et al., 2009; Pike et al., 2010; Rossi et al., 2008).

It has been proposed that this mechanism has evolved to better process fold-back flaps on Okazaki fragments (Pike et al., 2010). Fold-back flaps are stable DNA secondary structures which cannot be cleaved by Fen1 and Dna2 or bound by RPA. Pif1 stimulates Pol δ dependent strand displacement and unwinds the entire Okazaki fragment that contains fold-back flaps at its 5' ends *in vitro* (Pike et al., 2010). Importantly, while Pif1 (due to its 5'-3' polarity) would unwind the 3' of an Okazaki fragment, acting as an

accessory strand displacement stimulator of Pol δ, it would give to the Pol δ/Pif1 complex a potent capability to displace its 5' end (see discussion of this thesis).

Interestingly, while deletion of *PIF1* rescues the lethality of *dna2Δ* cells, *RRM3* deletion is synthetic lethal with *dna2* mutations and the triple mutant *dna2Δ pif1Δ rrm3Δ* is inviable (Budd et al., 2006).

1.3.1.5 Unwinding of DNA-RNA hybrids and fork-like substrates

Pif1 preferentially unwinds RNA-DNA hybrids *in vitro* (Boule and Zakian, 2007).

*h*PIF1 and *Sc*Pif1 unwind, with a 5' to 3' polarity, dsDNA with extend 5' ssDNA tail which corresponds to the leading strand of replication fork like substrates *in vitro* (George et al., 2009; Lahaye et al., 1993).

1.3.1.6 Break-induced replication

In response to DNA damage generated by ionizing radiations, Pif1 is recruited to DNA repair foci together with homologous recombination proteins (Wagner et al., 2006).

Moreover it has been found that Pif1 promotes the Break-Induced Replication (BIR), a recombination-dependent pathway for DSBs repair. In the context of BIR, Pif1 is important for the recruitment of Polδ, the DNA polymerase which lengthens the invading strand of the D-loop, and promotes D-loop extension. The ATPase/helicase activity of Pif1 stimulates the Polδ-dependent DNA synthesis and the bubble migration opening the double helix (Wilson et al., 2013).

1.3.2 Rrm3

Rrm3 (*ribosomal DNA recombination mutant 3*) is an ATP-dependent DNA helicase, with a 5'-3' polarity (Ivessa et al., 2002). Rrm3 is a 723 amino acids protein and its helicase domain shows 48% of identity and 60% of similarity with the helicase domain of Pif1, while the N- and C-terminal domains are divergent (Bessler et al., 2001). The N-terminus of Rrm3 is an unstructured region which regulates the protein abundance and it is essential

for the functions of the protein *in vivo*; indeed the expression of an N-terminal truncated form of *rrm3* has the same effects of *RRM3* deletion (Bessler and Zakian, 2004; Schmidt et al., 2002).

RRM3 was identified in 1993, as a gene encoding for a sequence-specific factor that suppresses the mitotic exchanges between tandem repeats; it was in fact observed that *RRM3* deletion increases the recombination frequency between repetitive sequences of ribosomal DNA (Keil and McWilliams, 1993).

Like *PIF1,* also *RRM3* is predicted to encode a nuclear isoform and a mitochondrial isoform and mitochondrial proteome analysis reveals that Rrm3 localizes to mitochondria (Prokisch et al., 2004). *RRM3* deletion does not cause mitochondria defects, but partially rescues the mitochondrial loss in *pif1* mutants (Ivessa et al., 2000; O'Rourke et al., 2005).

Like *PIF1*, also *RRM3* is a non-essential gene and the double mutant *pif1Δ rrm3Δ* is viable (Ivessa et al., 2000).

1.3.2.1 Rrm3 is a replisome component

Rrm3 associates with replication origins in early S-phase, probably throughout the interaction with Orc5 (Matsuda et al., 2007), and moves with the replication forks (Azvolinsky et al., 2006). Moreover Rrm3 interacts *in vivo* with Pol2, the catalytic subunit of DNA polymerase ε (Azvolinsky et al., 2006), and *in vitro* with the sliding clamp PCNA thanks to an 8 amino acids motif called PIP-box (p21-like PCNA interaction motif) localized in its N-terminus (Schmidt et al., 2002).

All these data suggest that the Rrm3 helicase travels with the replication fork as a replisome component, while Pif1 is though to be recruited to specific genomic regions post-replicatively (Azvolinsky et al., 2006; Paeschke et al., 2011).

1.3.2.2 Rrm3-dependent pausing sites

In the absence of *RRM3* replication forks pause, or the pausing is exacerbated, at more than 1400 genomic sites, defined as Rrm3-dependent pausing sites, which include rDNA

(Ivessa et al., 2000), telomeric and subtelomeric DNA (Ivessa et al., 2002), centromeres (Ivessa et al., 2003), *tRNA* genes, inactive replication origins (Ivessa et al., 2003; Ivessa et al., 2000), silent mating-type loci and transcriptional silencers (Ivessa et al., 2003).

These sites have been originally identified monitoring the replication fork progression by neutral/neutral 2D gel analysis (Ivessa et al., 2002) and subsequently were mapped genome-wide monitoring the ChIP on chip binding profile of DNA polymerase ε in *rrm3Δ* mutants (Azvolinsky et al., 2009). In the absence of *RRM3*, DNA polymerase ε is enriched at the level of the Rrm3-dependent pausing sites and this reflects a slowing down of the replication forks progression at these genomic loci (Azvolinsky et al., 2009).

rrm3Δ cells accumulate chromosome breakages at the Rrm3-dependent pausing sites (Szilard et al., 2010) and show an increased recombination frequency (Keil and McWilliams, 1993). *RRM3* deletion leads to a constant activation of the DNA damage checkpoint (Ivessa et al., 2003). *rrm3* mutants are considered *chromosomal instability* (CIN) mutants which adapt to replications stress; indeed, thanks to the upregulated level of dNTPs, *rrm3Δ* cells show enhanced DNA synthesis in hydroxyurea compared to wild type cells (Hashash et al., 2011; Poli et al., 2012).

Highly transcribed RNA Pol II genes are another group of natural pausing sites, but the fork pausing is not exacerbated in the absence of *RRM3* or *PIF1* (Azvolinsky et al., 2009), although the effect of the combined ablation of these two genes on fork pausing at RNA Polymerase II transcribed genes has not been tested. Recently, it has been proposed that another auxiliary helicase, the RNA/DNA helicase Sen1, assists fork progression at these sites (Alzu et al., 2012). *sen1* mutants accumulate aberrant DNA structures and RNA-DNA hybrids at the head-on collision sites between replication and transcription (Alzu et al., 2012).

On the contrary, in *S. pombe,* Pfh1 is required for the efficient fork progression, not only at the level of rDNA, tRNA, telomeres, centromeres and the silent mating type loci, but also at highly transcribed RNA Pol II genes (Sabouri et al., 2012).

It has been recently reported that the Structural Maintenance of Chromosomes (SMC) complex, Smc5/6, promotes, together with Rrm3, the replication fork progression through the RFB of the rDNA and through other natural pausing sites (Menolfi et al., 2015).

1.3.2.3 Ribosomal DNA replication

Ribosomal DNA locus is a highly fragile and recombinogenic genomic region, made of ~150 directed-tandem repeats of 9.1 Kb on the chromosome XII; each repeat contains the rRNA 5S gene, transcribed by RNA polymerase III, and the rRNA 35S coding sequence, transcribed by RNA polymerase I (Venema and Tollervey, 1999). The non-transcribed region of each repeat contains an ARS, but only 15 % of these origins of replication is fired in S-phase (Pasero et al., 2002). Replication proceeds bidirectionally until the forks reach the *replication fork barrier* (RFB), a polar replication block that arrests the progression of the leftward-moving fork, avoiding the head-on collision of replicative apparatus with the 35S transcriptional unit (Brewer and Fangman, 1988; Brewer et al., 1992; Linskens and Huberman, 1988). The rightward-moving fork proceeds for 5-10 repeats until it converges on a fork stalled at the RFB, completing the replication; RFB are therefore considered replication termination sites (*TER sites*).

Both Pif1 and Rrm3 are associated with the ribosomal DNA *in vivo* but they have opposite effects on DNA replication fork progression at the RFB. Rrm3 promotes the fork progression across the RFB, while Pif1 contributes to maintain fork pausing at the level of the RFB (Ivessa et al., 2000). 2D gel analysis reveals that *rrm3Δ* cells accumulate pausing signals in multiple sites throughout the ribosomal DNA, especially at the level of the RFB, meaning that Rrm3 is important to promote the movement of the rightward-moving forks, to favor the fork progression across the RFB and to resolve converged forks; the absence of Pif1 results on the contrary in a less efficient arrest of replication forks at the replication fork barrier (Ivessa et al., 2000). Replication defects in *rrm3Δ* cells are associated with breakages of stalled forks and increased recombination, which lead to the formation of extrachromosomal rDNA circles (ERCs). This means that Rrm3 suppresses, while Pif1

promotes, the Rad52-dependent formation of extrachmosomal rDNA circles (Ivessa et al., 2000; Sinclair and Guarente, 1997).

1.3.2.4 Disruption of protein-DNA complexes

All the Rrm3-dependent pausing sites are assembled in stable non-nucleosomal DNA-protein complexes and their artificial disassembly eliminates the Rrm3 dependency of DNA replication. *tRNA* genes, which are not able to assemble the transcription initiator complexes, do not cause the replication fork stalling in *rrm3Δ* (Ivessa et al., 2003); in the same way the deletion of *FOB1*, the gene encoding the protein that generates the RFB of the rDNA, abolishes the replication defect of *rrm3* mutants at the level of the RFB and partially suppresses the formation of extrachromosomal rDNA circles (Torres et al., 2004). Although *FOB1* deletion eliminates the protein barrier, in the case of the lack of transcription initiator complex assembly also tRNA transcription is inhibited. It will be interesting to dissect the contributions of tRNA transcription and protein occupancy to DNA replication fork progression across tRNAs.

The catalytically inactive *rrm3-K260A* mutant, in which the lysine in the ATP binding motif of the Walker A box is mutated to alanine, has the same replication defects of *rrm3Δ* cells (Ivessa et al., 2000; Torres et al., 2004), suggesting that Rrm3 uses its helicase activity to remove bulky, non-nucleosomal protein-DNA complexes which would impede DNA replication fork progression.

1.3.2.5 Telomere replication

Chromatin Immunoprecipitation experiments demonstrated that Rrm3 associates with telomeres *in vivo* (Azvolinsky et al., 2009).

Replication fork pausing at $C_{1-3}A/TG_{1-3}$ terminal telomeric sequences and at internal telomeric DNA tracts is exacerbated in *rrm3Δ* and *rrm3-K260A* cells and this effect is not suppressed by the ablation of Sir or Rif proteins associated with telomeric repeats. Rrm3

catalytically acts to promote fork progression also at specific sub-telomeric elements, such as inactive replication origins (Azvolinsky et al., 2009; Ivessa et al., 2002).

In the absence of Rrm3 telomeres are modestly longer, the telomeric silencing is reduced and the *de novo* telomere addition rate is the same of wild type cells, but *RRM3* deletion partially rescues the telomere lengthening and the telomere addition phenotype of *pif1* mutants (Ivessa et al., 2002).

1.3.2.6 Replication termination

Rrm3, like *S.pombe* Pfh1, has a role in replication termination (Fachinetti et al., 2010; Steinacher et al., 2012). Replication termination takes place at site-specific replication termini called *TER* sites, containing replication pausing elements, and the forks fusion is mediated by the topoisomerase Top2 and by Rrm3 (Fachinetti et al., 2010).

At the level of the RFB of the ribosomal DNA, Rrm3 controls the replication termination together with the checkpoint proteins Tof1 and Csm3; Fob1 and the Tof1-Csm3 complex protect the stalled forks at RFBs, counteracting the helicase activity of Rrm3 which promotes the progression of the replication forks likely displacing Fob1 from the RFB (Mohanty et al., 2006).

Tof1 and Csm3, like the *S.pombe* Swi1 and Swi3 orthologous (Dalgaard and Klar, 2000; Sabouri et al., 2012), are required for a stable fork arrest at TER sites, while Mrc1 and the checkpoint do not seem to control fork pausing and stalled fork stability at the RFBs (Calzada et al., 2005; Tourriere et al., 2005).

2. Materials and Methods

2.1 *E.coli* strains

Subcloning efficiency *DH5α*^{TM} *competent cells* (Invitrgen, Life Technologies)
Genotipo: F- φ80*lac*Z ΔM15 (*lac*ZYA-*arg*F)U169 *rec*A1 *end*A1 *hsd*R17(rκ-,mκ+) *pho*A *sup*E44 *thi*-1 *gyr* A96 *rel*A1 λ-

2.2 Yeast strains

All the strains used in this study are listed in Table 2.1 and are W303 derivatives with the wild type *RAD5* locus.

Name	Genotype	Origin
CY11360	*MAT a, ade2-1, ura3-1, his3-11,15, leu2-3,112, trp1-1, can1-100, GAL, PSI+, RRM3-13MYC-KANMX6*	This study
CY12404	*MAT a ade2-1, ura3-1, his3-11,15 leu2-3, 112 trp1-1,CAN1, RAD5 rad53-K227A-KANMX4*	This study
CY12406	*MAT a ade2-1, ura3-1, his3-11,15 leu2-3, 112 trp1-1,CAN1, RAD5+ rrm3::HIS3 rad53-K227A-KANMX4*	This study
CY12425	*MAT a, ade2-1, ura3-1, his3-11,15, leu2-3,112, trp1-1, CAN1, GAL, PSI+, rad53-K227A-KANMX6, RRM3-13MYC-HIS3*	This study
CY12422	*MAT a, ade2-1, ura3-1, his3-11,15, leu2-3,112, trp1-1, CAN1, GAL, PSI+, sml1::TRP1, rad53::KANMX6, RRM3-13MYC-HIS3*	This study
CY12443	*MAT a, ade2-1, ura3-1, his3-11,15, leu2-3,112, trp1-1, CAN1, GAL, PSI+, sml1::TRP1, rad53::KANMX6*	This study
CY12445	*MAT a, ade2-1, ura3-1, his3-11,15, leu2-3,112, trp1-1, CAN1, GAL, PSI+, sml1::TRP1*	This study
CY12448	*MAT a, ade2-1, ura3-1, his3-11,15, leu2-3,112, trp1-1, CAN1, GAL, PSI+, sml1::TRP1, rrm3::HIS3*	This study
CY12460	*MAT a, ade2-1, ura3-1, his3-11,15, leu2-3,112, trp1-1, CAN1, GAL, PSI+, sml1::TRP1, rad53::KANMX6, rrm3::HIS3*	This study
CY12470	*MAT a, ade2-1, ura3-1, his3-11,15, leu2-3,112, trp1-1, CAN1, GAL, PSI+, sml1::TRP1, RRM3-13MYC-HIS3*	This study
CY12484	*MAT a, ade2-1, ura3-1, his3-11,15, leu2-3,112, trp1-1, CAN1, GAL, PSI+, rrm3::HIS3*	This study
CY12486	*MAT a, ade2-1, ura3-1, his3-11,15, leu2-3,112, trp1-1, can1-100, GAL, PSI+*	Lab collection
CY12488	*MAT a ade2-1 ura3-1 his3-11,15 leu2-3,112, trp1-1 CAN1, GAL, PSI+, sml1::TRP1, ura3::7x-TKs-URA3*	This study
CY12493	*MAT a ade2-1 ura3-1 his3-11,15 leu2-3,112, trp1-1 CAN1, GAL, PSI+, sml1::TRP1, rad53::KANMX4, ura3::7x-TKs-URA3*	This study
CY12512	*MAT a ade2-1, ura3-1, his3-11,15 leu2-3,112, trp1-1, CAN1, GAL, PSI+, ura3::7x-TKs-URA3*	This study
CY12527	*MAT a ade2-1, ura3-1, his3-11,15 leu2-3,112, trp1-1, CAN1, RAD5+, rad53-K227A-KANMX4, ura3::7x-TKs-URA3*	This study

CY12674	*MAT a, ade2-1, ura3-1, his3-11,15, leu2-3,112, trp1-1, CAN1, GAL, PSI+, sml1::TRP1, rad53::KANMX6*	This study
CY12681	*MAT alpha, ade2-1, ura3-1, his3-11,15, leu2-3,112, trp1-1, CAN1, GAL, PSI+, sml1::TRP1, rad53::KANMX6, sac3::NATMX*	This study
CY12682	*MAT a, ade2-1, ura3-1, his3-11,15, leu2-3,112, trp1-1, CAN1, GAL, PSI+, sml1::TRP1, sac3::NATMX*	This study
CY12689	*MAT a, ade2-1, ura3-1, his3-11,15, leu2-3,112, trp1-1, CAN1, GAL, PSI+, sml1::TRP1, rad53::KANMX6, sac3::NATMX, rrm3::HIS3*	This study
CY12690	*MAT a, ade2-1, ura3-1, his3-11,15 leu2-3,112, trp1-1, CAN1, GAL, PSI+, sml1::TRP1 sac3::NATMX, rrm3::HIS3*	This study
CY12698	*MAT a, ade2-1, ura3-1, his3-11,15, leu2-3,112, trp1-1, CAN1, GAL, PSI+, POL1-9MYC-TRP1, rad53-K227A-KANMX6*	This study
CY12801	*MAT a, ade2-1, ura3-1, his3-11,15, leu2-3,112, trp1-1, can1-100, GAL, PSI+, rrm3-S85A-S86A-S87A-S90A-S92A-S95A*	This study
CY12803	*MAT a, ade2-1, ura3-1, his3-11,15, leu2-3,112, trp1-1, can1-100, GAL, PSI+, rrm3-S85A-S86A-S87A-S90A-S92A-S95A-13MYC-HIS3*	This study
CY12824	*MAT a, ade2-1, ura3-1, his3-11,15, leu2-3,112, trp1-1, can1-100, GAL, PSI+, rrm3-S85D-S86D-S87D-S90D-S92D-S95D*	This study
CY12831	*MAT a, ade2-1, ura3-1, his3-11,15, leu2-3,112, trp1-1, can1-100, GAL, PSI+, rrm3-S85D-S86D-S87D-S90D-S92D-S95D-13MYC-HIS3*	This study
CY12850	*MAT alpha, ade2-1, ura3-1, his3-11,15, leu2-3,112, trp1-1, can1-100, GAL, PSI+, sml1::TRP1 rad53::KANMX6, rrm3-S85D-S86D-S87D-S90D-S92D-S95D-13MYC-HIS3*	This study
CY12865	*MAT a, ade2-1, ura3-1, his3-11,15, leu2-3,112, trp1-1, CAN1, sml1::TRP1, rad53::KANMX6, RRM3-13MYC-HIS3*	This study
CY12867	*Mat a, ade2-1, ura3-1, his3-11,15, leu2-3,112, trp1-1, CAN1, GAL, PSI+, sml1::TRP1, RRM3-13MYC-HIS3*	This study
CY12927	*MAT a, ade2-1, ura3-1, his3-11,15, leu2-3,112, trp1-1, can1-100, GAL, PSI+, POL1-9MYC-TRP1*	This study
CY12934	*MAT a, ade2-1, ura3-1, his3-11,15, leu2-3,112, trp1-1, CAN1, GAL, PSI+, sml1::TRP1, pif1-m2-6HIS-3FLAG-KANMX4*	This study
CY12953	*MAT a, ade2-1, ura3-1, his3-11,15, leu2-3,112, trp1-1, can1-100, GAL, PSI+, sml1::TRP1, rrm3-S85A-S86A-S87A-S90A-S92A-S95A-13MYC-HIS3*	This study
CY12960	*MAT a, ade2-1, ura3-1, his3-11,15, leu2-3,112, trp1-1, CAN1, GAL, PSI+, sml1::TRP1, rad53::KANMX6, rrm3-S85A-S86A-S87A-S90A-S92A-S95A-13MYC-HIS3*	This study
CY13073	*MAT a, ade2-1, ura3-1, his3-11,15, leu2-3,112, trp1-1, can1-100, GAL, PSI+, sml1::TRP1, rad53::KANMX6, PIF1-6HIS-3FLAG-NATMX*	This study
CY13074	*MAT a, ade2-1, ura3-1, his3-11,15, leu2-3,112, trp1-1, can1-100, GAL, PSI+, sml1::TRP1, PIF1-6HIS-3FLAG-NATMX*	This study
CY13172	*MAT a, ade2-1, ura3-1, his3-11,15, leu2-3,112, trp1-1, CAN1, GAL, PSI+, sml1::TRP1, rad53::KANMX6, rrm3-K260A-13MYC-HIS3*	This study
CY13173	*MAT a, ade2-1, ura3-1, his3-11,15, leu2-3,112, trp1-1, CAN1, GAL, PSI+, sml1::TRP1, rrm3-K260A-13MYC-HIS3*	This study

CY13174	*MAT a, ade2-1, ura3-1, his3-11,15, leu2-3,112, trp1-1, CAN1, GAL, PSI+, sml1::TRP1, rad53::KANMX6, rrm3-K260A-13MYC-HIS3*	This study
CY13282	*MAT a, ade2-1, ura3-1, his3-11,15, leu2-3,112, trp1-1, CAN1, GAL, PSI+, POL1-6HIS-3FLAG-NATMX, sml1::TRP1, rad53::KANMX6*	This study
CY13284	*MAT a, ade2-1, ura3-1, his3-11,15, leu2-3,112, trp1-1, can1-100, GAL, PSI+, POL1-6HIS-3FLAG-NATMX, sml1::TRP1*	This study
CY13331	*MAT a, ade2-1, ura3-1, his3-11,15, leu2-3,112, trp1-1, CAN1, GAL, PSI+, sml1::TRP1, pif1-m2*	This study
CY13334	*MAT a, ade2-1, ura3-1, his3-11,15, leu2-3,112, trp1-1, can1-100, GAL, PSI+, sml1::TRP1, rrm3::HIS3, pif1-m2*	This study
CY13339	*MAT a, ade2-1, ura3-1, his3-11,15, leu2-3,112, trp1-1, CAN1, GAL, PSI+, sml1::TRP1, rad53::KANMX6, pif1-m2*	This study
CY13342	*MAT a, ade2-1, ura3-1, his3-11,15, leu2-3,112, trp1-1, can1-100, GAL, PSI+, sml1::TRP1, rad53::KANMX6, rrm3::HIS3, pif1-m2*	This study
CY13650	*MAT a, ade2-1, ura3-1, his3-11,15, leu2-3,112, trp1-1, CAN1, GAL, PSI+, POL1-6HIS-3FLAG-NATMX, sml1::TRP1, rad53::KANMX6, rrm3::HIS3, pif1-m2*	This study
CY13664	*MAT a, ade2-1, ura3-1, his3-11,15, leu2-3,112, trp1-1, can1-100, GAL, PSI+, sml1::TRP1, pif1-S131A-S140A-S143A-S147A-S148A-S169A-S170A-S178A-S180A-S184A-S210A-T212A-6HIS-3FLAG-NATMX*	This study
CY13668	*MAT a, ade2-1, ura3-1, his3-11,15, leu2-3,112, trp1-1, can1-100, GAL, PSI+, sml1::TRP1, pif1-S131D-S140D-S143D-S147D-S148D-S169D-S170D-S178D-S180D-S184D-S210D-T212D-6HIS-3FLAG-NATMX*	This study
CY13735	*MAT a ade2-1, ura3-1, his3-11,15 leu2-3, 112 trp1-1,CAN1, RAD5+, pif1-m2, rad53-K227A-KANMX4*	This study
CY13738	*MAT a ade2-1, ura3-1, his3-11,15 leu2-3, 112 trp1-1,CAN1, RAD5+, pif1-m2, rrm3::HIS3, rad53-K227A-KANMX4*	This study
CY14011	*MAT a, ade2-1, ura3-1, trp1-1, leu2-3,112, his3-11,15, GAL, PSI+, leu2::2X-LEU2-GAL1-rad53-D339A-NATMX, sml1::TRP1, pif1-S131A-S140A-S143A-S147A-S148A-S169A-S170A-S178A-S180A-S184A-S210A-T212A-6HIS-3FLAG-NATMX, RRM3-13MYC-HIS3*	This study
CY14012	*MAT a, ade2-1, ura3-1, trp1-1, leu2-3,112, his3-11,15, GAL, PSI+, leu2::2X-LEU2-GAL1-rad53-D339A-NATMX, sml1::TRP1, pif1-S131D-S140D-S143D-S147D-S148D-S169D-S170D-S178D-S180D-S184D-S210D-T212D-6HIS-3FLAG-NATMX, RRM3-13MYC-HIS3*	This study
CY14013	*MAT a, ade2-1, ura3-1, trp1-1, leu2-3,112, his3-11,15, GAL, PSI+, leu2::2X-LEU2-GAL1-rad53-D339A-NATMX, sml1::TRP1, Pif1-6HIS-3FLAG-NATMX, rrm3-S85A-S86A-S87A-S90A-S92A-S95A-13MYC-HIS3*	This study
CY14014	*MAT a, ade2-1, ura3-1, trp1-1, leu2-3,112, his3-11,15, GAL, PSI+, leu2::2X-LEU2-GAL1-rad53-D339A-NATMX, sml1::TRP1, Pif1-6HIS-3FLAG-NATMX, rrm3-S85D-S86D-S87D-S90D-S92D-S95D-13MYC-HIS3*	This study

CY14015	*MAT a, ade2-1, ura3-1, trp1-1, leu2-3,112, his3-11,15, GAL, PSI+, leu2::2X-LEU2-GAL1-rad53-D339A-NATMX, sml1::TRP1, pif1-S131D-S140D-S143D-S147D-S148D-S169D-S170D-S178D-S180D-S184D-S210D-T212D-6HIS-3FLAG-NATMX, rrm3-S85D-S86D-S87D-S90D-S92D-S95D-13MYC-HIS3*	This study
CY14076	*MAT a, ade2-1, ura3-1, his3-11,15, leu2-3,112, trp1-1, CAN1, GAL, PSI+, sml1::TRP1, rad53::KANMX6, ura3::URA3-pGAL-RNR1*	This study
CY14077	*MAT a, ade2-1, ura3-1, his3-11,15, leu2-3,112, trp1-1, can1-100, GAL, PSI+, sml1::TRP1, rad53::KANMX6, rrm3::HIS3, pif1-m2, ura3::URA3-pGAL-RNR1*	This study
TEMP17-I1	*MAT a, ade2-1, ura3-1, his3-11,15, leu2-3,112, trp1-1, can1-100, GAL, PSI+, leu2::GPD1-OsTIR1::LEU*	This study
TEMP17-F9	*MAT a, ade2-1, ura3-1, his3-11,15, leu2-3,112, trp1-1, can1-100, GAL, PSI+, leu2::GPD1-OsTIR::LEU, dna2-AID*-9myc::Hyg*	Branzei group
TEMP18-B4	*MAT a, ade2-1, ura3-1, his3-11,15, leu2-3,112, trp1-1, can1-100, GAL, PSI+, leu2::GPD1-OsTIR::LEU, NAT-pADH1-tc3-dna2-AID*-9myc::hphNT*	This study
TEMP17-G3	*MAT a, ade2-1, ura3-1, his3-11,15, leu2-3,112, trp1-1, can1-100, GAL, PSI+, leu2::GPD1-OsTIR::LEU, dna2-AID*-9myc::Hyg, pif1-m2*	This study
TEMP17-I5	*MAT a, ade2-1, ura3-1, his3-11,15, leu2-3,112, trp1-1, can1-100, GAL, PSI+, leu2::GPD1-OsTIR::LEU, dna2-AID*-9myc::hphNT, rad9::KANMX6*	This study
TEMP17-I6	*MAT a, ade2-1, ura3-1, his3-11,15, leu2-3,112, trp1-1, can1-100, GAL, PSI+, leu2::GPD1-OsTIR::LEU, dna2-AID*-9myc::hphNT, rad9::KANMX6*	This study
TEMP17-H4	*MAT a, ade2-1, ura3-1, his3-11,15, leu2-3,112, trp1-1, can1-100, GAL, PSI+, leu2::GPD1-OsTIR::LEU, Dna2-AID*-9myc::hphNT, rrm3::HIS3*	This study
TEMP18-C7	*MAT a, ade2-1, ura3-1, his3-11,15, leu2-3,112, trp1-1, can1-100, GAL, PSI+, leu2::GPD1-OsTIR::LEU, Dna2-AID*-9myc::Hyg, NAT-pADH1-tc3-3HA-rrm3*	This study
TEMP18-D6	*MAT a, ade2-1, ura3-1, his3-11,15, leu2-3,112, trp1-1, can1-100, GAL, PSI+, leu2::GPD1-OsTIR::LEU, Dna2-AID*-9myc::Hyg, NAT-pADH1-tc3-3HA-rrm3, pif1-m2*	This study
TEMP18-B1	*MAT a, ade2-1, ura3-1, his3-11,15, leu2-3,112, trp1-1, can1-100, GAL, PSI+, leu2::GPD1-OsTIR::LEU, dna2-AID*-9myc::Hyg, rad53-K227A-KANMX4*	This study
TEMP18-I2	*MAT a, ade2-1, ura3-1, his3-11,15, leu2-3,112, trp1-1, can1-100, GAL, PSI+, leu2::GPD1-OsTIR::LEU, dna2-AID*-9myc::Hyg, fob1::HIS3*	This study

Table 2.2. Yeast genotypes

2.3 Growth media

2.3.1 Media for *E. coli*

LB (DIFCO): 1% Bactotryptone, 0.5% Yeast extract, 1% NaCl, pH 7.25

LB Agar: LB + 2% agar (DIFCO)

LB Amp: LB + ampicillin (50 μg/ml)

2.3.2 Media for *Saccharomyces cerevisiae*

YP: 1% Yeast extract, 2% bactopeptone, pH 5.4

YP agar: YP + 2% agar (DIFCO)

YPD: YP + 2% glucose

YPD agar: YPD + 2% agar

SC: 0.67% yeast nitrogen base (YNB, DIFCO w/o AA), 2% glucose/galactose/raffinose, amino acids as required.

SC agar: SC + 2% agar

Sporulation media (VB): NaAc•$3H_20$ 1.36%, KCl 0.19%, NaCl 0.12%, $MgSO_4$ 0.35%, 1.5% agar.

5-Fluorootic Acid (5-FOA) media: 0.67% yeast nitrogen base (YNB, DIFCO w/o AA), 2% glucose, 1 mg/ml 5-FOA, 0.012 mg/ml uracile, amino acids as required, + 2% agar.

2.4 Yeast strains construction

2.4.1 *E. coli* transformation

50 μl of chemically competent DH5α^{TM} cells were thawed on ice for approximately 10' prior to the addition of plasmid DNA (1-10 ng). Cells were then incubated with DNA on ice for 30', subjected to a heat shock for 40'' at 42° C and returned to ice for 2'. Pre-warmed LB medium (950 μl) was added to the vial and cells were incubated at 37° C for 1

h in a shaking incubator. Finally the transformation reaction was plated onto LB+Amp plates.

2.4.2 Plasmid DNA isolation from *E. coli*

Clones picked from individual colonies were used to inoculate 5 ml LB supplemented with 50 μg/ml ampicillin and were grown overnight at 37°C. Plasmids extraction was performed with Wizard Plus SV Minipreps DNA Purification System (Promega) following the manufacturer's instructions.

2.4.3 Amplification of cassettes by PCR

Cassettes for genes deletion, generation of conditional alleles or epitope-tagged proteins have been generated by PCR, using specific oligonucleotides and the appropriate template as described in (De Antoni and Gallwitz, 2000; Kotter et al., 2009; Longtine et al., 1998; Morawska and Ulrich, 2013).

PCR reaction mix: 35 μl ddH_20
1 μl dNTPS
10 μl HF Buffer 5X (NEB)
1 μl Phusion High Fidelity DNA polymerase NEB, 2U/ml
1 μl Oligo Forward (10 mM)
1 μl Oligo Reverse (10 mM)
1 μl Template DNA (10 ng/ml)

PCR conditions: 2' 98°C
30'' 98°C, 30'' 55°C, 1'/kb 72°C (x 5 cycles)
30'' 98°C, 30'' 66°C, 1'/kb 72°C (x 35 cycles)
5' 72°C

2.4.4 Yeast transformation

Gene deletions, conditional alleles, mutant alleles expressing fusion proteins with different tags (De Antoni and Gallwitz, 2000; Kotter et al., 2009; Longtine et al., 1998; Morawska and Ulrich, 2013) were generated by one step replacement systems, using the following

high efficiency transformation protocol. The same procedure was used to obtain strains carrying the centromeric plasmid YCplacIII (Ivessa et al., 2002)

100 ml of log-phase cells ($5x10^6$ cells/ml) grown in YPD at 28°C were collected by centrifugation, washed with water, transferred to an Eppendorf tube and resuspended in 500 µl of water. A 100 µl aliquot was used for each transformation. Cells were centrifugated, supernatant was discarded and 360 µl of transformation mix (TMIX: 74 µl ddH_2O sterile, 240 µl PEG4000 (50% w/v in water) filtered, 36 µl LiAc 1M, 10 µl denatured ssDNA 10 mg/ml (Sigma) were added. 1 µg of PCR-amplified linear DNA cassette or of plasmid DNA were added, transformation mix was mixed and then cells were heat-shocked at 42°C for 40'.

Cells were then centrifuged for 1' at 3000 rpm. Finally, the pellet was re-suspended in distilled water and spread onto selective medium. In case of selection for resistance to antibiotic G418, nourseothricin (NAT) or hygromycin (HPH) after the heat shock, cells were incubated in 1 ml of YPD for 2 hours at 28°C to allow expression of the resistance gene before plating on selective plates. The resulting transformant colonies were streaked out to obtain single colonies that were checked for the correct integration by colony PCR or Western blotting (if required).

2.4.5 Colony PCR

The proper integration of PCR cassettes and the presence of point mutations, were monitored by colony PCR.

Approximately 1 ml of cells were collected with a yellow tip, resuspended in 3 ml of NaOH 20 mM in a PCR tube, boiled at 95°C for 10 minutes and kept at 4°C.

The following PCR reaction mix was added to each boiled solution:

14.325 µl ddH_20

0.5 µl dNTPS (20 mM)

5 µl HF Buffer 5X (NEB)

0.175 µl Phusion High Fidelity DNA polymerase NEB, 2U/ml

1 μl Oligo Forward (10 μM)

1 μl Oligo Reverse (10 μM)

PCR conditions: 2’ 98°C

30’’ 98°C, 30’’ 50-68°C (depending on the primers), 1’/kb 72°C (x 35 cycles)

5’ 72°C

2.4.6 *In vivo* site-directed mutagenesis using the Delitto Perfetto approach

rrm3 and *pif1* mutant alleles were generated using the “break-mediated Delitto Perfetto” strategy (Storici and Resnick, 2006), that allows the *in vivo* site-directed mutagenesis via homologous recombination, using synthetic oligonucleotides, without retention of heterologous sequences.

Mutagenesis is accomplished in two steps.

Step 1: a CORE (COunterselectable REporter) cassette, which contains the counterselectable *KlURA3* gene and the reporter gene *hyg* that provides resistance to hygromycin, was amplified from the pGSHU plasmid, adding two flanking targeting sequences. The CORE cassette was then inserted by standard DNA targeting procedures at the locus of interest, using the high efficiency transformation protocol previously described (see paragraph 2.4.4).

Step 2: cells containing the CORE cassette were transformed with Integrative Recombinant Oligonucleotides (IROs), carrying the desired mutations, which targeted the regions surrounding the inserted CORE cassette, inducing the loss of the CORE cassette and the introduction of the mutations. To improve the efficiency of this method we used a pair of complementary IROs of ~100 nt for each mutagenesis (listened below). IROs used were synthesized custom primers, HPLC purified (Eurofins MWG Operon).

The CORE cassette included also a galactose inducible I-SceI endonuclease and an I-SceI cut site; the generation of a DSB, prior to IROs transformation, was used to increase the oligonucleotide targeting efficiency.

> IROs for site-directed mutagenesis of K260 of Rrm3 to alanine:

F:TTAATCGTCAAAAAAAGAACAAATGTCTTTTACACCGGTAGTGCGGGTACAG
GT**GCG**TCGGTCATTTTGCAAACGATCATAAGACAATTGAGCTCTTTGTATGGG
AAAGAA

RC:TTCTTTCCCATACAAAGAGCTCAATTGTCTTATGATCGTTTGCAAAATGACC
GA**CGC**ACCTGTACCCGCACTACCGGTGTAAAAGACATTTGTTCTTTTTTTGACG
ATTAA

> IROs for site-directed mutagenesis of S85, S86, S87, S90, S92 and S95 of Rrm3 to alanine residues:

F:CTCCTAGGCCAAGATTAATACGGAATAAT**GCGGCTGCC**TTATTC**GCG**CAG**G
CT**CAAGGT**GCG**TTTGGAGATGATGATCCCGACGCAGAATTCAAAAAATT

RC:AATTTTTTGAATTCTGCGTCGGGATCATCATCTCCAAA**CGC**ACCTTG**AGC**C
TG**CGC**GAATAA**GGCAGCCGC**ATTATTCCGTATTAATCTTGGCCTAGGAG

> IROs for site-directed mutagenesis of S85, S86, S87, S90, S92 and S95 of Rrm3 to aspartic acid residues:

F:CTCCTAGGCCAAGATTAATACGGAATAAT**GACGATGAC**TTATTC**GAC**CAG**G
AC**CAAGGT**GAC**TTTGGAGATGATGATCCCGACGCAGAATTCAAAAAATT

RC:AATTTTTTGAATTCTGCGTCGGGATCATCATCTCCAAA**GTC**ACCTTG**GTC**C
TG**GTC**GAATAA**GTCATCGTC**ATTATTCCGTATTAATCTTGGCCTAGGAG

A variation of the "break-mediated Delitto Perfetto" strategy (Storici and Resnick, 2006), was used to mutagenized 11 serine residues (S131, S140, S143, S147, S148, S169, S170, S178, S180, S184, S210) and one threonine (T212) in the N-terminus of Pif1 to alanine or aspartic acid residues (Figure 3.20).

The external regions of the IROs (~30,40 nt) are required for efficient targeting and therefore only the central sequence can be used for mutagenesis. Since the standard method has a limited mutagenesis window, while the indicated Pif1 residues covered a region of ~250 nt, we took advantage of synthetic assembled N-terminal regions of *PIF1*, cloned into a plasmid, carrying the mutations to alanine residues or to aspartic acid residues of S131, S140, S143, S147, S148, S169, S170, S178, S180, S184, S210 and T212, (Life Technologies). The region of interest (of ~ 700 nt) was amplified by PCR using specific oligonucleotide. The two dsDNA cassettes obtained were then used to transform cells containing the CORE cassette in the N-terminal region of *PIF1*.

Transformation with IROs for pCORE cassette removal

Cells containing the CORE cassette were grown in YP + Raffinose 2% at 28ºC ON. Galactose (2% final concentration) was added in the media for 4 hours to express GAL1- I-SceI, which induced a DSB at the cloned target site. 50 ml of cells ($5x10^6$ cells/ml) were collected by centrifugation, washed with water and then with 5 ml of LiAc 0.1 M, TE 1X pH=7.5, transferred to an Eppendorf tube and resuspended in 250 ml of LiAc 0.1 M, TE 1X pH=7.5. A 50 μl aliquot was used for each transformation.

20 μl of the 50 μM solution of the pairs of fully complementary IROs (previously denatured at 100ºC for 2' and kept on ice) (or 7 μg of the PCR-amplified DNA fragment) and 300 ml of LiAc 0.1 M, TE 1X pH 7.5 in PEG 4000 50% were added. Cells were mixed briefly by vortexing, incubated at 30ºC for 30' shaking and then heat-shocked at 42°C for 15'. Cells were then centrifuged for 4' at 5000 rpm. Finally, the pellet was re-suspended in 100 μl of distilled water and dilutions of cells were plated on YPD plates ON. The day after cells were replica plated on 5-Fluorootic Acid (5-FOA) media in order to select the oligonucleotide transformants; in the presence of the counterselectable marker *KlURA3* of the CORE cassette cells were not able to growth on 5-FOA plates. Transformant colonies were selected for loss of *KlURA3*, checked for the loss of hyg markers and checked for the correct integration of IROs by PCR. The presence of the desired mutations was verified by sequencing.

2.4.7 Crossings and tetrads dissection

S. cerevisiae can grow in a diploid state or in an aploid state with two different mating type, *MATα* and *MATa.* Since haploid cells of opposite mating type conjugate generating diploid cells that can undergo meiosis in specific growth conditions, meiotic segregation is often used to produce mutants carrying multiple mutations.

Haploid strains of opposite mating type were crossed, mixing them on YPD plates and incubated at 28 °C ON to allow mating. The obtained diploid cells were isolated on

selective media and then starved for nutrients using VB plates, to induce the sporulation; each diploid cell formed an ascus with four haploid spores. After 3 days a sufficient number of tetrads were dissected with a micromanipulator in order to obtain the desired genotype combination. Genotype and correct allele segregation were checked by markers resistance and, if necessary, by colony PCR.

2.5 Cells growth, cell cycle arrests, drugs treatments and conditional depletions

Unless otherwise indicated, yeast cells were grown at 28ºC in YPD medium (2% glucose).

2.5.1 Synchronization in G1 phase

The mating pheromone α-factor, secreted by MATα cells, binds to the α-factor pheromone receptor on MATa cells, inducing the cell cycle arrest in G1 and morphological changes. MATa haploid cells grow projections called "shmoos" in preparation for fusion with MATα cells.

Exponentially growing MATa cells were synchronized using 4 μg/ml of the synthetic α-Factor peptide (Primm) at 28°C for 2/2.5 hours, or using 3 μg/ml of alpha factor with a second addition of 1.5 μg/ml after 1 hour from the first treatment. When >95% of cells were unbudded and had formed shmoos, cells were centrifuged and release in fresh medium.

2.5.2 Synchronization in G2/M phase

Nocodazole is a microtubule poisoning agent that causes their depolymerization, arresting cycling cells in metaphase.

Cells were arrested in G1 using α-factor, release into S phase, and block in G2/M by the addition in the media of 20 μg/ml of Nocodazole (Sigma-Aldrich) dissolved in DMSO (1% total). The arrest was maintained for a long time, in PFGE experiments, by re-adding 10

μg/ml of Nocodazole after 3h from the release into S phase.

2.5.3 Drug treatments and HU sensitivity spot assay

Cells, synchronized in G1 alpha factor, were harvested and resuspended in fresh medium containing 25 mM, 150 mM or 200 mM of the DNA replication inhibitor hydroxyurea (HU), or in the presence of the DNA alkylating agent methylmethane sulfonate (MMS) (0.033%).

Drug sensitivity assays were performed using ten-fold serial dilutions of stationary phase-grown cells spotted onto YPD plates, SD-leucine plates, or YP + Raffinose + Galactose plates, with the indicated HU concentrations. Pictures of the plates have been taken after 3 days of growth at 28°C.

2.5.4 Conditional depletions of Dna2 and Rrm3

The conditional degradation of Dna2, fused with the auxin-dependent degron sequence AID^{71-114}-9Myc (Morawska and Ulrich, 2013; Nishimura et al., 2009) (Figure 3.30), was induced treating cells with 0.5 mM of Auxin (IAA, indole-3-acetic acid sodium salt, SIGMA I5148).

To induce the conditional depletion of Dna2 and Rrm3, using the conditional *Tc-DNA2* and *Tc-RRM3* alleles carrying a tetracycline-dependent translational repressor (Kotter et al., 2009) (Figure 3.30), Tetracycline (SIGMA. 87128) was added in the media at a final concentration of 0.6 mM. When long kinetics were performed, half of the initial amount of the antibiotic was added after 3 hours to maintain an efficient inhibition of protein translation.

30 minutes of auxin and tetracycline treatments induced the complete degradation of *Tc-DNA2-AID,* while the complete degradation of *Tc-RRM3* was observed after 2 hours of treatment with tetracycline (unpublished observations).

To monitor the effect of the absence of Dna2 on the S-phase progression, *DNA2-AID* cells

or *Tc-DNA2-AID* cells were synchronized in G1 for ~2 hours and, 1 hour after the addiction of α-factor, respectively, 0.5 mM auxin and 0.5 mM auxin plus 0.6 mM tetracycline were added in the media to deplete *DNA2* in G1 before initiation of DNA replication. *DNA2* ablated cells were then released into S-phase in fresh medium with 0.5 mM auxin or 0.5 mM auxin plus 0.6 mM tetracycline. In the presence of the *Tc-DNA2-AID* allele, additional 0,3 mM tetracycline was added after 3 hours from the release into S-phase to reinforce the block of Dna2 translation.

The block of *Tc-RRM3* translation, in the experiment shown in Figures 3.36 and 3.37, was induced adding in the media, together with alpha factor, 0.6 mM tetracycline. *RRM3* ablated cells were released into S-phase in fresh medium with 0.6 mM tetracycline.

Cell viability assays were performed using ten-fold serial dilutions of stationary phase-grown cells spotted onto YPD plates containing 0.5 mM IAA and/or 0.6 mM tetracycline. Unless otherwise indicated, cells were grown at 28ºC for 3 days and then scanned.

2.6 Fluorescence Activated Cell Sorting (FACS) analysis of DNA content

Approximately 10^7 cells were fixed with 100% ethanol. Cells were centrifuge for 1' at maximum speed, resuspended in 500 µl Tris-HCl 50 mM pH 7.5 containing RNaseA (1mg/ml)(Sigma) and incubated ON at 37˚C. The day after cells were treated with 500 µl Tris-HCl 50 mM pH 7.5 containing Proteinase K (1mg/ml)(Roche) for 1h at 50˚C. Cells were then stained with Propidium Iodide (Sigma) 50 µg/ml in FACS Buffer solution (200 mM Tris-HCl pH 7.5, 200 mM NaCl, 80 mM $MgCl_2$). A 1:10 dilution in Tris-HCl 50mM pH 7.5 was sonicated for 6'' and analyzed in Becton Dickinson FACScan for FL2H fluorescence. For each sample, 10,000 events were counted and acquired data were analyzed with FlowJO Software.

2.7 TCA-based protein extraction

The yeast protein extraction has been performed with Trichloroacetic acid (TCA) method as described by (Reid and Schatz, 1982). (Reid and Schatz, 1982)(Reid and Schatz, 1982)(Reid and Schatz, 1982)(Reid and Schatz, 1982)(Reid and Schatz, 1982)(Reid and Schatz, 1982)(Reid and Schatz, 1982)(Reid and Schatz, 1982)(Reid and Schatz, 1982)(Reid and Schatz, 1982)(Reid and Schatz, 1982)(Reid and Schatz, 1982)(Reid and Schatz, 1982)(Reid and Schatz, 1982)(Reid and Schatz, 1982)10 ml of exponentially growing cells ($1x10^7$ cells/ml) are collected, washed with 1 ml TCA 20%, transferred in a 2 ml Eppendorf tube and resuspended in 50 µl TCA 20%. An equal volume of acid-washed glass beads (425-600 µm, Sigma-Aldrich) is added. Cells are broken by continuous vortexing for 3'. 100 µl of TCA 5% is added to have as final concentration of TCA 10%. The lysate is transferred to a new 1.5 ml tube and centrifuged for 10 minutes at 3000 rpm at RT. The pellet is re-suspended in 100 µl of Laemmli Buffer 2X (2X Laemmli Buffer: 4% SDS, 20% glycerol, 10% 2-mercaptoethanol, 0.004% bromphenol blue, 0.125 M Tris HCl pH6.8). The pH is neutralized with 60 µl of Tris Base 2M. The protein extract is boiled for 3' at 95˚C and centrifuged for 2' at top speed at RT. The supernatant is collected and the protein extract is subjected to SDS-PAGE analysis.

2.8 SDS polyacrylamide gel electrophoresis (SDS-PAGE)

Proteins are separated according to their molecular weight by polyacrylamide gel electrophoresis (PAGE) under denaturing conditions.

The polyacrylamide gels consist of two parts, running and stacking gels, and were prepared as described in Table 2.2. Gels were run in SDS-PAGE running buffer (Glicine 2 M, Tris 0.25 M, SDS 0.02 M, pH 8.3), through which an electric field was applied, and then proteins were transferred on nitrocellulose filters (see Western Blotting procedure below).

	Running gel			Stacking gel
	7.5 %	10 %	12.5%	
40% Acrylamide	3.76 ml	5 ml	6.25 ml	1.25 ml
2% bisacrylamide	0.98 ml	1.3 ml	1 ml	0.7 ml
0.5M Tris-HCl pH=6.8	/	/	/	2.5 ml
1.5M Tris-HCl pH=8.8	5 ml	5 ml	5 ml	/
SDS 10%	200 µl	200 µl	200 µl	100 µl
APS 10%	200 µl	200 µl	200 µl	200 µl
Temed 10%	20 µl	20 µl	20 µl	20 µl
Water until:	20 ml	20 ml	20 ml	10 ml

Table 2.2. SDS-PAGE gels composition.

2.9 Phosphate Affinity SDS-PAGE

Phosphate-affinity Mn^{2+}-Phos-tag SDS-PAGE allows the detection of the mobility shift of phosphorylated proteins (Kinoshita et al., 2009; Kinoshita et al., 2006).

The Phos-tag™ AAL-107 reagent is a molecule that, in the presence of manganese ions, specifically binds to the phosphate groups, trapping phosphorylated proteins during SDS-PAGE and allowing the separation of phosphorylated isoforms of a protein from their nonphosphorylated counterparts (Figure 2.1).

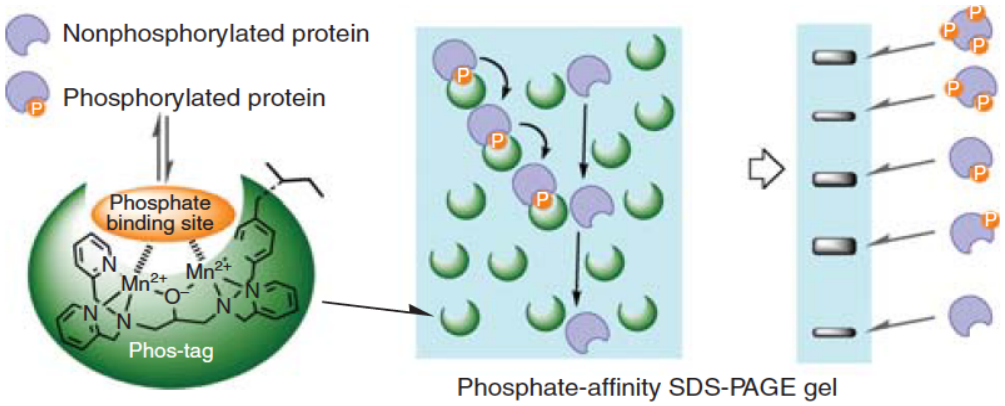

Figure 2.1. Schematic representation of the Phosphate-affinity SDS-PAGE system. Adapted from (Kinoshita et al., 2009)

Phospho-tag gels have been prepared according to manufacturer instructions (Kinoshita et al., 2009; Kinoshita et al., 2006). 7.5% polyacrylamide gels were used to resolve the phospho-specifc bands of Rrm3, while for Pif1 10% polyacrylamide gels were used (see Table 2.3). Gels were run in SDS-PAGE running buffer (Glicine 2 M, Tris 0.25 M, SDS

0.02 M, pH 8.3) through which an electric field was applied. After the run, before the electric transfer (see Western blot procedure described below), gels were incubated in 1X Transfer buffer (1% glycine, 0.02 M Tris base, 20% methanol) supplemented with 100 mM EDTA pH=8 for 30' to chelate the manganese ions and then washed for 15' in 1X Transfer buffer for three times.

	Running gel (7.5 %)	**Running gel (10 %)**	**Stacking gel**
40% Acrilammide	3.76 ml	5 ml	1.25 ml
2% bisAcrilammide	0.98 ml	1.3 ml	0.7 ml
0.5M Tris-HCl pH=6.8	/	/	2.5 ml
1.5M Tris-HCl pH=8.8	5 ml	5 ml	/
SDS 10%	200 µl	200 µl	100 µl
Phos-tag™ 5 mM	160 µl	160 µl	/
$MnCl_2$ 10 mM	320 µl	320 µl	/
APS 10%	200 µl	200 µl	200 µl
Temed 10%	20 µl	20 µl	20 µl
Acqua fino a	20 ml	20 ml	10 ml

Table 2.3. Phospho-tag gels composition.

2.10 Western blotting

Proteins were transferred, through electric transfer, on nitrocellulose filters (Whatman Protran, Nitrocellulose Transfer Membrane, Pore size 0.45 µm or 0.22 µm) in 1X Transfer buffer (1% glycine, 0.02 M Tris base, 20% methanol) at 200 mA ON. Ponceau staining (0.2% Ponceau S, 3% acetic acid) was used to roughly reveal the amount of protein transferred onto the filters. Unspecific protein binding was blocked for 1 h with 5% milk in PBST (80 g NaCl,2 g KCl, 2 g KH_2PO_4, 11.4 g $Na_2HPO_4 \cdot 2H_2O$ for 1liter of PBS + 0.2 % Tween 20). After blocking, membranes were incubated with the primary antibody for 2.5 hours at RT, followed by 3X 10' washes in PBST and then incubated with the horseradish peroxidase-conjugated secondary antibody for 1 h. The membranes were washed again 3 times for 10' each in PBST and the bound secondary antibody was revealed using SuperSignal West Pico Chemiluminescent Substrate (Thermo Scientific). Membranes were

then exposed to photographic films and developed.

The antibodies used in this work for western blot analysis are listened in the following table.

Primary antibodies	Dilution	**Secondary antibodies**	Dilution
Ab α myc Mouse monoclonal, 9E10 (IFOM) 1 mg/ml	1:2000	GAM (Anti-mouse, Goat polyclonal) (Bio-rad #170-6516) IgG-HRP	1:20000
Ab α FLAG Mouse monoclonal, M2 (SIGMA F1804) 1 mg/ml	1:5000	GAM (Anti-mouse, Goat polyclonal) (Bio-rad #170-6516) IgG-HRP	1:20000
Ab α FLAG Rabbit polyclonal, (SIGMA, F7425) 0.8 mg/ml	1:20000	GAR (Anti-rabbit, Goat polyclonal) (Bio-rad #170-6515) IgG-HRP	1:20000
Ab α HA Mouse monoclonal, 12CA5 (IFOM) 48 μg/ml in serum-free medium (HB101, Irvine)	1:24	GAM (Anti-mouse, Goat polyclonal) (Bio-rad #170-6516) IgG-HRP	1:20000
Ab α Tubulin Mouse monoclonal (IFOM) 6 mg/ml	1:8000	GAM (Anti-mouse, Goat polyclonal) (Bio-rad #170-6516) IgG-HRP	1:20000
Ab α Rnr1 Goat polyclonal IgG, yN-16 sc-11980 (Santa Cruz) 200 μg/ml	1:1000	Anti-Goat (Santa Cruz)	1:5000
Ab α γH2AX Rabbit polyclonal, ab15083 (Abcam) 0.3 mg/ml	1:1000	GAR (Anti-rabbit, Goat polyclonal) (Bio-rad #170-6515) IgG-HRP	1:20000
Ab α Pol12 Mouse monoclonal, 6D2 (IFOM)	1:1000	GAM (Anti-mouse, Goat polyclonal) (Bio-rad #170-6516) IgG-HRP	1:20000
Ab α Rad53 Mouse monoclonal, EL7 (IFOM) 50 μg/ml in serum-free medium (HB101, Irvine)	1:4	GAM (Anti-mouse, Goat polyclonal) (Bio-rad #170-6516) IgG-HRP	1:20000
Ab α Phospho-Rad53 Mouse monoclonal, F9 (IFOM) 50 μg/ml in serum-free medium (HB101, Irvine)	1:150	GAM (Anti-mouse, Goat polyclonal) (Bio-rad #170-6516) IgG-HRP	1:20000

Table 2.4. Antibodies used in this study for Immunoblotting.

2.11 Chromatin Immunoprecipitation on chip (ChIP on chip)

The ChIP on chip technique consists in the immunoprecipitation of the protein of interest, associated with chromatin, followed by DNA amplification and hybridization to high-density oligonucleotide arrays (chip) (Bermejo et al., 2009b). This technique allows the detection of the genome-wide binding profile of the protein of interest at a resolution of 300 bp.

In details, protein-DNA complexes are crosslinked by formaldehyde treatment, the chromatin is sheared by sonication and then the immunoprecipitation of the epitope-tagged protein is performed using specific antibodies. The IP fraction is enriched in the protein of interest, while the SUP fraction, containing the non-immunoprecipitated DNA, is used as hybridization control. After crosslink reversal and proteinase K and RNAse treatments, DNA fractions are amplified by tagged-random primer PCR in non-saturating conditions, DNAse digested and labeled with biotin. SUP and IP fractions are hybridized to independent high-density oligonucleotide arrays (chip) and after staining, washing and scanning, the comparison of the signal intensity of the two fractions will provide a measurement of the protein-DNA association along entire genome (see Figure 2.1).

The integration of the logarithmic expression of the IP/SUP signal ratio and the annotated sequence of *S. cerevisiae* genome allow the construction of maps displaying the binding pattern of the protein of interest along entire chromosomes.

In this PhD thesis ChIP on chip of DNA Polymerase α, Rrm3 and Pif1 were performed after the G1 release into S-phase in the presence of 25 mM or 150 mM of hydroxyurea.

ChIP on chip of replisome-DNA replication fork components allowed the precise localization of all active DNA replication forks in the genome of *Saccharomyces cerevisiae.*

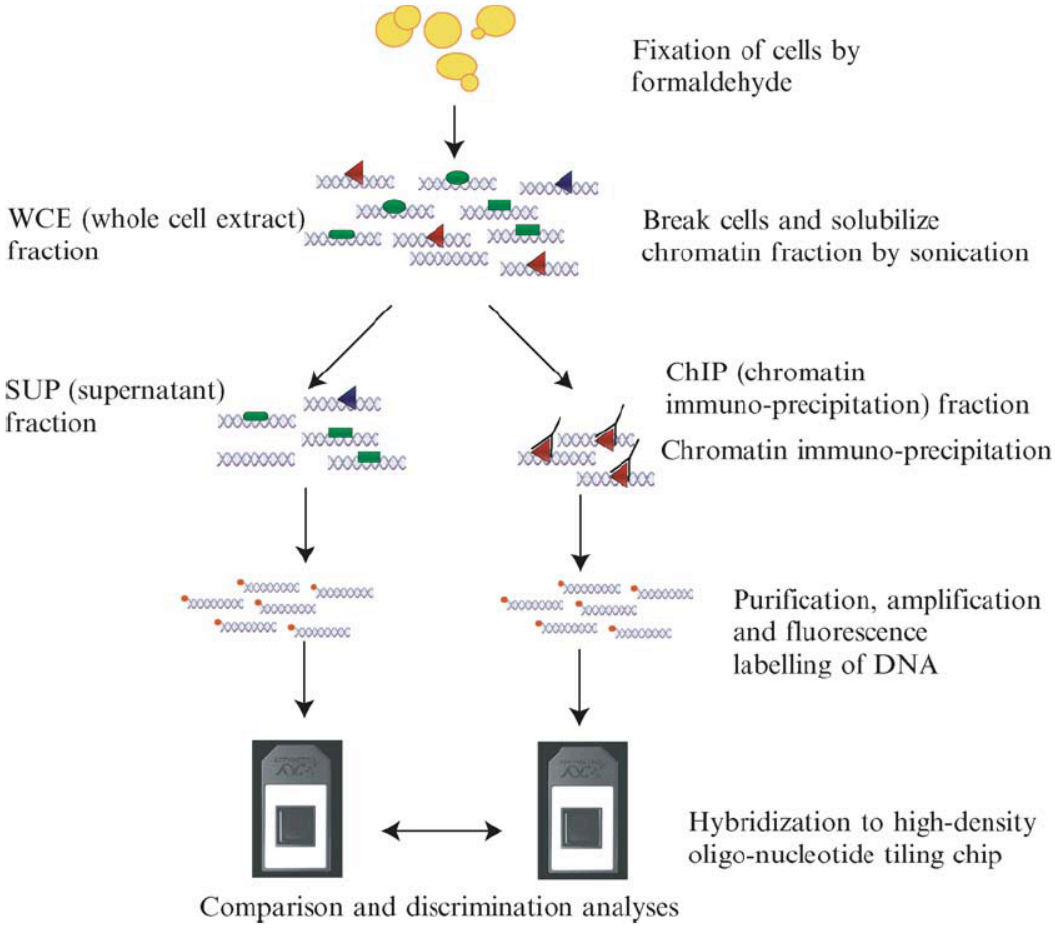

Figure 2.2. Schematic representation of ChIP on chip procedure. Adapted from (Katou et al., 2006)

Solutions (filtered 0,2 μm):

PBS (Phospate Buffered Saline): 137 mM NaCl, 10 mM PO_4 ph=7.4, 2.7 mM KCl.

TBS: 20 mM Tris-HCl pH=7.5, 150 mM NaCl.

TE 1X: 10 mM Tris-HCl pH=8, 1mM EDTA.

PBS/BSA: PBS 1X containing 5 mg/ml Bovine Serum Albumin

Lysis buffer: 50 mM Hepes–KOH, pH 7.5, 140 mM NaCl, 1 mM EDTA, 1% Triton-X100, 0.1% Na-deoxycholate.

Wash buffer: 10 mM Tris–HCl, pH 8.0, 250 mM LiCl, 0.5% NP-40, 0.5% Na-deoxycholate, 1 mM EDTA.

Elution buffer: 50 mM Tris–HCl, pH 8, 10 mM EDTA, 1% SDS.

TE/1% SDS: TE with 1% SDS.

10X One-Phor-All-Buffer: 100 mM Tris-Acetate pH=7.5, 100 mM Mg-Acetate, 500 mM K-Acetate.

Magnetic beads preparation (Protein A)

1. Transfer 60 µl of magnetic beads (Dynabeads, Invitrogen) in a 1.7-ml prelubricated Costar tube, for each 100 ml of cell culture

2. Place the tube in a magnetic grid and aspirate the supernatant with a vacuum pump.

3. Wash beads twice with 0.5 ml of ice cold PBS/BSA by removing the tube from the magnetic grid and gently shaking

4. Resuspend the beads in 60 µl of PBS/BSA and add 20 µg of anti-Flag monoclonal antibody M2 (SIGMA F1804) or anti-myc antibody (9E10, IFOM)

5. Incubate with rotation overnight at 4°C

6. Immediately before use, remove the antibody containing solution; wash twice with ice-cold PBS/BSA and resupend in 60 µl of PBS/BSA (15 µl of magnetic beads are added to each 0.4 ml Lysis Buffer aliquot)

Chromatin extracts preparation and immunoprecipitation

1. Collect 100 ml of culture after treatment.

2. Transfer the culture into two 50-ml centrifuge tubes containing formaldehyde to a 1% final concentration.

3. Incubate at room temperature for 30' gently shaking.

4. Wash cells 3 times with 20 ml of ice-cold 1x TBS. After the last washing step discard the supernatant and carefully remove the remaining liquid with a vacuum pump.

5. Resuspend each pellet in 0.8 ml of Lysis Buffer, supplemented to 1 mM PMSF (Phenylmethanesulphonyl fluoride) and 1x Antiproteolytic Cocktail (Complete protease inhibitor tablets, Roche) immediately before use, and transfer cells into 2-mL O-ring screw-cap tubes. Add zirconium beads up to 1 mm below the buffer's meniscus.

6. Break cells at 4 °C in the cold room, with a multibeads shocker using the following pattern: speed: 6,5 m/sec., 20 sec/cycle, 4 cycles.

7. Recover cell lysate as follows: wipe each O-ring tube with a tissue paper, puncture the bottom with a hypodermic syringe needle (27G1/2), fix the tube on a 1,5 ml eppendorf tube, centrifuge at 0.8 g for 5 min at 4 °C to recover the lysate.

8. Centrifuge the extracts at 13400 g for 1 min at 4 °C. Add a 5 µl aliquot of the soluble fraction to 5 µl of 2x Laemli Buffer for Western blot analysis of IP efficiency. Discard the supernatant containing the soluble protein fraction Add 0.45 ml of supplemented Lysis Buffer without resuspending the pellet.

9. Shear chromatin by applying 5 sonication cycles of 15 sec at 1.5 tune. After each sonication cycle pellet the chromatin by centrifuging at 2300 g for 1 min at 4 °C.

10. Centrifuge at 16000 g for 5 min at 4 °C. Transfer the supernatant to a 1.7-ml prelubricated tube. Add a 5 µl aliquot of this Whole Cell Extract (WCE) to 5 µl of 2x Laemli Buffer for Western blot analysis

11. Add previously washed antibody-bound magnetic beads: 30 µl per tube**.** Incubate on a rotating wheel at 4°C overnight.

Beads washing and crosslink reversal

1. Place beads-containing tubes in a magnetic grid. Wait until the beads attach to the magnet leaving a clear supernatant.

2. IMPORTANT: Transfer 5 µl of the supernatant to a 1.5 ml microcentrifuge tube containing 95 ml of TE-1% SDS).

3. Transfer another 5 µl to a tube containing 5 µl of 2x Laemli Buffer for Western blot analysis of IP efficiency.

4. Wash beads as follows:

- 2x with 1 ml of ice cold Lysis Buffer (without antiproteolytics).
- 2x with 1 ml of ice cold Lysis Buffer supplemented with 360 mM NaCL.

- 2x with 1 ml of ice cold Wash Buffer.

- 1x with 1 ml of ice cold TE pH 8.

5. Remove the TE with a micropipette in order to avoid bead aspiration and centrifuge the beads at 800 g for 3 min at 4 °C. Place the tubes back in the magnetic grid and remove thoroughly the remaining liquid with a vacuum pump.

6. Add 80 μl of Elution Buffer to each tube, resuspend the beads by pipetting up and down and incubate at 65 °C for 10'.

7. Centrifuge the tubes for 1 min at 16000 g at RT.

8. Place the tubes back in the magnetic grid and transfer 5 μl from a fraction in a tube containing 5 μl of 2x Laemmli Buffer.

9. For the Western blot analysis of IP efficiency boil the samples at 95 °C for 30 min prior to SDS-PAGE.

10. Transfer the remaining IP fractions (75-80 μl) to new 1.5-ml microcentrifuge tubes containing 4 volumes (300-320 μl) of TE-1% SDS.

11. Add 95 μl of TE-1% SDS to the SUP fraction (collected on step 2)

Incubate both the IP and the Supernatant samples overnight at 65 °C in order to reverse the crosslink.

DNA purification

1. Consolidate the samples by pulse-spinning

2. Add 25 μl of TE to the IP sample containing 375 μl (the sample used for the gel control)

3. Add:

- 179 μl of TE, 6 μl of glycogen (20 mg/ml) and 15 μl of Proteinase K (50 mg/ml) to the IP samples

- 44.75 μl of TE, 1.5 μl of glycogen (20 mg/ml) and 3.75 μl of Proteinase K (50 mg/ml) to the SUP sample.

4. Mix, without vortexing, and incubate at 37 °C for 2 hours.

5. Pulse-spin to consolidate the samples

6. Add: - 24 μl of a 5M NaCl stock to the IP samples

- 6 μl of a 5M NaCl stock to the SUP samples.

7. Extract twice by adding an equal volume of phenol /chlorophorm / isoamylalcohol, pH 8.0 at RT: 600 μl for IP samples and 150 ml for SUP samples. Vortex and spin at 13400 g for 5 min at RT.

8. Add 2 volumes of cold 100% ethanol: 600 μl for the IP samples and 300 μl for the SUP samples. Vortex and incubate at -20 °C for at least 20 min or O.N.

9. Centrifuge at ≥ 13400 g for 10 minutes at 4 °C.

10. Discard supernatant using a Gilson pipette and wash with 1 ml of cold 80% ethanol.

11. Centrifuge at ≥ 13400 g for 10 minutes at 4 °C.

12. Discard the supernatant using a Gilson pipette and spin again; discard the remaining ethanol with a gel loading tip.

13. Let the pellet dry, resuspend in 30 μl of TE containing 10 mg of RNase A (stock 10 mg/ml).

14. Incubate 1h at 37 °C

15. Consolidate the samples by pulse spinning.

16. Pool 30 μl IP samples together to obtain two 60 μl samples and purify the IP/SUP DNA using a PCR purification kit following the manufacturer's instructions. Elute the DNA with 50 ml of EB buffer.

17. Pool the two 50 μl IP samples together and precipitate the DNA by adding:

- 5 μl of 3M Sodium Acetate, 2 μl of glycogen (20 mg/ml) to the IP SAMPLE

- 2.5 μl of 3M Sodium Acetate, 1 μl of glycogen (20 mg/ml) to the SUP SAMPLE

18. Add 2.5 volumes of cold 100% ethanol: - 267.50 µl to the IP samples

- 133.75 µl to the SUP samples

19. Incubate at -20 °C for at least 20 min. or O.N.

20. Centrifuge at ≥ 13400 g for 10 minutes at 4 °C.

21. Discard supernatant using a Gilson pipette and wash with 0.5 ml of cold 70% ethanol.

22. Centrifuge at ≥ 13400 g for 10 minutes at 4° C.

23. Discard the supernatant using a Gilson pipette and spin again; discard the remaining ethanol with a gel loading tip.

24. Leave 5' at 37° C and resuspend the pellet in 10 µl of ddH_20.

25. Vortex then pulse-spin for three times to recover the precipitate

DNA amplification

Amplification of the IP and SUP DNA, in non-saturating conditions, is required to obtain a sufficient amount (≥ 4/5 µg) of DNA to be labeled and used as hybridization probe.

Use WGA2 GenomePlex Complete Genome Amplification (WGA) Kit. Follow manufacturer's instructions from the *Library Preparation* step on:

a) Add 2 µl of 1X Library preparation Buffer to each sample

b) Add 1 µl of Library stabilization solution

c) Vortex thoroughly, consolidate by centrifugation and place in thermal cycler at 95° C for 2 minutes

d) Cool the sample on ice, consolidate the sample by centrifugation, and return to ice.

e) Add 1 µl Library Preparation Enzyme, vortex thoroughly and centrifuge briefly.

f) Place sample in a thermal cycler and incubate as follows:

16° C for 20 minutes

24° C for 20 minutes

37° C for 20 minutes

75° C for 5 minutes

4° C hold

g) Remove samples from thermal cycler and centrifuge briefly.

Amplification step:

A master mix may be prepared by adding the following reagents:

Nuclease-free water: 48.5 µl

10X Amplification Master Mix: 7.5 µl

Reaction from step g): 14.0 µl

WGA DNA Polymerase: 5.0 µl

Vortex thoroughly, centrifuge briefly, and begin thermocycling.

Initial Denaturation: 95° C for 3 minutes

Perform 14 cycles as follows:

Denature: 94° C for 15 seconds

Anneal/Extend: 65° C for 5 minutes

1. Pulse-spin the samples.
2. Check the amplified DNA by loading a 1.9 µl aliquot of the reaction in a 1.2% agarose gel; a smear ranging from 100-1000 bp should be observed.
3. Purify the IP/SUP DNA using a PCR purification kit following the manufacturer's instructions. Elute the DNA with 50 µl of EB buffer. Add other 50 µl of EB buffer and elute again in the same tube
4. Precipitate the DNA by adding:

5 µl of 3M Sodium Acetate, 2 µl of glycogen (20 mg/ml), and 267.5 µl of EtOH 100%.

5. Vortex and incubate at -20 °C for at least 20 min or O.N.
6. Centrifuge at ≥ 13400 g for 10 minutes at 4 °C.
7. Discard supernatant using a Gilson pipette and wash with 1 ml of cold 80% ethanol.
8. Centrifuge at ≥ 13400 g for 10 minutes at 4 °C.

9. Discard the supernatant using a Gilson pipette and spin again; discard the remaining ethanol with a gel loading tip.

10. Let the pellet dry, resuspend in 42 µl of bidistilled water

11. Measure DNA concentration by spectrometry at 260 nm (Nanodrop)

NB: The minimal DNA concentration should be 100 micrograms/µl

12. If the concentration of the sample is lower, the purified sample can be further amplified by performing 2 additional cycles of the amplification reaction.

DNAse digestion

Short DNAse incubation is performed to reduce the size of amplified DNA and increase it's suitability for the hybridizatation on the array.

1. Prepare DNAse reaction mix (for 13 samples):

ddH_2O	14,8 µl
10X One-Phor-All-Buffer plus	2 µl
25mM $CoCl_2$	1.2 µl
DNAse I (1U/ml)	2 µl

2. Prepare the following reaction mix:

10X One-Phor-All-Buffer plus	4.85 µl
25mM $CoCl_2$	2.9 µl
DNAse I reaction mix	1.5 µl
DNA (5-10 mg) + ddH_2O (IP/SUP) samples	40.75 µl

3. Vortex and pulse-spin to pack the sample.

4. Incubate at 37° C for 30'' and then transfer to 95°C for 15'.

DNA labeling

1. Spin to pack the sample

2. Transfer DNA into a new 1.5ml-microcentrifuge tube.

3. Add: 5ml of TdT reaction buffer

1 μl Biotin-N11-ddATP (1nMole/ μl)

1 μl terminal transferase (400 U/ μl)

4. Vortex and Pulse-spin to recover the sample

5. Incubate at 37° C for 1hr.

Hybridization, washing, staining and scanning of chips

The amount of DNA used to hybridize the Affymetrix chips (*S.cerevisiae* Tiling 1.0R, P/N 900645) was normalized to 4 μg within the different samples to preserve quantitative ratios. Hybridization, washing, staining, and scanning were performed according to the manufacturer's instructions (Affymetrix).

2.12 ssDNA-BromodeoxyUridine Immunoprecipitation on chip (ssDNA BrdU-IP on chip)

Yeast cells were engineered to express thymidine kinase of *Herpes simplex* virus to incorporate into replicating DNA 5-bromo-2'-deoxyuridine (BrdU), a synthetic nucleoside that is a thymidine analog. The immunoprecipitation, using anti-BrdU antibodies, of the newly-synthesized BrdU-labeled DNA was followed by PCR amplification, labeling with a fluorophore and cohybridization along with a reference sample onto DNA microarrays.

Experiments were performed as in (Katou et al., 2006).

ssDNA BrdU-IP on Chip allowed to monitor the chromosome replication dynamic and, combined with ChIP on chip analysis of replisome-DNA replication fork components, allowed us to precisely localize, genome-wide, all the active DNA replication forks in our experimental conditions. Superimposition analysis of binding and BrdU incorporation profiles can be used to locate a factor of interest at active DNA replication forks (Rossi et al., 2016)

Magnetic beads preparation

Protein A Magnetic Beads preparation, for each 150 ml culture:

1) Take 20 µl of dynabeads for each IP and put in a Costar prelubricated tube

2) Wash the beads two times with 1 ml of PBS 1X, 5 mg/ml BSA, 0.1% Tween20

3) Resuspend in 20 µl of PBS, 5mg/ml BSA, 0.1% Tween20; add 4 µg of anti-BrdU antibody MBL M1-11-3

5) Incubate the beads ON at 4°C, rotating

6) Wash the antibody-beads complex two times with 1 ml of PBS 1, 5 mg/mL BSA, 0,1% Tween20

7) Resuspend the antibody-beads complex in 20 µl of PBS 1X, 5 mg/ml BSA, 0.1% Tween20

Day 1: DNA extraction

1) Synchronize with α-Factor 250 ml of cells ($1x10^7$ cells/ml) growth O/N in SC-URA medium

2) Release cells from G1 arrest into YPDA medium containing HU (25 mM or 150 mM) and BrdU (200-500 mg/ml).

3) Add Na-Azide 10% at a final concentration of 0.1% and keep on ice for at least 45 min.

4) Centrifuge the culture using the Beckman centrifuge and the JA-14 rotor:
5000 rpm, 5 min at 4°C and discard the supernatant

5) Resuspend the pellet in 20 ml of cold and sterilized TE 1X

6) Centrifuge the culture at 3220 g, 5 min at 4°C. Discard the supernatant and carefully remove the remaining liquid with a vacuum pump

7) Extract the DNA with QIAGEN GENOMIC DNA ISOLATION KIT (Cat. No. 19060).

a. Resuspend cell pellet in 50 ml Falcon tube with 5 ml of spheroplasting buffer (1 M sorbitol, 100 mM EDTA pH 8.0, 0.1% β –mercaptoethanol).

b. Place the cell suspension at 30°C until spheroplasts are visible under microscope

c. Discard the supernatant and re-suspend the pellet in 5 ml of G2 buffer of the QUIAGEN

kit.

d. Add 100 µl of RNase (10 mg/ml) and incubate the tube for 30 min at 37°C

e. Add 100 µl of Proteinase K (20 mg/ml) and incubate for 1 hour at 37°C

f. Collect the supernatant by centrifugation at 5000 rpm, 4°C, for 5 min

g. Equilibrate the Genomic tip 100/G with 4 ml of QBT

h. Gently mix the supernatant with 5 ml of QBT and apply it to the equilibrated Genomic tip 100/G.

i. Wash 2 times the columns with 7.5 ml of QC

j. Elute the DNA into an isopropanol-containing corex tube with 5ml of QF pre-warmed at 50°C

k. Centrifuge for 10 min at 8100 rpm RT in a proper swing out rotor

l. Wash the pellet with 1 ml ethanol 70%

m. Centrifuge for 5min at 8100 rpm RT

n. Let the corex containing the pellet to air-dry

o. Add 250 µl of Tris HCl 10 mM pH 8 and let the pellet resupending ON at 4°C

Day 2: chromatin shearing and BrdU immunoprecipitation

1) Shear the BrdU containing DNA by sonication to a length of 200-1000bp

Using the Bandelin UW2070 sonicator you can use the following parameters:

Power: 20%, 20 seconds/pulse, 6 pulses

After each sonication cycle, pellet the chromatin by centrifuging at 2300xg for 1' at 4°.

2) Quantify the DNA

The average amount of genomic DNA should range from 50 to 200ng/mL

3) Centrifuge for 5 min at 3000 rpm at 4°C

4) Normalisation: Depending of the quantification, use the same quantity of DNA for all your conditions. Do the appropriate dilution to have two tubes of 1.5 ml containing 100 µl of the DNA solution of the fixed concentration.

5) Denaturate the DNA at 100°C for 10 min and immediately put on ice

6) Add rapidly to each tube:

100 µl of ice cold 2x PBS

200 µl of ice cold PBS, 2% BSA, 0,2% Tween20

7) Add the DNA solution from each tube to the 10 µl antibody-beads complex and incubate o/n at 4°C, rotating.

Day 3: beads washes and DNA purification

1) Place beads containing tubes in a magnetic grid. Wait until the beads attach to the magnet leaving a clear supernatant.

2) Collect 2.5 µl +2.5 µl of supernatant from each precipitation tube and put into a new eppendorf tube with 45 µl of Elution Buffer 1X (Sup fraction); keep R.T.

3) Wash the beads as follows:

- 2X with 1 ml of ice cold Lysis buffer
- 2X with 1 ml of ice cold Lysis buffer +500 mM NaCl
- 2X with 1 ml of ice cold Washing buffer
- 1X with 1 ml of ice cold TE 1X pH8

4) Place on the magnetic grid;

Remove the TE with a micropipette to avoid beads aspiration

Centrifuge 3 min at 800 g 4°C

Place the tubes back in the magnetic grid and remove thoroughly the remaining liquid with a vacuum pump.

5) Resuspend the beads in 50 µl of elution buffer;

incubate at 65°C for 10 min mixing 3 times during the incubation

6) Centrifuge 1 min at 16000 g at RT

7) Place the tubes back in the magnetic grid and transfer the eluted material into new tubes

8) Add to the IP and to the SUP: 49 µl of TE 1X and 1 µl of Proteinase K (Stock 50 mg/mL)

9) Mix, without vortexing, and incubate at 37°C for 1h.

10) Purify DNA by Qiagen PCR purification Kit. Elute with 50 µL of EB buffer

11) Pool the two identical IP samples together and precipitate the DNA adding:

5 µl of 3M Sodium Acetate, 1 µl glycogen to the IP samples

2.5 µl of 3M Sodium Acetate, 0.5 µl glycogen to the SUP samples

12) Add 2.5 volumes of cold 100% ethanol:

265 µl to the IP samples

132,5 µl to the SUP samples

13) Incubate at -20 °C for at least 20 min. or O.N.

14) Centrifuge at ≥ 13400 g for 10 minutes at 4 °C.

15) Discard supernatant using a Gilson pipette and wash with 0.5 ml of cold 70% ethanol.

16) Centrifuge at ≥ 13400 g for 10 minutes at 4° C.

17) Discard the supernatant using a Gilson pipette and spin again; discard the remaining ethanol with a gel loading tip.

18) Leave 5' at 37° C. Resuspend the pellet in 10 µl of ddH_20

19) Vortex then pulse-spin for three times to recover the precipitate

20) Proceed as for ChIP on chip, starting from the DNA amplification step, using only 10 cycles of amplification instead of 14.

2.12.1 ChIP on chip and BrdU-IP on chip data analysis

PCR amplification steps in our ChIP on chip and ssDNA BrdU-IP on chip analysis were carried out under non saturating conditions and the amounts of DNA used to hybridize the affymetrix chips were normalized.

Data analysis was performed as described in (Rossi et al., 2016).

CEL files, obtained by scanning of the hybridized Affymetrix chips were analyzed using a modified version of the Tiling Array Suite software (TAS) from affymetrix. The software does a linear scale normalization of input CEL files (IP and Sup) intensity so that the median value is equal to a selected target intensity of 500. Signals and the p-value changes

obtained from TAS per each probe position were subsequently used by the software to detect clusters of enriched signals as ranges within the chromosomes. Conditions for clusters detection in whole range (at least 600 bps), except for segments within the range shorter than 600 bps, were: log2 signal (IP/SUP binding ratio) positive and change in p-value (evaluated using Wilcoxon signed rank test) <0.2, as described in (Bermejo et al., 2009a).

BrdU incorporation profiles have been generated as described for protein binding profiles. Genome-wide binding and BrdU incorporation profiles can be superimposed and the statistical significance of binding and BrdU cluster overlappings can be calculated using a confrontation against a null hypothesis model generated with a Montecarlo-like simulation (Bermejo et al., 2009a).

The average binding signals of Polα, Rrm3 and Pif1 and the average BrdU incorporation at 141 early ARSs were plotted using the sitepro function in CEAS (Cis-regulatory Element Annotation System) (Shin et al., 2009). log2 signal (IP/SUP binding ratio) bed files obtained from protein binding and BrdU incorporation analysis were wig converted and used to draw average signals around 141 active DNA replication origins (Autonomously Replicating Sequences, ARSs), setting 50 bps as the profiling resolution and 10 or 20 kbps as the size of flanking regions from the center of each ARS. For the calculation of average binding or BrdU incorporation signals, negative values were set to zero. Total average binding or BrdU incorporation signals around 141 ARSs have been derived as average of the average of signals from the 50 bp bins created by the sitepro CEAS script where negative values were set to zero.

2.13 ChIP quantitative PCR (ChIP-qPCR)

The quantitative ChIP-qPCR technique consists in the ChIP of the target protein followed by the quantitative PCR amplification of the immunoprecipitated DNA. A DNA-binding dye is included in the PCR reaction in order to have a proportional increase in the

fluorescent signal and in the amount of DNA, allowing the determination of the amount of the starting template. At the beginning of the PCR reaction fluorescence is at a background level, then progressively increases reaching an exponential phase, during which the amount of PCR products and consequently the fluoresce signals double at each cell cycle. The Real Time PCR monitors the threshold cycle (C_T), the cycle number at which the fluorescent signal is detectable and rises above a threshold.

Chip-qPCR analysis was carried out as described in (Alzu et al., 2012).

Beads and chromatin extracts preparation, immunoprecipitation and DNA purification were performed as described for ChIP on chip (see paragraph 2.11). Differently from ChIP on chip, 10 μl of Whole Cell Extract were taken before the immunoprecipitation step and were used as the control sample (INPUT) in the PCR reaction. Levels of immunoprecipitated DNA were then measure by quantitative Real-Time PCR by using the SYBR Green technique (LighCycler 480 SYBR Green I Master, Roche) and run in Roche Light Cycler 480 Real-Time PCR System, using the following PCR program:

I	5’ 95°C
II Quantification (40 cycles)	10’’ 95°C, 30’’ 60°C
III Melting curve	10’’ 95°C, 97°C

The fold enrichment of the target protein was measured with the following formula:

$$\text{Fold increase} = 2^{(C_T \text{ input} - C_T \text{ IP})} / 2^{(C_T \text{ input} - C_T \text{ IPbackgound})}$$

ChIP-qPCR were normalized using the CT IP background, obtained performing the same ChIP experiment with an unrelated antibody (Ab α Vinculin, IFOM).

The magnitude of Polα-myc and Rrm3-myc bindings, shown in Figure 3.3A, were determined by quantitative ChIP-qPCR, using the oligos 305L3F (CCATGACTTTGGCACATCAG) and 305L3R (CGCTGCCTCCTTAGTAATCG), that map in a region located 6 kb upstream the *ARS305*.

The magnitude of Polα-Flag and Pif1-Flag bindings, shown in Figure 3.3B, were determined on a region located 9.2 kb upstream the *ARS305* using the oligos 305L8F (TCAAAGCAGATGCCATGAAC) and 305L8R (CTGTTTGCACGAAGGAATCA). Showed data represent the mean ±SD of three independent experiments.

2.13 Neutral-neutral two-dimensional agarose gel electrophoresis (2D gel)

Neutral-neutral two-dimensional agarose gel electrophoresis (2D gel) technique allows separation and identification of the replication intermediates, arising in a specific DNA fragment, according to their mass and shape complexity (Bell and Byers, 1983). This technique, further developed by Brewer and Fangman (Brewer and Fangman, 1987), has been used to map DNA replication origins in yeast chromosomes and to study replication and recombination related DNA structures in many organisms.

The technique consists on a DNA extraction, that utilizes the cationic detergent CTAB and Chloroform/isoamylalcohol, followed by a defined strategy of DNA digestion with specific restriction enzymes. Restriction fragments are separated through a first electrophoretic run, in conditions that emphasize the mass differences and minimize the contribution of shape to the mobility (low agarose concentration, low voltage, no ethidium bromide). Subsequently, each sample lane is cut out and separated by the second dimension gel, where DNA runs orthogonally with respect to the first dimension gel. The second gel, on the contrary, is run under conditions that maximize the contribution of the shape to the mobility by means of a delay of complex structures during migration (high agarose concentration, high voltage and in the presence of ethidium bromide). Finally a Southern blot with a specific radio-labeled probe is performed.

As a result of the two consecutive electrophoretic runs, each DNA structure assumes in the two dimensional area a specific position dictated by the unique combination of mass and

shape, measured by the deviation from the line that would be followed by a linear molecule of DNA that doubled in size (see Figure 2.3).

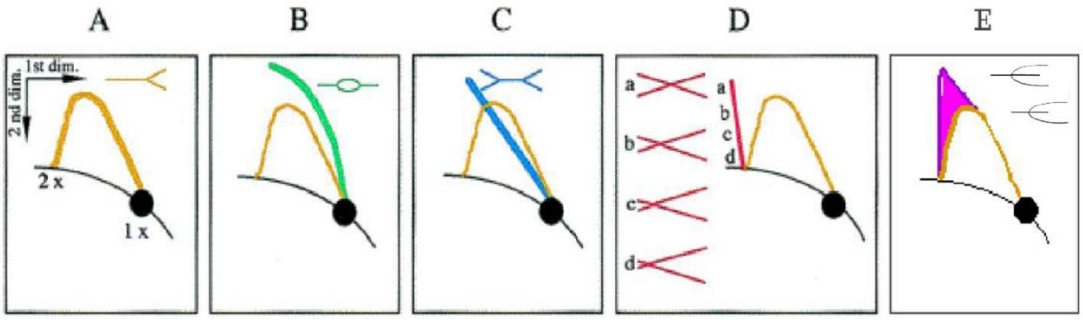

Figure 2.3. Schematic representation of the 2D gel migration patterns of replication intermediates. Adapted from (Lucas et al., 2000)

The 1X spot at the lower right corner of each panel (monomer spot) depicts the position at which non-replicating molecules migrate. The diagonal curve intersecting the 1X spot depicts the line formed by all linear molecules in the population. DNA fragment containing an origin of replication generates two sister replication forks, with a "bubble" like structure that enlarges with the progression of replication, resulting in two linear DNA molecules when forks proceed outside the restriction fragment analyzed (Figure 2.3B). In case the replication origin is not precisely positioned in the center of the analyzed DNA region, one fork of the bubble will exit the fragment before the other, generating a Y-shaped structure. Passively replicated DNA assumes a characteristic "Y" shape for the progression of the replication forks emanating from a flanking replication origin (Figure 2.3A). Converged replication forks generate double Ys signals (Figure 2.3C) and X-shape molecules. Recombination intermediates and hemicatenates assume a "X" shape due to the presence of a physical link between the two newly replicated DNA molecules (Figure 2.3D).

In specific pathological conditions, the formation of cruciform intermediates (also called reversed forks) and their derivatives generate a "spike-cone" signal (Lopes et al., 2001) (Figure 2.3E).

2.13.1 *In vivo* psoralen-crosslinking of genomic DNA

Psoralen efficiently intercalates in the double strand DNA and upon irradiation with ultraviolet (UV) light (366 nm) forms covalent crosslinks between pyrimidines of opposite strands. Psoralen derivatives easily penetrate the membranes of living cells and Trimethylpsoralen (TMP) is the most commonly used for *in vivo* crosslinking of DNA to stabilize and protect weak replication intermediates (Wellinger and Sogo, 1998).

Material and solutions:

- Sodium azide 10%, store at 4°C.

- Psoralen solution: 0.2 mg/ml Trioxalen (SIGMA) in 100% Ethanol. Keep in the dark. Dissolve by stirring overnight at 4°C. Store at -20°C.

- UV stratalinker (Stratagene), 365 nm and 265 nm UV bulbs

Procedure:

1. 2 x 10^9 cells (200 ml from a 1 x 10^7 cells/ml culture) were collected.

2. Block cells by treating with sodium azide (0.1% final) for at least 40 min on ice.

3. Pellet the cells and wash twice with 20 ml of ice-cold water.

4. Re-suspend in 5 ml of ice-cold water and transfer in a 6 well plate (FALCON) (1 sample/well).

5. Keep the 6 well dish always on ice while performing psoralen-crosslinking.

6. Add 300 µl of psoralen solution, mix well and incubate for 5 minutes (on ice)

7. Mix again within the 5 minutes and irradiate for 10 minutes (on ice) in a Stratalinker (Stratagene) with 365 nm UV bulbs, at a distance of 2-3 centimeters from the bulbs.

8. Repeat steps 6-7 for three more times. Cover with aluminum wrap during incubation with psoralen to keep samples as much as possible in the dark.

9. Transfer cells in falcon tubes and wash the dish with 5 ml of ice-cold water to collect all cells

10. Pellet the cells, wash twice with 20 ml of ice-cold water and proceed with DNA

extraction.

2.13.2 Isolation of total genomic DNA using the CTAB procedure.

Solutions

-10 mg/ml Zymolyase stock (1000U/ml).

- Spheroplasting buffer: 1M sorbitol, 100 mM EDTA pH 8.0, 0.1%

β-mercaptoethanol, 100 U Zymoliase.

- Solution I: 2% w/v CTAB (FLUKA-cetyltrimethylammonium bromide),

1.4 M NaCl,

- Solution II: 1% w/v CTAB, 50 mM Tris HCl pH 7.6, 10 mM EDTA

- Solution III: 1.4 M NaCl, 10 mM Tris HCl pH 7.6, 1 mM EDTA

- RNase 10 mg/ml (DNase free)

- Proteinase K 20 mg/ml

- 100 mM Tris HCl pH 7.6, 25 mM EDTA pH 8.0

- 24:1 Chloroform/isoamylalcohol

-Phenol:Chloroform:Isoamyl Alcohol 25:24:1 Saturated with 10 mM Tris, pH 8.0, 1 mM EDTA (SIGMA)

- Isopropanol

- 70% Ethanol

- 10 mM Tris-HCl pH 8.0

Procedure

1. After psoralen crosslinking harvest cell samples in ice.

2. Collect the cells by centrifugation at 4000 rpm 5-10 min, wash two times with cold water and re-suspend in 50 ml Falcon tube with 4.5 ml of spheroplasting buffer and 0.5 ml of 10 mg/ml Zymolyase.

3. Place the cell suspension at 30°C until spheroplasts are visible under microscope.

Usually this step takes 40 min, but the appropriate time has to be calculated based on the

stock of zymolyase and mainly on the cell growth conditions, which influence the dimension of the cell wall.

4. Collect the spheroplasts by centrifugation at 4000 rpm for 10 min at 4°C; carefully remove the supernatant and replace it with 2 ml of water. Vigorously re-suspend the spheroplasts on vortex and sub-sequentially add 2.5 ml of Solution I; kindly mix the suspension and place it at 50°C with 300 µml of 10 mg/ml RNasi for 30 min.

5. Add 300 µl of 20 mg/ml Proteinase K and protract the incubation for further 1 hour at 50°C. Note that at this step the solution has to become clear, with no visible aggregates of cellular component; if necessary, incubate over night at 30°C.

6. Separate the solution by centrifugation at 4000 rpm for 10 min at room temperature and process separately the obtained supernatant and the pellet as indicated in the following sections.

Supernatant

1. Transfer the supernatant into a 15 ml Falcon tube and add 2.5 ml Chloroform/isoamylalcohol 24:1 and 0.5 ml of Phenol:Chloroform:Isoamyl Alcohol 25:24:1 (Sigma).

2. Mix vigorously 6 times and separate the two phases by centrifugation at 4000 rpm for 10 min.

3. Carefully transfer the clear upper phase into 15 ml Falcon tube and add 2.5 ml Chloroform/isoamylalcohol 24:1.

4. Mix vigorously 6 times and separate the two phases by centrifugation at 4000 rpm for 10 min.

5. Carefully transfer the clear upper phase into a Corex glass tube with a pipette and add two volumes (10 ml) of Solution II. Note that at this step the prolonged incubation (1-2 hours) with Solution II might help DNA precipitation in the next step.

6. Separate the solution by centrifugation at 11.000 rpm for 20 min in a swing out rotor, discard the supernatant and re-suspend the pellet in 2.5 ml of Solution III.

Briefly incubate at 37°C to help the dissolution of the pellet.

Pellet

1. Energetically re-suspend the pellet into 2 ml of Solution III and incubate 1 hour at 50°C.

2. Transfer the solution into a 15 ml Falcon tube and extract with 1 ml of Chloroform/isoamylalcohol 24:1. Separate the two phases by centrifugation at 4000 rpm for 10 min at full speed in an appropriate centrifuge.

3. Carefully transfer the clear upper phase (Solution III) into the Corex glass tube containing Solution III obtained from the treatment of the supernatant (see treatment of "supernatant" step 6).

4. Precipitate the DNA with 1 volume (10 ml) of isopropanol at 11.000 rpm in swing out rotor for 30 min at 10°C.

5. Briefly wash the pellet with 2 ml of ice cold ethanol 70%.

6. After centrifugation (5 min 8.500 rpm), carefully remove the ethanol with a pipette as much as possible and dissolve the DNA into 250 µl of 10 mM Tris-HCl pH 8.

2.13.3 DNA digestion

After preparation of DNA samples, 1-2 µg of DNA preps are quantified using a DNA fluorimeter or using standard gel electrophoresis. An aliquot of sample, corresponding to 10µg of total DNA, is digested with 100 U of the appropriated restriction enzyme and subjected to neutral-neutral 2D gel electrophoresis.

After the restriction digestion (from 5h to 16h), DNA is precipitated by adding 1/8 volume of KAc 2.5M and 2V of Isopropanol, kept for al least 1 h on the bench and centrifuged 1h at maximum speed at 15°C. The DNA then is washed with 0.5ml of ice cold EtOH 70% and re-suspended in 20µl of 10 mM Tris-HCl pH 8.

2.13.4 2D-gel procedure

Prepare a 0.35% agarose gel without ethidium bromide (US Biological-LOW EEO) in

fresh TBE1X and fill an appropriate gel tray in cold room (we routinely use apparatus WxL=20x25). Wait 1 h, and put the gel in the box at room temperature containing a suitable volume of TBE1X for at least 30'. Handle the gel very carefully because it is very fragile. Load the DNA samples and a molecular weight DNA marker, leaving one empty well in between each sample and run the gel at constant low voltage (50 V, c.a. 1V/cm) for 24 h.

Stain the gel in TBE 1X with 0.3µg/µl ethidium bromide for 30 min. Use a big knife to cut out the gel lanes under a UV trans-illuminator with the aid of a ruler. If the fragment of interest is for example an origin of replication contained in a 5kb restriction fragment, the gel slice will contain all DNA molecules ranging from 5kb up to 10kb. The intermediates with a complex shape, such as bubbles and joint molecules, migrate up to 10 kb; hence, we recommend to cut a piece larger than is expected just based on the molecular weight of the fragment; generally, we manage slices from 9.5 to 6.5 cm for DNA fragment ranging from 3-6 kb. With the aid of a flexible piece of plastic, rotate gel slices by 90° before put them in the second dimension gel try. It is possible to use an apparatus of the same size of the one used for 1st dimension and set 4 to 6 slices, depending on their dimension. At the same time, prepare a 0.9% agarose gel in TBE1X, with ethidium bromide 0.3µg/µl. Pour the gel, this time at room temperature, around the gel slices and wait 1h for solidification. Put the tray in gel box with an appropriate volume of TBE1X containing 0.3µg/µl ethidium bromide and run at constant high voltage in a cold room with the following settings: 100V 30' and 150V 15 h (limiting current: 150 mA).

During the run, linear DNA molecules will distribute along a characteristic arc that is visible under a UV lamp. When DNA molecules with lower molecular weight reach the bottom of the gel, stop the run and, using the knife, cut gel pieces 10x20 cm containing 2 or 3 DNA samples.

2.13.5 Southern blot

Revert the psoralene crosslinking by irradiating the gel for 10 minutes with 265 nm UV lamps in a Stratalinker (Stratagene) and proceed with the blotting (see Southern blot procedure described in paragraph 2.15).

The signals are analyzed using Typhoon scanner (GE Healthcare) and eventually quantified using Image Quant program.

2.13.6 Quantification of replication intermediates

It is possible to quantify the 2D gels signals using the Image Quant software (GE Healthcare). This tool allows the numeric quantification of the radiolabelled signals of specific and selectable regions after the acquisition by the Typhoon scanner (GE Healthcare).

Quantification of X-shaped intermediates, generating the spike/cone signals in Figure 3.5A, reported in Figure 3.5C, has been generated in the following way.

For each time point, areas corresponding to the monomer spot (M), the X-spike/cone signal (X) and a region without any replication intermediates as background reference were selected and the signal intensities (SI) in percentage of each signal were obtained. The values for the X and monomer were corrected by subtracting from the SI value the background value after the latter was multiplied for the ratio between the dimension of the area for the intermediate of interest and for background. Thus, the values for X and M were calculated in the following way:

$$X = SI(Xs) - \frac{SI(backgroud) * A(Xs)}{A(background)}$$

$$M = SI(M) - \frac{SI(backgroud) * A(M)}{A(background)}$$

The relative signal intensity for the X was then determined by dividing the value for X with the sum of the total signals (the sum of the X and monomer values).

$$Spike\ cone\ \ signal = \frac{X}{X + M}$$

The same method was used to quantify the signal of the tip of the spike arc, generated by the converged forks at the RFB of the ribosomal DNA, showed in Figure 3.26A. The signals were normalized against the intensity of their corresponding monomer spots and were then reported into the histogram as values relative to the wild type signal.

2.14 Pulse Field Gel Electrophoresis (PFGE)

Pulse Field Gel Electrophoresis (PFGE) is a technique that allows the separation of large DNA molecules (up to several million base pairs in length), thanks to periodical changes in the direction of the electric field applied during the run.

Intact cells are immobilized in agarose and treated to disrupt the cell walls and remove cellular proteins; in this way agarose plugs containing the genomic DNA are obtained, avoiding the fragmentation caused by the manipulation of naked DNA. Agarose-embedded DNA is then subjected to electrophoretic run and fully replicated chromosomes enter into gels and can be separated according to their size, while replicating chromosomes are retained into the wells.

DNA isolation in agarose plugs

1. 50 ml of 5 x 10^6 / 1 x 10^7 cells/ml are fixed with 0.1 % Sodium Azide in ice for at least 40'.

2. Spin down cells in 50 ml falcon tube by centrifugation at 4000 rpm for 5' at 4°C.

3. Wash cells with ice cold water.

4. Resuspend cells in 10 ml of ice cold Buffer 1 (Tris-HCl 10 mM pH 7.5, 50 mM EDTA/NaOH pH 8)

5. Spin down cells by centrifugation, resuspend them in 1 ml of Buffer 1 and transfer in 2 ml Eppendorf tubes.

6. Spin down cells by centrifugation at 4000 rpm for 1' at 4°C and remove supernatant with a pipette.

7. Resuspend cells in 300 or 400 μl of ZYMOBUFFER (50 mM Phosphate Buffer pH 7, 50 mM EDTA) and pre-warm cells in a thermoblock at 37°C for about 5'.

8. Mix gently the cells with an equal volume of 1.5% agarose (Pulsed Field Certified Agarose, Bio-Rad), previously melted and stored in waterbath at 50°C.

9. Quickly fill the plugs mold using an aliquot of 90 μl of cell/agarose mix for each plug.

10. Leave the molds at 4°C for at least 40' in order to allow blocks to solidify.

11. Eject plugs in 50 ml falcon tubes and containing 5 ml of ZYMOBUFFER supplemented with 10 mM DTT and 0.2 mg/ml zymolyase (100U/ml).

12. Leave at 37°C ON in a waterbath.

13. Gently remove the buffer and add the Lysis Buffer (Tris-HCl 100 mM pH 7.5, 200 mM EDTA, 1% sarkosyl, 2 mg/ml proteinase K)

14. Leave at 42°C for 24-48 hours.

15. Gently discard the Lysis Buffer, wash the plugs twice with 10 ml of Buffer 1.

16. Resuspend the plugs in Tris-HCl 50 mM pH 7.5 containing 0.5 mg/ml RNAse.

17. Incubate at 37°C ON.

18. Discard the buffer and wash 2 times with 10 ml of Buffer 1 for 1 hour.

19. Resuspend the plugs in 5 ml of Buffer 1.

Gel & run conditions

20. Use 150 ml of 0.5X TBE to prepare a 0.8% or 1 % agarose gel (Agarose Low EEO, USBiological), using a one-tooth to obtain one big well.

21. Using a spatula put the plugs in the well and seal them using 0.5% agarose gel.

22. Install the gel in the electrophoresis tank of the Amersham gene navigator system, filled with pre-cooled running buffer (3 liters of 0.5X TBE).

23. Run conditions:

> Run condition used to detect chromosome III fragmentation (1 % agarose gel):

165 V, 30 seconds pulses step wise, 24 h (water bath at 4°C).

> Run conditions used to detect chromosome XII size (0.8 % agarose gel):

100 V, 68 h, with pulses times ramping from 300 to 900 seconds (water bath at 10°C).

24. After electrophoresis, stain the gel with 0,5 μg/μl ethidium bromide in 0.5X TBE for 30'.

25. Gels are then subjected to Southern Blot and hybridized using specifically genomic probes (see Southern blot procedure described in paragraph 2.15).

2.14.1 DNA digestion in agarose plugs

DNA-contained in agarose plugs can be digested, as well as DNA in solution, and separated using standard electrophoresis technique if the resulting DNA fragments are small enough.

a. Cut each plugs in two equal parts with a razor blade.

b. Wash twice the half-plug with 1 ml of Tris-HCl 10 mM pH 8 for 30' with gentle agitation.

c. Carefully remove the buffer and wash the plug with 400 ml of required digestion buffer (1X) (NEB) for 30' with gentle agitation to equilibrate the agarose-embedded DNA in endonuclease digestion conditions.

d. Remove the buffer and add 200 ml of the required digestion mix, containing 100 U of the appropriate restriction enzyme, and incubate O/N at 37°C.

e. Following the restriction endonuclease digestion, wash two times with 1 ml of Tris-HCl 10 mM pH 8 for 30' with gentle agitation.

f. Equilibrate the agarose-embedded DNA with 1 ml of TBE 1X for 30' on a rotating wheel.

g. Using a spatula put the plugs in the well of 0.8% or 1 % agarose gel (Agarose Low EEO, USBiological in TBE1X) and seal them using 0.5% agarose gel.

h. Run at 100V in TBE1X for the appropriate time.

i. Gels are then subjected to Southern Blot and hybridized using specifically genomic probes (see Southern blot procedure described in paragraph 2.15).

2.15 Southern blot hybridization

Southern blot

Depurinate the gel 30 min in 0.25N HCl, denaturate 30 min in 0.5M NaOH, 1.5M NaCl and finally neutralize for 30 min in 1M $AcNH_4$, 0.02M NaOH.

Transfer the gel in standard Southern Blot conditions using Gene Screen (Perkin Elmer) membrane in SSC10X for an over night. Remove the membrane from the gel, wash it with SSC5X and fix the DNA onto the membrane by UV irradiation (autocrosslinking program, with 265 nm UV lamps on *Stratalinker*).

DNA probes

The membranes are subjected to hybridization with a radiolabel probe of interest. Probes were amplified by PCR reactions on genomic DNA using the indicated oligonucleotides.

***ARS305* probe**
Fw: GGCAATATATGAATGCAGTGC
Rw: GTTGGTAGCACTTTGATGAGG

***YCLO44C* probe**
Fw: TGGAATTGATGAGTTCAATGG
Rw: GTAATAGCAATTCCACCGACC

Ribosomal DNA (probe for the BglIIB fragment)
Fw: GTTGATCGGACGGGAAACGGTG
Rw: GTGACAGGTGCCCCGGGTAACCC

$tRNA^A$ (*HIS2* probe)
Fw: TCCTCGAGGTCATGCACTCACACCATTCACAC
Rw: CAGATGCGGCCGAGTCGGCGAGCAAACAGGG

***TEF2* probe**
Fw: CAGAGATGATCGAGCCGGTAG
Rw: CCTGGCTTGATGACACCGG

***CEN12* probe**

Fw: GCATAAAAATTTGTTTTCGGGG

Rw: ATCAGATTTTTCACTGGGCG

***CEN14* probe**

Fw: GATATCTGCGTTTAGGCGCC

Rw: CCACCATTTATGAAGTTGCCCC

Poly(GT) telomere-specific probe

Poly(GT) probe was obtained from the EcoRI-digested plasmid pSP100, followed by gel extraction using the Wizard SV Gel and PCR Clean-Up system (Promega).

Hybridization of the filters

50 ng of purified DNA probe is labeled with 50 μCi of α^{32}P dCTP using a random prime kit (prime-a-gene labelling kit (Promega).

Boil the DNA probe with water for 10min before adding the rest of the reagents:

- 12 μl DNA (50 ng)
- 30.4 μl H_20
- 10 μl Labeling Buffer 5X
- 2 μl BSA
- 0.7 μl dATP (20 μM)
- 0.7 μl dTTP (20 μM)
- 0.7 μl dGTP (20 μM)
- 1 μl DNA Polymerase I Large (Klenow) Fragment 100U/ml
- 2.5 μl of α^{32}P dCTP (50 μCi)

Incubate at RT for at least 1 hour to allow incorporation of the radioactive nucleotides in the DNA fragments.

The reaction is then passed through ProbeQuant™ G-50 Micro Columns (GE Healthcare) to remove the non-incorporated nucleotides. During the preparation of the radiolabelled probe, the membranes are rinsed with water and pre-hybridized with 20-30 ml of PerfectHyb™ Plus Hybridization Solution (SIGMA) for at least 1 h at 65°C in a rotating tube. The labeled probe is boiled 10 min at 95°C and added to pre-hybridization mix. The

hybridization is prolonged at 65°C over night.

The filters are washed for 30’ with ~100 ml 2X SSC, 1% SDS at 65°C in a rotating tube and two times (30’ each) with ~500 ml 2X SSC, 1% SDS at 65°C in a tray with agitation. The hybridized membranes are briefly airdried, covered with saran wrap and expose to a storage phosphor screen in an appropriate cassette.

The signals are analyzed using Typhoon scanner (GE Healthcare) and eventually quantified using ImageQuant program.

2.16 Transmission electron microscopy

Analysis of replication forks by transmission electron microscopy has been performed as described (Neelsen et al., 2014).

3. Results

3.1 Rad53 counteracts Rrm3/Pif1-mediated fork reversal and chromosome fragmentation under replication stress

3.1.1 Rrm3 and Pif1 associate with the forks following replication stress in a Rad53-independent manner

We investigated whether Rrm3 and Pif1 associate with forks in the presence of HU, in a Rad53-dependent manner, using the Chromatin Immunoprecipitation on chip (ChIP on chip) (Bermejo et al., 2009a; Bermejo et al., 2009b) and in parallel ssDNA-BromodeoxyUridine Immunoprecipitation on chip (ssDNA BrdU-IP on chip) was used to visualize the newly synthesized DNA (Bermejo et al., 2009b; Katou et al., 2003). We compared the Pif1 and Rrm3 binding sites with those of DNA polymerase α, 90 minutes from the G1 release in 150 mM HU, in WT *RAD53* background or in *rad53Δ* cells (Figure 3.1). Polα clusters co-localized with BrdU peaks, generated by forks emanating from active origins (Figure 3.1A). The average binding signals of Polα, to a 40 kbps window centered on 141 active ARSs (Figure 3.1C), exhibited a bimodal distribution in *sml1Δ* cells due to the advancements of the two sister forks from the origins, while in *sml1Δ rad53Δ* cells the binding signals were more centered on the origin point due to impaired fork progression. Moreover, compared to the WT condition, we observed a decrease in the average Polα binding (2.86 folds less) and in BrdU incorporation (2.21 folds less) in the absence of *RAD53* on 141 active ARSs (Figure 3.1B,C), which likely reflects the extensive fork collapse and the replisome dissociation from the stalled replication forks, typical of HU–treated *rad53* cells (Cobb et al., 2005; Lopes et al., 2001; Lucca et al., 2004).

Rrm3 and Pif1 were associated to the same chromosome sites bound by Polα under replication stress, either in the presence or in the absence of Rad53 functions, and their

distributions paralleled the ones of Polα, also at late and dormant origins that were specifically fired in *rad53* cells (Figure 3.1A) (Rossi et al., 2016) (Santocanale and Diffley, 1998; Shirahige et al., 1998). Statistical analysis produced highly significant p-values of genome-wide overlap between Polα, Rrm3 and Pif1 clusters, both in *sml1Δ* and in *sml1Δ rad53Δ* cells, indicating that these three proteins shared the same chromosome binding sites (Figure 3.1A). The average binding signals of the three proteins at 141 early ARSs showed that the distribution of Rrm3 and Pif1 clusters paralleled the ones of Polα in *sml1Δ* cells and even in *sml1Δ rad53Δ* cells (Figure 3.1D,E) (Rossi et al., 2016). While Pif1 and Rrm3 bound with the same magnitude of Polα to the early ARSs in *sml1Δ* cells (Figure 3.1D), in *sml1Δ rad53Δ* the magnitude of their binding was higher than that of Polα binding (Figure 3.1E). These observations suggest that additional binding sites for the two DNA helicases may be created at collapsing forks of *rad53* cells treated with HU, leading to an additional recruitment of Rrm3 and Pif1 at inactivated forks.

To further validate these data and to check if the results were dependent upon the Rad53 kinase activity, we performed the same kind of analysis in wild type strain and in cells carrying the kinase-dead mutant allele *rad53-K227A*, released in 150 mM of hydroxyurea for 90 minutes (Figure 3.2). In line with the previous experiment (Figure 3.1), we observed a bimodal distribution of the average binding signals of Polα and Rrm3 around 141 active *ARS*s in the wild type strain (Figure 3.2B), even if the two sister forks emanating from early replication origins progressed less compared to the *sml1Δ* background in which the levels of dNTPs is 2.5 folds higher (Zhao et al., 1998). Rrm3 binding sites co-localized with the ones of Polα, in a statistically significant way, in wild type strain (p-value = 6.1E-50) and also in *rad53-K227A* mutant (p-value = 6.6E-117), in which we observed a great reduction of Rrm3 and Polα binding due to the DNA replication fork collapse (Figure 3.2A,B). Surprisingly, while the magnitude of Rrm3 binding to 141 early ARSs is higher than Polα magnitude in *sml1Δ rad53Δ* cells (Figure 3.1E), Rrm3 and Polα bind inactivated

forks of *rad53-K227A* cells with the same magnitude (Figure 3.2B). This evidence could suggest that deletion of *RAD53* induces a more penetrant phenotype on the collapsing forks, which leads to the formation of additional substrates and induces additional Pif1 and Rrm3 recruitments.

Binding of Polα, Rrm3 and Pif1 around the *ARS305* origin in *rad53-K227A* and *sml1Δ rad53Δ* mutants was confirmed by ChIP-qPCR (Figure 3.3A,B).

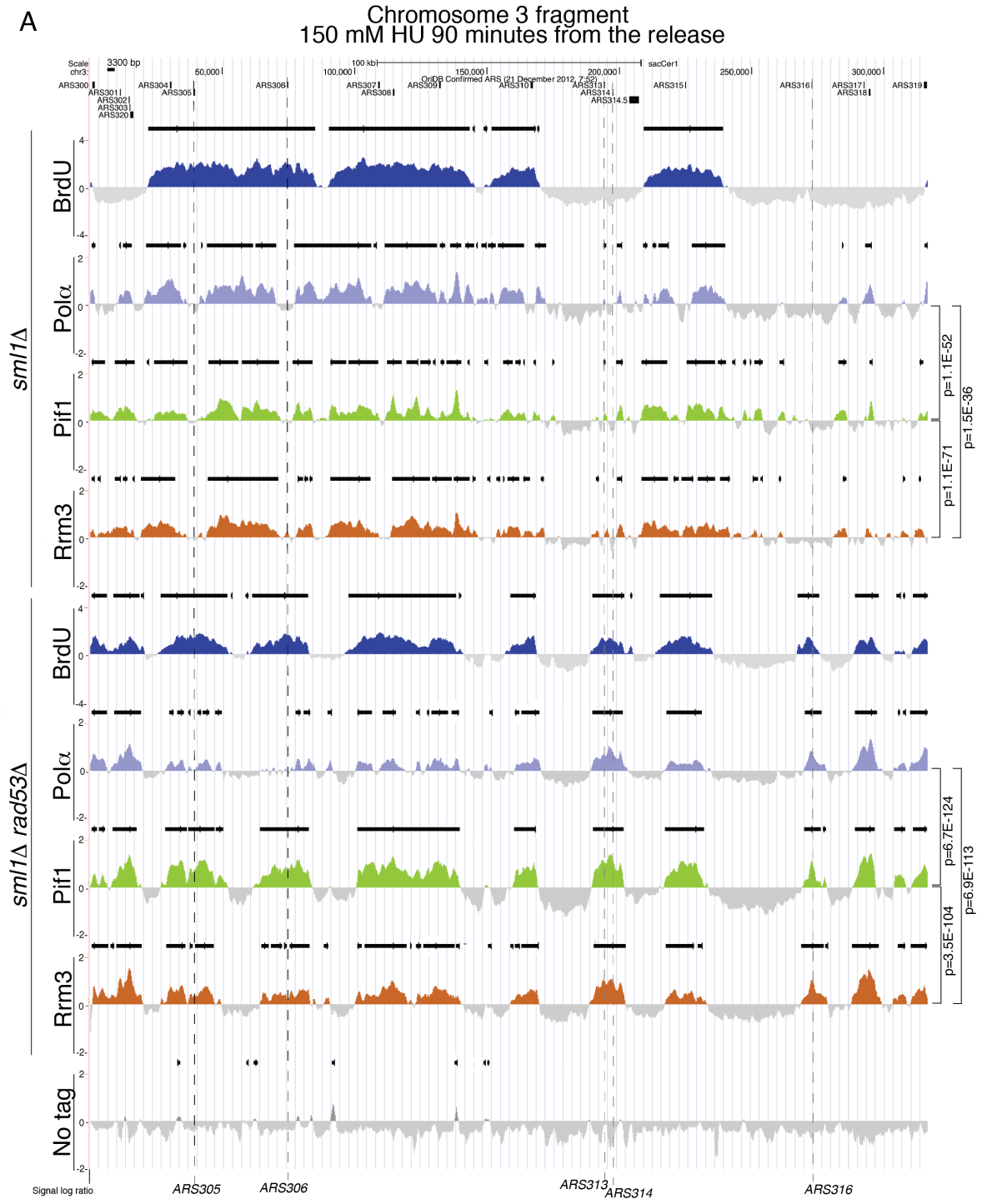

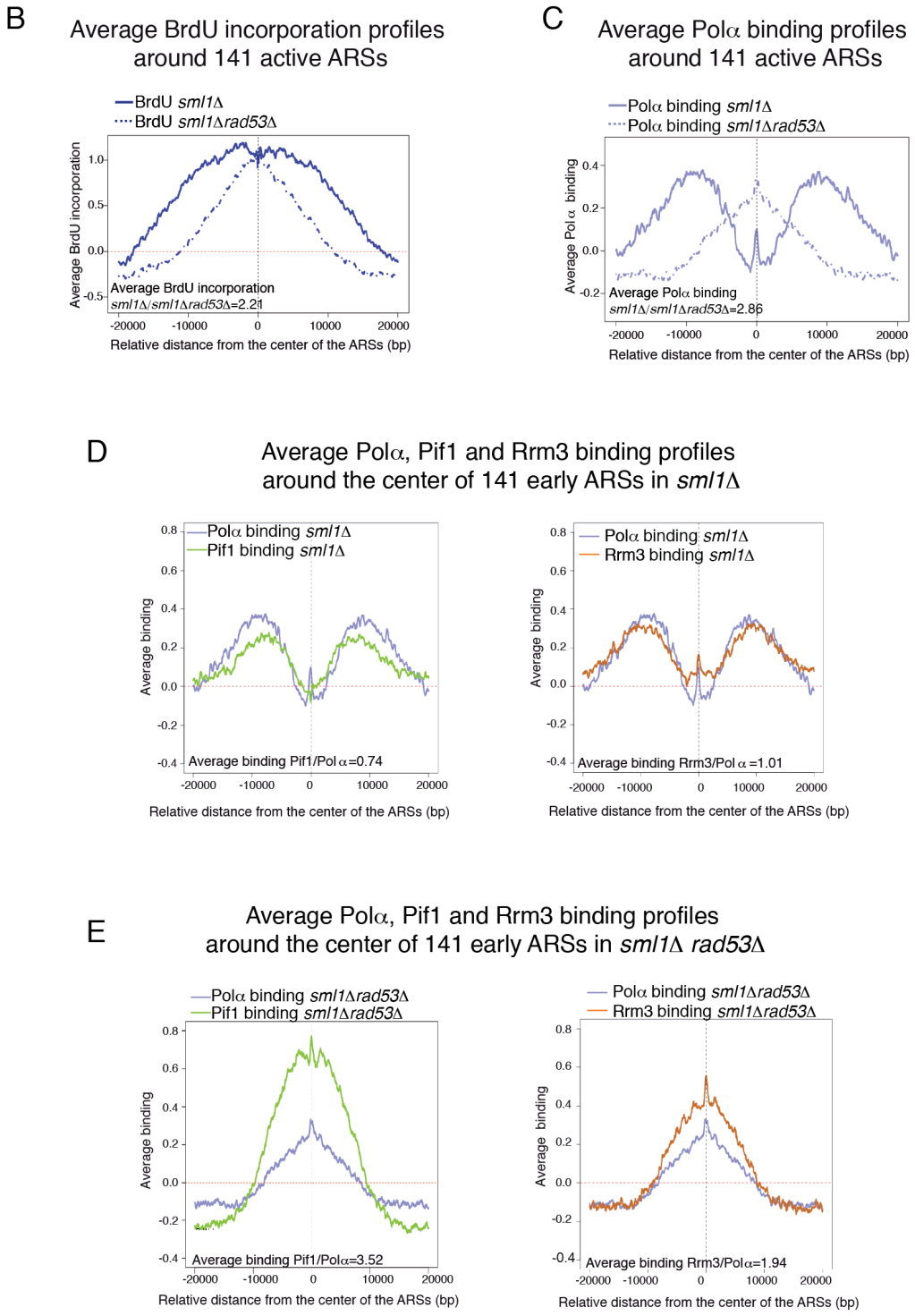

Figure 3.1. Rrm3 and Pif1 associate with stalled DNA replication forks independently of *RAD53*. A) BrdU incorporation (dark blue) and Polα-Flag (light blue), Rrm3-Myc (orange) and Pif1-Flag (green) binding profiles were determined, respectively, by ssDNA-BrdU IP on chip and ChIP on chip in the strains CY12488, CY13284, CY12470, CY13074, CY12493, CY13282, CY12422 and CY13073 released from G1 into S-phase in the presence of 150 mM of HU for 90 min. Dashed black lines indicate early (*ARS305* and *ARS306*) and dormant (*ARS313, ARS314* and *ARS316*) origins. Black horizontal bars above the binding profiles indicate the statistically significant binding or BrdU clusters. A black scale bar indicates the distance corresponding to 3300 base pairs (bp) on the chromosome III map. The y axis show the signal log2 IP/SUP ratios, which express enrichments in the IP fractions and are related to the magnitude of protein-DNA bindings or BrdU incorporations in the reported chromosome III region. p-values of the significance of the

genome-wide overlap between the considered protein clusters are indicated. **B)** Average BrdU incorporation profiles in *sml1Δ* and *sml1Δ rad53Δ* cells in a window of 40 kbps centered on 141 ARSs have been determined in the experiment shown in panel A. The ratio of average BrdU incorporation signals in *sml1Δ* versus *sml1Δ rad53Δ* cells around 141 ARSs is 2.21. **C-D-E)** The profiles in the graphs express the average of the ChIP on chip binding signals, from the experiment shown in panel A, for the indicated proteins in a window of 40 kbps centered on each of the 141 early active DNA replication origins in *sml1Δ* and *sml1Δ rad53Δ* cells (see Materials and Methods). Ratio of indicated total average binding signals is reported in each graph.

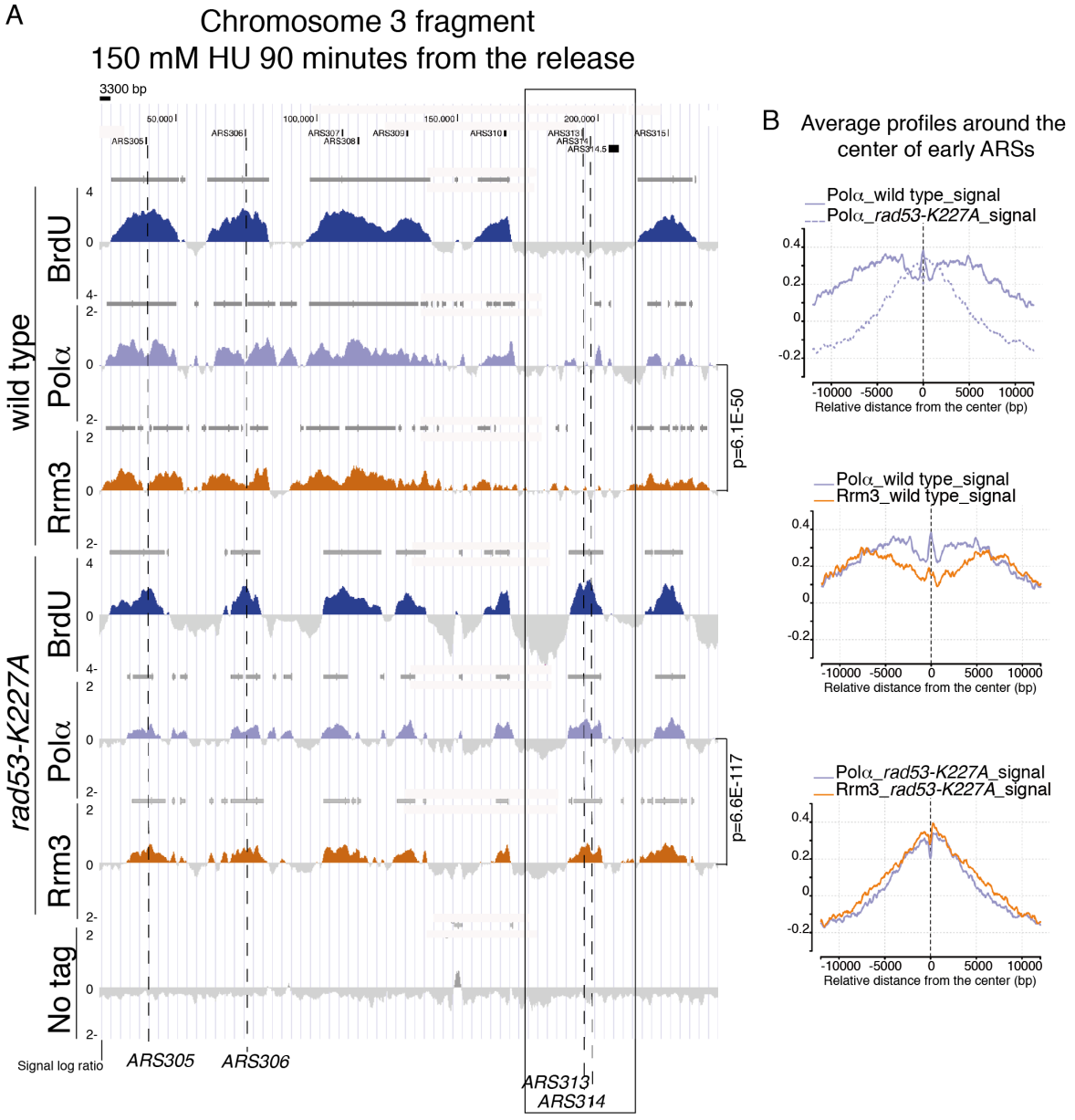

Figure 3.2. Rrm3 association with stalled DNA replication forks does not require Rad53 kinase activity. A) Rrm3-13Myc (orange) and Polα-9Myc (light blue) binding profiles were determined in CY11360, CY12425, CY12927 and CY12698 strains, released from G1 into S-phase in the presence of 150 mM HU for 90 min. BrdU-chip profiles were determined in strains CY12512, CY12527. Dashed black lines indicate early (*ARS305* and *ARS306*) and dormant (*ARS313* and *ARS314*) origins. Dark grey horizontal bars above the binding profiles indicate the statistically significant binding or BrdU clusters. A black scale bar

indicates the distance corresponding to 3300 base pairs (bp) on the chromosome III map. The y axis show the signal log2 IP/SUP ratios, which express enrichments in the IP fractions and are related to the magnitude of protein-DNA bindings or BrdU incorporations in the reported chromosome III region. p-values of the significance of the genome-wide clusters overlap are reported. **B)** The profiles in the graphs express the average of the ChIP on chip binding signals, from the experiment shown in panel A, for the indicated proteins in a window of 24 kilobases centered on each of the 141 early active DNA replication origins in the indicated genetic backgrounds (see Materials and Methods).

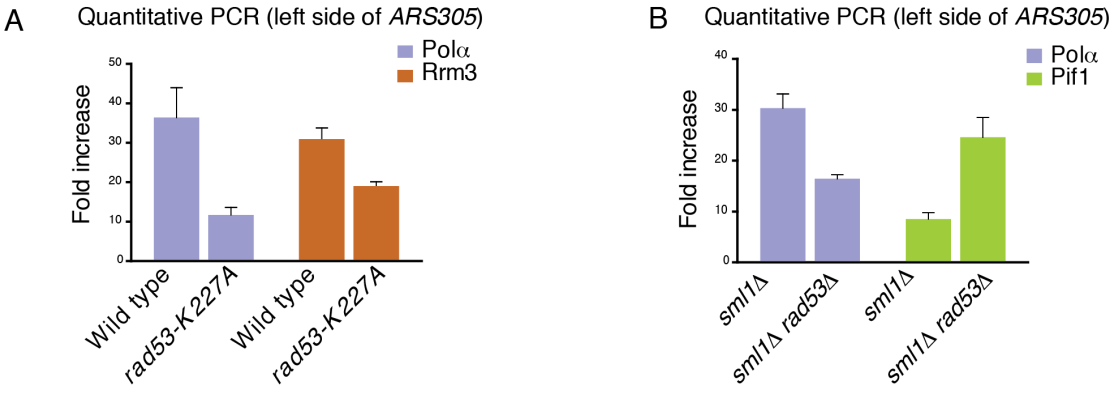

Figure 3.3. DNA polymerase α dissociates from the stalled DNA replication forks in *rad53* mutants. A) The magnitude of Polα and Rrm3 binding to the chromosomes in S-phase was determined in the experiment shown in Figure 3.2A by quantitative ChIP-qPCR, in wild type and *rad53-K227A* strains. The protein binding was monitored in a region located 6 kb upstream the *ARS305* which contained the majority of the replication forks in this experimental condition. **B)** The magnitude of Polα and Pif1 binding was determined in the experiment shown in Figure 3.1A by quantitative ChIP-qPCR, in *sml1Δ* and *sml1Δ rad53Δ* cells, on a region located 9.2 kb upstream the *ARS305* due to the longer advancement of replication forks in strains carrying the deletion of *SML1*. Showed data (A-B) represent the mean ±SD of three independent experiments.

We performed the same kind of analysis on G1-synchronized cells, released for 45 minutes in the presence of low dose of HU (25 mM) (Figure 3.4), a condition that allowed more fork progression compared with the previous experiments performed in the presence of 150 mM HU (Figures 3.1,3.2).

As revealed by the highly significant p-values of genome-wide clusters overlap, also at low HU concentrations, Rrm3 and Pif1 binding clusters co-localized with the ones of Polα in a statistically significant way (Figure 3.4), in *sml1Δ* cells and also in *sml1Δ rad53Δ* cells, in which the DNA replication fork progression was impaired (Lopes et al., 2001; Sogo et al., 2002).

Altogether these observations suggest that, under replication stress, Rrm3 and Pif1 likely associate with the replisome, the fork or both and that the distribution of the binding clusters of Rrm3 and Pif1 is not altered by the absence of *RAD53*.

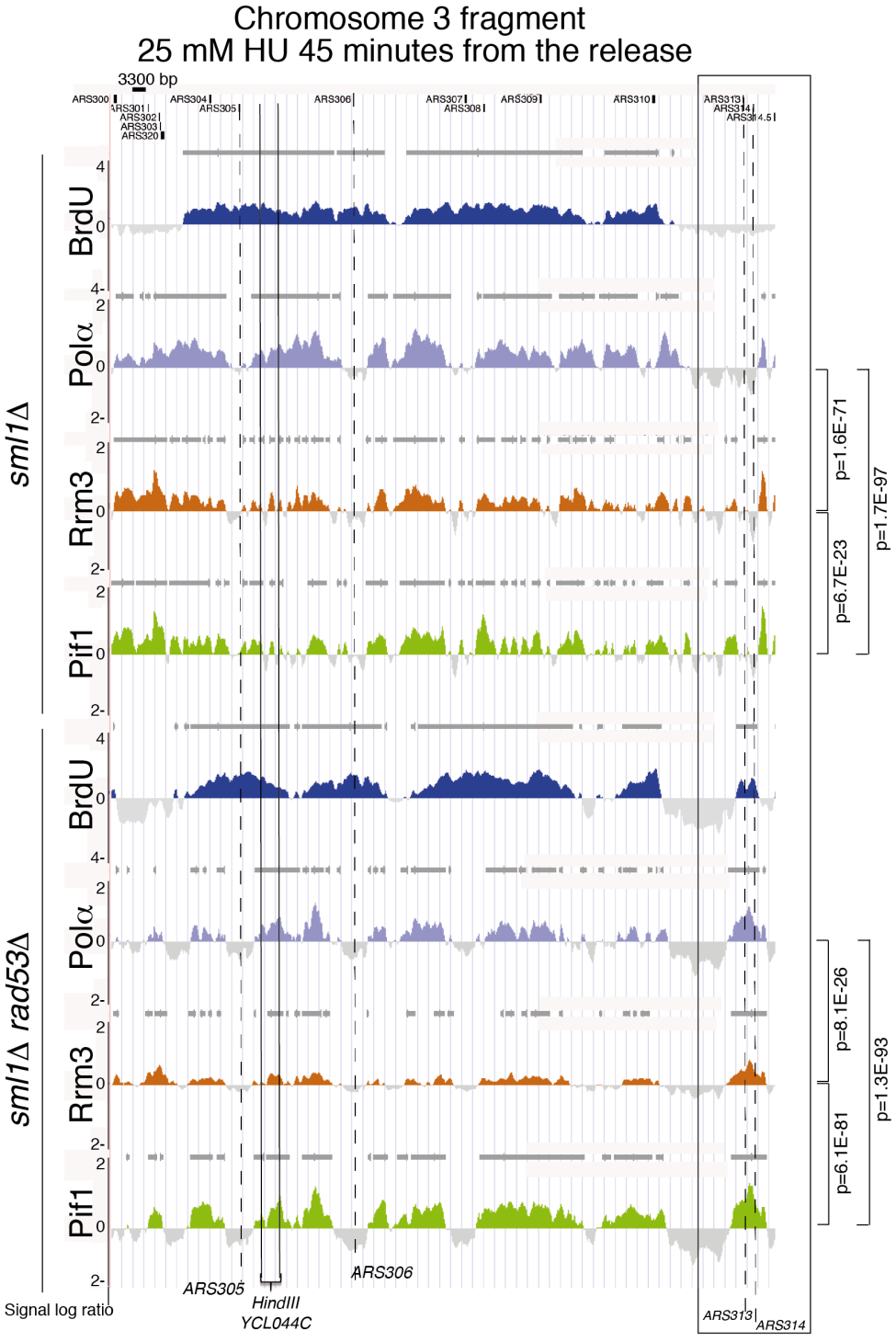

Figure 3.4. Rrm3 and Pif1 associate and move with the DNA replication forks in the presence of low HU concentrations and are loaded on the dormant DNA replication origins, which are fired in *rad53* mutants under replication stress. Polα–Flag (light blue), Rrm3-Myc (orange) and Pif1-Flag (green) binding profiles were determined in strains CY13284, CY13282, CY12470, CY12422, CY13074 and

CY13073 following the G1 release into S-phase in the presence of 25 mM HU for 45 min. BrdU-chips profiles (blue) were determined in strains CY12488 and CY12493. Dashed black lines indicate early (*ARS305* and *ARS306*) and dormant (*ARS313* and *ARS314*) origins. Grey bars indicate statistically significant binding or BrdU clusters. p-values of the genome-wide overlap of the considered protein clusters are indicated. The position of the HindIII-*YCL044C* restriction fragment, analysed by 2D gel in Figure 3.5, is shown on the ChIP on chip maps.

3.1.2 Fork abnormalities in *rad53* mutants treated with HU depend on Rrm3 and Pif1

Since it has been reported that Pif1 is phosphorylated in HU (Makovets and Blackburn, 2009), that hPIF1 and *Sc*Pif1 can unwind replication fork like substrates *in vitro* (George et al., 2009; Lahaye et al., 1993) and since we have found that Pif1 and Rrm3 bind stalled replication forks even in the absence of Rad53, we investigated whether Rrm3 and Pif1 influence the fate of the forks in *rad53* cells following replication stress. In order to test this hypothesis, we ablated *RRM3* and the *PIF1* nuclear form, using the *pif1-m2* allele, which retains only the mitochondrial isoform of Pif1 (Schulz and Zakian, 1994), in *sml1Δ* and *sml1Δ rad53Δ* strains; we released the resulting strains from G1 in 25 mM of hydroxyurea for 90 minutes and we analysed the replication intermediates accumulating in the HindIII-*YCL044C* genomic fragment (positioned around 5kb on the right side of the *ARS305* origin and indicated in Figure 3.4) through neutral-neutral 2D gels after *in vivo* chromatin psoralen-crosslinking (Figure 3.5) (Liberi et al., 2006).

From the experiment reported in Figure 3.4 we observed that, 45 minutes from the G1 release in 25 mM HU, the majority of the forks in *sml1Δ* cells had already passed through the *YCL044C* locus (as shown by the distribution of Polα binding clusters on the right side of *ARS305*), while in *sml1Δ rad53Δ* most forks were still localized within the *YCL044C*-containing fragment. In line with these observations, we failed to visualize replication intermediates in the *RAD53* WT set of strains (Figure 3.5A, upper panels), while *sml1Δ rad53Δ* cells exhibited a strong 2D gel signal, characterized by the presence of the Y-arc, generated by the rightward moving forks emanating from the *ARS305*, and the spike-cone

signal, which corresponds to the formation of cruciform intermediates (also called reversed forks) and their derivatives (Figure 3.5A, yellow arrow) (Bermejo et al., 2011; Doksani et al., 2009; Lopes et al., 2001). The deletion of *RRM3*, or the ablation of *PIF1*, only partially suppressed fork abnormalities in *rad53* mutants (Figure 3.5A,C). Interestingly, in the quadruple mutant *sml1Δ rad53Δ rrm3Δ pif1-m2* the spike-cone signal was almost completely abolished (Figure 3.5A,C). Since in the quadruple mutant both large Ys and X shaped molecules were less abundant, due to forks movement outside the analysed *YCL044C* locus, to confirm our data we analysed by 2D gels, the replication intermediates accumulated in the same genomic locus at earlier time points in *sml1Δ rad53Δ* and in *sml1Δ rad53Δ pif1-m2 rrm3Δ* cells (Figure 3.5D). We found that the cruciform structures were under-represented throughout the kinetic in the *sml1Δ rad53Δ pif1-m2 rrm3Δ* strain while they accumulated, as expected, in *sml1Δ rad53Δ* (Figure 3.5D). These data suggest that the combined absence of Pif1 and Rrm3 suppressed, not only the accumulation of reversed forks, but also the DNA replication fork block induced by HU in *rad53* mutants; indeed FACS profiles showed that the quadruple mutant almost completed the S-phase within 90 minutes after the release in HU (Figure 3.5A, red arrow), like the *sml1Δ* set of strains, while *sml1Δ rad53Δ* cells remained blocked in early S-phase (Figure 3.5A).

To further verify that Rrm3 and Pif1 ablations suppress DNA replication fork stalling in *rad53* mutants under replication stress, we analysed the Polα binding clusters at 60 minutes from the G1 release in 150 mM of HU in *sml1Δ rad53Δ* and *sml1Δ rad53Δ pif1-m2 rrm3Δ* cells (Figure 3.6). According to our data obtained by 2D gels, Polα clusters (which marked the position of the replisomes) remained very close to the replication origin *ARS305* in *rad53* mutants, while they were localized more far away from the same DNA replication origin in the quadruple mutant as a result of replisome progression. Interestingly, *RRM3* and *PIF1* ablations were able to suppress the fork stalling, but not the

unscheduled origin firing of late and dormant origins typical of *rad53* mutants exposed to replication stress conditions (Figure 3.6, black arrow).

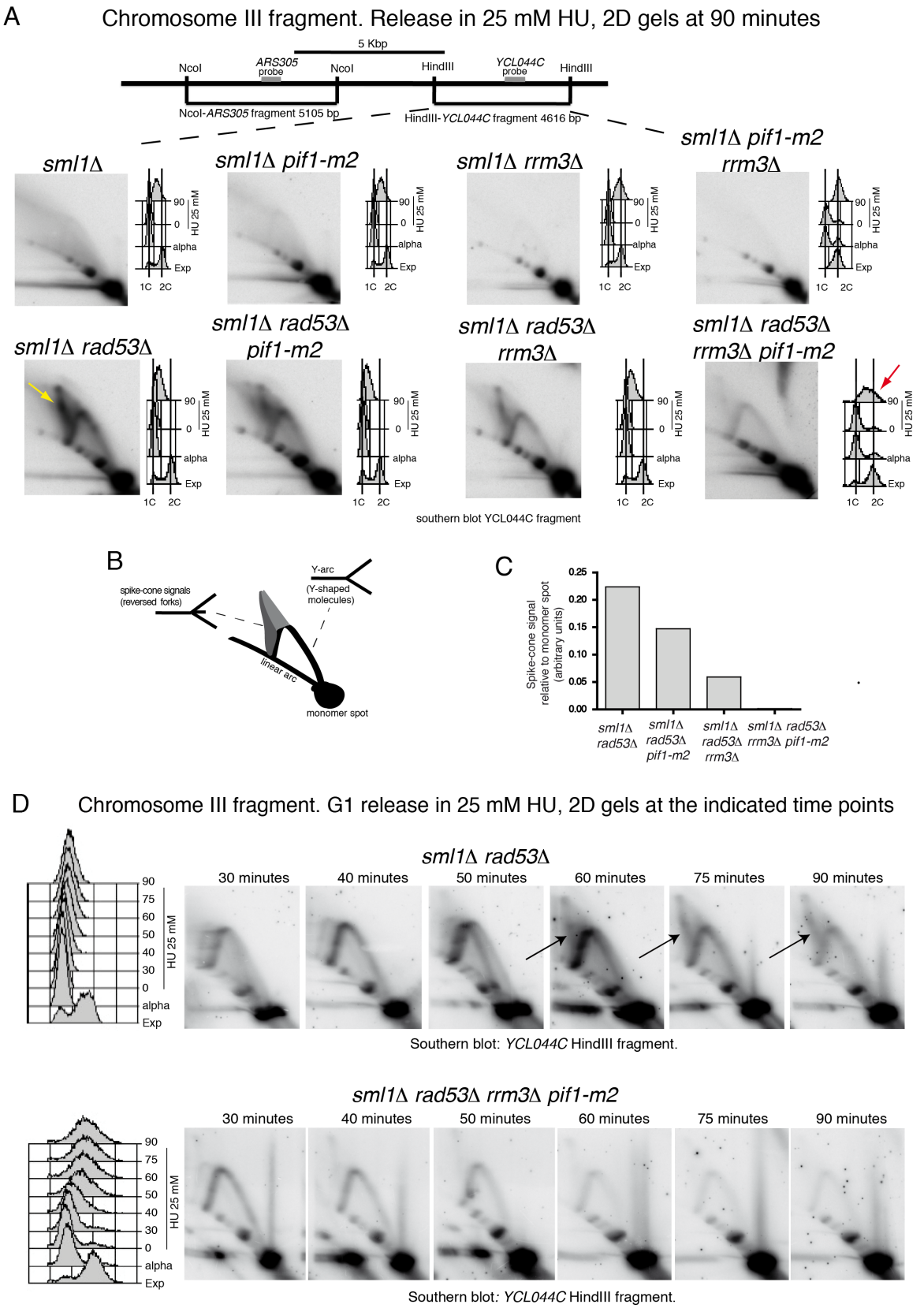

Figure 3.5. Rrm3 and Pif1 synergistically promote fork reversal in *rad53* cells under replication stress.

A) DNA replication intermediates have been analysed by 2D gel electrophoresis after *in vivo* psoralen cross

linking on the HindIII-*YCL044C* fragment, in strains CY12445, CY13331, CY12448, CY13334, CY12443, CY13339, CY12460 and CY13342, released from G1 into S-phase in the presence of 25 mM HU for 90 min. FACS profiles showing the cellular DNA content during the experiments and schematic representation of the 2D signals detectable in this experimental condition **(B)** are shown. The yellow arrow indicates the spike/cone 2D gel signal corresponding to cruciform DNA intermediates accumulating at stalled replication forks in the absence of *RAD53* while the red arrow indicates the cell cycle progression in the quadruple mutant *sml1Δ rad53Δ rrm3Δ pif1-m2.* **C)** Intensities of the spike/cone signals detected in the 2D gels of panel A were normalized against the intensities of their monomer spots and reported into the histogram (a. u.) for the indicated strains. **D)** The strains CY12443 and CY13342 were synchronized in G1 and released into S-phase in the presence of 25 mM of HU. As in panel A, 2D gel profiles of replication intermediates, accumulating at the HindIII-*YCL044C* fragment, and FACS analysis showing the cellular DNA content at the indicated time points are shown.

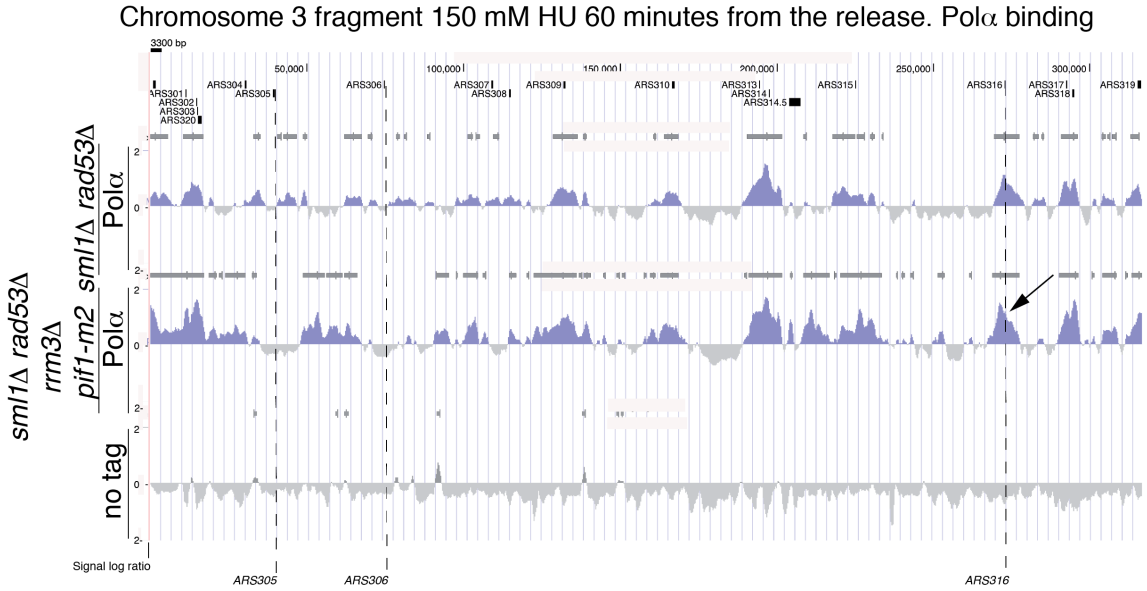

Figure 3.6. Rrm3 and Pif1 promote fork stalling in *rad53* mutants under replication stress. The strains *sml1Δ rad53Δ* (CY13282) and *sml1Δ rad53Δ rrm3Δ pif1-m2* (CY13650) carrying the *POL1-6His-3Flag* allele have been released from G1 into S-phase in the presence of 150 mM HU for 60 minutes. Polα binding profiles (light blue), determined by ChIP on chip and relative to the indicated region of the chromosome III, are shown. Y-axis shows the signal log2 IP/SUP ratio, which expresses the magnitude of protein-DNA binding in the chromosome loci represented. Dark grey horizontal bars above the binding profiles indicate the statistically significant binding clusters. Dashed black lines indicate the positions of the early origins *ARS305* and *ARS306* and the late origin *ARS316*, which is fired (and bound by Polα) in HU only in checkpoint defective cells.

To exclude the possibility that these results were due to alterations in origin firing in *rad53* cells in the absence of the Pif1 helicases, we monitored the kinetics of the firing of the early replication origin *ARS305,* after the G1 release in high concentration of HU, in *sml1Δ*

rad53Δ and *sml1Δ rad53Δ pif1-m2 rrm3Δ* cells by neutral-neutral 2D gels (Figure 3.7). In this condition, the appearance of 2D gel signals in correspondence of the bubble and Y arcs indicated that *ARS305* was fired in the strain analysed. As it can be appreciated in Figure 3.7, there is a difference of 10 minutes in the kinetic of *ARS305* firing between *sml1Δ rad53Δ* and *sml1Δ rad53Δ pif1-m2 rrm3Δ* cells (Figure 3.7, black arrows), which is unlikely to be the cause of the suppression effects observed.

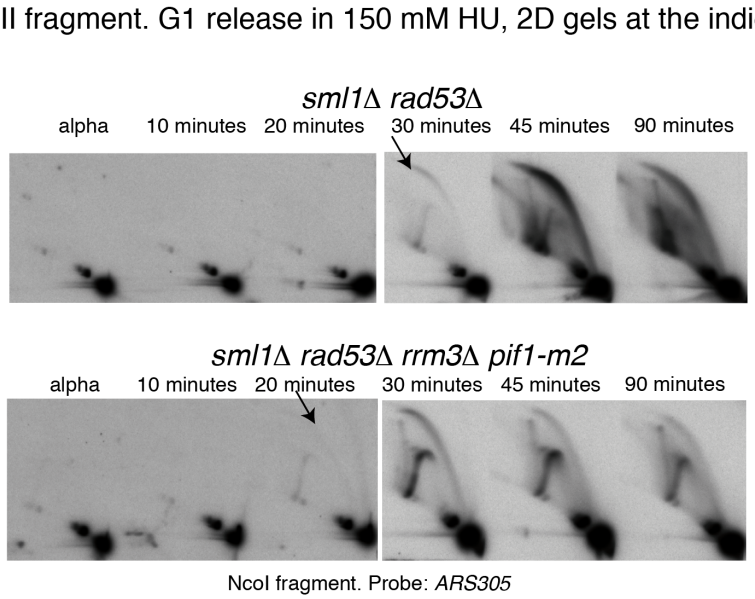

Figure 3.7. *sml1Δ rad53Δ pif1-m2 rrm3Δ* cells fire origins 5-10 minutes earlier that *sml1Δ rad53Δ* cells. Strains CY12443 and CY13342 were arrested in G1 and released into S-phase in the presence of 150 mM of HU. After *in vivo* psoralen cross linking, DNA replication intermediates accumulating on the NcoI-*ARS305* restriction fragment have been analysed by 2D gel electrophoresis at the indicated time points. Black arrows indicate the time points in which *ARS305* is fired as shown by the presence of DNA replication bubbles and Y arc signals that appear in the 2D gels profiles.

3.1.3 Rrm3 and Pif1 promote chromosome fragility in hydroxyurea-treated *rad53* cells

Since low HU concentrations induce late and massive chromosome breakages in *rad53* cells when the replication forks reach replication risk elements, such as the replication slow zones (RSZs) (Cha and Kleckner, 2002; Hashash et al., 2011), we investigated whether the Pif1 helicases contributed to the chromosome fragility of *rad53* cells.

sml1Δ, sml1Δ pif1-m2, sml1Δ rrm3Δ, sml1Δ pif1-m2 rrm3Δ, sml1Δ rad53Δ, sml1Δ rad53Δ pif1-m2, sml1Δ rad53Δ rrm3Δ and *sml1Δ rad53Δ rrm3Δ pif1-m2* strains were released from G1 into 25 mM HU and the migration pattern of chromosome III was analysed by pulsed field gel electrophoresis (PFGE) and southern blotting at the indicated time points (Figure 3.8 A-F). The non-replicating G1 chromosomes were able to enter into the gels, while replicating chromosomes in exponentially growing cells or in HU-arrested cells were retained into the wells. The set of control strains (*sml1Δ, sml1Δ pif1-m2, sml1Δ rrm3Δ, sml1Δ rrm3Δ pif1-m2*) accumulated a basal level of endogenous fragmentation only after 5 hours of HU treatment (Figure 3.8 A,B,C), which was not detectable in *sml1Δ rrm3Δ* cells (Figure 3.8B). Interestingly, *sml1Δ, sml1Δ pif1-m2, sml1Δ rrm3Δ* cells accumulated a strong high molecular weight PFGE signal (HPFGES) (migrating between the wells and the chromosome III signals), at 5 hours from the G1 release in HU (see Figure 3.8 A,B black arrows). The appearance of this HPFGES correlated with the acquisition of the 2C DNA content and, likely, with the late steps of DNA replication or with the beginning of mitosis (see FACS profiles in Figure 3.8 A,B). Importantly, this signal is not present in the G1 samples excluding that it can be due to plugs manipulation during in-agarose isolation of the chromosomal DNA (Figure 3.8 A,B,C). Taking in consideration the kinetics of generation and the migration position of this signal, it likely reflects the accumulation of chromosome entanglements, which arise during late S-phase or mitosis, after DNA replication in the presence of HU. Interestingly, in *sml1Δ rrm3Δ pif1-m2* cells this signal already appeared at 1.5 hours form the G1 release in HU (Figure 3.8C, black arrow), suggesting that in these cells the S-phase is faster and they already reached mitosis at this time point.

In *sml1Δ rad53Δ* cells, the chromosome III migrated into the gel in G1, while, after the release in HU, it was retained into the wells and after 3 and 5 hours form the G1 release in hydroxyurea cells accumulated massive chromosome fragmentation, which was partially

suppressed by the *pif1-m2* or *rrm3Δ* mutations (Figures 3.8D,E,G,H). It is of note that even after 5 hours from the G1 release in HU, chromosome III did not re-enter in the PFGE gel in *sml1Δ rad53Δ, sml1Δ rad53Δ rrm3Δ and sml1Δ rad53Δ pif1-m2* cells (Figures 3.8D,E,G,H). Strikingly, in the quadruple mutant *sml1Δ rad53Δ rrm3Δ pif1-m2,* the chromosome fragmentation was almost completely abolished and chromosome III was fully replicated and re-entered the gel with minimal fragmentation, already 1.5 hours after the G1 release in HU (Figure 3.8F,I). FACS analysis showed that the combined ablation of *RRM3* and *PIF1* allowed *rad53* cells to complete replication and progress into the next cell cycle, while in their presence *sml1Δ rad53Δ* were stuck in S-phase (Figure 3.8F, yellow arrows).

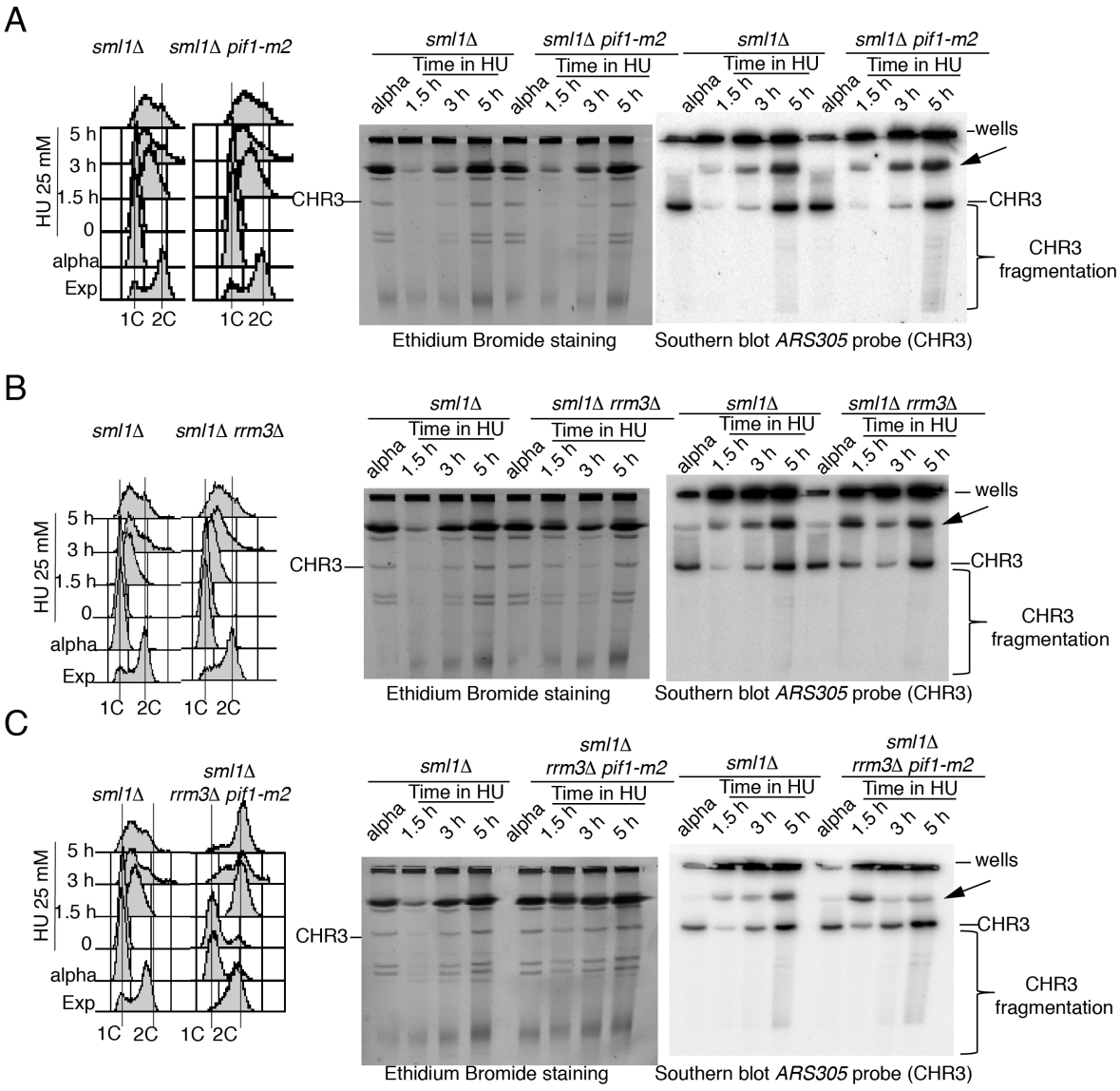

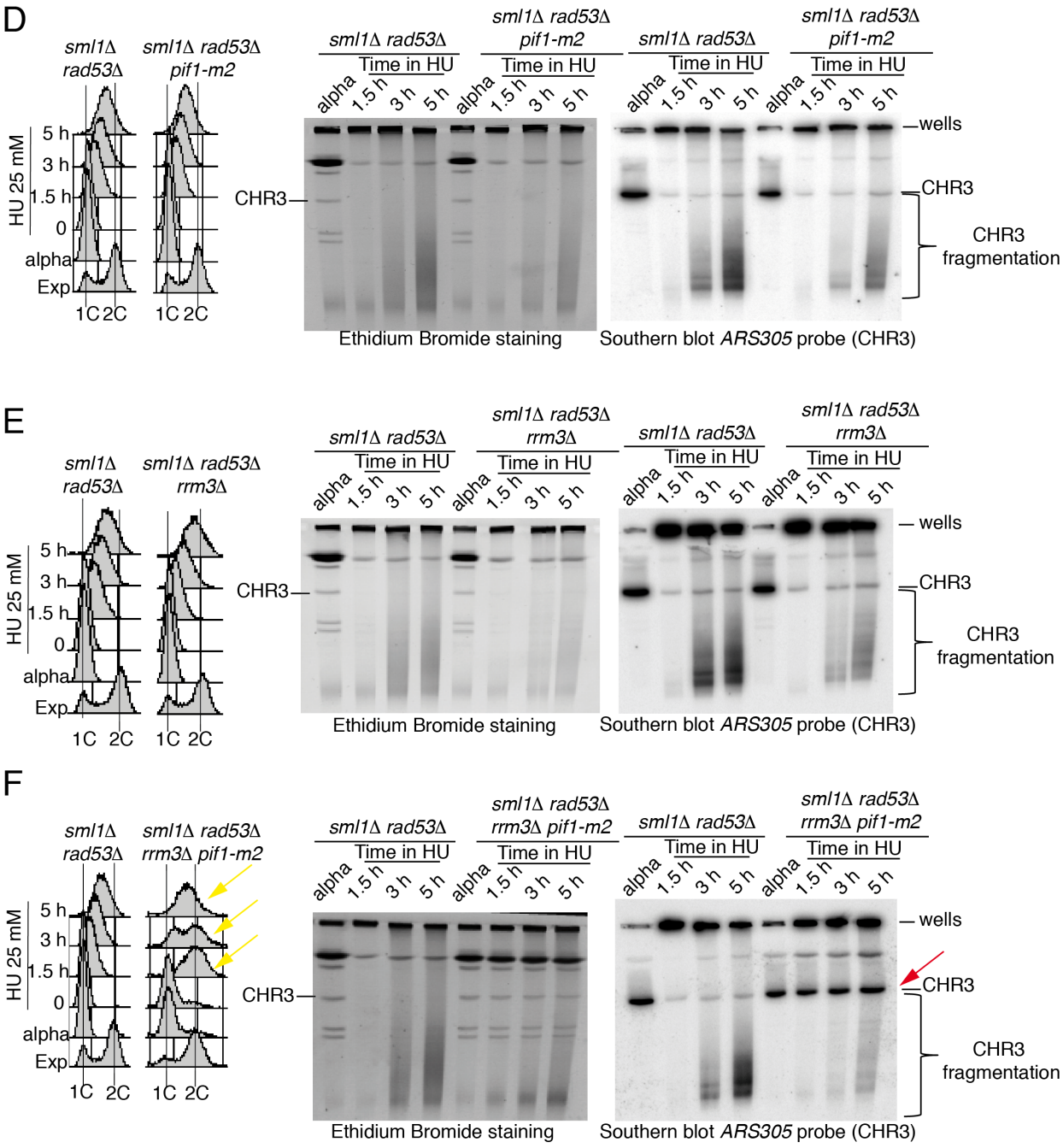
D
sml1Δ rad53Δ
sml1Δ rad53Δ pif1-m2
HU 25 mM
5 h
3 h
1.5 h
0
alpha
Exp
1C 2C 1C 2C
CHR3
sml1Δ rad53Δ
Time in HU
alpha 1.5 h 3 h 5 h
wells
CHR3
CHR3 fragmentation
Ethidium Bromide staining
Southern blot ARS305 probe (CHR3)
E
sml1Δ rad53Δ
sml1Δ rad53Δ rrm3Δ
F
sml1Δ rad53Δ rrm3Δ pif1-m2

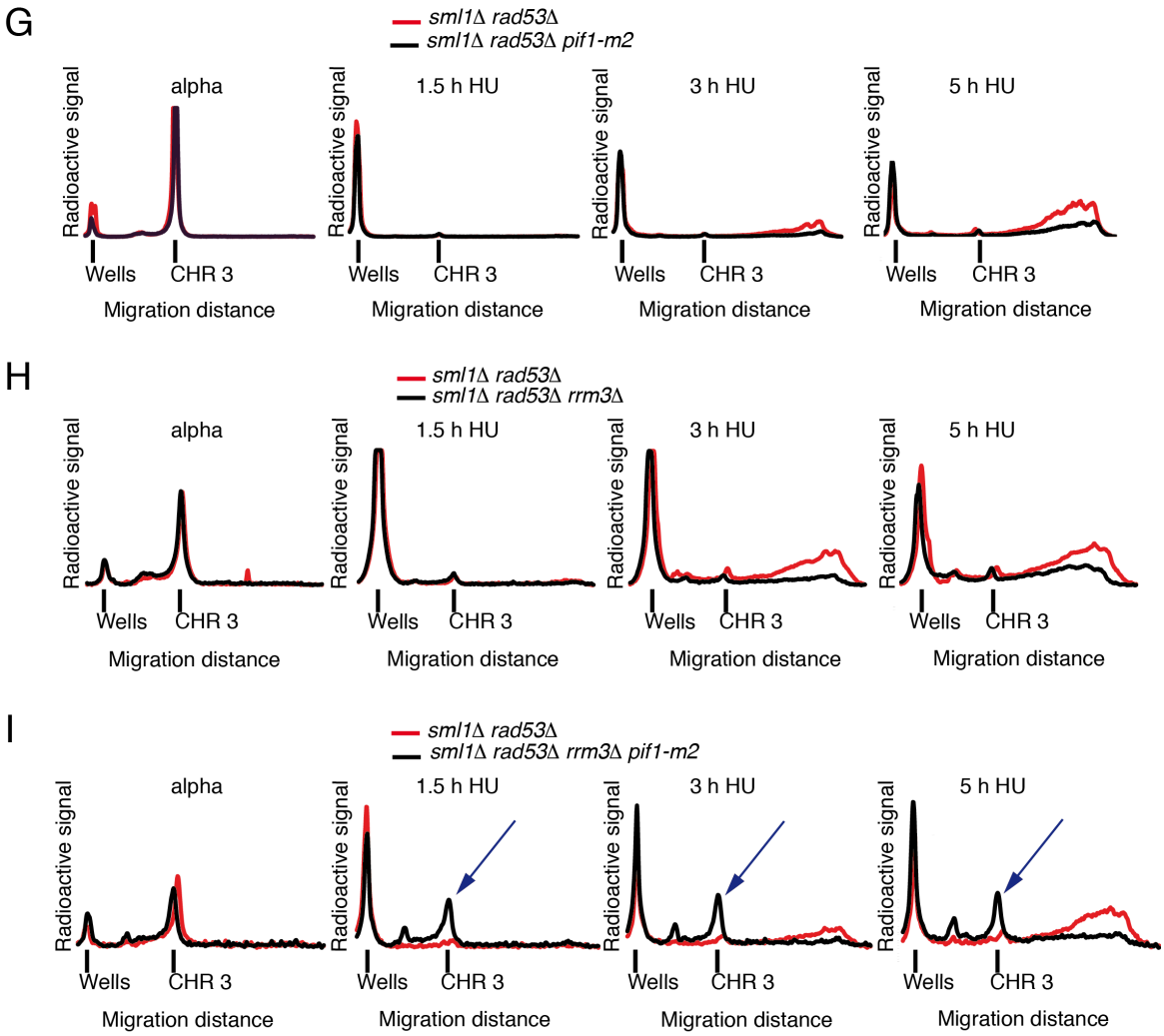

Figure 3.8. *RRM3* and *PIF1* ablations suppress replication stress-induced chromosome fragility in *rad53* mutants. A-B-C-D-E-F) The migration pattern of the chromosome III was analysed by PFGE and southern blotting (using an *ARS305* recognizing probe) at the indicated time points in the strains CY12445, CY13331, CY12448, CY13334, CY12443, CY13339, CY12460 and CY13342 released from G1 into S-phase in the presence of 25 mM HU. Pictures of the ethidium bromide stained PFGE gels are reported. A black line and a black bracket indicate, respectively, the migration position of the entire chromosome III and the region of the gel in which chromosome fragmentation is detectable. The position of the wells is indicated. The black arrows in panel A and B indicate an high molecular weight PFGE signal (HPFGES). The red arrow in panel F indicates the southern blotting signal of the chromosome III, which re-enters in the gel in HU only in the strain *sml1Δ rad53Δ rrm3Δ pif1-m2* cells. FACS profiles are shown and the yellow arrows indicate the cell cycle progression into mitosis in the quadruple mutant *sml1Δ rad53Δ rrm3Δ pif1-m2*. **G-H-I)** Quantitative profiles of the PFGE experiments shown in panels D-E-F are reported. The intensity of the radioactive signal in each lane of the PFGE gels shown in panels D-E-F was plotted against the migration distance. In order to quantify and better appreciate the difference in the chromosome fragmentation between different strains, quantitative profiles of the indicated strains analysed at different time points are overlapped. Blue arrows indicate the signals corresponding to the chromosome III, which re-enters into the gel in the quadruple mutant *sml1Δ rad53Δ rrm3Δ pif1-m2* treated with HU.

Since, in the experiments presented Figure 3.8F, we compared the chromosome fragility of two strains (*sml1Δ rad53* and *sml1Δ rad53Δ rrm3Δ pif1-m2*) that were in different phases of the cell cycle, we performed the same experiment adding nocodazole in the media after the G1 release in HU to arrest the cells at metaphase-anaphase transition, preventing the progression into mitosis of the *sml1Δ rad53Δ rrm3Δ pif1-m2* strain (Figure 3.9). *rad53* mutants, released from G1 into S-phase in the presence of Nocodazole, after 3 and 5 hours of HU treatment, accumulated chromosome breakages that were suppressed by combined *RRM3* and *PIF1* ablations. We concluded that chromosome fragility induced by HU in *rad53* mutants, did not require the metaphase-anaphase transition and that suppression of chromosome fragmentation in *sml1Δ rad53Δ rrm3Δ pif1-m2* cells was not due to the differences in cell cycle progression of this strain compared to *sml1Δ rad53Δ* cells.

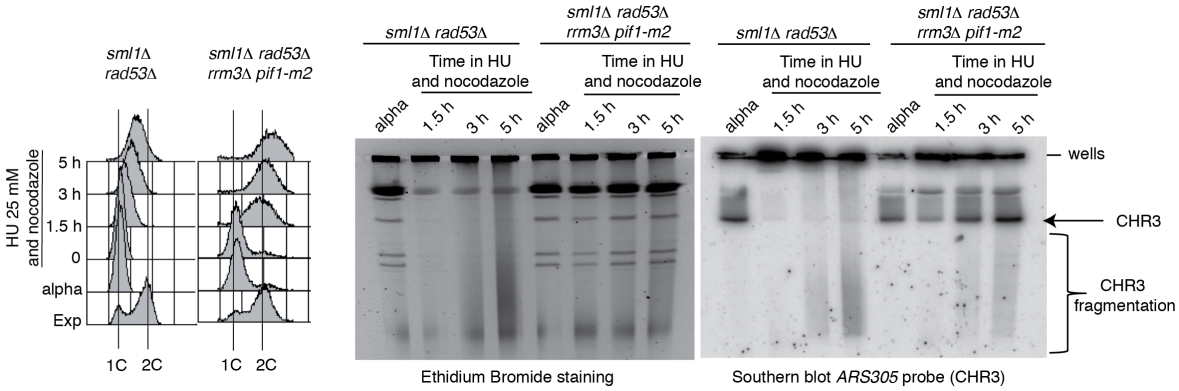

Figure 3.9. Metaphase to anaphase transition is not required for the replication stress induced chromosome fragmentation, detectable in *rad53* cells treated with low HU concentrations. CY12443 and CY13342 strains were synchronized in G1 and released into S-phase in the presence of 25 mM of HU and nocodazole (20 μg/ml). Fresh nocodazole was added (10 μg/ml) after 3 h from the G1 release in S-phase to maintain the metaphase arrest. The migration pattern of chromosome III was analysed, at the indicated time points, by PFGE and southern blotting, using an *ARS305* recognizing probe. A black arrow indicates the southern blot signal corresponding to the migration position of the chromosome III, which re-enters in the gel in HU only in the strain CY13342. A black bracket indicates the region of the gel in which the chromosome fragmentation is detectable. Position of the wells is shown. Pictures of the ethidium bromide-stained PFGE gels and FACS profiles, indicating the cellular DNA content during the experiment, are shown.

Almost all the experiments presented in the previous part of this thesis were performed using the *SML1* deletion, to minimize the contribution of dNTP levels. *SML1* deletion leads to a 2.5 folds increase of the cellular pool of dNTPs (Zhao et al., 1998).

To further sustain the conclusion that the suppression phenotypes induced by *RRM3* and *PIF1* ablations in *rad53* cells under replication stress were not due to indirect effects of their ablations on the dNTPs level, we analysed the replication stress-induced chromosome fragmentation in *rad53* mutants in which *SML1* was deleted and *RNR1* was over-expressed using the *GAL1-10* promoter (Figure 3.10). It has been shown that *RNR1* over-expression leads to a 10-folds increase in the dNTPs level compared WT cells (Chabes and Stillman, 2007). One expectation of this experiment was that, if the suppression of chromosome fragmentation in *rad53* cells treated with HU was due to an indirect effect of *RRM3* and *PIF1* ablations on the cellular pool of dNTPs, *SML1* deletion and *RNR1* over-expression would have reduced, at least partially, the chromosome fragmentation induced in *rad53* cells exposed to HU. *sml1Δ rad53Δ* cells, over-expressing Rnr1 under the control of the *GAL1-10* promoter, were released in S-phase in the presence of 25 mM of hydroxyurea, in non-inducing (raffinose) or inducing (galactose) conditions and the migration pattern of chromosome III was analysed by PFGE and southern blotting. Chromosome breakages appeared in *rad53* mutants, 8 hours after the release in HU, even in the presence of high dNTPs levels and *RRM3* and *PIF1* ablations were still able to suppress the chromosome fragility of *rad53* mutants both in non-inducing and in the presence of high levels of Rrn1 (Figure 3.10), strongly suggesting that the suppression effects detected in this thesis work are likely not due to indirect effects of *RRM3* and *PIF1* ablations on the cellular level of dNTPs.

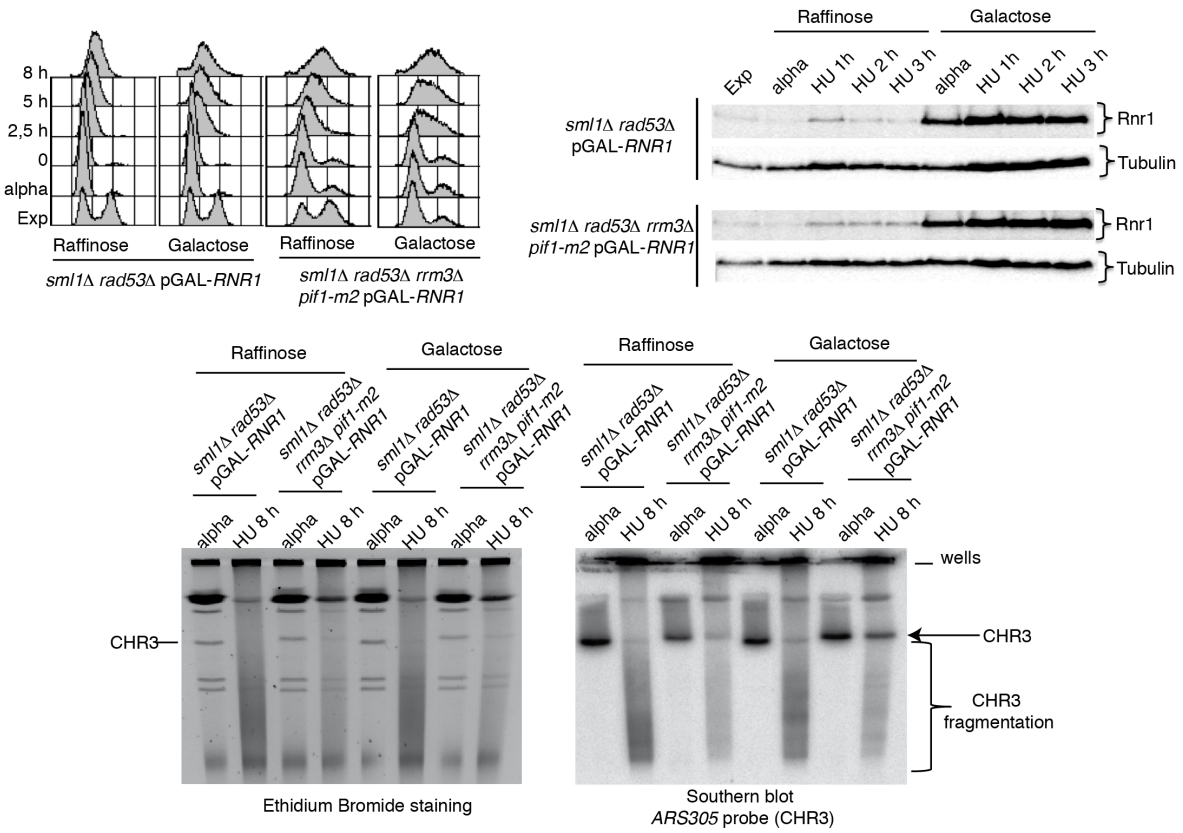

Figure 3.10. High dNTPs levels induced by *SML1* deletion and *RNR1* over-expression do not suppress the chromosome fragmentation caused by the treatment of *rad53* mutants with low HU doses. CY14076 and CY14077 strains, carrying the *RNR1* gene under the control of the *GAL1/GAL10* promoter, were grown in YP+raffinose, synchronized with alpha factor in the presence or absence of galactose and released from the G1 arrest into S-phase with 25 mM of HU for 8 hours, in the presence or absence of galactose. FACS profiles are shown and Rnr1 protein levels were monitored by western blotting, using an anti-Rnr1 antibody. The level of the tubulin was monitored in parallel as loading control. Chromosome III migration pattern was analysed by PFGE and southern blotting using an *ARS305* recognizing probe, at the indicated time points. A picture of the ethidium bromide stained PFGE gel is reported. A black arrow indicates the southern blot signal corresponding to the migration position of the chromosome III, which re-entered in the gel in HU only in the strain CY14077. The region of the gel in which chromosome fragmentation is detectable is indicated by a black bracket. Position of the wells is shown.

With the aim of checking if high HU doses induce chromosome fragmentation in checkpoint defective cells, we released the *rad53Δ* strain from G1 into S-phase in the presence of 200 mM of HU. Migration pattern of the chromosome III and chromosome fragmentation were analysed by PFGE and southern blotting using a probe recognizing the *ARS305* locus (Figure 3.11). As it can be seen in figure 3.11 chromosome III was retained into the wells and only a low level of chromosome fragmentation was detectable, even after 5 hours from the G1 release in HU, both in *sml1Δ rad53Δ* and *sml1Δ rad53Δ rrm3Δ*

pif1-m2 cells. High HU concentrations suppress the fragile sites expression in *rad53* cells, probably because forks immediately stall and collapse close to the replication origins, with a very low level of fork breakage, even after very long incubation times (up to seven hours in high HU) (Figure 3.11 and our unpublished observations) (Cha and Kleckner, 2002; Hashash et al., 2011). Differently, when *rad53* cells are released in low HU concentrations, there is still a substantial level of DNA replication fork progression (even in the absence of *RAD53*- see Figure 3.4) and forks reach the replication slow zones (RSZs), where they get fragmented with a mechanism still unknown, mediated by Toposoimerase II (Top2) and condensins, while it does not require spindle tension, anaphase, cytokinesis and a series of structure specific DNA endonucleases and helicases involved in DNA recombination and DNA replication fork re-start (Hashash et al., 2012).

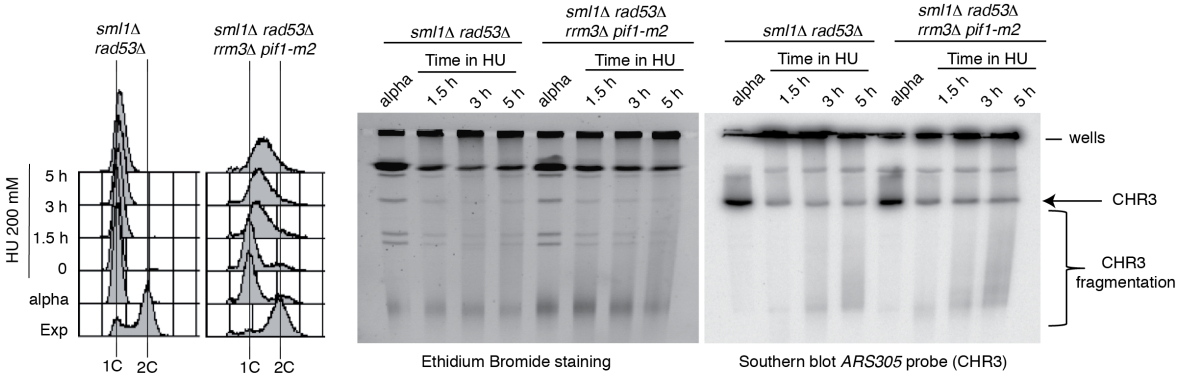

Figure 3.11. Treatment of *rad53* cells with 200 mM HU induces low levels of chromosome fragmentation. CY12443 and CY13342 strains were synchronized in G1 and released into S-phase in the presence of 200 mM HU. The migration pattern of chromosome III was analysed, at the indicated time points, by PFGE and southern blotting, using an *ARS305* recognizing probe. A low level of chromosome fragmentation (indicated by a black bracket) was detectable in the two strains even after 5 hours of treatment with 200 mM of HU. A black arrow indicates the southern blot signal of the chromosome III. Position of the wells is shown. Picture of the ethidium bromide stained gels and FACS profiles with the cellular DNA content during the experiment are shown.

3.1.4 Rrm3 and Pif1 promote cell lethality in *rad53* mutants exposed to replication stress

Since replication fork defects and chromosome fragmentations are thought to promote cell lethality in *rad53* mutants under replication stress and since we found that ablations of the

Pif1 helicases ameliorate these phenotypes, we decided to test whether the absence of *RRM3* and *PIF1* suppresses the cellular lethality of *rad53* cells treated with HU. For this purpose, we used the colony assay to compare the viability of the strains indicated in figure 3.12 in the presence of hydroxyurea. In agreement with our expectation, we found that *PIF1* and *RRM3* ablations synergistically suppressed the HU sensitivity of *rad53* mutants. In particular, *RRM3* deletion partially rescued the HU sensitivity of *rad53* mutants, while the *pif1-m2* mutation alone did not influence *rad53* viability in HU. This result can be rationalized hypothesizing that *PIF1* ablation exerts its suppression only when *RRM3* is ablated (Figure 3.12 and see Discussion).

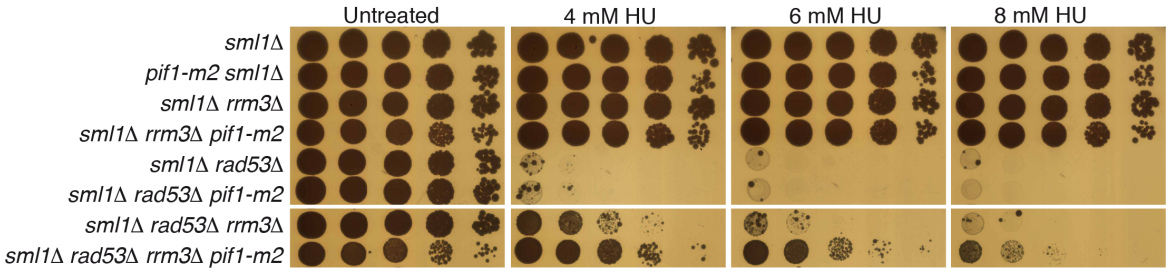

Figure 3.12. Ablations of *RRM3* and *PIF1* synergistically suppress the cell lethality of *rad53* mutants exposed to HU. HU sensitivity at the indicated dosages was determined by drop assay in strains CY12445, CY13331, CY12448, CY13334, CY12443, CY13339, CY12460 and CY13342. Pictures of the plates were taken after 3 days of growth at 28°C.

PIF1 and *RRM3* ablations were not able to rescue the UV sensitivity of *rad53* mutants (Figure 3.13), suggesting that the suppression effect of *pif1-m2* and *rrm3Δ* was specific for replication stress induced by dNTPs deprivation and not by DNA replication perturbations arising in consequence of the presence of DNA lesions.

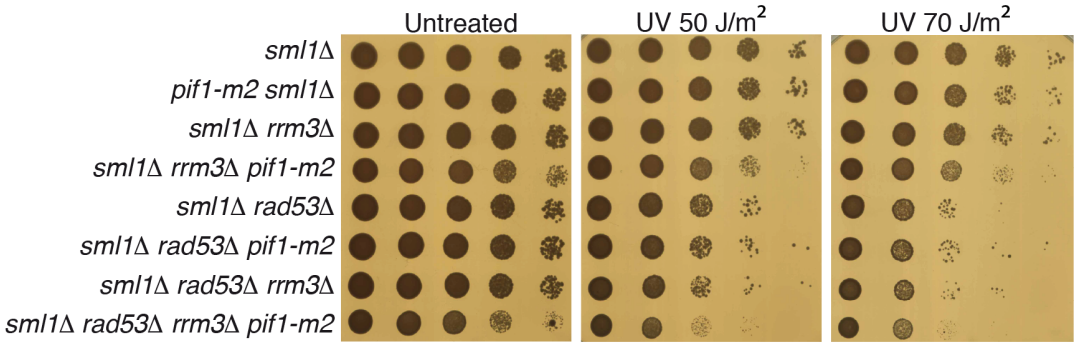

Figure 3.13. *RRM3* and *PIF1* ablations do not suppress the UV sensitivity of *rad53* cells. Viability of the indicated strains, following UV-induced DNA damage, was determined by drop assay. After cells deposition,

the plates were irradiated with the indicated UV dosages (expressed in J/m^2). Picture of the plates were taken after 3 days of growth at 28°C.

Using the "Delitto Perfetto" approach (Storici and Resnick, 2006), we generated the ATPase/helicase-dead allele *rrm3-K260A*, in which the lysine in the ATP binding pocket of Rrm3 was mutated to alanine (Ivessa et al., 2000). We observed that the *rrm3-K260A* mutation was able to rescue the HU sensitivity of *sml1Δ rad53Δ* cells, at the same level of *RRM3* deletion (Figure 3.14). This result strongly suggests that Rrm3 executes its toxic activity in *rad53* cells treated with HU through its DNA helicase activity.

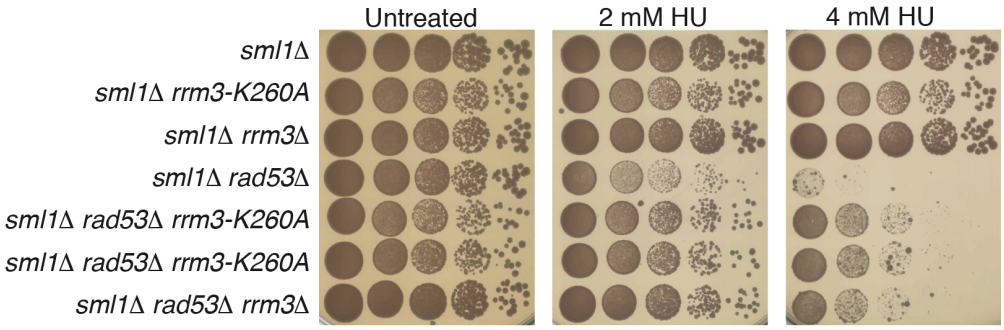

Figure 3.14. The helicase-dead allele *rrm3-K260A* suppresses the HU sensitivity of *rad53* mutants at the same extent as *RRM3* deletion. HU sensitivity was determined by drop assay at the indicated dosages in strains CY12867, CY13173, CY12448, CY12865, CY13172, CY13174 and CY12460. Pictures of the plates were taken after 3 days of growth at 28°C.

To exclude that the suppression of the *rad53* HU sensitivity in the strain *sml1Δ rad53Δ rrm3Δ pif1-m2* was due to the presence of other mutations, we complemented the quadruple mutant with a plasmid expressing either the wild type form of Rrm3 or the helicase-defective *rrm3-K260A* mutant (Figure 3.15) (Ivessa et al., 2002). The presence of the centromeric plasmid carrying the wt *RRM3* gene abolished the suppression of the HU sensitivity in *sml1Δ rad53Δ rrm3Δ pif1-m2* cells, while the empty vector or the plasmid expressing the *rrm3-K260A* mutant protein did not alter the viability of the quadruple mutant in hydroxyurea (Figure 3.15A). Moreover, FACS analysis of G1 released cells in 25 mM of hydroxyurea, revealed that the expression of Rrm3 in *sml1Δ rad53Δ rrm3Δ pif1-m2* cells was also able to restore the replication block caused by the absence of *RAD53* in the presence of HU (Figure 3.15B).

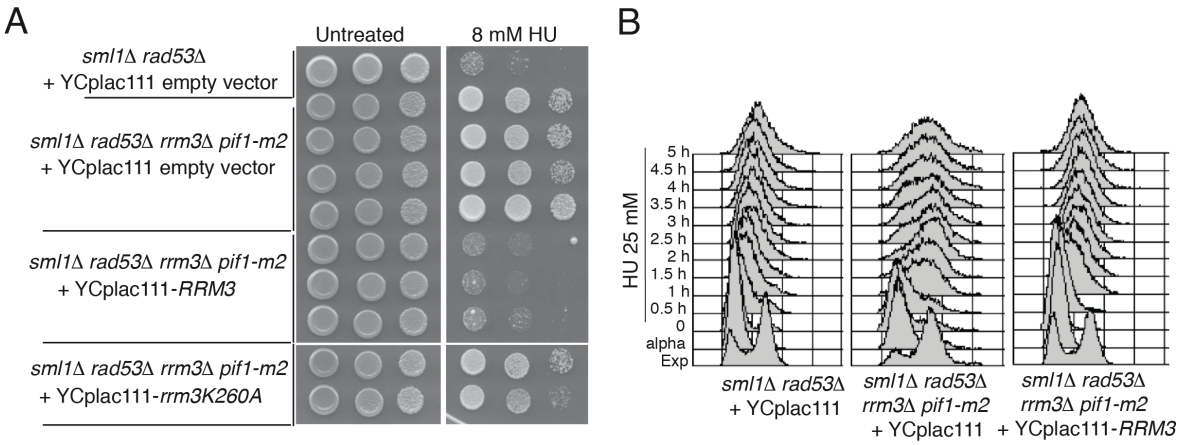

Figure 3.15. Expression of Rrm3, but not of the helicase-dead variant *rrm3-K260A*, is able to restore the HU sensitivity and HU-induced S-phase block in the strain *sml1Δ rad53Δ rrm3Δ pif1-m2*. A) HU sensitivity was determined by drop assay for the strains CY12443 and CY13342, transformed with the plasmid *YCplac111* (empty vector), *YCplac111-RRM3* or *YCplac111-rrm3-K260A* (Ivessa et al., 2002) expressing either the wt form of Rrm3 or the helicase dead variant *rrm3-K260A*. **B)** The strains CY12443 (transformed with *YCplac111*) and CY13342 (transformed either with *YCplac111* or *YCplac111-RRM3*) were arrested in G1 and released in 25 mM of HU. The cellular DNA content was determined by FACS analysis at the indicated time points.

Checkpoint-mediated down-regulation of gene gating is one of the key mechanisms to prevent the replication stress-induced cell lethality in *rad53* mutants (Bermejo et al., 2011). It has been shown that, in the presence of HU, Rad53 phosphorylates the nuclear pore protein Mlp1 leading to inhibition of the mRNA export into the cytoplasm, a process called gene gating. Rad53 dependent release of the transcribed chromatin from the nuclear envelope under replication stress is though to release chromosomal topological constrains that can be deleterious in the context of the stabilization of the stalled replication fork (Bermejo et al., 2011). According to this mechanism, ectopic ablation of *SAC3* (an essential gene for gene gating) partially suppresses the HU sensitivity of *rad53* cells (Bermejo et al., 2011).

We decided to analyse the genetic relationships between the *SAC3* and the *RRM3/PIF1* dependent pathways of suppression of HU sensitivity of *rad53* cells. To do this we deleted *SAC3* in *sml1Δ rad53Δ rrm3Δ* cells and monitored the HU sensitivity. We found that *SAC3* and *RRM3* deletions had additive effects on the suppression of the HU sensitivity of

rad53 mutants (Figure 3.16), suggesting that the Pif1 helicases and the gene gating influence the viability of HU-treated *rad53* cells through distinct genetic mechanisms.

We also generated the quintuple mutant *sml1Δ rad53Δ rrm3Δ pif1-m2 sac3Δ*, but the analysis of the HU sensitivity of this strain was impeded by its extremely slow growth phenotype (data not shown).

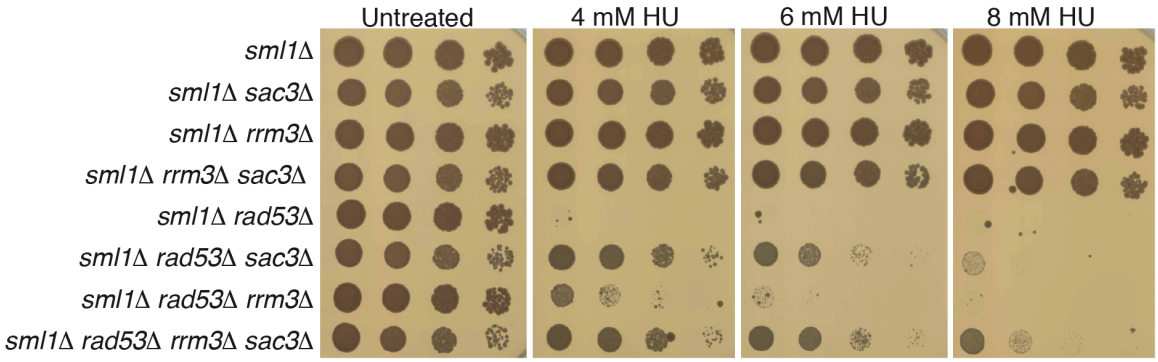

Figure 3.16. Ablations of the Pif1 helicases and gene gating have additive effects in the suppression of the HU sensitivity of *rad53Δ* cells. HU sensitivity at the indicated dosages was determined by drop assay on the following strains: CY12445, CY12682, CY12448, CY12690, CY12674, CY12681, CY12460 and CY12689. Pictures of the plates were taken after 3 days of growth at 28°C.

We confirmed the results obtained in the *sml1Δ rad53Δ* background also in the *rad53-K227A* background. We verified that the *pif1-m2* and the *rrm3Δ* mutations synergistically suppressed the HU sensitivity of *rad53-K227A* cells (Figure 3.17A). As in *rad53Δ* cells, the *RRM3* deletion partially alleviated the HU sensitivity of *rad53-K227A* mutants, while the *pif1-m2* mutation did not have any effects on cell viability in HU (Figure 3.17A). Coherent with this, we also found that the combined ablation of *RRM3* and *PIF1* rescued the cell cycle arrest in S-phase of *rad53-K227A* mutants after the G1 release in 25 mM of HU (Figure 3.17B)

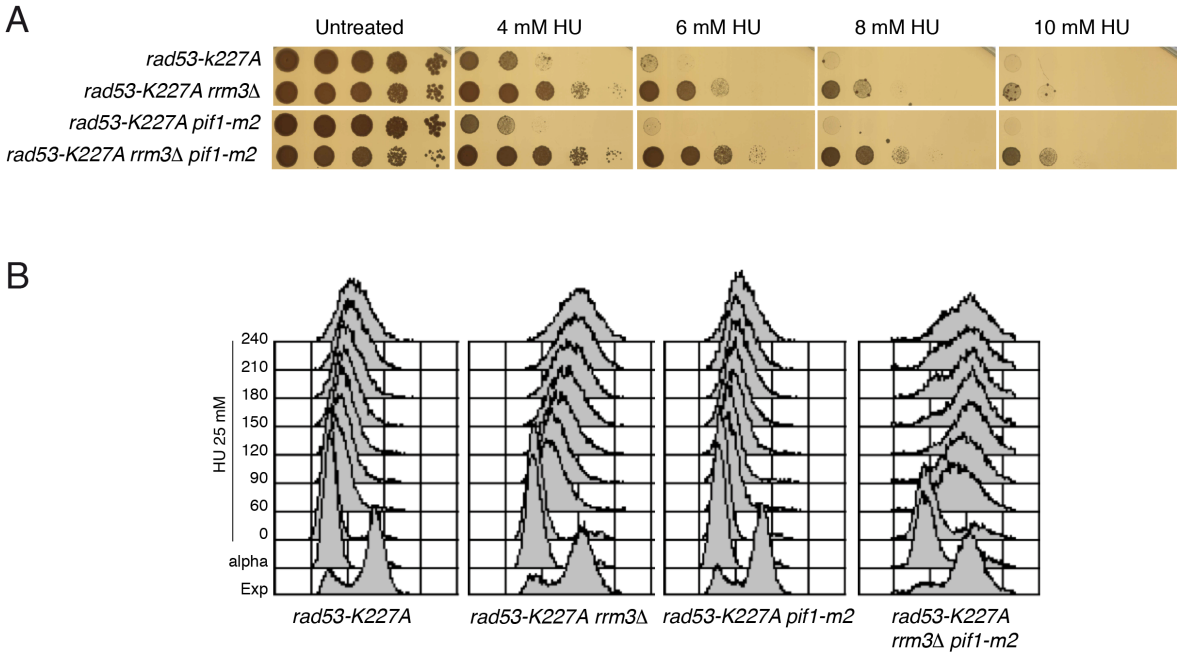

Figure 3.17. Ablation of the Pif1 helicases suppresses the HU sensitivity and replication fork arrest induced by treatment of *rad53-K227A* mutant cells with low HU doses. A) HU sensitivity of CY12404, CY12406, CY13735 and CY13738 strains has been determined by drop-assay, at the indicated HU dosages. **B)** The same strains as in A were synchronized in G1 and released into S-phase in the presence of 25 mM of HU. Samples were collected at the indicated time points, and the cellular DNA content was determined by FACS analysis.

3.1.5 Rrm3 and Pif1 are hyperphosphorylated in a Rad53-dependent manner following replication stress

It has been reported that Pif1 is phosphorylated after induction of a single double strand break, in a Mec1-, Rad53- and Dun1-dependent manner, and that this checkpoint dependent regulation activates Pif1 and prevents deleterious *de novo* telomere addition at DSBs sites (Makovets and Blackburn, 2009). In the same report, it has been shown that Pif1 gets hyperphosphorylated when the cells are treated with HU, but the physiological role and the genetic dependences of the HU-induced phosphorylation of Pif1 have not been investigated in this report. Since we have shown that Pif1 and Rrm3 localize at the stalled DNA replication forks and their combined ablations suppress replication fork defects and chromosome fragmentation in *rad53* cells treated with HU, we decided to investigate whether the checkpoint directly controls the Pif1 helicases at the stalled DNA replication forks. To address this question, G1 synchronized cells were release in the presence of 150

mM HU and the phosphorylation status of Rrm3-Myc (Figure 3.18A) and Pif1-Flag (Figure 3.18B) was monitored, at the indicated time points, by western blotting using phospho-tag gels to maximize the mobility shifts specifically due to phosphorylation (Kinoshita et al., 2006). Rrm3 and Pif1 were hype-phosphorylated between 30 and 45 minutes from the release into S-phase, when cells started the DNA replication in the presence of HU, reaching the maximum level of phosphorylation at 90 minutes from the G1 release (Figure 3.18A,B).

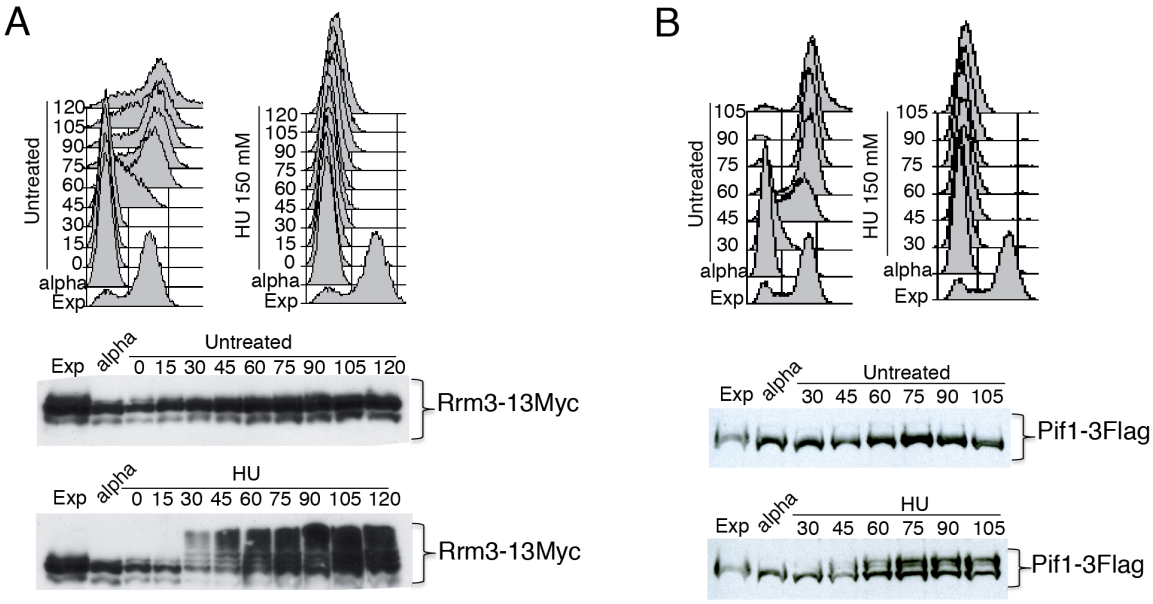

Figure 3.18. Rrm3 and Pif1 get hyperphosphorylated during S-phase in the presence of HU. A-B) The strain CY11360 and the strain CY13074 were arrested in G1 and released into S-phase in the presence or absence of 150 mM HU. The phosphorylated isoforms of Rrm3-Myc and of Pif1-Flag were separated using phospho-tag gels (Kinoshita et al., 2006) and visualized by western blotting using anti-Myc and anti-Flag antibodies, at the indicated time points.

Since Pif1 phosphorylation was observed after the induction of a single double strand break (Makovets and Blackburn, 2009), we wanted to investigate if also DNA replication perturbation through the presence of alkylated DNA bases would have induced this post translational modification of Pif1. To do this, we released yeast strains carrying Rrm3-myc and Pif1-flag tagged versions into S-phase in the presence of the alkylating agent methyl methane sulfonate (MMS). We found that Rrm3 and Pif1 were phosphorylated also in the

presence of this kind of DNA damage in S-phase. In particular, Rrm3 and Pif1 were hype-phosphorylated around 30 minutes after the release in S-phase (Figure 3.19).

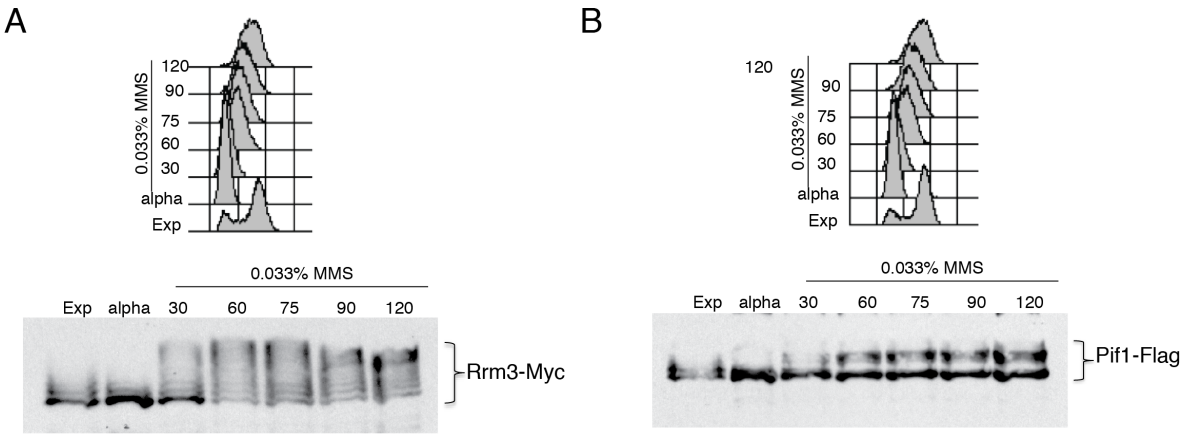

Figure 3.19. Rrm3 and Pif1 get phosphorylated during S-phase in the presence of the DNA alkylating agent MMS. A-B) The strain CY12867 and the strain CY13074 were arrested in G1 and released into S-phase in the presence of 0.033% MMS. The phosphorylated isoforms of Rrm3-Myc and of Pif1-Flag were separated using phospho-tag gels (Kinoshita et al., 2006) and visualized by western blotting using anti-Myc and anti-Flag antibodies, at the indicated time points.

We then addressed whether the HU-induced Rrm3 and Pif1 hyperphosphorylations were dependent on Rad53, by western blotting using phospho-tag gels. We observed that, 90 minutes after the G1 release in 150 mM of hydroxyurea, the mobility shifts of Rrm3 and Pif1 were abolished in *rad53Δ* cells (Figure 3.21). We conclude that both Rrm3 and Pif1 are regulated through phosphorylation in a Rad53-dependent manner under replication stress.

3.1.6 The phospho-defective *rrm3* and *pif1* mutations reduce the HU- and Rad53-dependent hyperphosphorylation of the Pif1 helicases, while the phospho-mimick *rrm3* allele rescues the HU sensitivity of *rad53* mutants

We identified six serines, clustered in a sequence of twelve amino acids, in the N-terminal region of Rrm3 and 11 serine residues and one threonine in the N-terminus of Pif1, which could be considered potential consensus motifs for Rad53 or for PI3K-like kinases (Figure 3.20) (Smolka et al., 2007). Mutagenesis of these residues to alanine or aspartic acid residues, using the "Delitto Perfetto" technique (Storici and Resnick, 2006), gave rise,

respectively, to the phospho-defective *rrm3-6SA* and *pif1-12A*, or the phospho-mimicking *rrm3-6SD* and *pif1-12D* mutants.

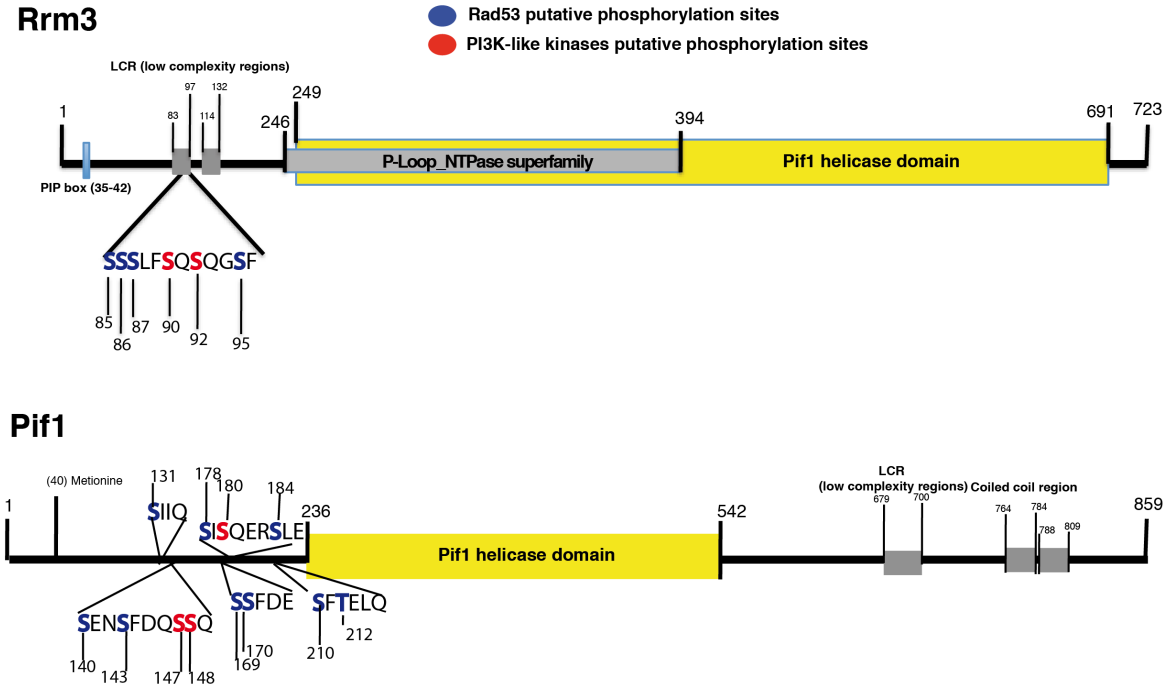

Figure 3.20. Schematic representation of the putative PI3K-like kinases and Rad53-dependent phosphorylation sites of Rrm3 and Pif1. Cartoons of Rrm3 and Pif1 proteins with the functional domains and the putative phosphorylation sites for PI3K-like kinases (red) or Rad53 (blue), substituted to alanine in the *rrm3-6SA* and *pif1-12A* phospho-deficient alleles or to aspartate in the corresponding phospho-mimicking alleles.

First, to confirm that the phospho mutant alleles did not have any indirect effect on protein stability, we measured the protein levels of the *rrm3-6SA, pif1-12A, rrm3-6SD* and *pif1-12D* mutant forms and found that they are expressed at the same level of their wild type counterparts (Figures 3.21, 3.24). We also verified that the phospho-mutant alleles of Rrm3 and Pif1 do not influence Rrm3 and Pif1 functions in unperturbed conditions (Figures 3.22, 3.23, 3.25).

By western blotting, on exponentially growing cells in untreated conditions, we verified that the *rrm3-6SA* and *rrm3-6SD* mutations did not alter the Rrm3 protein levels and did not induce the phosphorylation of Rad53 and of the histone H2A, while, as expected, *RRM3* deletion induced a mild checkpoint activation (Ivessa et al., 2003; Szilard et al., 2010) (Figure 3.21).

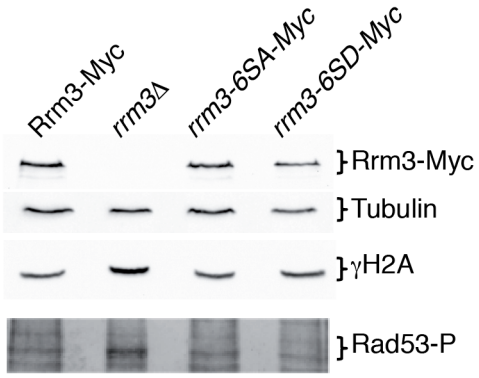

Figure 3.21. The *rrm3-6SA* and *rrm3-6SD* alleles do not influence Rrm3 protein levels and do not induce checkpoint activation in unperturbed conditions. The yeast strains RRM3-13MYC (CY11360), *rrm3Δ* (CY12484), *rrm3-6SA-13MYC* (CY12803), *rrm3-6SD-13MYC* (CY12831) carrying the indicated *RRM3* alleles have been grown to mid log phase in unperturbed conditions. Protein extracts were prepared and separated by SDS-page. Rrm3 variants, tubulin, histone H2A phosphorylation and Rad53 phosphorylation were visualized by western blotting using specific antibodies.

Since in the absence of Rrm3, DNA replication forks pause at the level of different kind of pausing elements, we verified the functionality of the *rrm3-6SA* and *rrm3-6SD* alleles by monitoring in 2D gels the fork progression dynamic across two typical Rrm3-dependent pausing sites: the $tRNA^A$ locus (Figure 3.22B) (Ivessa et al., 2003) and the replication fork barrier (RFB) of the rDNA (Figure 3.22A) (Ivessa et al., 2000). We found that the strains carrying the phospho-mutant alleles of *RRM3* exhibited the same 2D gel profiles of wild type cells in unperturbed conditions, while *rrm3Δ* mutants accumulated strong pausing signals at the RFB of the rDNA (Figure 3.22A) and at the level of the $tRNA^A$ gene (Figure 3.22B).

These results suggest that the Rad53-mediated phosphorylation of Rrm3 and Pif1 do not impact on the role that Rrm3 has in assisting DNA replication fork progression across pausing elements in untreated conditions.

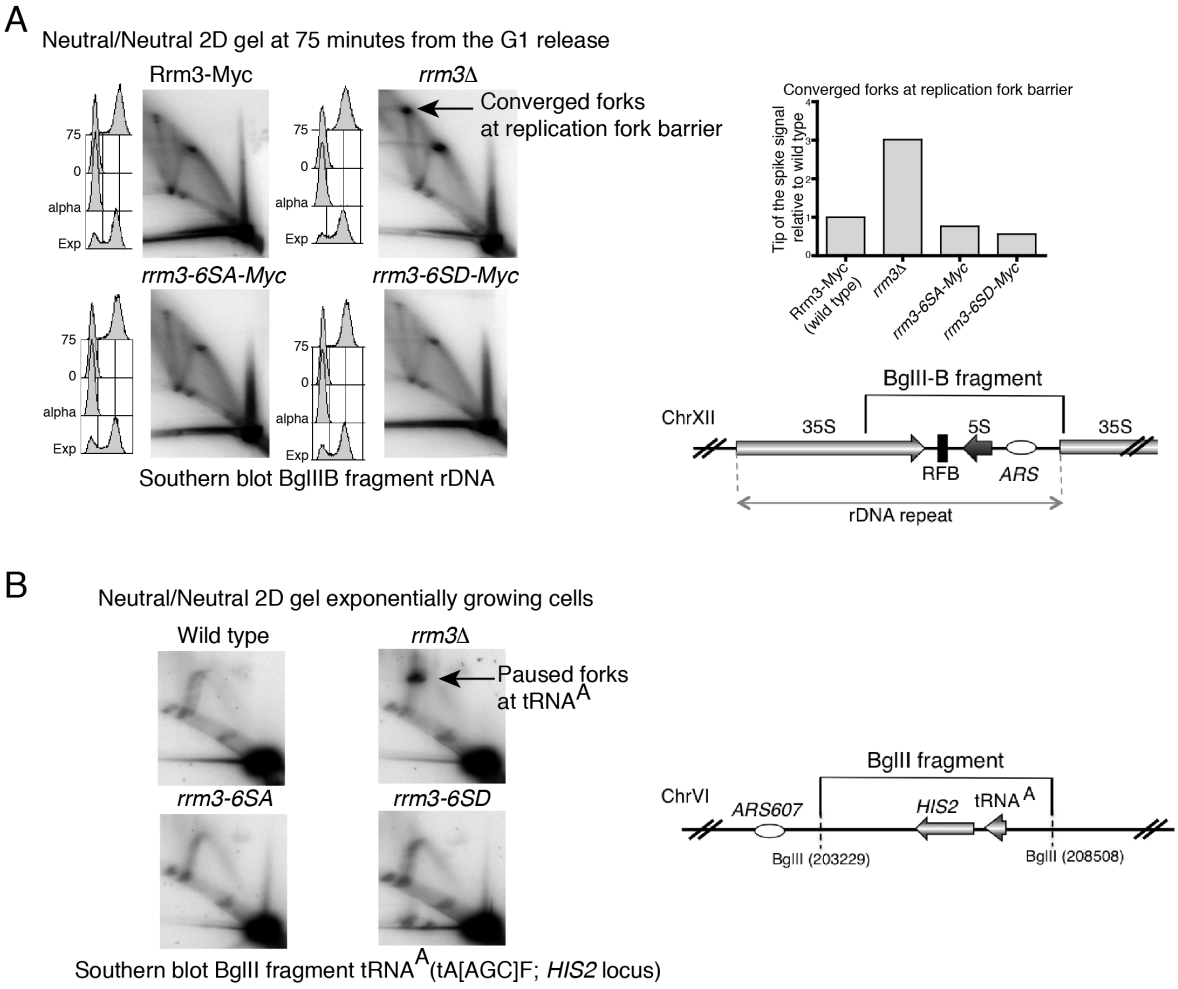

Figure 3.22. The *rrm3-6SA* and *rrm3-6SD* alleles do not induce replication forks pausing at rDNA and tRNA^A gene in unperturbed conditions. A) DNA replication intermediates accumulating in the BglIIB fragment of the rDNA (Ivessa et al., 2000), were visualized through neutral-neutral 2D gel electrophoresis in the yeast strains CY11360, CY12484, CY12803 and CY12831 at 75 minutes from the G1 release into an unperturbed S-phase. FACS profiles, which show the cellular DNA content during the experiments, are shown. The signals at the tip of the spike arc (corresponding to converged replication forks at the replication fork barrier in the rDNA) (Ivessa et al., 2000), were normalized against the intensity of their corresponding monomer spots and reported into the histogram as values relative to the wild type signal. A map of the fragment analysed by neutral-neutral 2D gels is shown. **B)** DNA replication intermediates accumulating in the BglII fragment containing the *HIS2* and the tRNA^A tA[AGC]F genes, have been visualized through neutral-neutral 2D gel electrophoresis in the yeast strains CY12486, CY12484, CY12801 and CY12824 grown to mid log phase in unperturbed conditions (Ivessa et al., 2003). A map of the fragment analysed by neutral-neutral 2D gels is shown.

To further investigate the connection between Rad53 and the Pif1 helicases at the natural pausing sites and to clarify if Rad53 has roles in assisting DNA replication fork progression across Rrm3 dependent pausing elements, we monitored the fork progression at tRNAs in the absence of Rad53 (Figure 3.23). By 2D gel analysis we failed to detect pausing signals in *sml1Δ* and *sml1Δ rad53Δ* cells at the tRNA^A locus in unperturbed

conditions and even when cells were treated with 25 mM of hydroxyurea, while *rrm3Δ* cells accumulated a strong pausing signal in both conditions (Figure 3.23, black arrows). These results suggest that Rad53 and the Rad53-mediated phosphorylation of Rrm3 and Pif1 do not impact on replication fork progression across natural pausing elements.

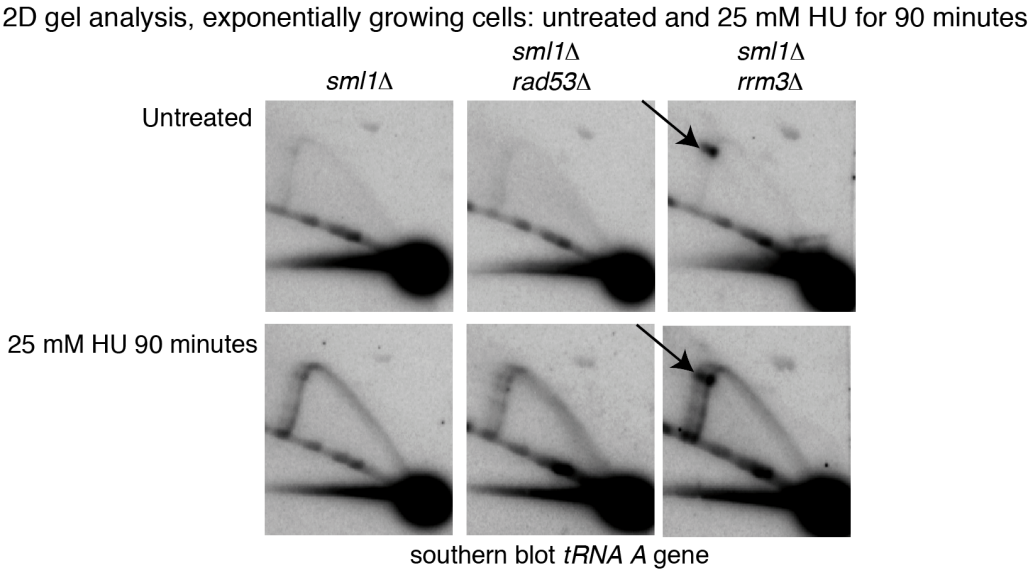

Figure 3.23. Exponentially-growing wild type and *rad53Δ* cells do not accumulate DNA replication pausing signals at the tRNA^{A} gene, in unperturbed conditions or in the presence of 25 mM HU. CY12445, CY12443 and CY12448 strains were grown to mid log phase and DNA replication intermediates, accumulating on the BglII-*HIS2* restriction fragment containing the tRNA^{A} gene, were analysed by 2D gel electrophoresis, in unperturbed conditions or after 90 minutes of treatment of exponentially growing cells with 25 mM of HU. A black arrow indicates the DNA replication pausing signal induced at the tRNA^{A} locus by the absence of *RRM3*.

By western blotting, we confirmed that also the *pif1-12A* and *pif1-12D* mutations did not affect Pif1 protein levels in exponentially growing cells (Figure 3.24).

Moreover the phospho-mutant and phospho-defective alleles of *PIF1* did not influence the length of the telomeres (Figure 3.25), while it has been published that in the absence of a functional nuclear isoform of Pif1 telomeres are longer (Schulz and Zakian, 1994).

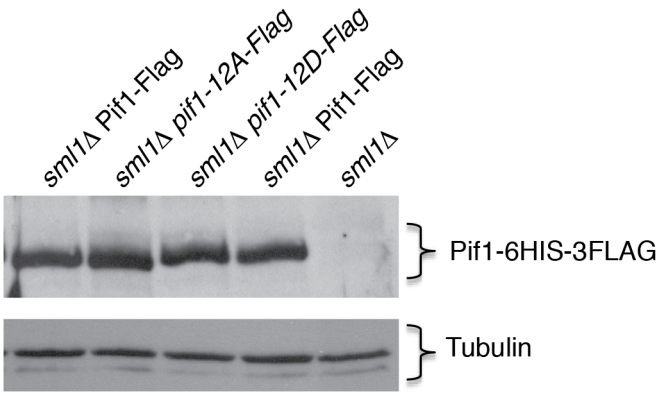

Figure 3.24. The *pif1-12A* and *pif1-12D* alleles do not influence Pif1 protein levels. The following yeast strains: *sml1Δ PIF1-6HIS-3FLAG* (CY13074), *sml1Δ pif1-12A-6HIS-3FLAG* (CY13664), *sml1Δ rad53Δ pif1-12D-6HIS-3FLAG* (CY13668), *sml1Δ* (CY12445), have been grown to mid log phase in unperturbed conditions. The protein levels of Pif1-6His-3Flag, *pif1-12A-6His-3Flag* and *pif1-12D-6His-3Flag* and of the tubulin (as loading control), have been analysed by western blotting, respectively, using anti-flag antibodies and anti tubulin antibodies.

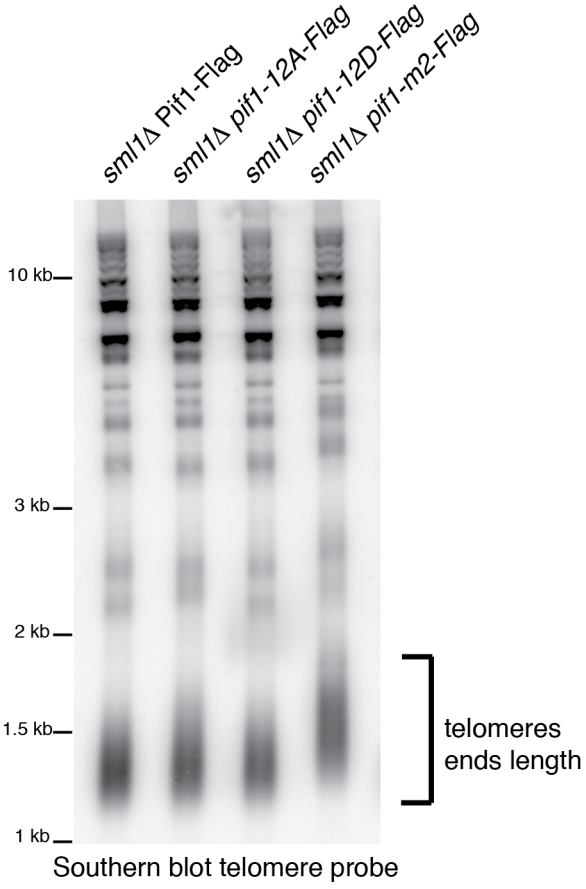

Figure 3.25. The *pif1-12A* and *pif1-12D* alleles do not induce elongation of telomeric DNA. The length of the telomeres has been analysed by southern blotting using a telomere specific probe as previously described (Longhese et al., 2000) in the yeast strains used in D and in the *sml1Δ pif1-m2-6His-3Flag* strain (CY12934), which have been grown to mid log phase in unperturbed conditions.

Once we verified that the phospho-mutants of Rrm3 and Pif1 did not influence protein levels or protein functions in unperturbed conditions, the phosphorylation state of *rrm3-*

6SA, pif1-12A and the corresponding wild type proteins were compared 90 minutes after the alpha-factor release in HU (150 mM) using phospho-tag gels (Figure 3.26). The phospho-defective *rrm3-6SA* and *pif1-12A* mutants showed a strongly-reduced HU- and Rad53- dependent phosphorylation (Figure 3.26).

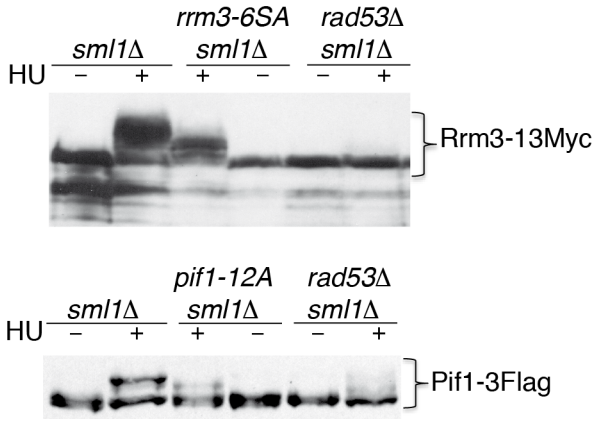

Figure 3.26. HU-induced Rrm3 and Pif1 hyperphosphorylation is Rad53-dependent and is almost completely abolished in the *rrm3-6SA* and *pif1-12A* phospho-deficient mutants. The phosphorylation states of the *rrm3-6SA* and *pif1-12A* mutant proteins were analysed at 90 minutes from G1 release into S-phase in the presence of 150 mM HU in the strains CY12867, CY12953, CY12865, CY13074, CY13664 and CY13073 using phospho-tag gels (Kinoshita et al., 2006) and western blotting.

To further investigate the physiological role of the HU-induced and checkpoint dependent Rrm3 and Pif1 phosphorylations, we combined the phospho-deficient and the phospho-mimicking alleles of *RRM3* with the deletion of *RAD53* and tested the HU sensitivity of the obtained strains by drop assay (Figure 3.27). Interestingly, the *rrm3-6SD* mutant allele rescued the HU sensitivity of *sml1Δ rad53Δ* cells with the same magnitude of *RRM3* deletion, while the phospho-defective *rrm3-6SA* allele did not affect the HU sensitivity of *rad53* mutants (Figure 3.27).

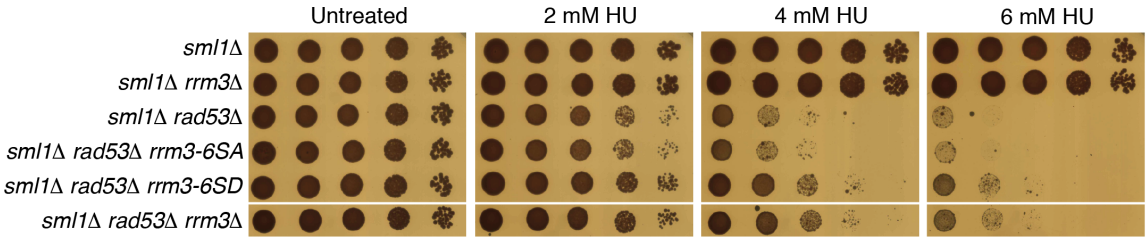

Figure 3.27. The phospho-mimicking *rrm3-6SD* allele rescues the HU sensitivity of *rad53* cells at the same extent of *RRM3* deletion. HU sensitivity was determined by drop assay at the indicated HU dosages in strains CY12867, CY12448, CY12865, CY12960, CY12850 and CY12460. Pictures of the plates have been taken after 3 days of growth at 28°C.

To further characterize the genetic interactions between Pif1 helicases and Rad53 under replication stress we took advantage of a conditional system through which it is possible to over-express the kinase-defective *rad53-D339A* dominant negative allele under the control of the *GAL1* promoter (Pellicioli et al., 1999). In this system, the expression of the mutant protein *rad53-D339A* is directed by a construct integrated into the genome. Using this conditional system it is possible to inactivate Rad53 functions through the addition of galactose to the cell culture, which induces the over expression of the dominant negative protein *rad53-D339A* and makes the cells HU sensitive (Figure 3.28). Consistent with the previous results (Figure 3.27), we observed that the phospho-defective *rrm3-6SA* and *pif1-12A* alleles did not alter the HU sensitivity of cells in which the *rad53-D339A* mutant allele was over-expressed, while the phospho-mimicking *rrm3-6SD* mutation alleviated the HU sensitivity of *rad53-D339A* overexpressing cells (Figure 3.28). The double phospho-mimicking mutant *rrm3-6SD pif1-12D* did not further improve the viability of *rad53-D339A* mutants in HU, compared to the single *rrm3-6SD* mutant (Figure 3.28). One possible explanation for the lack of this expected result is that not all the Pif1 phosphorylated residues have been mutagenized or that the *pif1-12D* mutant protein did not fully resemble a constitutively phosphorylated protein.

The fact that the phospho-mimicking mutant of Rrm3 ameliorates the checkpoint mutant phenotypes strongly suggests that the Rad53-dependent phosphorylation of the Pif1 helicases has an inhibitory role on their activities at the stalled replication fork.

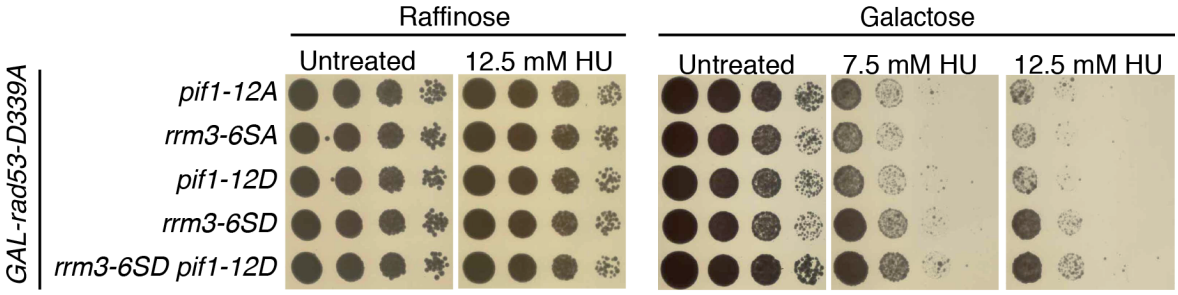

Figure 3.28. The phospho-mimicking mutants of Rrm3 and Pif1 rescue the HU sensitivity of *rad53* cells. HU sensitivity has been determined by drop assay at the indicated HU dosages in YP+2%Raffinose or YP+2%Raffinose+2%Galactose in strains: *leu2::2X-LEU2-GAL1-rad53-D339A sml1Δ pif1-12A-6HIS-*

3FLAG RRM3-13MYC (CY14011), *leu2::2X-LEU2-GAL1-rad53-D339A sml1Δ Pif1-6HIS-3FLAG rrm3-6SA-13MYC* (CY14013), *leu2::2X-LEU2-GAL1-rad53-D339A sml1Δ pif1-12D-6HIS-3FLAG RRM3-13MYC* (CY14012), *leu2::2X-LEU2-GAL1-rad53-D339A sml1Δ Pif1-6HIS-3FLAG rrm3-6SD-13MYC* (CY14014), *leu2::2X-LEU2-GAL1-rad53-D339A sml1Δ pif1-12D-6HIS-3FLAG rrm3-6SD-13MYC* (CY14015). Pictures of the plates were taken after 3 days of growth at 28°C.

3.1.7 Rrm3 and Pif1 promote fork reversal and formation of ssDNA tracks at branching points of stalled replication forks in *rad53* cells

We used the transmission electron microscopy (EM) (Neelsen et al., 2014) to directly visualize the replication intermediates accumulated in the absence of *RAD53,* 90 minutes after the G1 release in 150 mM of hydroxyurea (Figure 3.29). In *sml1Δ rad53Δ* cells we observed the typical abnormal structures previously described (Sogo et al., 2002): 41% were resected forks, either in hemireplicated (Figure 3.29A) or gapped conformation (Figure 3.29B,C), 10 % were reversed forks (Figure 3.29D) and 7 % were broken forks (Figure 3.29E). We found that the ablation of the Pif1 helicases reduced the overall accumulation of these pathological structures in *rad53* mutants; in *sml1Δ rad53Δ rrm3Δ pif1-m2* cells 28 % of the forks analysed were resected forks, 2 % reversed forks and 2 % broken forks (Figure 3.29F).

Moreover we found that, while the length of the ssDNA tracks at the fork branching point in *sml1Δ rad53Δ* cells was distributed around 800 nt, in *sml1Δ rad53Δ rrm3Δ pif1-m2* mutants the gaps at forks were significantly shorter (Figure 3.29G).

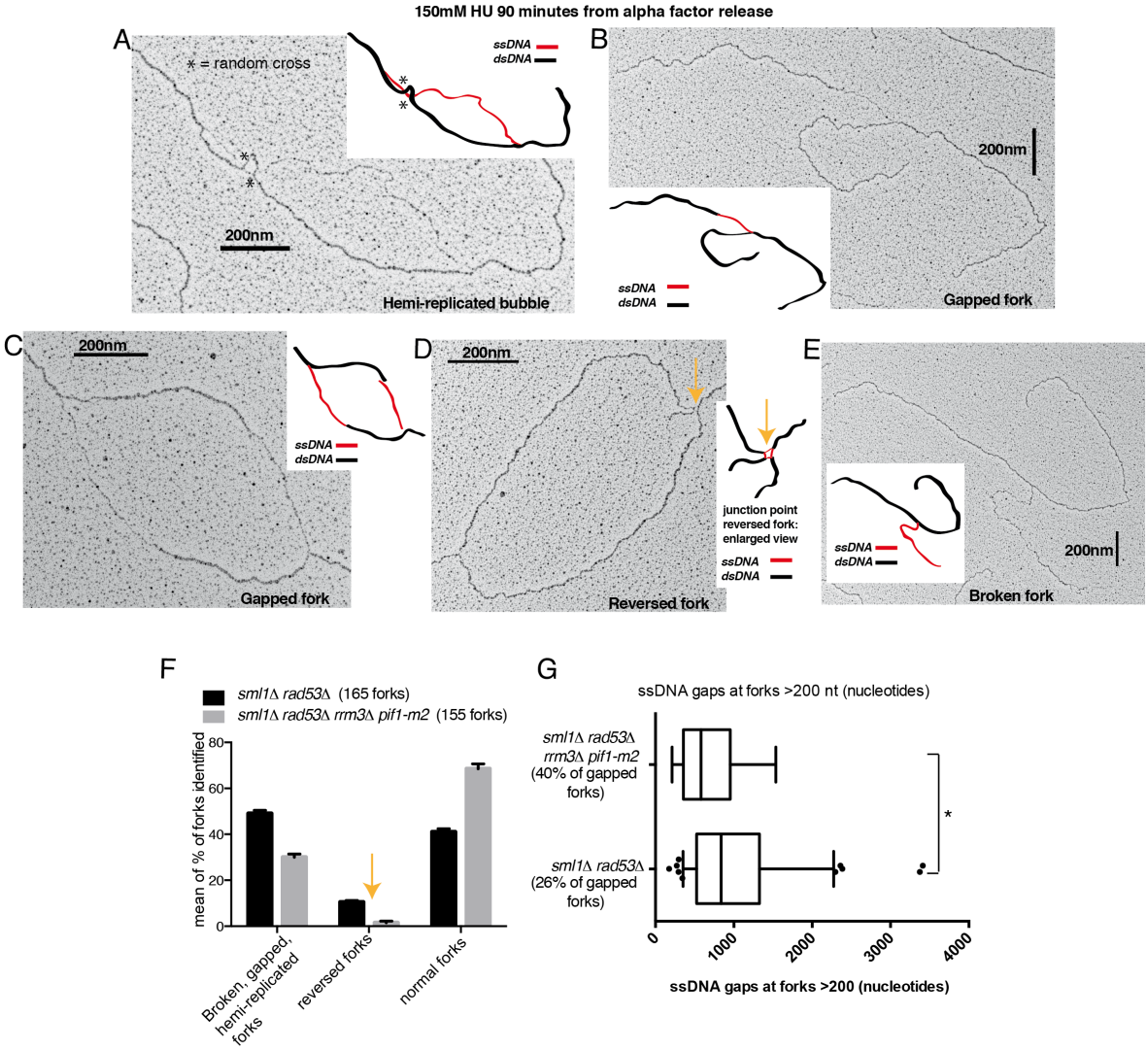

Figure 3.29. Rrm3 and Pif1 contribute to fork abnormalities in *rad53* cells treated with HU. A–E) Representative transmission electron microscopy (TEM) pictures of *in vivo* psoralen crosslinked DNA replication forks with different structural features (hemi-replicated forks, gapped forks, reversed forks, and broken forks), isolated from strains CY12443 and CY13342 at 90 min from G1 release into S-phase in the presence of 150 mM HU are shown. The 200 nm scale bars are reported in black in each TEM picture. **F)** A plot representing the means of the percentages and standard deviations of the DNA replication fork structures found in two independent experiments is reported. At least 80 DNA replication forks were analysed for each experiment. The number of samples (molecules) in the dataset is 165 forks for CY12443 and 155 forks for CY13342. The orange arrows indicate the structural features of the reversed forks and the distribution of these replication intermediates in the indicated genetic backgrounds. **G)** Distributions of the length of the ssDNA gaps measured at the fork branching points in the two strains. The ssDNA data representation is as follows (box plot): center line, median; box limits, 10th and 90th percentiles; whiskers, 1st and 99th percentiles; black dots, outliers. * $p < 0.05$ by two-tailed t test. Means of the percentages of gapped forks identified in the two strains in the two independent experiments are reported.

3.2 Crosstalk between Dna2, the Pif1 helicases and Rad9 in unperturbed DNA replication

3.2.1 A single S-phase in the absence of *DNA2* does not influence the bulk of DNA synthesis, but induces a cell cycle arrest in M-phase, with fully phosphorylated Rad53 and 2C DNA content

It has been recently reported that the *S. pombe* effector kinase Cds1 phosphorylates the nuclease Dna2 to process stalled replication forks, counteracting fork reversal (Hu et al., 2012). Interestingly, it has been also published that deletion of *PIF1* suppresses the lethality of *dna2Δ* cells, while *RRM3* deletion causes synthetic lethality when combined with *dna2* mutations (Budd et al., 2006). Moreover the mutations of the checkpoint mediators *rad9* and *mrc1* can rescue, partially, the lethality of *dna2Δ* cells (Budd et al., 2011).

Considering these data and the results reported in this thesis on the Rad53 dependent regulation of Pif1 and Rrm3 at the replication fork under replication stress, we decided to further investigate the crosstalk between Dna2, the Pif1 helicases and Rad9 in the maintenance of the DNA replication fork integrity in unperturbed conditions and under DNA replication stress, either in absence or in the presence of Rad53.

Since *DNA2* is an essential gene (Budd and Campbell, 1995), we took advantage of conditional systems to study its functions. We applied to *DNA2* the auxin-inducible degron system (*DNA2*-AID, Figure 3.30A) (Morawska and Ulrich, 2013; Nishimura et al., 2009), which uses the plant hormone auxin (indole-3 acetic acid, IAA) to induce the proteasomal dependent degradation mediated by the F-box protein *Os*Tir1 of the target protein, fused with an auxin-dependent degron sequence, AID^{71-114}-9Myc. We further improved the conditional ablation of *DNA2*, combining the AID system with the tetracycline-dependent translation control system (*Tc-DNA2-AID*, Figure 3.30B) (Kotter et al., 2009), which

prevents translation upon tetracycline binding to the three tc aptamers introduced in the 5' UTR of *DNA2*.

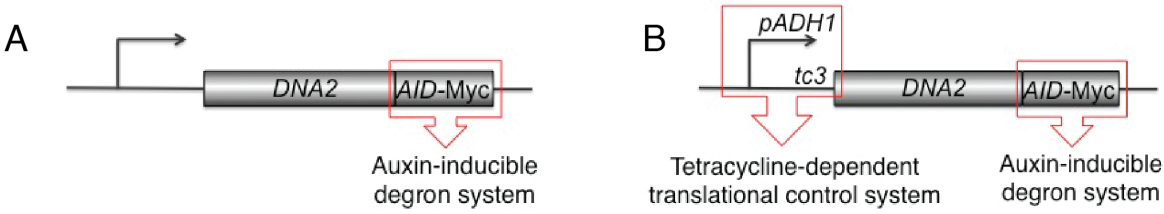

Figure 3.30. Schematic representation of systems used to induce the conditional depletion of Dna2. A) Schematic representation of the auxin-inducible degron system (Morawska and Ulrich, 2013; Nishimura et al., 2009), with the auxin-dependent degron sequence, AID^{71-114}, and the tag 9-Myc, located at the C-terminus of Dna2. In this degron system, the plant hormone auxin (indole-3 acetic acid, IAA) and the presence of the plant derived E3 enzyme Tir1 induce a rapid proteasomal-mediated degradation of Dna2. **B)** Schematic representation of the translational degron system (Kotter et al., 2009), used to deplete Dna2 in the presence of tetracycline. In this system the expression of the gene of interest is put under the control of a modified version of the *ADH1* promoter. In particular, three DNA sequences called tc aptamers, which bind strongly the tetracycline molecule and inhibit protein translation, have been inserted at the 5' UTR, to prevent the translation of *DNA2* mRNA in the presence of tetracycline. This system was used in combination with the auxin-inducible degron system to improve the conditional ablation of *DNA2*.

We first verified the efficiency of the conditional ablation of *DNA2*. *DNA2-AID* and *Tc-DNA2-AID* strains were not viable, respectively, in the presence of 0.5 mM of auxin and in the presence 0.5 mM of auxin plus 0.6 mM of tetracycline, confirming the efficient degradation of Dna2 (Figure 3.31). In the experiments presented in this second part of the thesis, if the presence of auxin or tetracycline will be indicated, it means that the two molecules are present at the above indicated concentrations, which cause a degradation of Dna2 at a level that induces cell lethality and the protein is no longer detectable by western blotting (Figure 3.32B).

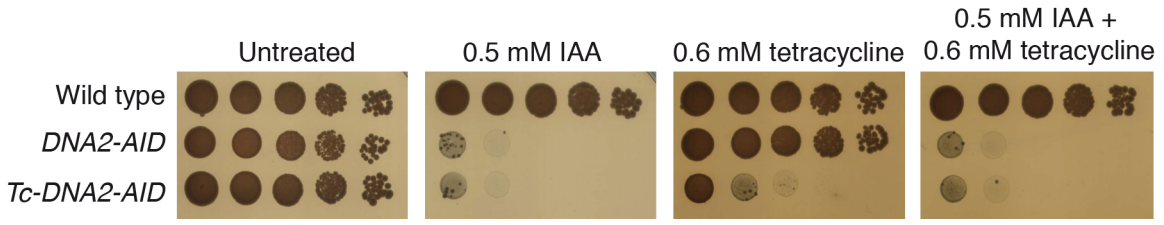

Figure 3.31. Conditional depletion of Dna2 leads to cell lethality. Ten fold serial dilutions of the strains TEMP17-I1, TEMP17-F9 and TEMP18-B4 were plated on YPD plates with or without 0,5 mM IAA and 0,6 mM tetracycline. Pictures of the plates were taken after 3 days of growth at 28°C.

Several studies, using separation-of-function *dna2* alleles, have established that the nuclease activity of the protein is required for cell survival, but the essential function of Dna2 remains elusive (Budd and Campbell, 1995; Budd et al., 2000; Lee et al., 2000). Since *dna2* point mutations, even in the helicase domain, cause severe growth defects and reduced life span (Budd et al., 2006; Hoopes et al., 2002), we decided to uncover the essential role of Dna2 by characterizing the phenotype of *DNA2*-ablated cells, using the conditional allele *Tc-DNA2-AID* (Figure 3.30B).

Since Dna2 is thought to participate in Okazaki fragment processing, we monitored the effect of the absence of Dna2 in the S-phase progression. To do this, *Tc-DNA2-AID* cells were synchronized in G1 for 2 hours and, 1 hour after the addiction of α-factor, auxin and tetracycline were added in the media to deplete *DNA2* in G1, before initiation of DNA replication. *DNA2*-ablated cells were released into S-phase in fresh medium with auxin and tetracycline for 3 hours and an untreated cell culture (without auxin and tetracycline) was kept in parallel as a control sample in which Dna2 is not degraded (Figure 3.32). Interestingly, FACS profiles, taken at the indicated time points after the G1 release in S-phase showed that *DNA2*-ablated cells were not deficient in the bulk of DNA synthesis; indeed, at 60 minutes from the G1 release, both untreated cells and *DNA2*-depleted cells completed the S-phase reaching a 2C DNA content (Figure 3.32A). While control cells entered in the second cell cycle after 2 hours from the G1 release, *DNA2*-ablated cells remained blocked, with 2C DNA content and 98% of dumbbell shaped cells even after 3 hours from the G1 release (Figure 3.32A and data not shown). This result is in line with previous studies that have reported that temperature-sensitive *dna2* mutants grown at the restrictive temperature arrest the cell cycle at G2/M-phase in a Rad9- and Mec1-dependent manner (Fiorentino and Crabtree, 1997).

With the aim of verifying, at a biochemical level, that the arrest caused by ablation of Dna2 really occurs at mitosis and it is due to a fully active DNA damage checkpoint we decided to analyse, by western blotting, the phosphorylation state of the DNA polymerase

α-primase B subunit and Rad53, which are markers, respectively, of mitosis (Foiani et al., 1995; Palou et al., 2015) and of DNA damage checkpoint activation (Pellicioli et al., 1999). We also verified that, in the presence of auxin and tetracycline, Dna2 was rapidly depleted in G1 and was not detectable along the entire experiment (Figure 3.32B). As expected, we found that in control cells Pol12, which is phosphorylated in an M-CDK-dependent way (see Introduction), was unphosphorylated in G1 arrested cells, hyperphosphorylated at 60-90 minutes form the G1 release when the cells reached mitosis with 2C DNA content and unphosphorylated when cells entered in the second cell cycle at 2 hours from the G1 release (Figure 3.32A,B). Moreover Rad53 was not phosphorylated in control cells without auxin and tetracycline along the entire experiment (Figure 3.32B) suggesting that control cells underwent through a normal S-phase.

Dna2-ablated cells entered in mitosis with the same kinetic of control cells; Pol12 was hyperphosphorylated at 60 minutes from the G1 release but, differently from control cells, it remained fully phosphorylated until the end of the experiment (Figure 3.32B). Importantly, while Rad53 was not activated in control cells, in the absence of Dna2 the kinase started to be hyperphosphorylated at 90 minutes from the G1 release, when Dna2 ablated cells were already in mitosis, according to the hyperphosphorylated state of Pol12 corresponding to high M-CDK activity (Figure 3.32B).

These results demonstrate that *DNA2*-ablated cells are not deficient in the bulk of DNA synthesis, which occurs without Rad53 activation; on the contrary the lack of Dna2 for a single S-phase induces checkpoint activation and cell cycle arrest when the cells enter into mitosis (Figure 3.32).

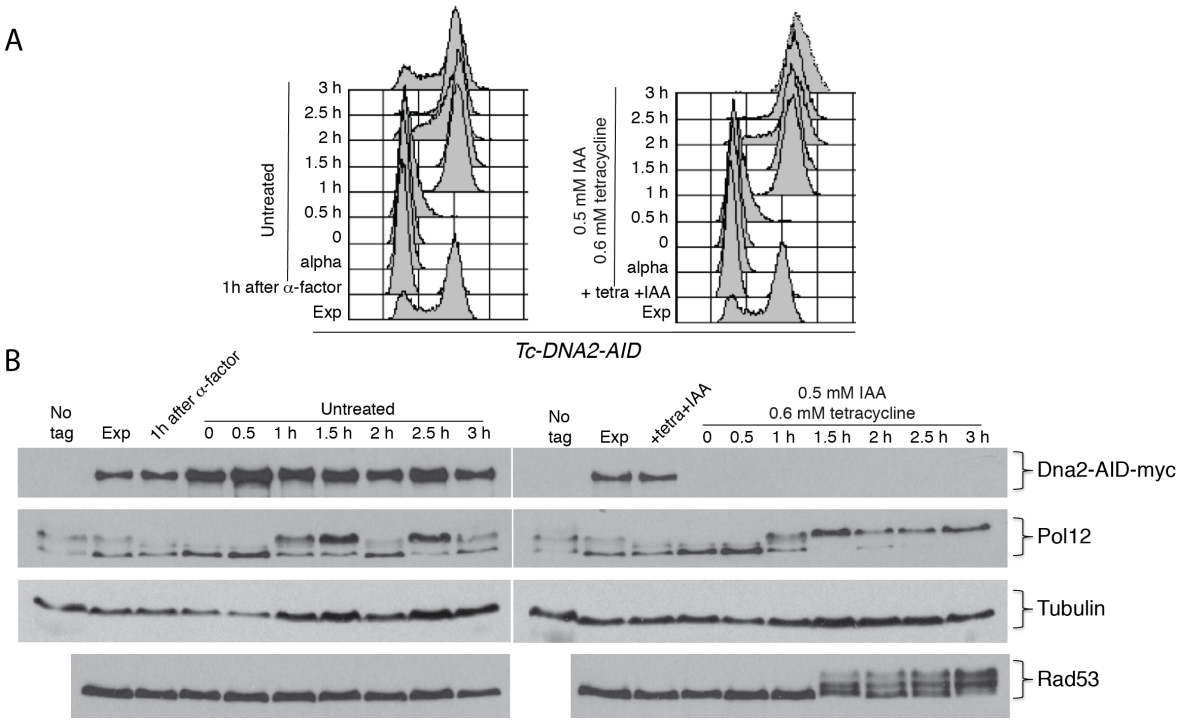

Figure 3.32. *dna2*-ablated cells are proficient in the bulk of DNA replication but, after a single S-phase, remain blocked in M-phase with 2C DNA content and with phosphorylated Rad53 and B subunit of the DNA plolymerase α. *Tc-DNA2-AID* (TEMP18-B4) cells were arrested in G1 for 2 hours and, 1h before the release into the cell cycle, 0,5 mM IAA and 0,6 mM tetracycline were added in the media in order to achieve complete depletion of Dna2 in G1 before starting DNA replication. Cells were released into S-phase in the presence of 0,5 mM IAA and 0,6 mM tetracycline. 2 hours after the G1 release, additional 0,3 mM tetracycline was added to reinforce the block of Dna2 translation. An untreated culture, in which IAA and tetracycline were not added and Dna2 was not degraded, was kept as a control. FACS samples for the determination of the cellular DNA content **(A)** and samples for protein analysis **(B)** were collected at the indicated time points. The protein levels of Dna2 and of tubulin (as loading control) were analysed by western blotting, respectively, using anti-myc antibodies and anti tubulin antibodies. Rad53 activation and Pol12 phosphorylation were monitored by western blotting, respectively, using anti-Rad53 antibody (EL7) and anti-Pol12 antibodies (D6).

To better characterize whether specific stages of mitosis (like metaphase to anaphase transition), are required for checkpoint activation when Dna2-depleted cells enter into mitosis, we synchronized the *DNA2-AID* strain in G1 in the presence of auxin and released cells in fresh medium without alpha factor and with auxin and nocodazole to block the cells in metaphase (Figure 3.33). Western blotting was used to monitor the efficiency of *DNA2* depletion and the checkpoint activation, through the analysis of Rad53 phosphorylation. Even if the metaphase-anaphase transition was impeded, in the absence of Dna2, Rad53 started to be phosphorylated 90 minutes after the G1 release in S-phase

and remained hyperphosphorylated throughout the rest of the experiment (Figure 3.33), with the same kinetic observed in the previous experiment (Figure 3.32B). The fact that the absence of Dna2 induced checkpoint activation also in nocodazole-arrested cells strongly suggests that the activity of Dna2 is essential after the S-phase and before the metaphase to anaphase transition.

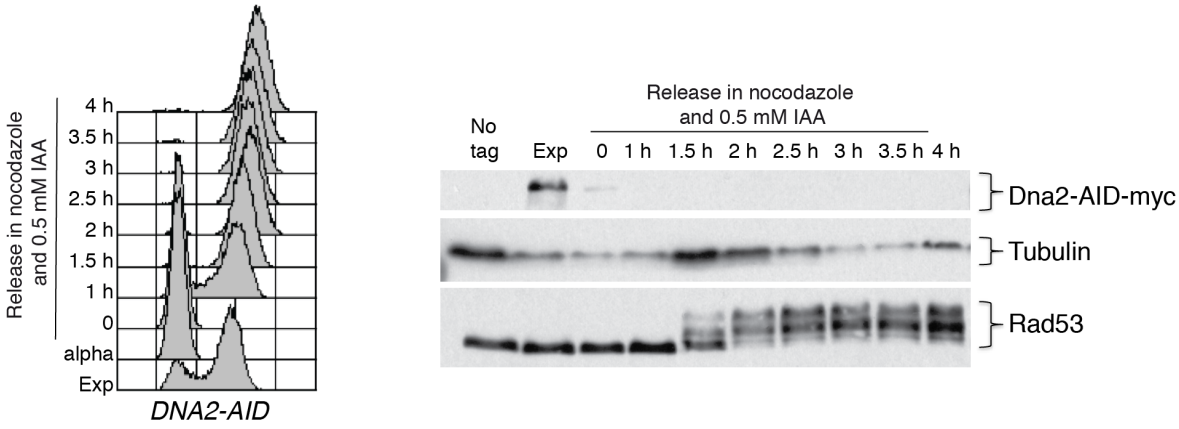

Figure 3.33. Metaphase to anaphase transition inhibition by nocodazole does not prevent Rad53 hyperphosphorylation induced by a single S-phase in the absence of Dna2. *DNA2-AID* (TEMP17-F9) cells were synchronized in G1, in the presence of 0.5 mM of IAA (added in the media 1h after the α-factor) to induce the degradation of *DNA2-AID* in G1 before the beginning of the S-phase, and released into S-phase in the presence of nocodazole (20 μg/ml) to block the methaphase-anaphase transition and 0.5 mM IAA to maintain Dna2 degradation. Rad53 phosphorylation and the protein levels of Dna2-AID-9Myc and of the tubulin were analysed by western blotting using specific antibodies at the indicated time points. FACS analysis are shown.

3.2.2 The ablation of *PIF1* rescues the G2/M arrest and checkpoint activation caused by a single S-phase in the absence of Dna2

Since it has been shown that the lethality of *dna2Δ* cells can be rescued by deleting the nuclear isoform of Pif1 (Budd et al., 2006) and is partially suppressed by the deletion of the checkpoint mediator *RAD9* (Budd et al., 2011), while *RRM3* deletion is synthetic lethal with *dna2* mutations (Budd et al., 2006), we validated these *DNA2* genetic interactions in the *DNA2-AID* background, testing the viability of the cells by drop assay in the presence of auxin (Figure 3.34). We confirmed the opposite synthetic genetic effects caused by *RRM3* and *PIF1* ablations on the survival of *dna2* cells (Budd et al., 2006); indeed we

observed that the *RRM3* deletion did not alter the cell lethality of *DNA2* ablated cells, while the ablation of the nuclear isoform of Pif1, using the *pif1-m2* allele, completely suppressed the auxin-induced cellular lethality of *DNA2-AID* cells (Figure 3.34).

RAD9 deletion only partially rescued the auxin-induced lethality of *DNA2-AID* cells and a light rescue was observed also in the presence of the kinase-defective *rad53-K227A* allele (Figure 3.34).

Rad9 is the DNA damage checkpoint adaptor, that in the presence of DNA damage is phosphorylated by Mec1, associates with the FHA domains of Rad53 mediating the interaction between Mec1 and Rad53 and act as a scaffold to allow the full activation of Rad53 through auto-phosphorylation (Pellicioli and Foiani, 2005). The presence of long 5'-DNA flaps, generated by Pif1 on unprocessed Okazaki fragments in the absence of Dna2, is thought to induce the DNA damage checkpoint activation that leads to a permanent cell cycle arrest and cell lethality in *dna2* cells (Budd et al., 2011; Budd et al., 2006; Levikova and Cejka, 2015; Pike et al., 2009; Pike et al., 2010; Rossi et al., 2008). One expectation is that ablation of *RAD9*, which is a fundamental regulator of the G2/M DNA damage checkpoint, would allow *dna2* cells to proceed in the cell cycle, likely at the expense of an increased genome instability/chromosome alterations due to the inappropriate processing of the Okazaki fragments at the DNA replication forks (see next paragraphs and discussion). In agreement with to previous reports (Budd et al., 2011), *RAD9* deletion partially rescued the lethality of *DNA2*-ablated cells (Figure 3.34). We note that the dimension of the colonies in *dna2 rad9* cells is much smaller than the dimension of the colonies in *dna2 pif1-m2* cells, suggesting that the growth rate in *dna2 rad9* cells may be lower than wild type or *dna2 pif1-m2* cells growth rate (Figure 3.34). It is reasonable to think that *dna2 rad9* cells could suffer the genome instability caused by Pif1-induced abnormalities at the DNA replication forks. In agreement with the small dimension of the colonies of *dna2 rad9* cells, we have recently discovered that Dna2 depletion in the

absence of *RAD9* allows cells to execute only a defined number of generations and after that *dna2 rad9* cells die with chromosomal alterations (Figure 3.43 and Figure 3.45).

The same considerations can be likely applied to the suppression of *dna2* cell lethality caused by the ablation of *RAD53* through the *rad53-K227A* allele. As it can be noted in figure 3.34, *dna2 rad53-K227A* cells showed a severe growth defect, compared to the control cells and to *dna2 pif1-m2* cells.

The ablation of *PIF1* rescues the cell lethality caused by the absence of Dna2 and restores a grow rate similar to the wild type cells; on the contrary, suppression of the lethality of *dna2* cells induced by checkpoint ablation is likely to generate mutant cells that have high levels of genomic instability due to the progression into the cell cycle in the presence of continued unscheduled actions of Pif1 on the Okazaki fragments of the lagging strand and the subsequent creation of fork abnormalities and chromosome alterations.

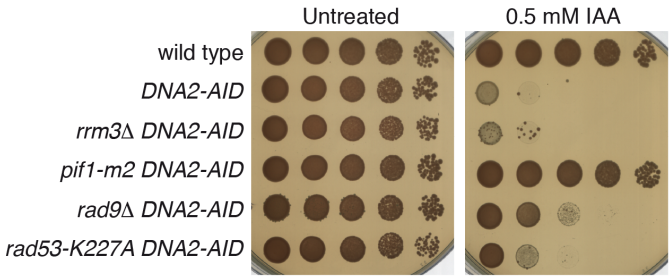

Figure 3.34. *PIF1* and *RAD9* ablations and the *rad53-K227A* allele rescue the lethality of *dna2* cells, while *rrm3 dna2* cells die after a single S-phase. Viability of strains TEMP17-I1, TEMP17-F9, TEMP17-H4, TEMP17-G3, TEMP17-I5 and TEMP18-B1 was determined by drop assay in the absence and in the presence of 0.5 mM IAA. Pictures of the plates were taken after 3 days of growth at 28°C.

To study the genetic interactions between *DNA2, RRM3* and *PIF1,* overcoming the fact that the double mutant *pif1-m2 rrm3Δ* displays a strong slow growth phenotype, we had applied the tetracycline-dependent translation control systems (Kotter et al., 2009) to *RRM3* (*Tc-RRM3*) and we generated the triple mutant *pif1-m2 Tc-RRM3 DNA2-AID.*

We observed that *RRM3* ablation, as well as *RRM3* deletion, did not have any effect on the auxin-induced lethality of *DNA2-AID* cells (Figure 3.35).

In the triple mutant *pif1-m2 Tc-RRM3 DNA2-AID,* cell lethality was induced only on plates containing both IAA and tetracycline, where combined degradation of Dna2 and Rrm3 occurred (Figure 3.35).

Based on this data, we conclude that Rrm3 is essential for cell viability in the absence of Pif1 and Dna2, and this is in line with previously reported observations (Budd et al., 2006).

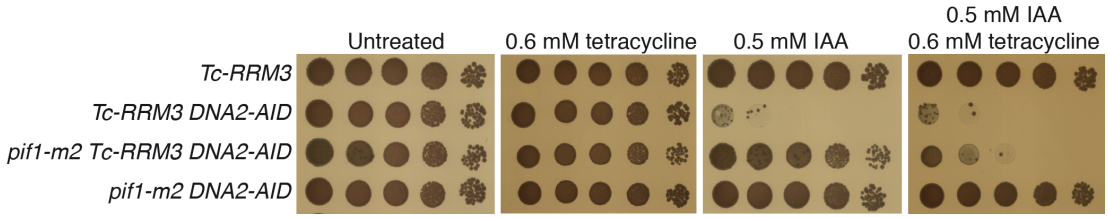

Figure 3.35. *RRM3* deletion in *pif1-m2 dna2* cells is synthetic lethal. Viability of strains TEMP18-D2, TEMP18-C7, TEMP18-D6 (which carry the *pADH1-Tc3-HA-RRM3* allele) and TEMP17-G3 was determined by drop assay in the absence and in the presence of 0.5 mM IAA and 0.6 mM tetracycline. Pictures of the plates were taken after 3 days of growth at 28°C.

To better understand the crosstalk between *PIF1*, *RRM3*, *RAD9* and *DNA2* during an unperturbed S-phase at a biochemical level, we decided to monitor Rad53 activation during a single S-phase in the presence of auxin in a series of strains carrying combinations of mutations of the above genes with the *DNA2-AID* allele. In particular, *DNA2-AID*, *DNA2-AID pif1-m2*, *DNA2-AID rad9Δ*, *DNA2-AID rrm3Δ* cells were synchronized in G1 in the presence of auxin to deplete *DNA2* and released into S-phase in conditions in which Dna2 degradation was continuously induced (Figure 3.36). The same experiment was performed with *DNA2-AID Tc-RRM3* and *DNA2-AID Tc-RRM3 pif1-m2* cells, adding in the media also tetracycline in order to induce a block in the *RRM3* translation and subsequent Rrm3 degradation (Figure 3.36, 3.37).

We verified, through western blotting, that the depletions of Dna2 and Rrm3 were effective and the two proteins were absent or barely detectable along the entire experiment (Figure 3.36B, 3.37B).

The FACS analysis of DNA content showed that, while *DNA2-AID*, *DNA2-AID rrm3Δ*, *DNA2-AID Tc-RRM3* and *DNA2-AID Tc-RRM3 pif1-m2* cells underwent an M phase arrest, *DNA2-AID pif1-m2* and *DNA2-AID rad9Δ* strains completed the mitosis and progressed into the second cell cycle (Figures 3.36A, 3.37A). In agreement with these data, Rad53 was not phosphorylated in *DNA2-AID pif1-m2* and *DNA2-AID rad9Δ* strains, while it was heavily hyperphosphorylated in *DNA2-AID rrm3Δ* and *DNA2-AID Tc-RRM3* strains with the same kinetic observed in *DNA2-AID* cells (Figure 3.36B).

Moreover, as previously reported (Ivessa et al., 2003), a mild checkpoint activation was detectable in *rrm3Δ* mutants in the samples taken form exponentially growing cells and 1 hour after the G1 release in S-phase.

Interestingly, in the triple mutant *DNA2-AID Tc-RRM3 pif1-m2,* Rad53 was modestly phosphorylated even at very late stages of S-phase or mitosis and 4 hours after the G1 release the hyperphosphorylated level of Rad53 was not detectable (Figure 3.37B). This evidence strongly suggests that the observed cell cycle arrest in *DNA2-AID Tc-RRM3 pif1-m2* cells is not a consequence of the DNA damage checkpoint activation, but rather it can be caused either by the activation of other surveillance pathways (like the spindle assembly checkpoint), or by the presence of chromosome entanglements, which likely do not contain DNA structures able to induce checkpoint activation. Another possible explanation is that Dna2, Pif1 and Rrm3 synergize in the direct activation of Mec1 or Rad53 as it has already been reported for Dna2, Ddc1 and Dpb11 ((Kumar and Burgers, 2013; Majka et al., 2006; Mordes et al., 2008; Navadgi-Patil and Burgers, 2009; Navadgi-Patil et al., 2011) and see Discussion).

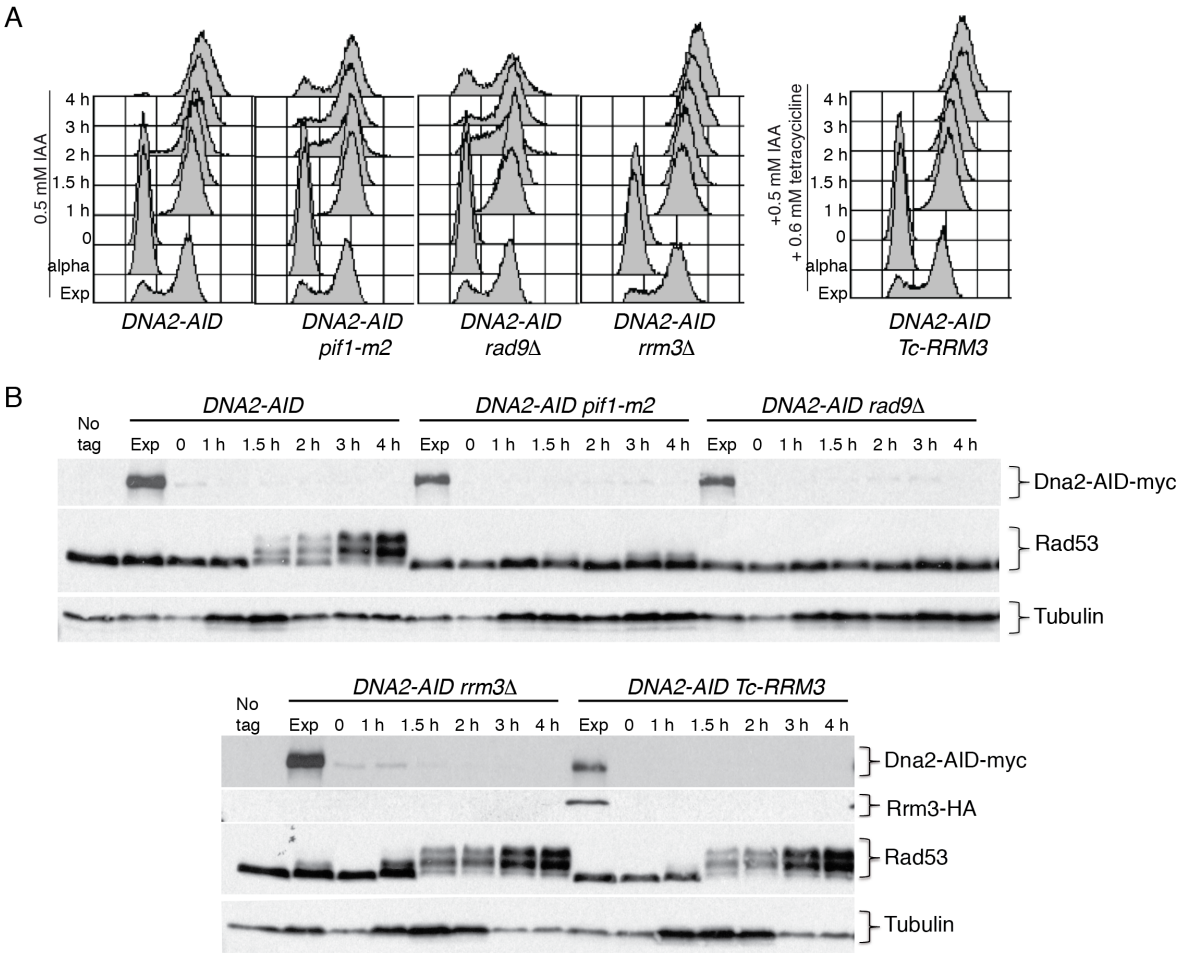

Figure 3.36. *PIF1* and *RAD9* ablations rescue checkpoint activation and the G2/M arrest induced by a single S-phase in the absence of Dna2. *DNA2-AID* (TEMP17-F9), *DNA2-AID pif1-m2* (TEMP17-G3), *DNA2-AID rad9Δ* (TEMP17-I6) *DNA2-AID rrm3Δ* (TEMP17-H4) cells were synchronized in G1 in the presence of 0,5 mM IAA (added in the media 1h after α-factor addition) to induce the degradation of *DNA2-AID*, and released in 0.5 mM IAA for 4 h. *DNA2-AID Tc-RRM3* (TEMP18-C7) cells were synchronized in G1 in the presence of 0,5 mM IAA (to induce the degradation of *DNA2-AID)* and 0,6 mM tetracycline (to block the translation of *RRM3* mRNA); cells, depleted for Dna2 and Rrm3, were released in fresh medium containing 0,5 mM IAA and 0,6 mM tetracycline. Dna2 and Rrm3 degradation, and Rad53 activation, were monitored by western blotting using specific antibodies at the indicated time points (**B)**. Tubulin was used as loading control. FACS analysis are shown **(A)**.

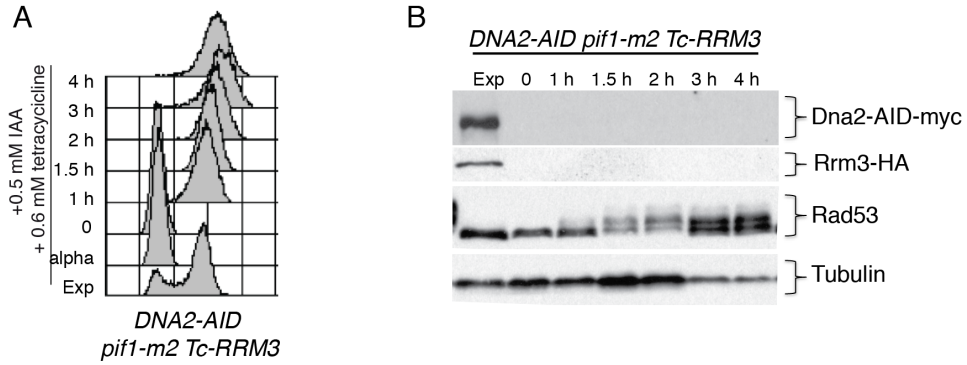

Figure 3.37. *dna2 rrm3 pif1* triple mutant arrests in M-phase with 2C DNA content and mild Rad53 phosphorylation. *DNA2-AID Tc-RRM3 pif1-m2* (TEMP18-D6) cells were synchronized in G1 in the presence of 0,5 mM IAA (to induce the degradation of *DNA2-AID)* and 0,6 mM tetracycline (to block the translation of *RRM3* mRNA). Cells, depleted for Dna2 and Rrm3, were released into S-phase in fresh medium containing 0,5 mM IAA and 0,6 mM tetracycline. FACS profiles showing the cellular DNA contents during the experiments are shown **(A).** Dna2 and Rrm3 degradations, and Rad53 activation were monitored by western blotting, using specific antibodies at the indicated time points **(B)**. Tubulin levels were detected in the experiment by western blotting using specific antibodies and were used as loading control.

3.2.3 Deletion of the DNA damage checkpoint, combined with a reduced fork speed, suppresses the G2/M arrest, Rad53 activation and cell lethality caused by the absence of Dna2

Since it has been reported that Dna2, Ddc1 and Dpb11 directly stimulate the Mec1 kinase activity through the physical interactions with Mec1 (Kumar and Burgers, 2013; Majka et al., 2006; Mordes et al., 2008; Navadgi-Patil and Burgers, 2009; Navadgi-Patil et al., 2011), specifically in S-phase, to initiate the replication checkpoint, we explored the effects of *DNA2* ablation on Rad53 activation in the presence of hydroxyurea. *DNA2-AID* cells, with or without *DNA2*, were synchronized in G1 and released in S-phase in the presence of 25 mM of HU. The efficiency of Dna2 depletion and Rad53 phosphorylation were analysed by Western blotting at the indicated time points after the release in S-phase (Figure 3.38). FACS analysis of DNA content showed that, in the presence of 25 mM HU, the S-phase was prolonged compared to unperturbed conditions and control cells completed the mitosis and progressed into the next cell cycle between 2.5 and 3 hours after

the G1 release into S-phase (Figure 3.38A); surprisingly also *DNA2* ablated cells were able to progress in the second cell cycle (Figure 3.38A, yellow arrow), while they experienced a terminal cell cycle arrest in the M-phase of the first cell cycle in the absence of hydroxyurea (see FACS profiles in Figure 3.32A). These data suggest that the arrest in the mitosis of the first cell cycle, caused by a single S-phase in the absence of Dna2, is suppressed by low HU concentrations.

Control cells that proceed into S-phase in the presence of 25 mM of HU exhibited Rad53 phosphorylation at 60 minutes from the G1 release, after that the Rad53 kinase was completely inactivated when the cells entered into mitosis and proceeded in the next cell cycle at 2 hours from the G1 release in HU (Figure 3.38B). *DNA2-AID* cells, released into S-phase in the presence of auxin and HU, showed a complete degradation of Dna2 and the same kinetic of Rad53 activation and inactivation of the control cells (Figure 3.38B).

Therefore, we conclude that, in the presence of low HU doses, the S-phase checkpoint signalling is not compromised in *DNA2* ablated cells, as previously suggested (Kumar and Burgers, 2013).

Surprisingly, we found that the presence of low doses of hydroxyurea avoids the permanent checkpoint activation and, consequently, the terminal first cell cycle arrest at mitosis caused by the absence of *dna2* in a single S-phase. Indeed, strikingly, even after 120 minutes after the release into S-phase with low HU, Rad53 was almost completely dephosphorylated in *DNA2*-ablated cells (Figure 3.38B). As it can be appreciated from the FACS analysis, cells ablated for *DNA2* and released in S-phase in the presence of 25 mM HU were able to enter in the second cell cycle around 3 hours after the release, with a low level of Rad53 phosphorylation. On the contrary the same cells exhibited a very strong cell cycle arrest with hyperphosphorylated Rad53 when released in S-phase in the absence of HU (compare Figures 3.32 and 3.38). Moreover, wild type cells proceeded synchronously and entered in the third cell cycle at 4 hours from the G1 release (showing that they can replicate their genome several times in the presence of 25 mM of HU). On the contrary,

DNA2 ablated cells remained blocked in the M-phase of the second cell cycle and progressively exhibited a dumbbell conformation (Figure 3.38 and unpublished observations). This likely happened because, even if low HU concentration was very effective in suppressing the first cell cycle arrest caused by the absence of Dna2, a mild Rad53 activation was detectable in *dna2* cells in the second cell cycle in the presence of HU (Figure 3.38B).

This result strongly suggests that, even if *DNA2* ablated cells are able to pass through the first mitosis and proceed into the second cell cycle in the presence of low HU concentrations, the residual fork abnormalities accumulated after two subsequent S-phases without Dna2 will likely induce the arrest of these cells in the second cell cycle with activated Rad53 (Figure 3.38).

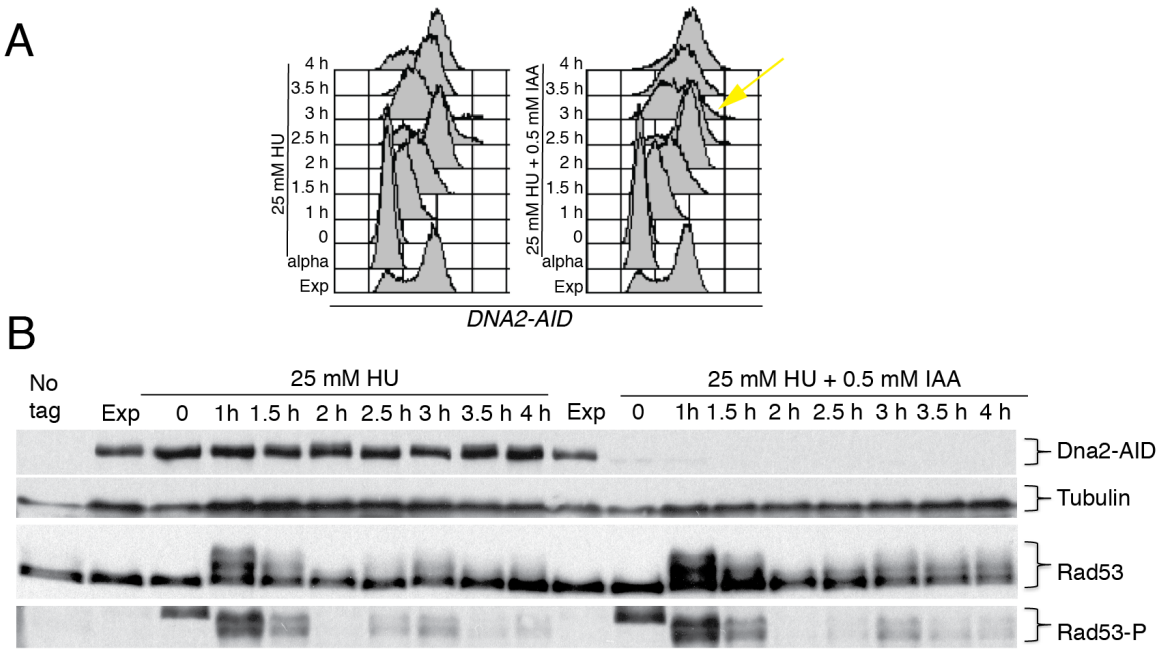

Figure 3.38. HU treatment abolishes Rad53 activation and the G2/M arrest induced by the absence of *Dna2* in a single S-phase. *DNA2-AID* (TEMP17-F9) cells were synchronized in G1 with or without 0.5 mM IAA (to deplete Dna2 in G1) and released into S-phase in the presence of 25 mM of HU, with or without 0.5 mM IAA. FACS profiles, showing the cellular DNA content during the experiment, are shown (**A)** and a yellow arrow indicates the cell cycle progression into mitosis observed in *DNA2* ablated cells in the presence of 25 mM HU. Dna2 protein level, tubulin and Rad53 phosphorylation were visualized by western blotting using specific antibodies at the indicated time points (**B).**

Since we observed that slowing down of the speed of the replication forks with low HU dose was able to suppress the first cell cycle arrest caused by the ablation of *DNA2* but did not prevent the arrest of *dna2* cells at the mitosis of the second cell cycle we did not expect that low HU doses would rescue the cellular lethality of *DNA2* ablated cells. Accordingly, we found that *DNA2* ablated cells did not grow better in plates containing auxin and 10 mM of HU compared to plates with HU (Figure 3.39). As positive control of the effectiveness of the HU in this experimental condition we spotted *rad53* mutant cells, which showed pronounced HU hypersensitivity (Figure 3.39). Interestingly, the capability of the *pif1-m2* mutation to suppress the cellular lethality associated to the absence of Dna2 was not influenced by the slowing down of the rate of DNA replication, indeed *DNA2-AID pif1-m2* cells were alive on plates with 10 mM of HU and auxin and grew at the same extent of untreated cells (Figure 3.39). Moreover, the presence of HU did not suppress the lethality caused by the combined absence of Dna2 and Rrm3 as shown by the lethality of *DNA2-AID rrm3Δ* cells in the presence of HU and auxin (Figure 3.39).

It has been reported that the ablation of the G2/M DNA damage checkpoint (through the deletion of *RAD9*), partially suppresses the lethality of *DNA2* depleted cells, likely at the expense of an increased genome instability (see results paragraph 3.2.2 and (Budd et al., 2011)). We have found that *DNA2-AID rad9Δ* cells, in the presence of auxin, are able to divide but when the replication defects, caused by the ablation of Dna2, are propagated for more than a defined number of generations, *dna2 rad9* cells arrest in mitosis with high percentage of dumbbell cells and die (see figure 3.43A). Based on what previously proposed (Budd et al., 2011; Budd et al., 2006; Levikova and Cejka, 2015; Pike et al., 2009; Pike et al., 2010; Rossi et al., 2008), we hypothesize that if the DNA replication defects caused by the absence of Dna2 are due to abnormal formation of 5' flaps in consequence of extensive DNA polymerase δ/Pif1-mediated strand displacement events on the lagging strand, slowing down of the speed of the DNA replication forks would be very effective in ameliorating the cell growth of *dna2 rad9Δ* cells. According to this hypothesis

we found that *DNA2-AID rad9Δ* cells grew much better on plates with auxin when 10 mM of HU was present (Figure 3.39). Importantly, while the colonies of *DNA2-AID rad9Δ* cells on auxin have a smaller dimension compared to the colonies of control cells or *DNA2-AID pif1-m2* cells, the combined presence of auxin and low HU almost completely suppressed the slow growth defect of *dna2 rad9* cells (Figure 3.39).

Low HU concentrations were not able to alleviate the slow growth defect of the *DNA2-AID rad53-K227A* strain grown in the presence of auxin likely because the HU sensitivity induced by the presence of the *rad53-K227A* allele is so high that already at 10 mM of HU a large fraction *rad53-K227A* cells was died (Figure 3.39).

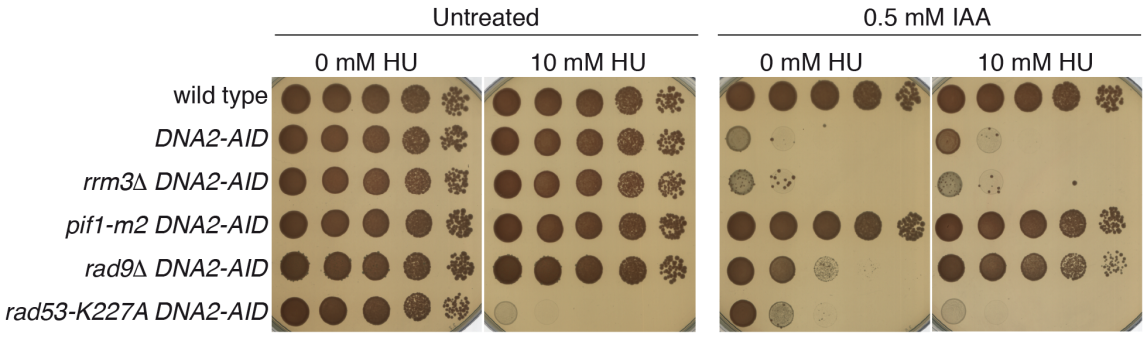

Figure 3.39. The ablation of the *RAD9*-dependent DNA damage checkpoint, combined with a reduced fork speed induced by treatment with a low dose of HU, rescues the lethality *of DNA2*-ablated cells. A) Ten fold serial dilutions of strains TEMP17-I1, TEMP17-F9, TEMP17-H4, TEMP17-G3, TEMP17-I5 and TEMP18-B1 were spotted on 0 mM HU plates and 10 mM HU plates, with or without 0.5 mM IAA. Pictures of the plates were taken after 3 days of growth at 28°C.

To further validate the hypothesis that growth defects of *dna2 rad9* cells (and *dna2 rad53-K227A* cells) can be suppressed by slowing down the speed of DNA replication, we incubated the *DNA2-AID rad9Δ* and *DNA2-AID rad53-K227A* cells at low temperatures (16ºC or 20ºC) in the presence of auxin. We found that low temperature was able to suppress the growth defects of *dna2 rad9* and *dna2 rad53* cells and mildly rescued the lethality of *dna2* cells (Figure 3.40A).

Another implication of our findings is that high growth temperature and the corresponding increase of the DNA replication speed should worsen the growth capability of *DNA2-AID*

rad9Δ and *DNA2-AID rad53-K227A* cells plated on auxin. Accordingly, we found that high growth temperatures (33ºC) in the presence of auxin, decreased the growth capability of the *DNA2-AID rad9Δ* and *DNA2-AID rad53-K227A* cells (Figure 3.40B).

Based on this experimental evidence we conclude that the ablation of the Rad9-dependent DNA damage checkpoint and the slowing down of the replication fork speed (through the treatment with low HU doses or incubation at low temperature), synergistically rescue the lethality of *DNA2*-ablated cells.

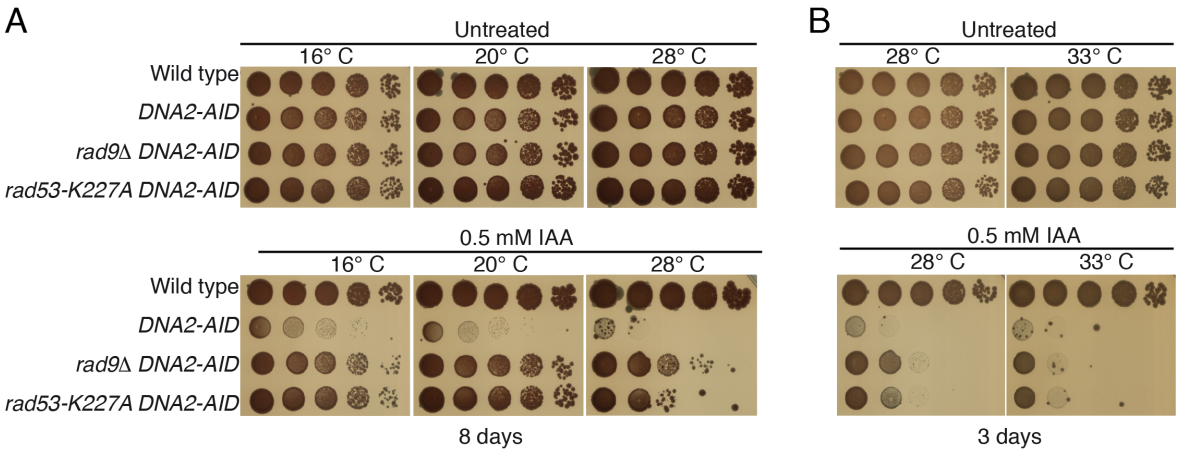

Figure 3.40. The ablation of the DNA damage checkpoint and reducing the fork speed, through incubation at low temperature, rescue the lethality of *DNA2*-ablated cells. Cell viability of strains TEMP17-I1, TEMP17-F9, TEMP17-I5 and TEMP18-B1 was determined by drop assay in the absence and in the presence of 0.5 mM IAA. Pictures of plates, taken after 3 days of growth at 28°C and at 33°C, are reported in panel **B,** while in panel **A** are shown pictures of plates incubated at 16°C, 20°C and 28°C until 8 days.

3.2.4 *DNA2* ablation in a single S-phase does not induce replication fork pausing at rDNA, tRNA^{A} and RNA-Polymerase-II-transcribed genes, but causes the shortening of rDNA after 4.5 generations in *rad9Δ* cells

Considering our previous results, a single S-phase in the absence of Dna2 leads to the accumulation of DNA damage that activate the checkpoint in mitosis and induces a strong first cell cycle arrest. Therefore, we hypothesised that Dna2 could play an essential role in the replication of specific pausing elements, the replication of which has been reported to

occur in late S-phase or in mitosis (Deshpande and Newlon, 1996; Fachinetti et al., 2010; Greenfeder and Newlon, 1992; Ivessa et al., 2003; Mechali et al., 2013; Menolfi et al., 2015).

Since *FOB1* deletion rescues the slow growth phenotype and the bleomycin sensitivity of *dna2-2* mutant, carrying a point mutation in the helicase domain, and since *dna2-2* causes Fob1-dependent replication fork stalling and double strand breaks in the ribosomal DNA (Weitao et al., 2003b), we hypothesized that Dna2 could be essential for replication fork progression across the ribosomal DNA, an Rrm3-depenent pausing site (Ivessa et al., 2003). To address this possibility, we first checked if the lethality of *DNA2*-ablated cells was rescued by the absence of Fob1, the protein required for the polar replication fork arrest at the replication fork barrier (RFB) of the rDNA. Unexpectedly, drop assay showed that *FOB1* deletion did not rescue the auxin-induced lethality of *DNA2-AID* cells (Figure 3.41).

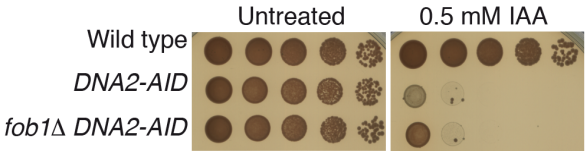

Figure 3.41. Cell lethality induced by *DNA2* ablation is not suppressed by *FOB1* deletion. Cell viability of strains TEMP17-I1, TEMP17-F9, TEMP18-I2 was determined by drop assay in the absence and in the presence of 0.5 mM IAA. Pictures of the plates were taken after 3 days of growth at 28°C.

Coherent with this, we also found that the ablation of *DNA2* did not affect the replication fork progression across the rDNA, which was monitored by neutral-neutral 2D gels in cells depleted or not for *DNA2,* 45 minutes after the G1 release in S-phase (Figure 3.42A,B).

tRNA genes have been shown to be potent natural pausing sites, which induce strong DNA replication fork pausing, especially in the absence of *RRM3* (Deshpande and Newlon, 1996; Ivessa et al., 2003). We hypothesised that Dna2 could be needed for the replication of tRNA genes and to test this hypothesis we monitored replication fork progression across the $tRNA^{A}$ locus (Ivessa et al., 2003), 45 minutes after the release into S-phase, but we

failed to detect any differences in the 2D gels signals, between cells that progressed through S-phase in the presence or in the absence of Dna2 (Figure 3.42A,C).

Dna2 did not seem to play a role even in the replication of RNA Pol II transcribed genes, which have been reported to be strong DNA replication impediments (Azvolinsky et al., 2009). We found that, 45 minutes after the G1 release in S-phase in the presence of auxin, *DNA2* depleted cells did not accumulate 2D gel pausing signals at the level of the RNA PolII transcribed gene *TEF2* (Figure 3.42A,D).

This preliminary evidence obtained by 2D gels suggests that the DNA replication fork defects caused by the absence of Dna2 in a single S-phase do not influence DNA replication fork progression at three most representative pausing sites identified in the genome of *S.cerevisiae* (Azvolinsky et al., 2009; Deshpande and Newlon, 1996; Ivessa et al., 2003). It is of note that in the experimental conditions used to detect replication fork pausing (45 minutes from the release in S-phase), both control and Dna2-ablated cells were in late S-phase and were close to reach the 2C DNA content (as shown in the FACS profiles in figure 3.42A). Importantly, in this condition, both control cells and Dna2 ablated cells entered into mitosis 60 minutes from the G1 release as it can be seen by the phosphorylation of DNA polymerase α-primase B subunit (see Figure 3.32B), while Rad53 phosphorylation rised at 90 minutes in Dna2 ablated cells when they were already in mitosis (see Figure 3.32B). We cannot exclude that DNA replication pausing signals, due to the absence of Dna2, are induced between 45 minutes and 90 minutes from the G1 release although we favour the hypothesis that Dna2 is not required for DNA replication across the analysed pausing sites (see discussion).

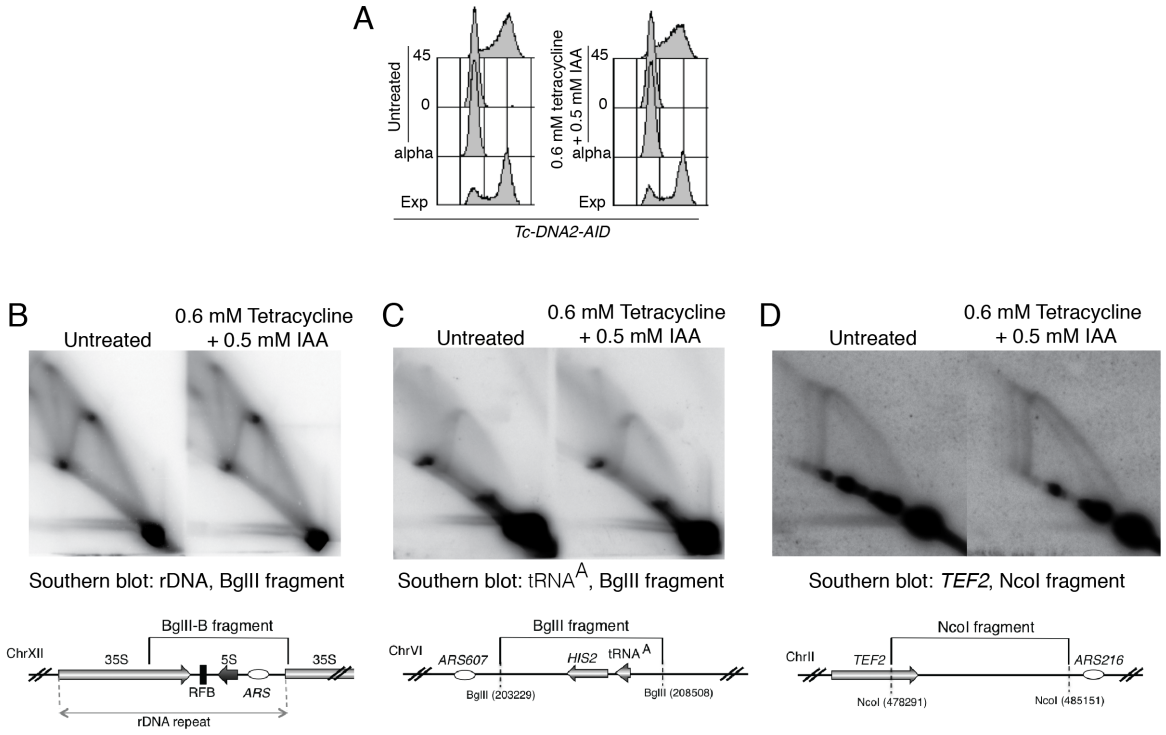

Figure 3.42. *DNA2* ablation in a single S-phase does not induce pausing of the DNA replication forks at rDNA, tRNA^A and RNA Pol II transcribed genes. *Tc-DNA2-AID* (TEMP18-B4) cells were synchronized in G1 in the presence of 0,5 mM IAA and 0.6 mM tetracycline (added in the media 1h after the α-factor addition) to induce the degradation of Dna2 in G1, and released into S-phase in the presence of 0.5 mM IAA and 0.6 mM tetracycline. Cells that were not treated with auxin and tetracycline were kept in parallel as a control. FACS profiles with the cellular DNA content during the experiment are shown (**A**). DNA replication intermediates isolated after *in vivo* psoralen DNA crosslinking, were analysed by neutral-neutral 2D gels 45 minutes from the release from the G1 into S-phase in the presence and in the absence of Dna2, respectively, in the BglII B fragment of the rDNA (Ivessa et al., 2000) (**B),** in the BglII fragment containing the *HIS2* and the tRNA^A tA[AGC]F genes (Ivessa et al., 2003) **(C)** and in the NcoI fragment, which contains the RNA PolII transcribed gene *TEF2* (Ivessa et al., 2003) (**D**). Maps of the genomic fragments analysed by neutral-neutral 2D gels are shown in each panel.

Based on the reported evidence, we failed to detect replication defects caused by *DNA2* ablation in a single S-phase that could justify the checkpoint activation and the lethality of *dna2* mutants. Therefore, to uncover the essential role of Dna2, we decided to monitor the effects of *DNA2* ablation on the fate of specific genomic loci in *DNA2-AID rad9Δ* cells, in which the first cell cycle arrest due to the absence of Dna2 is abolished and cells can divide for several generations in the absence of the 5'-flap endonuclease.

DNA2-AID rad9Δ cells were synchronized in G1 and Dna2 degradation was induced before the release in S-phase. An untreated cell culture without Dna2 degradation was kept

in parallel as a control (Figures 3.43, 3.44, 3.45). The growth rate of *DNA2-AID rad9Δ* was measured in condition in which Dna2 was continuously degraded. Growth curve in Figure 3.43A revealed that, after the G1 release, *dna2 rad9* mutants proliferated slower compared to *rad9Δ* control cells, being able to perform less than 5 cell divisions and, after 11-12 hours from the G1 release, they stopped to proliferate and accumulated an increasing percentage of dumbbell cells. Therefore, *RAD9* deletion allows only few additional generations in the absence of Dna2, after that the absence of Dna2 induces cell lethality and cell cycle arrest (Figure 3.43A).

With the aim of identifying chromosome alterations (or chromosome breakages) induced by cell cycle progression in the absence of Dna2 we decided to analyze the migration pattern of the chromosome III by PFGE in *DNA2-AID rad9Δ* mutants grown 12 and 15 hours after the G1 release in the presence of auxin (Figure 3.43B). As it can be noted in figure 3.43B, at 12 hours from the G1 release in the presence of auxin *DNA2-AID rad9Δ* started to accumulate a certain level of chromosome fragmentation, which was not present in the same cells released in the absence of auxin. Although the experimental conditions of Figure 3.43B can be adjusted to maximize the induction of chromosomal breakages in the absence of Dna2 (our unpublished observations), the experiment presented in figure 3.43B strongly supports the hypothesis that 4.5 cell cycles in the absence of Dna2 induce chromosome fragmentation and cell lethality

At the same time points we failed to detect any alteration in centromeres size or integrity (Figure 3.44A) and in the telomere length (Figure 3.44B) in *dna2 rad9* mutants.

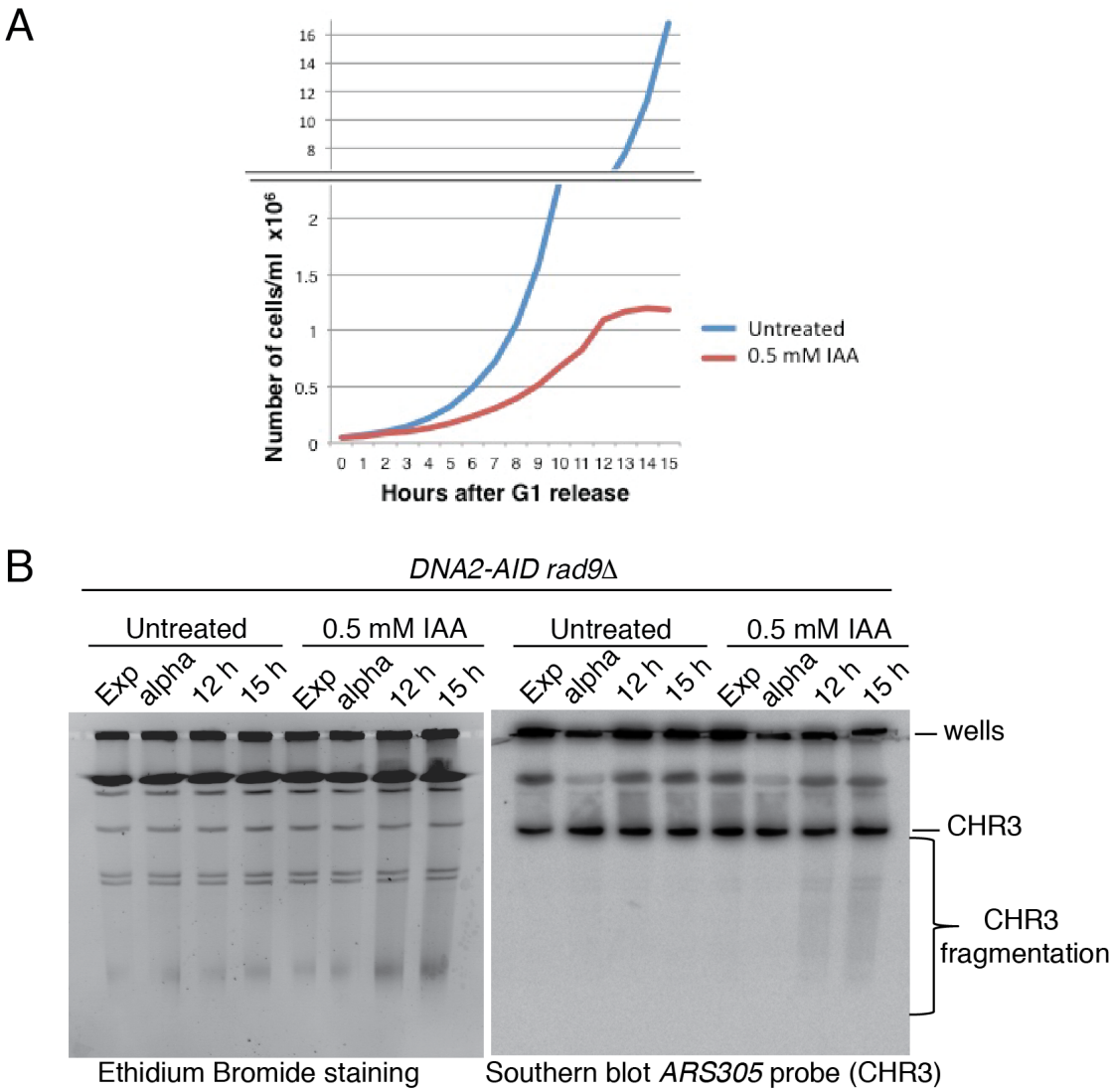

Figure 3.43. Cells ablated for *RAD9* and *DNA2* die after 4.5 generations and accumulate chromosome breakages. A) *DNA2-AID rad9Δ* (TEMP17-I6) cells were synchronized in G1 and 1h before the release into S-phase 0,5 mM IAA was added in the media in order to induce the degradation of Dna2 in G1 and to allow the cells to enter into S-phase in the absence of Dna2. Cells were released in fresh medium, in the presence of 0,5 mM IAA, to maintain Dna2 degradation along the entire experiment. An untreated cell culture (without IAA) was kept in parallel as a control of the experiment. After the release into S-phase cellular concentration was determined every hour for 15 h to generate the reported growth curve. Genomic DNA (from exponentially growing cells, G1 synchronized cells and cells release from G1 for 12 and 15 hours) was isolated in agarose plugs. **B)** The migration pattern of the chromosome III has been analysed by PFGE and southern blotting, using an *ARS305* recognizing probe, on samples obtained from the experiment described in panel A at the indicated time points. Picture of the ethidium bromide stained gel is reported. A black line and a black bracket indicate, respectively, the migration position of the entire chromosome III and the region of the gel in which chromosome fragmentation is detectable. The position of the wells is indicated.

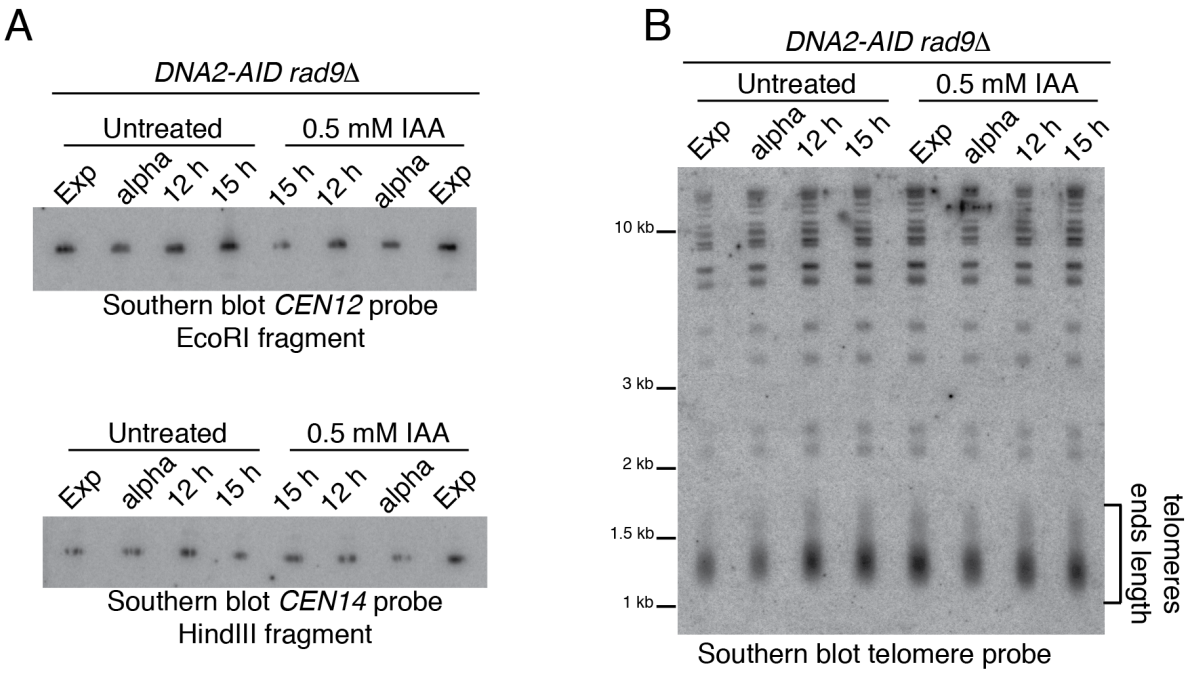

Figure 3.44. *DNA2* and *RAD9*-deleted cells, grown for 4.5 generations, do not accumulate alterations in centromeres and telomeres length. A) DNA samples isolated in agarose plugs, obtained from the experiment described in Figure 3.43A, were digested with EcoRI or with HindIII, to obtain, respectively, a 3340 bp fragment containing the *CEN12* DNA sequence and a 2330 bp fragment containing the *CEN14* DNA sequence. Digested genomic DNA into the plugs has been run on a monodimensional agarose gel electrophoresis and the migration patterns of the DNA fragments containing the centromeric DNA sequences have been analysed by southern blotting with specific probes. **B)** Genomic DNA into the agarose plugs, from experiment described in Figure 3.43A, was digested with the XhoI restriction enzyme, and subjected to agarose gel electrophoresis. The average length of telomeric DNA has been analysed by southern blotting using a telomere specific probe as previously described (Longhese et al., 2000).

Since it has been recently reported that the interaction of Dna2 with Ctf4, the adaptor that connects the DNA polymerase α with the CMG helicase complex, is important for the maintenance of multiple directed-tandem repeats that form the ribosomal DNA locus (Villa et al., 2016), we monitored the fate of the BamHI fragment of chromosome XII, which contains the rDNA repeats, by PFGE and southern blotting in *DNA2-AID rad9Δ* strain at 12 and 15 hours after the G1 release in the presence of auxin (Figure 3.45).

Despite we had previously showed that *DNA2* ablation in a single S-phase did not induce DNA replication fork pausing at rDNA locus (Figure 3.42A,B), we found that 12 and 15 hours after the G1 release in the presence of auxin, the ablation of *DNA2* induced a

shortening of the BamHI fragment of the chromosome XII in *dna2 rad9* cells, likely caused by the loss of rDNA repeats (Figure 3.45).

Taken together these results suggest that a penetrant phenotype due to the absence of Dna2 is the alteration of the fate of the chromosome XII, which can be caused by accumulation of fork abnormalities at the rDNA and subsequent induction of chromosome breakages.

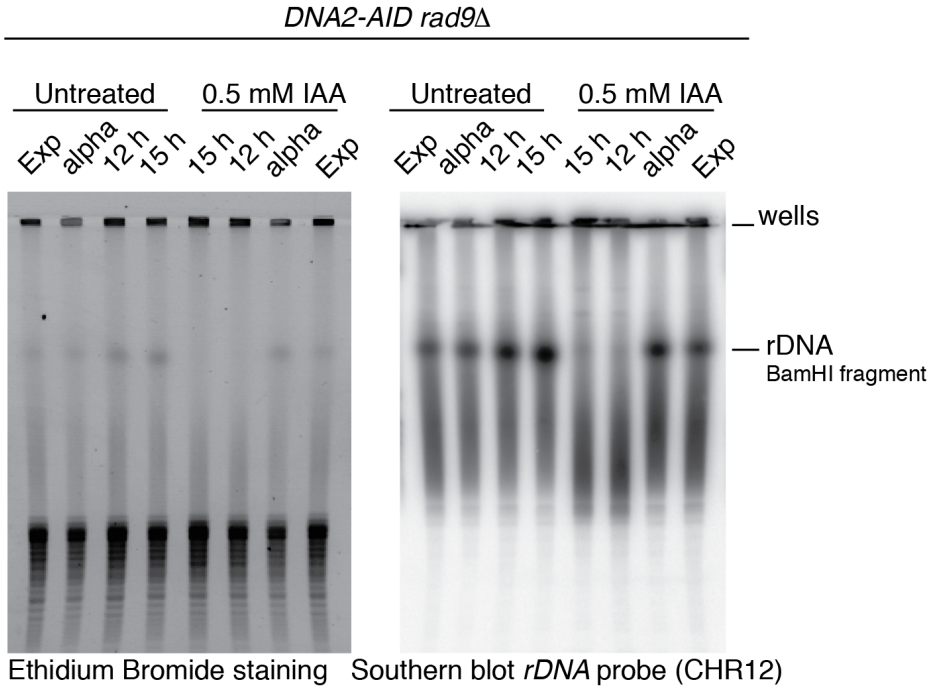

Figure 3.45. Ablation of Dna2 for 4.5 cellular generations leads to a strong decrease in the size of the rDNA in *rad9* mutant cells. Genomic DNA isolated into agarose plugs, from experiment described in Figure 3.43A, was digested with the BamHI restriction enzyme, and the migration pattern of the BamHI fragment of chromosome XII, containing the rDNA repetas, was analysed by PFGE and southern blotting at the indicated time points, using a rDNA recognizing probe. Picture of the ethidium bromide stained gel is reported. A black line indicates the migration position of the BamHI fragment of chromosome XII in wild type cells.

4. Discussion

4.1 Rad53-mediated regulation of Pif1 and Rrm3 contributes to maintain the stability of stalled DNA replication forks and to preserve chromosome integrity under replication stress

Eukaryotic cells have evolved the highly conserved *ATR/hCHK1, Mec1/Rad53* kinase mediated signal transduction pathways, called DNA replication checkpoints. These surveillance pathways control several complex cellular responses, which are activated in the presence of DNA replication perturbations and constitute the cellular response to DNA replication stress. One important function of the DNA replication checkpoint is to maintain the stability of stalled DNA replication forks, which have an intrinsic fragility and can undergo spontaneous or genetically mediated DNA decays (Branzei and Foiani, 2009). Early and recent studies contributed to clarify that the $Mec1^{Rad3/ATR}$-$Rad53^{Cds1/CHK1}$ kinase axis controls replication fork components and regulates the dynamic of association and activity of several enzymes to the replication fork. Accordingly, HU treatments induce Mec1-Rad53 dependent phosphorylations of Rpa2, Exo1, Dna2, Psf1, Mcm2-7 and Mrc1 in budding yeast and Rad3/Cds1-dependent phosphorylations of Dna2 and Mus81 have been reported in fission yeast (see Introduction). In line with the role of the $Mec1^{Rad3/ATR}$-$Rad53^{Cds1/CHK1}$ kinase axis in controlling fork components or fork modifier enzymes, it has been recently shown that HU treatment induces ATR-dependent phosphorylation of SMARCAL1 (Couch et al., 2013) and ATR dependent recruitment of FANCD2 to the MCM complex at stalled replication forks in the presence of replication stress (Lossaint et al., 2013). Interestingly, ATR has also been shown to prevent RNF4/PLK1/SLX4 mediated fork cleavage in the presence of aphidicolin or HU (Couch et al., 2013; Ragland et al., 2013).

Due to the multiple pathways regulated by Mec1$^{Rad3/ATR}$-Rad53$^{Cds1/CHK1}$ kinase axis under DNA replication stress, the intricate networks, which are necessary to ensure the stability of stalled DNA replication forks and the integrity of chromosomes under replication stress, are not completely clarified.

The aim of this thesis work was to uncover new Rad53-mediated regulations at stalled replication forks.

A first possible connection between the Pif1 DNA helicases and the cellular response to DNA replication stress emerged when it was shown that Pif1 becomes hyperphosphorylated when cells are exposed to HU (Makovets and Blackburn, 2009). In this study, neither the genetic dependences of this Pif1 modification, nor the physiological role of this regulation were reported. Moreover, Pif1 is able to unwind synthetic structures resembling stalled DNA replication forks *in vitro*, which gives Pif1 the potential activity to be a fork modifier enzyme (George et al., 2009; Lahaye et al., 1993). Although Pif1 was shown to be recruited at late stages of the S-phase at genome sites that contain G-quadruplex structures (Paeschke et al., 2011), it was not clear if this DNA helicase is a fork component and associates to the stalled DNA replication forks in the presence of HU. On the contrary, Rrm3 was shown to associate and move with the replication forks in unperturbed conditions, through its interaction with PCNA and DNA polymerase ε (Azvolinsky et al., 2006; Schmidt et al., 2002).

At the beginning of this thesis work we decided to investigate if Rrm3 and Pif1 bind the stalled DNA replication forks and if also Rrm3, as Pif1 (Makovets and Blackburn, 2009), undergoes to an HU induced hyperphosphorylation.

4.1.1 Pif1 and Rrm3 associate with stalled DNA replication forks and their association to the forks is not influenced by Rad53

We used the Chromatin Immunoprecipitation on chip (ChIP on chip) approach to compare genome-wide the binding clusters of Rrm3 and Pif1 with the ones of DNA polymerase α,

in S phase in the presence of hydroxyurea. In this experimental condition, we were able to precisely localize, genome-wide, all the active DNA replication forks, thanks to the comparison of the ChIP on chip profiles of DNA Polα, with the ssDNA-BromodeoxyUridine Immunoprecipitation on chip (ssDNA-BrdU IP on chip) profiles (Rossi et al., 2016).

We showed that Rrm3, Pif1 and DNA Polα binding clusters co-localized in a statistically significant way, either in presence of high or low HU doses and both in the control *sml1Δ* cells and in *rad53* mutants in which the replication fork progression was clearly impaired by the presence of HU. Based on the fact that in all our experiments/genetic backgrounds the distribution of DNA polymerase α binding clusters overlapped with Pif1 and Rrm3 binding clusters in a statistically significant way, we strongly support the idea that Rrm3 and Pif1 are replication fork components under replication stress and their association to the stalled forks is not influenced by Rad53 activity.

Rrm3 has the capacity to displace proteins from the DNA (Ivessa et al., 2003; Ivessa et al., 2002; Ivessa et al., 2000) and Pif1 can unwind DNA structures resembling DNA replication forks, Okazaki fragments like structures, DNA-RNA hybrids and G-quadruplexes (Boule and Zakian, 2007; Paeschke et al., 2013; Paeschke et al., 2011; Pike et al., 2010). Although in unperturbed conditions, Rrm3 and Pif1 activities, on non-nucleosomal DNA protein complexes and other bulky DNA structures at the fork or ahead of it promote fork progression across pausing elements (Bochman et al., 2010), we reasoned that the same activities, if not regulated, could have deleterious effects on the structure and functionality of the stalled replication fork. For example, Pif1 mediated unwinding events on the lagging strand could be deleterious when the fork is blocked (see following paragraphs). It is not known if Rrm3 and Pif1 preferentially bind leading or lagging strands (although based on *in vitro* evidences Pif1 has been suggested to localize at the lagging strand). Considering that Rrm3 binds DNA polymerase ε, it could be located at the leading strand and its unscheduled activity could unwind the 3' end of the nascent

strand and/or displace replisome components from the leading strand (see following paragraphs).

Because Rrm3 and Pif1 localize at the stalled forks and their unscheduled activities could modify the composition or the structure of the replisome or the DNA replication fork we decided to investigate which was the physiological role of the Rad53-mediated regulation of Rrm3 and Pif1 under replication stress and which were the consequences of the lack of this regulation on the structure and the functionality of the stalled replication fork. In the context of these studies we have been able to confirm previously reported evidence which showed massive accumulation of abnormal DNA replication fork intermediates and dissociation between replisome components and the DNA replication fork in *rad53* mutants treated with HU (Cobb et al., 2005; Lopes et al., 2001; Lucca et al., 2004; Sogo et al., 2002).

4.1.2 Incubation of *rad53* cells with high HU doses leads to DNA polymerase-α dissociation from the DNA replication fork and induces the formation of abnormal DNA replication intermediates

In the presence of high doses of hydroxyurea DNA polymerases (Polα, Polδ e Polε) and MCM helicase have been shown to dissociate from the stalled replication forks of *rad53* cells (Cobb et al., 2003; Cobb et al., 2005; Lucca et al., 2004). Together with the dissociation of replisome components from the replication fork, *rad53* mutants exposed to HU show accumulation of abnormal DNA structures at the replication forks named resected-forks, hemi-replicated bubbles and reversed forks (Lopes et al., 2001; Sogo et al., 2002).

In agreement with these reported data, we found that the average Polα binding signal, to a 40 kb window centered on 141 early ARSs, in the presence of 150 mM of HU, was 2.86 folds less in *sml1Δ rad53Δ* cells compared to *sml1Δ* cells and the average BrdU incorporation at the same genomic *loci* was 2.21 fold less in the absence of *RAD53*.

Moreover, while average DNA polymerase α binding and BrdU incorporation profiles showed a bimodal distribution around the replications origins of *sml1Δ* cells, as a result of a certain level of DNA replication fork progression, their distribution was centered on the origin points in the absence of *rad53* strongly supporting the previous reported evidences of DNA replication fork inactivation in *rad53* cells exposed to HU (Cobb et al., 2003; Cobb et al., 2005; Lopes et al., 2001; Lucca et al., 2004; Sogo et al., 2002).

We also confirmed by ChIP-qPCR the decreased binding of DNA Polα to flanking regions of the early replication origin *ARS305* of *rad53-K227A* and *sml1Δ rad53Δ* cells treated with HU.

We noticed that, while the average distribution of the binding sites of Pif1 and Rrm3 around 141 active ARSs co-localized with average Polα binding in *sml1Δ* and *sml1Δ rad53Δ* cells, the magnitude of their binding was higher than Polα binding magnitude in *sml1Δ rad53Δ* cells. These data strongly support the conclusion that, in the absence of *RAD53*, replication intermediates generated at collapsing forks may induce additional recruitments of Pif1 and Rrm3.

Recently, Labib's laboratory showed that a phenomenon reminiscent to the replication stress-induced dissociations of Mcm4 and Polα from the replication fork occurs only at a subset of very early DNA replication origins in *rad53* mutants (De Piccoli et al., 2012). The authors proposed that the lack of bindings of Polα and Mcm4 at these origins was due to the movements of these proteins in the surrounding regions and in their view this was due to incomplete depletion of the pool of dNTPs at the time in which these origins were fired. We did not observe this phenomenon; indeed Polα average binding clusters were always localized close to the origin points of 141 ARSs, either in *sml1Δ rad53Δ* or in *rad53-K227A,* and Polα binding clusters in the surrounding regions of these origins were not observed. Importantly, the magnitude of Polα binding in the absence of Rad53 was always lower than in the control cells as it was verified either by ChIP on chip or ChIP-

qPCR. Labib's group also showed that pulling down individual replisome components, intact replisomes were recovered from *rad53* cells treated with high doses of HU (De Piccoli et al., 2012). Thus they proposed that replisome stability at defective DNA replication forks is independent of S-phase checkpoint kinases. Although biochemical purification of the replisomes at a given time point is a powerful technique, it does not guaranty that the purified replisomes were really associated to DNA replication forks *in vivo*. Moreover, *rad53* cells do not inhibit *de novo* origins firing in the presence of HU, creating a dynamic situation in which replication forks fired early will collapse early, while the ones fired late, due to continuous *de novo* origin firing, will collapse later. If a sufficient time to obtain complete fork collapse is not given, the purification of the total amount of replisomes in *rad53* cells in HU at a given time will reflect the presence of assembled replisomes, which are likely generated through *de novo* origin firing. Although Labib's group tried to inhibit *de novo* origin firing in *rad53* cells treated with HU, with the aim of dissecting the contribution of newly assembled replisomes to the replisome pool, the efficiency of their procedure was not checked by 2D gels or ssDNA-BrdU-IP on chip.

4.1.3 Rrm3 and Pif1 induce replication fork stalling, abnormal fork structures and chromosome fragmentation in *rad53* cells treated with HU

Based on the fact that Rrm3 and Pif1 were associated with stalled replication forks in *rad53* mutants and that additional recruitment of the two DNA helicases were detected at collapsing forks of checkpoint mutants under replication stress, we investigated whether Rrm3 and Pif1 influenced the fate of the stalled forks, which are not protected by Rad53. Interestingly, we observed that the combined ablation of *RRM3* and *PIF1* synergistically suppressed the spike-cone signal, detectable through neutral-neutral 2D gels electrophoresis in *rad53* mutants, which corresponds to cruciform intermediates generated at the replication forks (Lopes et al., 2001). Electron microscopy analysis confirmed that, even in the presence of high doses of HU, in the quadruple mutant *sml1Δ rad53Δ rrm3Δ*

pif1-m2, the formation of the typical abnormal fork structures observed in *rad53* mutants, which include hemireplicated bubbles, gapped forks, reversed forks and broken forks (Sogo et al., 2002), was reduced and the ssDNA tracks at the fork branching points of the different categories of resected forks identified were significantly shorter.

These evidences are compatible with synergistic Rrm3 and Pif1-mediated unscheduled unwinding activities on the nascent strands of the collapsing forks (see following paragraphs).

In *rad53* mutants, treated with hydroxyurea, replisome-fork dissociation and the accumulation of abnormal replication intermediates are thought to impair fork progression. Consistent with a detrimental activity of Rrm3 and Pif1 on the stalled forks of *rad53* cells, we observed that combined ablation of the two DNA helicases was able to restore a significant capability of Polα to progress from replication origins towards flanking regions in *rad53* mutants, either at low HU doses or in the presence of 150 mM HU.

Moreover, we found that the Pif1 helicases synergistically promoted the chromosome fragility observed in *rad53* cells treated with low HU doses (Cha and Kleckner, 2002; Hashash et al., 2011); indeed, in the presence of 25 mM of HU, in the quadruple mutant *sml1Δ rad53Δ rrm3Δ pif1-m2* the chromosome fragmentation observed in *sml1Δ rad53Δ* cells was almost completely abolished. Neither the relationships between chromosome fragmentation, incubation time in HU and HU dose, nor the location of the RSZs at which forks break in *rad53* cells are defined. For example, in *rad53* cells, high HU doses induce fork collapse and fork inactivation close to replication origins without chromosome fragmentation, while low HU doses allow a certain level of fork progression and massive chromosome breakage at the RSZs. In both cases *rad53* cells manifest cell lethality and are not capable to restart DNA replication forks after incubation with HU (Hashash et al., 2011; Lopes et al., 2001).

According to their deleterious roles in the induction of abnormal fork structures and chromosome fragmentation in *rad53* cells exposed to replication stress *PIF1* and *RRM3*

ablations synergistically suppressed the HU hypersensitivity of *rad53* mutants. Intriguingly, *PIF1* ablation executes its suppression effect on the HU hypersensitivity of *rad53* cells only if *RRM3* is not present. These imply that there may be a sequential action of the two DNA helicases on the stalled forks of *rad53* and that, in some way, when Rrm3 is present it could counteract Pif1 (see following paragraphs and models presented in the last part of this discussion).

RRM3 deletion has been previously identified as a suppressor of the chromosome fragmentation observed after the thermal inactivation of the *mec1-4* allele and as a mild suppressor of its temperature sensitivity (Hashash et al., 2011). Also *SML1* deletion, which induces a 2.5 fold increase in dNTPs level (Zhao et al., 1998), was shown to have a similar suppression effect on the phenotypes caused by Mec1 inactivation (Hashash et al., 2011). Since *rrm3Δ* cells are considered chromosomal instability mutants (CIN), with a slightly higher level of dNTPs due to a mild and constant activation of the intra-S phase checkpoint (Poli et al., 2012), it has been proposed that *RRM3* deletion suppresses chromosome fragmentation due to Mec1 inactivation because it slightly increases the dNTPs levels and therefore prevents collapse of the replication fork and chromosome fragmentation at RSZs in *mec1* cells (Hashash et al., 2011). In this scenario, the suppression of fork abnormalities, chromosome fragmentation and cell lethality observed in the quadruple mutant *sml1Δ rad53Δ rrm3Δ pif1-m2* could be caused by indirect effects of *RRM3* and *PIF1* deletions on dNTPs level. In this view, we would like to point out that fork abnormalities and chromosome fragmentation are still detectable in *rad53Δ* cells in which *SML1* is deleted. Moreover, we confirmed that chromosome fragility induced in *sml1Δ rad53Δ* cells by low doses of HU is not abolished by *RNR1* over-expression, which leads to a 10-folds increase in the dNTP levels compared to WT cells (Chabes and Stillman, 2007). The observation that high dNTP levels were not able to suppress the massive chromosome fragmentation of *rad53Δ* cells treated with low HU doses, indicates that the suppression of the chromosome

fragility in the quadruple mutant *sml1Δ rad53Δ rrm3Δ pif1-m2* is likely not due to indirect effects of *RRM3* and *PIF1* ablations on the cellular level of dNTPs. Moreover, it has also been recently shown, above 2.5-fold, further increase of the dNTPs levels does not promote fork progression in HU (Poli et al., 2012), but on the contrary high dNTP levels can induce cytotoxicity (Chabes and Stillman, 2007; Kumar et al., 2011).

The relationship between chromosome fragility and replication fork defects of *rad53* mutants under replication stress has not been clarified yet. Interestingly, we found that chromosome breakages started to appear in *sml1Δ rad53Δ* cells only 3 hours after the G1 release in 25 mM of HU, while fork abnormalities were already detectable starting from 60 minutes after the release into S-phase at the early replication origin *ARS305*. We propose that, in the absence of *RAD53*, fork stalling followed by fork collapse and the formation of resected and reversed forks, is a prerequisite for chromosome breakages at the RSZs; in particular, unresolved topological constrains due to defects in the gene gating release, together with the unscheduled activities of DNA helicases and/or endo/exonucleases could act on the stalled forks at late stages of S-phase or mitosis leading to the formation of abnormal DNA replication intermediates which can undergo DNA breakage. Accordingly, broken forks can be visualized by TEM in *rad53* cells treated with HU.

Condensins and Top2 have been identified as two factors required for the fragile sites expression after the thermal inactivation of the *mec1* mutant (Hashash et al., 2012). Whether and how Top2 and condensins affect the chromosome fragility of HU-treated *rad53* cells remain to be investigated. As in the case of chromosome fragmentation at the RSZs in the *mec1-4* allele (Hashash et al., 2012), the chromosome breakages in HU-treated *rad53* cells do not require the metaphase to anaphase transition.

One important function of the $Mec1^{Rad3/ATR}$-$Rad53^{Cds1/CHK1}$ kinase axis is to inhibit origin firing upon DNA replication inhibition. In human cells, ATR ablation induces unscheduled origin firing and replication fork catastrophe, due to the exhaustion of the cellular pool of RPA, which is no more sufficient to stabilize the increased pool of active replication forks

(Toledo et al., 2013). Intriguingly, while replication fork collapse and chromosome fragmentation were suppressed in *sml1Δ rad53Δ rrm3Δ pif1-m2* cells, unscheduled firing of late and dormant origins was still detectable. These data imply that the uncontrolled origin firing has a secondary role in the fragile sites expression in *rad53* cells treated with low doses of HU. These results are consistent with early evidences obtained through the separation of function allele *mec1-100*, which is proficient in the stabilization of the DNA replication forks under replication stress but still induces unscheduled DNA replication origin firing (Paciotti et al., 2001; Tercero et al., 2003). We also conclude that the suppression of replication fork defects, chromosome fragmentation and HU sensitivity of *rad53* cells treated with HU, can be uncoupled from the defect in the regulation of DNA replication origins firing.

4.1.4 Rrm3 and Pif1: new Rad53 targets at the stalled replication forks

We showed that Rrm3 and Pif1 are hyperphosphorylated during S-phase in response to replication stress in a Rad53-dependent manner, suggesting that the checkpoint directly controls Rrm3 and Pif1 at the stalled DNA replication forks.

To investigate the physiological role of this phosphorylation, through bioinformatics analysis, we identified putative consensus motifs for Rad53 or for Mec1 and Tel1 (Smolka et al., 2007), located in the N-terminus of Rrm3 and Pif1, and we mutagenized these serine and threonine residues to generate the phospho-defective or phospho-mimicking mutants of the Pif1 helicases. We focused our attention on the unstructured N-terminal regions of Rrm3 and Pif1, which do not contain the ATPase or the helicase domains, but seem to have regulatory roles; indeed the N-terminus of Rrm3 has been showed to be essential for the protein functions *in vivo* and to regulate the protein abundance (Bessler and Zakian, 2004; Schmidt et al., 2002) and the N-terminal domain of human PIF1 stimulates the binding to ssDNA and the unwinding activity *in vitro* (Gu et al., 2008).

Post-translational modifications of Rrm3 have not been previously reported, while Pif1 is known to be phosphorylated in response to DNA damage, in a Mec1-, Rad53- and Dun1-dependent manner, to prevent deleterious telomere additions at DSB sites (Makovets and Blackburn, 2009). Interestingly, in the presence of DSBs Pif1 is phosphorylated by the checkpoint at its C-terminus (Makovets and Blackburn, 2009), differently from the HU-induced and checkpoint dependent phospho-sites identified in this thesis work, which are located in the N-terminal region of Pif1.

We found that the phospho-defective *rrm3-6SA* mutant reduced the HU-induced and Rad53 dependent hyperphosphorylation of Rrm3, while the phospho-mimicking *rrm3-6SD* mutant alleviated the HU sensitivity of *rad53* cells at the same extent of *RRM3* deletion, strongly suggesting that Rad53 mediated phosphorylation events on Rrm3 down regulate Rrm3 activities under replication stress.

Although the phospho-defective *pif1-12A* mutant was able to abolish (almost completely) the accumulation of the Pif1 hyperphosphorylated isoforms in hydroxyurea, we failed to detect the expected synergistic effect of the combination of *rrm3-6SD* and *pif1-12D* alleles in the suppression of the HU sensitivity of *rad53* mutants. These data might be explained by the inability of the *pif1-12D* mutant protein to fully resemble the constitutively phosphorylated isoform of Pif1; otherwise the fact that the *pif1-12A* mutant was lightly phosphorylated in replication stress conditions might suggest that some of the key HU- and Rad53-dependent phosphorylation sites have not been identified yet.

Interestingly, we observed that *rrm3-6SA* and *pif1-12A* phospho-mutants did not influence Rrm3 and Pif1 functions in unperturbed conditions. The fact that the absence of Rad53 dependent phosphorylation sites on Rrm3 does not influence DNA replication fork progression across tRNAs and RFB at rDNA is in line with the lack of requirement of Rad53 to assist DNA replication across the same pausing elements, either in the absence or in the presence of low HU concentrations. Importantly, lack of effects on DNA replication fork progression at *RRM3* dependent pausing elements in *rrm3-6SA* cells indicates that

Rad53-mediated Rrm3 phosphorylation is necessary but not sufficient to down regulate the DNA helicase activity of Rrm3. In this view we envisage the existence of an HU-induced inhibitor of Rrm3 that could recognize and bind the phosphorylated form of the DNA helicase leading to its down regulation at stalled forks. A similar mechanism of regulation has been recently showed to act on hExo1 and *S.cerevisiae* Exo1 proteins (Andersen et al., 2012; Engels et al., 2011).

4.1.5 Uncontrolled Rrm3 and Pif1 unwinding activities on stalled forks promote fork reversal in *rad53* cells under replication stress

Our observations suggest altogether that Rad53 negatively regulates through phosphorylation the helicase activity of Pif1 and Rrm3 at stalled replication forks. We showed that Rrm3 and Pif1 ablations synergistically rescued cell lethality, chromosome fragmentation, replisome collapse, fork reversal and ssDNA gaps formation at DNA replication fork branching points in checkpoint-defective cells exposed to replication stress.

Nevertheless, Rrm3 and Pif1 ablations were not able to suppress completely the lethality of *rad53* mutants in the presence of hydroxyurea; this indicates that additional pathways exist or that complete suppression of HU hyper-sensitivity of *rad53* cells is not achievable. Our lab has recently shown that, in replication stress conditions, Rad53 stabilizes stalled DNA replication fork through the phosphorylation of the nuclear pore protein Mlp1 (Bermejo et al., 2011). We showed that ablation of Rrm3 and Pif1 DNA helicases activities at stalled replication forks and gene gating ablation constitute two genetically distinct pathways of suppression of the HU hyper-sensitivity of *rad53* cells. These conclusions imply that Rad53 dependent regulations of gene gating and of Pif1 helicases synergize in the maintenance of the stability of the stalled replication forks.

Due to its interaction with PCNA (Schmidt et al., 2002), Rrm3 is thought to be localized mainly on the lagging strand of the replication fork. Moreover Rrm3 interacts *in vivo* with

Pol2, the catalytic subunits of DNA polymerase ε (Azvolinsky et al., 2006), which acts in conjunction with the Cdc45-Mcm-GINS (CMG) complex on the leading strand (Langston et al., 2014). Although Rrm3 is thought to act as a snow plough, which removes DNA-protein complexes ahead of the replication fork, we cannot rule out that a fraction of Rrm3 is also present on the leading strand, and that this DNA helicase executes occasional backtrackings of the replisome or participates to the recently-hypothesized Polε-mediated proofreading activity of Polδ synthesis on the leading strand (Johnson et al., 2015). Importantly, if Rrm3, based on its polarity, localizes on the lagging strand it would move (on the DNA template) in the same direction of replication fork and, in this case, the protein could promote lagging strand advancement, not only by removing bulky obstacles ahead of the fork, but also by unwinding the 3' ends of blocked Okazaki fragments.

Also Pif1 could act on the lagging strand as Rrm3 (although Rrm3 activities at the replication forks are not known), but based on *in vitro* evidences Pif1 should unwind the 5' ends of a fraction of nascent Okazaki fragments, which are subsequently cut by Dna2 (Budd et al., 2006; Levikova and Cejka, 2015; Pike et al., 2009; Pike et al., 2010; Rossi et al., 2008). Based on Pif1 polarity, the DNA helicase would not be able to unwind directly the 5' end of an Okazaki fragment but, based on *in vitro* evidences, it has been proposed that it does it by stimulating the Polδ dependent strand displacement activity (Budd et al., 2006; Levikova and Cejka, 2015; Pike et al., 2009; Pike et al., 2010; Rossi et al., 2008). Considering the *in vitro* evidence present in the literature and the findings reported in this thesis work, it is time to speculate that Pif1 could be a replication fork component and that it acts as an accessory strand displacement factor, which stimulates Polδ activities on the 5' flaps of Okazaki fragments.

While the final outcome of Rrm3 and Pif1 activities at the DNA replication fork, or ahead of it, is an optimal fork progression across several DNA replication pausing elements in unperturbed conditions, the exact nature of these activities and the potential effects they could have on the structure of the replisome and the replication fork are poorly understood.

According to the literature and to the enzymatic properties of Rrm3 and Pif1, the two DNA helicases seem to promote replication fork progression in unperturbed conditions, assisting mainly the lagging strand synthesis (Figure 4.1, left panel). The replication forks stall at the level of the replication fork barrier (RFB) of the rDNA in a nearly symmetric conformation (with only 3 nt protruding in the lagging strand), without exposing ssDNA (Gruber et al., 2000). Importantly, the stability of the stalled replication forks at the the RFB is not controlled by the checkpoint (Calzada et al., 2005) and we found that replication fork progression across tRNA genes does not requires Rad53. Based on our observations and on published data, we propose that the checkpoint-dependent regulation of Rrm3 and Pif1 is not required at genomic sites that contain proteinaceous fork barriers (like RFB), or at the tRNA transcripts that induce fork pausing, due to clashes in head-on conformation between transcription and DNA replication. In agreement with previously reported evidences (Calzada et al., 2005) we propose that, in unperturbed conditions and in the presence of proteinaceous barriers or transcripts in head-on conformation, DNA replication fork progression is assisted by Rrm3 and Pif1 without needing Rad53 (see Figure 4.1). In particular, the combined actions of Rrm3 and Pif1 (either ahead of the fork or directly acting on the DNA replication fork architecture) would prevent uncoupling events between DNA polymerases and the DNA helicase or between leading and lagging strands, thus maintaining a symmetric structure of the DNA replication fork (with paired leading and lagging strands and close proximity between DNA polymerases and DNA helicases) (Figure 4.1).

On the contrary, in HU-induced replication stress conditions stalled replication forks exhibit an asymmetric accumulation of approximately 100 nt of ssDNA at the fork branching point (Sogo et al., 2002). We propose that this asymmetric configuration of stalled forks in the presence of HU is caused by the Rad53-mediated inhibition of Rrm3 and Pif1 helicase activities, that would preferentially inhibit the polymerization of the lagging strand, generating a stalled replication fork with an advanced leading strand; this

may facilitate, in some way, fork restart and checkpoint deactivation following HU removal (Figure 4.1, right panel). The described mechanism is consistent with the observation that the lagging strand-bound PCNA is specifically unloaded at HU-stalled replication forks, in a Mec1- and Rad53-dependent manner (Yu et al., 2014).

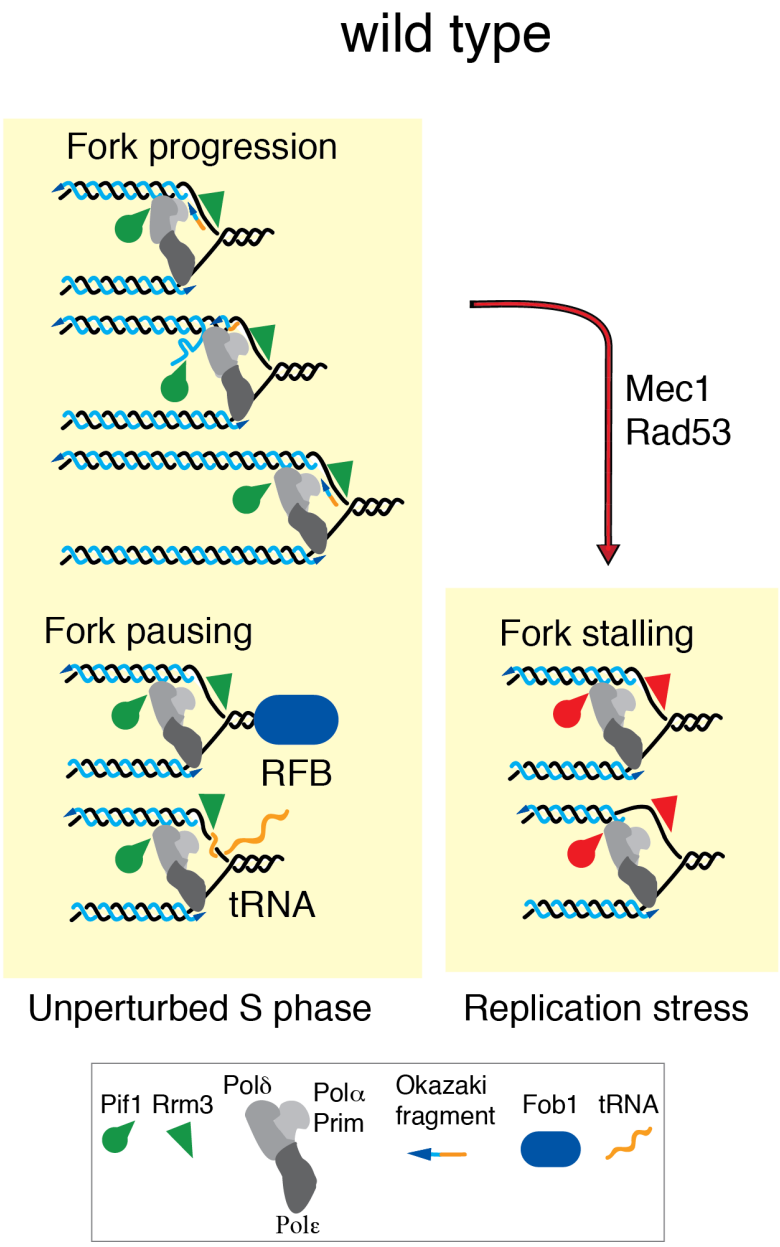

Figure 4.1. Model of the Rad53-dependent regulation of Rrm3 and Pif1 at stalled replication forks. The model represents replication forks progression in unperturbed S-phase, at natural pausing sites and in replication stress conditions. The left panel represents Rrm3 and Pif1 which regulate DNA replication fork progression across pausing elements without the need of Rad53 (green triangles). The right panel refers to a replication stress condition in which the checkpoint inhibits lagging strand unwinding activities of Rrm3 and Pif1 (indicated in red). Directions of the newly synthesized strands (light blue) are depicted by blue arrows. RNA is indicated in orange.

The Rad53-dependent down regulation of Rrm3 and Pif1 would therefore stabilize the stalled replication forks in a slightly asymmetric conformation, with reduced uncoupling between leading and lagging strands. In the absence of Rad53, the unscheduled activity of the Pif1 helicases would promote aberrant transitions at the stalled replication forks (Figure 4.2). In particular, Rrm3 and Pif1 would remain unphosphorylated and active and their unscheduled unwinding activities may generate asymmetric stalled forks with a protruding lagging strand and a long track of ssDNA on the leading strand. These asymmetric forks could account for the consistent percentage of gapped and resected forks detectable by transmission electron microscopy in *sml1Δ rad53Δ* cells treated with HU (see model in Figure 4.2, left panel). In this scenario, Rrm3 (with an unknown mechanism) might facilitate RNA priming on the lagging strand, inducing the formation of unusually long RNA primers (see Figure 4.2 left panel). One possibility is that Rrm3 moves in direction 5'-3' on the parental strand, thus inducing the advancement of DNA primase, which would be less sensitive to dNTPs deprivations. In this context, Rrm3 unscheduled activity would also displace the MCM complex ahead of the fork leading to DNA replication fork inactivation (see Figure 4.2 left panel). On the contrary, leading strand synthesis would suffer dNTPs deprivation, causing the formation of an asymmetric stalled fork with advanced lagging strand. In this condition, if the last long Okazaki fragment forms a 5' flap, it would generate an ideal substrate for Pif1/Polδ dependent strand displacement events leading to the formation of long protruding 5' flap at the lagging strand of the collapsing fork (see Figure 4.2 left panel). In this scenario, leading strand Rrm3 might promote the dissociation of DNA polymerase ε/δ and the unwinding of the 3' end of the nascent leading strand creating long 3' flaps (see Figure 4.2 left panel). Pif1 and Rrm3 unscheduled unwinding activities on the collapsing forks may have different efficiencies and processivity, creating different classes of gapped replication forks. If the unwound nascent strands re-anneal to each other, a reversed fork with a 5' protruding end on the regressed arm is expected to be created (see model in Figure 4.2, left panel). The

proposed idea that in the absence of Rad53 and in the presence of HU long RNA primers could be created at the stalled forks, is consistent with the following observations: *rad53* mutants are not able to induce the unloading of the lagging strand-bound PCNA at HU-stalled replication forks (Yu et al., 2014); DNA primase can produce longer RNA primers when uncoupled from DNA polymerase alpha (Badaracco et al., 1985); DNA polymerase alpha-primase phosphorylation state is modulated by Rad53 (Pellicioli et al., 1999); DNA polymerase alpha-primase has been proposed to be negatively regulated in a Rad53 dependent manner (Marini et al., 1997).

The experimental evidence reported in this thesis work is also compatible with a model in which extended Rrm3 and Pif1 unwinding activities on the lagging strand of the DNA replication forks of *rad53* cells treated with HU would promote the formation of gapped replication forks and reversed forks, without the need of creating long RNA primers on the lagging strand (see model in Figure 4.2, right panel). In this scenario, Rrm3 would unwind the 3' end of the Okazaki fragments of the collapsing forks of *rad53* cells treated with HU, while Pif1/Polδ strand displacement events would occur on the 5' ends. Importantly, Rrm3 would counteract Pif1/Polδ activity on the 5' of Okazaki fragments with a reminiscent mechanism of the one acting at the RFB in unperturbed conditions ((Ivessa et al., 2000) - see model in Figure 4.2, right panel).We observed that Rrm3 and Pif1 synergistically promote fork reversal, chromosome fragmentation and consequently cell lethality in *rad53* mutants treated with HU, indeed combined ablation of the two genes induced the maximum suppression effect on the HU hyper-sensitivity of *rad53* cells. Accordingly to this synergistic role, *RRM3* deletion alone partially rescued fork reversal, chromosome fragmentation and the HU sensitivity of *rad53* mutants. On the contrary, *pif1-m2* mutation alone showed a very mild effect in suppressing fork reversal and chromosome fragmentation in *rad53* cells treated with HU and it did not have any suppression effect on their HU hyper-sensitivity. These data imply that Rrm3 has a key role in promoting fork

abnormalities in *rad53* cells exposed to HU, while Pif1 would execute its deleterious activity only when Rrm3 is absent.

The model presented in figure 4.2 (right panel) provides a possible explanation of the reason why *PIF1* ablation, through the *pif1-m2* allele, executes its suppression effects on the HU hyper-sensitivity of *rad53* cells only in the absence of *RRM3*. In particular, Rrm3 would unwind the 3' ends of Okazaki fragments at the stalled forks of *rad53* cells and, contextually, it would counteract Pif1/Polδ dependent deleterious unwindings on the 5' ends (Figure 4.2, right panel). If Rrm3 is present, the toxic effects of Pif1/Polδ dependent deleterious strand displacement events would be counteracted, while if Rrm3 is absent, this toxic effects on the 5' ends of the Okazaki fragments would be revealed.

Other possible explanations for the lack of suppression of *PIF1* ablations on the HU hypersensitivity of *rad53* cells treated with HU lay on the fact that Pif1 could have both positive and negative roles in the absence of *RAD53* under replication stress or that the *pif1-m2* mutation is leaky.

We propose two possible mechanisms that are not mutually exclusive and can account for Rrm3 and Pif1 dependent induction of fork abnormalities at the stalled forks of *rad53* cells treated with HU. In the first scenario Rrm3 unscheduled activities could promote Primase dependent hyper-polymerization of RNA primers on the lagging strand leading to aberrant protruding 5' ends (Figure 4.2, left panel), while in the second scenario Rrm3 and Pif1 would synergize in the complete unwinding of the Okazaki fragments on the lagging strand of *rad53* cells treated with HU (Figure 4.2, right panel). Both models proposed are in agreement with recently reported *in vitro* activities of human Pif1 and *S. cerevisiae* Pif1 (George et al., 2009; Lahaye et al., 1993).

Importantly, in both cases Exo1 and Dna2 activities on the long 5' flaps on the lagging strand would counteract fork asymmetry and prevent fork reversal (Figure 4.2). Accordingly, Exo1 has been shown to counteract fork reversal in *rad53* mutants under

replication stress (Cotta-Ramusino et al., 2005) and Cds1 was shown to activate Dna2 at the stalled forks to prevent the formation of long 5' flaps (Hu et al., 2012). Although it is not clear whether Rad53 dependent regulation of Dna2 at the stalled forks is conserved in *S. cerevisiae,* lack of Rad53 regulation of Dna2 at the stalled forks can account for the additional recruitment of Pif1 and Rrm3 to the stalled forks of *rad53* mutant treated with HU.

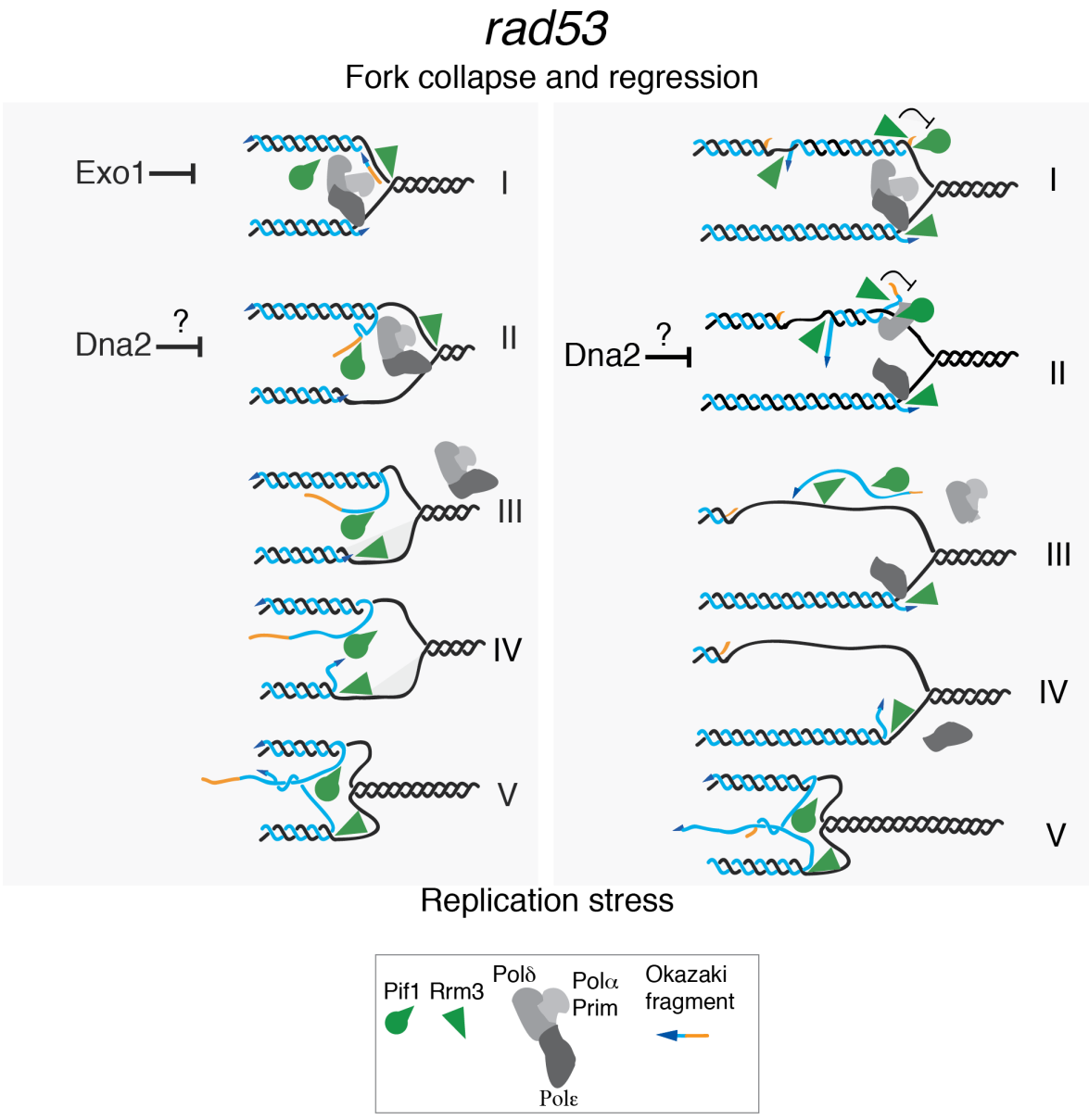

Figure 4.2. Models of unscheduled Rrm3- and Pif1-dependent unwinding activities that lead to the generation of reversed forks and gapped molecules at stalled forks, in the absence of *RAD53*, in replication stress conditions. Left and right panels represent two mutually non-exclusive mechanisms which could cause pathological transitions at stalled replication forks of *rad53* mutants in replication stress conditions.

Our work provides a new mechanistic insight into the cellular response to replication stress and highlights a new Rad53 dependent regulation of replisome components under replication stress. Taken together, our results clearly locate Pif1 at the stalled DNA replication fork. It remains to be investigated whether this important DNA helicase binds and moves with the forks also in unperturbed conditions. Another important insight into the activities of these two DNA helicases and the mechanism of DNA replication across the pausing elements would come from the exact localization of the two DNA helicases on the nascent strands of the replication forks. Although in specific conditions (checkpoint deficient backgrounds under replication stress) and with negative outcomes in terms of DNA replication fork dynamics and stability, in this first part of the thesis we clearly detected Rrm3 and Pif1 dependent activities, which can modify the structure of the DNA replication fork and/or the replisome *in vivo* (Rossi et al., 2015; Rossi et al., 2016). These activities clearly show that, at least in certain conditions, Pif1 and Rrm3 can act as fork modifier enzymes. It remains to be clarified whether and how these capabilities of Rrm3 and Pif1 to modify the structure of the DNA replication fork play essential roles in the efficient DNA replication fork progression across natural pausing elements. In this direction it will also be interesting to investigate the role of the pausing complex Csm3-Tof1-Mrc1 in the regulation of the replication fork functions of Pif1 and Rrm3.

4.2 Dna2, Rrm3, Pif1 and Rad9 functionally interplay in the maintenance of the DNA replication fork integrity

A pioneering study from Judith L. Campbell and colleagues showed that deletion of *PIF1* suppresses the lethality of *dna2Δ* cells (Budd et al., 2006). Since the authors also discovered that Dna2 is involved in the alternative pathway of Okazaki fragments processing (OFP) (Budd and Campbell, 1997), they interpreted this genetic interaction and *in vitro* evidences proposing that Dna2 counteracts Pif1 unwinding activities on the lagging strand by cutting the resulting long 5' flaps, which cannot be cleaved by the Fen1

endonuclease (Budd et al., 2006; Pike et al., 2009; Pike et al., 2010; Rossi et al., 2008). Intriguingly, the same authors showed that *RRM3* deletion causes synthetic lethality when combined with *DNA2* mutations and that *RAD9* ablation can suppress, at least partially, the phenotypes associated to *dna2* mutations (Budd et al., 2011; Budd et al., 2006).

Moreover, recently it has been reported that the *Sp*Cds1 effector kinase targets the nuclease Dna2 to counteracts fork reversal (Hu et al., 2012). In details, it was shown that, following HU treatments, Cds1 phosphorylates Dna2 in order to prevent its dissociation from stalled replication forks. In this context, Cds1 dependent association of Dna2 to the stalled forks would allow Dna2 action on 5' flaps, which counteracts fork reversal (Hu et al., 2012).

Considering the opposite genetic effects caused by *RRM3* and *PIF1* ablations on the survival of *dna2* cells in *S. cerevisiae* (Budd et al., 2006), the results reported in the first part of this PhD thesis about the Rad53 dependent regulation of Pif1 and Rrm3 under replication stress and the recent data obtained in *S.pombe* on the Cds1 dependent regulation of Dna2 (Hu et al., 2012), we decided to investigate the crosstalk between Dna2, the Pif1 helicases and Rad9 in the maintenance of the DNA replication fork integrity in unperturbed conditions and under DNA replication stress, either in absence or in the presence of Rad53.

4.2.1 Dna2 manifests essential functions in the M-phase of the cell cycle

DNA2 is an essential gene for cell viability (Budd and Campbell, 1995). Several studies, performed using temperature-sensitive and hypomorphic alleles of *DNA2*, or the recovered *pif1Δ dna2Δ* double mutant, were not able to unequivocally and exhaustively uncover the essential role of Dna2 *in vivo*. Based on genetic interactions and *in vitro* data, Dna2 is thought to act in the Okazaki fragment processing, but a direct evidence of its role in this pathway *in vivo* is still missing (Budd et al., 2011; Budd et al., 2006; Levikova and Cejka, 2015; Pike et al., 2009; Pike et al., 2010; Rossi et al., 2008). Therefore, to uncover the essential role of Dna2, we established a conditional allele of *DNA2*, combining the auxin-

inducible degron system (Morawska and Ulrich, 2013; Nishimura et al., 2009), and the tetracycline-dependent translation control system (Kotter et al., 2009), which allowed the rapid and efficient depletion of Dna2, leading to cell lethality.

It is clear from our data that the conditional ablation of *DNA2* during a single S-phase did not impeed the bulk of DNA synthesis, but caused a terminal cell cycle arrest in M phase, before the metaphase-anphase transition, induced by the presence of an active checkpoint. In the absence of Dna2, we observed that Rad53 started to get hyper-phosphorylated 90 minutes from the G1 release, after that cells had reached a 2C DNA content and the mitosis, as revealed by the hyper-phosphorylation of the M-CDK target, Pol12.

Although Dna2 is thought to participate to the Okazaki fragment processing, implicating a role of Dna2 in the processing of long 5' flaps generated by Pif1 during the replication of all the genome and, most importantly, at all the active replication forks, our data rather suggest that if Dna2 is involved in DNA replication it will execute its function at specific genomic *loci* replicated in late S or, more likely, in the processing of replication or intermediates in mitosis.

In this direction we would like to highlight that our evidences and the available data in the literature do not exclude that the essential role of Dna2 could be ascribed to mitotic recombination events, which occur at specific genome loci and are required for the proper propagation of the chromosomes to the daughter cells. Based on its genetic interactions with *RRM3* and *PIF1*, we hypothesised that Dna2 could play an essential role in the replication of specific pausing elements, or of genomic *loci*, such as telomeres and ribosomal DNA, which are replicated in late S-phase or in mitosis (Deshpande and Newlon, 1996; Fachinetti et al., 2010; Greenfeder and Newlon, 1992; Ivessa et al., 2003; Mechali et al., 2013; Menolfi et al., 2015), but we failed to detect replication fork pausing or defects (after 45 minutes form the G1 release into an single S-phase in the absence of Dna2), at the level of rDNA, tRNA genes and RNA Pol II transcribed genes, which are three well characterized replication pausing elements (Azvolinsky et al., 2009; Deshpande

and Newlon, 1996; Ivessa et al., 2003). It is to be noted that in this experimental condition both control cells and Dna2 ablated cells already reached the 2C DNA content. Since in *DNA2* ablated cells the checkpoint activation is detectable only after 90 minutes from the G1 release in S-phase when the cells are in mitosis, there is still the possibility that replication fork pausing or fork abnormalities induced by the absence of Dna2 at pausing sites arise between 45 minutes and 90 minutes from the G1 release. Even if we will monitor the fork progression at the same sites also at later time points, we disfavor this possibility based on the fact that DNA replication pausing signals induced by ablation of *RRM3*, at the same pausing sites, are detectable at very early stages of replication and can persist also thorough mitosis (our unpublished observations). Based on the available data, we tend to favor the hypothesis that Dna2 does not have any role in assisting DNA replication fork progression at the analysed pausing elements.

A possible caveat of the results presented in the second part of this thesis could be due to the lack of penetrance of the conditional allele *TC-DNA2-AID*. In particular, residual levels of Dna2, caused by the lack of fast and efficient degradation of the nuclease, could explain the absence of phenotypes in the bulk of DNA synthesis and in the replication across the pausing sites. About that, we would like to point out that we saw complete degradation of *dna2-AID* already after 30 minutes from the addition of auxin and tetracycline to the cell culture medium and, in all the experiments presented in this thesis, cells were kept at least one hour in conditions that induce the degradation of the nuclease before the cells were released in S-phase. Since Dna2 degradation has been analysed by western blotting, we cannot exclude that there is a residual level of the protein that is not detectable by this technique. Moreover, using our *DNA2* conditional allele we were able to recapitulate all the already known *DNA2* phenotypes and genetic interactions caused by the downregulation of Dna2 functions (Budd et al., 2011; Budd et al., 2006), indeed we confirmed several phenotypes previously observed using different mutant alleles of *DNA2* (Fiorentino and Crabtree, 1997; Villa et al., 2016). Based on these considerations and

results we support the conclusion that our *TC-DNA2-AID* allele is sufficiently penetrant to allow us to investigate the essential roles of Dna2.

To better understand the consequences of several S-phases in the absence of Dna2, we generated the double mutant *DNA2-AID rad9Δ*, that allowed to bypass the terminal first cell cycle arrest caused by the DNA damage checkpoint after a single S-phase in the absence of Dna2. Indeed, *dna2* mutants lethality was proposed to be caused by the presence of unprocessed long 5' ssDNA flaps on the lagging strand, generated by Pif1 during the Okazaki fragments maturation. This long 5' flaps at forks are thought to induce the Rad9-mediated activation of the DNA damage checkpoint, which arrests the cells at the metaphase/anaphase transition even after a single S-phase without Dna2 (Budd et al., 2011; Budd et al., 2006; Levikova and Cejka, 2015; Pike et al., 2009; Pike et al., 2010; Rossi et al., 2008). In agreement with this model, we observed that *RAD9* deletion suppressed the checkpoint activation and the M-phase arrest after a single S-phase in the absence of Dna2 and partially rescued the auxin-induced lethality of *DNA2-AID* cells. Thus, it seems that, differently from *PIF1* deletion, *RAD9* deletion does not counteract the formation of toxic replication intermediates in S-phase in the absence of Dna2, but it abolishes the DNA damage checkpoint signaling, preventing the terminal M phase arrest after a single S-phase in the absence of Dna2. If this was the case, we would expect that the deletion of *RAD9* allowed few more cell divisions in the absence of Dna2, but also induced an increased genome instability in *dna2 rad9* cells, caused by the presence of Pif1-induced abnormal replication intermediates, which couldn't be processed by Dna2. Indeed, we found that cells ablated for *RAD9* and *DNA2* proliferated only for 4.5 generations, and then accumulated chromosome breakages and a terminal phenotype caused by an increased percentage of dumbbell cells.

The fact that Dna2 is involved in telomere maintenance and localizes to telomeres in late S/G2 phase (Budd and Campbell, 2013; Choe et al., 2002), when we observed the checkpoint activation after a single S-phase in the absence of Dna2, together with the

previously reported evidences that also Rrm3 and Pif1 localize at telomeres and play a role in telomeres replication (Ivessa et al., 2002; Schulz and Zakian, 1994), made the hypothesis that Dna2 had an essential role in telomere replication or maintenance very attractive, but we unfortunately failed to detect any alterations in telomere length in *DNA2-AID rad9* cells grown for 4.5 generations in the absence of Dna2. However, whether telomere structure is altered in the absence of Dna2 or stochastic loss of single telomere or subtelomeric regions in the cell population accounts for the lethality of Dna2 ablated cells remain to be investigated. Indeed, it has been shown that *dna2* mutants have slightly shortened telomeric single stranded G-rich tails and accumulate small tracts of newly synthetized telomeric lagging strand DNA (Budd and Campbell, 2013).

Moreover *DNA2-AID rad9Δ* cells grown for 4.5 generations without Dna2, did not show alterations in the integrity or in the size of centromeric regions, but showed a strong reduction in the dimension of the chromosome XII, which was likely due to a reduction in the rDNA repeats copy numbers. This data suggests that Dna2 could be required for the processing of Okazaki fragments (as previously suggested), but its function can be specifically required at the rDNA locus. It will be interesting to measure the variation of the rDNA copy number in *DNA2-AID rad9Δ* cells grown for 4.5 generations with or without auxin and analyze the fine ultrastructure of the purified rDNA through transmission electron microscopy (TEM).

An early study utilized the slow growth hypomorphic *dna2-2* mutant allele defective in the helicase activity, but not in the nuclease activity of Dna2, to propose that Dna2 prevents fork stalling and breakages at the replication fork barrier (RFB) of rDNA (Weitao et al., 2003b). *dna2* mutants have a reduced life span, but do not accumulate extrachromosomal rDNA circles, and *dna2-2* old mother cells exhibit increased level of recombination and amplification of the rDNA locus compared to wild type cells (Hoopes et al., 2002). The deletion of *FOB1* suppresses the fork pausing and the fragility at the RFB in *dna2-2* mutants (Weitao et al., 2003b) and is also able to extend the short life span of *dna2-2*

mutants (Hoopes et al., 2002). Interestingly, the *dna2-2* mutation has been identified for its synthetic lethality with the deletion of *CTF4* (Formosa and Nittis, 1999), which encodes a replisome associated factor that connects DNA polymerase α with the CMG helicase complex. It has been recently shown that Dna2 physically interacts with Ctf4 and that the *dna2* mutant, in which this interaction is abolished, is viable but, differently from old *dna2-2* mutants (Hoopes et al., 2002), shows a strong reduction in the number of rDNA repeats (Villa et al., 2016).

The implication of these works is that the essential function of Dna2 could be executed at the rDNA. rDNA locus is highly recombinogenic and fragile; the recombination mediated expulsion of extrachromosomal rDNA circles (ERCs) occurs at high rate and was associated with replicative aging (Kobayashi, 2008; Sinclair and Guarente, 1997). Nowadays, high level of genome instability at the rDNA locus, rather than ERCs accumulation, is proposed to be the cause of aging (Ganley and Kobayashi, 2014).

The opposite genetic interactions of *RRM3* and *PIF1* with *DNA2* could be at least partially explained considering their roles in the context of a combined action of the three factors on rDNA replication; indeed, both Rrm3 and Pif1 associate with the ribosomal DNA but while Rrm3 promotes fork progression across the RFB, Pif1 induces fork pausing (Ivessa et al., 2000). In this view, ablation of *RRM3* and *DNA2* would amplify fork pausing, recombination and breakages at the rDNA while *PIF1* deletion, reducing the replication forks pausing at the RFB and the formation of extrachromosomal rDNA circles, could suppress the rDNA defects of *DNA2* ablated cells and their cell lethality. Ablation of *PIF1* in *rrm3Δ* cells induces a very penetrant slow growth phenotype while its ablation in *dna2* cells suppresses cell lethality restoring a wild type growth rate (Budd et al., 2006). In the light of their role at rDNA one possibility is that high fork speed at the RFB (induced by ablation of *PIF1*) is beneficial for *dna2* cells while fork stalling at RFB (induced by *RRM3* ablation) is detrimental. In this view the lethality of the triple mutant *pif1 rrm3 dna2* could be due to an unfavorable net balance of the fork speed at the RFB.

However, it is still to be further clarified whether the shortening of rDNA, observed in the *dna2 rad9* mutants, is the cause of the cell lethality. Indeed, the mutation of the Ctf4-interacting domain of Dna2 causes rDNA shortening but *dna2* mutant cells are alive (Villa et al., 2016). Even if *FOB1* deletion suppresses ribosomal DNA instability, fork stalling at the RFB, ERCs formation and decreased lifespan in different genetic backgrounds defective in rDNA functions (Hoopes et al., 2002; Kobayashi, 2008; Menolfi et al., 2015; Saka et al., 2016; Torres et al., 2004; Versini et al., 2003; Weitao et al., 2003a), it did not rescue the auxin-induced lethality of *DNA2-AID* cells. This data suggests that cell lethality of *dna2* cells is not caused by the polar pausing of the replication forks at the RFB or by rDNA shortening. One possible explanation is that the observed lethality of *DNA2* ablated cells in the absence of *FOB1* is caused by the presence of the Tof1-Csm3 complex that has a general role in replication and also promotes, together with Fob1, a stable fork arrest at the RFB; but, like *FOB1* deletion, also *TOF1* and *CSM3* deletions are known to be synthetic lethal with *dna2* mutations (Budd et al., 2005). Otherwise the rDNA instability of *dna2* mutants, could not depend on the RFB of the rDNA.

In this context, the observation that *FOB1* deletion did not rescue the auxin-induced lethality of *DNA2-AID* cell, together with the fact that no replication forks defects or pausing were detectable after a single S-phase in the absence of Dna2, did not support the hypothesis that the essential function of Dna2 was only to participate in the replication (and consequently in the maintenance of the stability) of the rDNA locus.

Differently from the suppression of *dna2* mutants lethality carried out by the deletion of *RAD9*, the deletion of *PIF1* completely rescued the lethality and the growth defects of *DNA2* ablated cells, even if *dna2Δ pif1Δ* cells retain some residual replication and repair defects, which are suppressed by deleting the Polδ subunit responsible for the strand displacement activity (Budd et al., 2006). *RAD9* deletion allows the proliferation of *dna2* mutant for 4.5 generations, likely at the expense of genome stability, while the ablation of nuclear isoform of *PIF1* is thought to suppress the formation of toxic replication

intermediates that induce cell death in the absence of Dna2 (Budd et al., 2011; Budd et al., 2006; Levikova and Cejka, 2015; Pike et al., 2009; Pike et al., 2010; Rossi et al., 2008). In line with published data (Budd et al., 2006), the *pif1-m2* mutation suppressed the auxin-induced lethality of *DNA2-AID* cells, the checkpoint activation and the consequent cell cycle arrest in M phase, after a single S-phase in the absence of Dna2, while *RRM3* deletion did not alter the lethality of *dna2* mutant cells.

Moreover we observed that *RRM3* ablation in *pif1-m2 dna2* cells was synthetic lethal. *pif1-m2 rrm3 dna2* triple mutant arrested in M-phase, similarly to *DNA2* ablated cells, but in the case of the triple mutant Rad53 was only modestly phosphorylated. While a possible explanation of the lethality of the triple mutant *rrm3 pif1-m2 dna2* has been proposed in the context of a role of Rrm3 Pif1 and Dna2 in the replication and maintenance of the rDNA (see above paragraphs in this Discussion session) the fact that *rrm3 pif1-m2 dna2* cells arrest at M-phase without activating Rad53 was an unexpected result.

Dna2 was proposed to stimulate the checkpoint activation through its physical interaction with Mec1, which occurs through two aromatic residues, located in the unstructured N-terminal domain of Dna2 (Kumar and Burgers, 2013). A similar mechanism of Mec1 activation through physical interactions was also observed for the two other checkpoint sensors, Ddc1 (Navadgi-Patil and Burgers, 2009) and Dpb11 (Navadgi-Patil et al., 2011). Since also Rrm3 and Pif1 contain unstructured N-terminal domains with several aromatic amino acid, we could hypothesize that they synergize with Dna2, in stimulating the Mec1 kinase activity and this could be the reason why there is low level of Rad53 activation in *rrm3 dna2 pif1-m2* cells arrested in mitosis. However, the fact that Rrm3 or Pif1 are not able to stimulate the Mec1 kinase activity *in vitro* is against this hypothesis (Kumar and Burgers, 2013). Another possible explanation is that the terminal cell cycle arrest in the triple mutant was not caused by the DNA damage checkpoint, but by other surveillance mechanisms that are not mediated by Rad53, like the spindle assembly checkpoint (Kim and Burke, 2008; Musacchio, 2015). This hypothesis implies that there are no abnormal

DNA replication or recombination structures in *rrm3 dna2 pif1-m2* arrested in M-phase that are able to induce Rad53 activation, which is really surprising considering the replication problems usually induced by the single mutations (Bochman et al., 2010; Budd and Campbell, 1995, 1997; Budd et al., 2000). Since the cause of the G2/M arrest in the *pif1-m2 rrm3 dna2* mutant is not clear this results will need to be further investigated.

4.2.2 Dna2 essential role could be counteracting strand displacement events due to elevated fork speed at specific genomic *loci*

We also explored the effects of the ablation of *DNA2* in the presence of hydroxyurea.

It is has been proposed that Dna2, thanks to its unstructured N-terminal domain, stimulates the Mec1 kinase activity by direct physical interaction and it is therefore an activator of the checkpoint signaling cascade, specifically in S-phase under replication stress conditions (Kumar and Burgers, 2013). We failed to detect any alteration in the checkpoint signaling in the presence of 25 mM of HU in the absence of Dna2; indeed Rad53 was correctly activated and inactivated when Dna2 ablated cells were released in S-phase in the presence of 25 mM of HU. This result can be explained considering that Dna2 synergizes with the 9-1-1 complex and Dpb11 in the S-phase checkpoint activation under replication stress (Kumar and Burgers, 2013).

Dna2 has been proposed to be a checkpoint target under replication stress conditions indeed in *S.pombe,* the checkpoint kinase Cds1 targets Dna2 to localize it at the stalled replication forks where its nuclease activity is thought to counteract accumulation of long flaps, which can induce fork reversal (Hu et al., 2012).

Whether this replication stress induced checkpoint dependent regulation of Dna2 is conserved in the budding yeast *S. cerevisiae* is currently under investigation in the lab. Preliminary results, that we recently obtained, seem to rule out that Dna2 is a component of the stalled DNA replication forks (our unpublished observations). Indeed, if genome-wide binding sites of DNA polymerase α and Dna2, detected by ChIP on chip in budding

yeast cells released from G1 into S-phase for 90 minutes in the presence of 150 mM of HU, are compared we do not detect a statistically significative overlap between the binding clusters of these two proteins (our unpublished observations). Moreover, in the same conditions, Dna2 does not seem to be hyper-phosphorylated as it is judged by analysing its migration pattern in SDS-PAGE using phospho-tag gels (Kinoshita et al., 2006) (our unpublished observations). So far, we do not have indications that Dna2 is a checkpoint target at the stalled replication forks and that its absence induces accumulation of abnormal DNA replication fork structures. According to the proposed Dna2 role as a factor that protects the stability and the architecture of the stalled DNA replication fork (Hu et al., 2012), one expectation was that the phenotypes, due to its absence in a single S-phase, should be worsened if the absence of Dna2 was combined to the presence of HU. Surprisingly, we noticed that the strains *dna2 pif1-m2* and *dna2 rad9* double mutants did not show sensitivity when plated on 10 mM of HU. Strikingly, when *DNA2* ablated cells were released in S-phase in the presence of 25 mM of HU, Rad53 was activated and inactivated with the same kinetic of the control cells and the strong and prolonged activation of the checkpoint kinase detected during a single unperturbed S-phase in the absence of Dna2 was suppressed. Importantly, Dna2 ablated cells, released in presence of low HU concentrations, do not arrest at the first cell cycle but they proceed through the next S-phase and get arrested at the mitosis of the second cell cycle likely because of a residual low level of Rad53 activation. This second cell cycle arrest is likely the reason why low HU does not suppress cell lethality caused by Dna2 ablation. Strikingly, when *RAD9* was deleted and Dna2 ablated and cells were allowed to proceed in the cell cycle, the presence of low HU doses almost completely rescued the growth defect of *dna2 rad9* mutants. This data strongly suggests that the replication defects, induced during several S-phases in the absence of Dna2, and the DNA damage checkpoint can be alleviated by slowing down the DNA replication fork speed using low does of HU.

An attractive hypothesis, which could explain the HU mediated suppression of Rad53 hyper-activation in Dna2 ablated cells, was that the presence of hydroxyurea at the beginning of the S-phase would induce a Rad53 mediated phosphorylation and inhibition of Pif1, which would alleviate replication defects induced by the absence of Dna2. One consequence of this hypothesis is that the combination of the phospho-mimicking allele *pif1-12D* with the *DNA2-AID* allele should rescue the lethality of *DNA2-AID* cells in the presence of auxin. Unfortunately, this was not the case, indeed *DNA2-AID pif1-12D* cells showed cell lethality when plated in the presence of auxin (our unpublished observations).

The idea that growth phenotypes and DNA replication phenotypes caused by the absence of Dna2 can be suppressed by slowing down the speed of the DNA replication fork is strongly supported by the fact that growth defects of *dna2 rad9* and *dna2 rad53* cells are alleviated by the incubation of these cells at low temperatures.

It is clear from our data that the deletion of the Rad9-dependent DNA damage checkpoint, combined with the slow down of the replication fork speed almost completely rescued the lethality of *DNA2* ablated cells. Based on published data and on these results, we propose that the slowing down of the DNA replication forks speed would limit the strand displacement activities of DNA polymerase δ and Pif1, reducing the formation of long 5' ssDNA flaps and making the role of Dna2 in processing the DNA flaps partially dispensable.

Although, the essential role of Dna2 in DNA replication and its relationships with Rrm3 and Pif1 still need to be further investigated, in this second part of this thesis we set up a panel of reagents and experimental conditions that will likely allow us to shed new lights on the roles of these three important factors during DNA replication.

6. References

Admire, A., Shanks, L., Danzl, N., Wang, M., Weier, U., Stevens, W., Hunt, E., and Weinert, T. (2006). Cycles of chromosome instability are associated with a fragile site and are increased by defects in DNA replication and checkpoint controls in yeast. Genes & development *20*, 159-173.

Aguilera, A. (2005). Cotranscriptional mRNP assembly: from the DNA to the nuclear pore. Curr Opin Cell Biol *17*, 242-250.

Alcasabas, A.A., Osborn, A.J., Bachant, J., Hu, F., Werler, P.J., Bousset, K., Furuya, K., Diffley, J.F., Carr, A.M., and Elledge, S.J. (2001). Mrc1 transduces signals of DNA replication stress to activate Rad53. Nature cell biology *3*, 958-965.

Allen, J.B., Zhou, Z., Siede, W., Friedberg, E.C., and Elledge, S.J. (1994). The SAD1/RAD53 protein kinase controls multiple checkpoints and DNA damage-induced transcription in yeast. Genes & development *8*, 2401-2415.

Alvino, G.M., Collingwood, D., Murphy, J.M., Delrow, J., Brewer, B.J., and Raghuraman, M.K. (2007). Replication in hydroxyurea: it's a matter of time. Molecular and cellular biology *27*, 6396-6406.

Alzu, A., Bermejo, R., Begnis, M., Lucca, C., Piccini, D., Carotenuto, W., Saponaro, M., Brambati, A., Cocito, A., Foiani, M.*, et al.* (2012). Senataxin Associates with Replication Forks to Protect Fork Integrity across RNA-Polymerase-II-Transcribed Genes. Cell *151*, 835-846.

Andersen, S.D., Keijzers, G., Rampakakis, E., Engels, K., Luhn, P., El-Shemerly, M., Nielsen, F.C., Du, Y., May, A., Bohr, V.A.*, et al.* (2012). 14-3-3 checkpoint regulatory proteins interact specifically with DNA repair protein human exonuclease 1 (hEXO1) via a semi-conserved motif. DNA repair *11*, 267-277.

Aparicio, O.M., Weinstein, D.M., and Bell, S.P. (1997). Components and dynamics of DNA replication complexes in S. cerevisiae: redistribution of MCM proteins and Cdc45p during S phase. Cell *91*, 59-69.

Azvolinsky, A., Dunaway, S., Torres, J.Z., Bessler, J.B., and Zakian, V.A. (2006). The S. cerevisiae Rrm3p DNA helicase moves with the replication fork and affects replication of all yeast chromosomes. Genes & development *20*, 3104-3116.

Azvolinsky, A., Giresi, P.G., Lieb, J.D., and Zakian, V.A. (2009). Highly transcribed RNA polymerase II genes are impediments to replication fork progression in Saccharomyces cerevisiae. Molecular cell *34*, 722-734.

Badaracco, G., Bianchi, M., Valsasnini, P., Magni, G., and Plevani, P. (1985). Initiation, elongation and pausing of in vitro DNA synthesis catalyzed by immunopurified yeast DNA primase: DNA polymerase complex. The EMBO journal *4*, 1313-1317.

Bailis, J.M., Luche, D.D., Hunter, T., and Forsburg, S.L. (2008). Minichromosome maintenance proteins interact with checkpoint and recombination proteins to promote s-phase genome stability. Molecular and cellular biology *28*, 1724-1738.

Bartkova, J., Horejsi, Z., Koed, K., Kramer, A., Tort, F., Zieger, K., Guldberg, P., Sehested, M., Nesland, J.M., Lukas, C.*, et al.* (2005). DNA damage response as a candidate anti-cancer barrier in early human tumorigenesis. Nature *434*, 864-870.

Bastos de Oliveira, F.M., Kim, D., Cussiol, J.R., Das, J., Jeong, M.C., Doerfler, L., Schmidt, K.H., Yu, H., and Smolka, M.B. (2015). Phosphoproteomics reveals distinct modes of Mec1/ATR signaling during DNA replication. Molecular cell *57*, 1124-1132.

Baxter, J., Sen, N., Martinez, V.L., De Carandini, M.E., Schvartzman, J.B., Diffley, J.F., and Aragon, L. (2011). Positive supercoiling of mitotic DNA drives decatenation by topoisomerase II in eukaryotes. Science *331*, 1328-1332.

Bazzi, M., Mantiero, D., Trovesi, C., Lucchini, G., and Longhese, M.P. (2010). Dephosphorylation of gamma H2A by Glc7/protein phosphatase 1 promotes recovery from inhibition of DNA replication. Molecular and cellular biology *30*, 131-145.

Bell, L., and Byers, B. (1983). Separation of branched from linear DNA by two-dimensional gel electrophoresis. Anal Biochem *130*, 527-535.

Bell, S.P., and Stillman, B. (1992). ATP-dependent recognition of eukaryotic origins of DNA replication by a multiprotein complex. Nature *357*, 128-134.

Bermejo, R., Capra, T., Gonzalez-Huici, V., Fachinetti, D., Cocito, A., Natoli, G., Katou, Y., Mori, H., Kurokawa, K., Shirahige, K.*, et al.* (2009a). Genome-organizing factors Top2 and Hmo1 prevent chromosome fragility at sites of S phase transcription. Cell *138*, 870-884.

Bermejo, R., Capra, T., Jossen, R., Colosio, A., Frattini, C., Carotenuto, W., Cocito, A., Doksani, Y., Klein, H., Gomez-Gonzalez, B.*, et al.* (2011). The replication checkpoint protects fork stability by releasing transcribed genes from nuclear pores. Cell *146*, 233-246.

Bermejo, R., Doksani, Y., Capra, T., Katou, Y.M., Tanaka, H., Shirahige, K., and Foiani, M. (2007). Top1- and Top2-mediated topological transitions at replication forks ensure fork progression and stability and prevent DNA damage checkpoint activation. Genes & development *21*, 1921-1936.

Bermejo, R., Katou, Y.M., Shirahige, K., and Foiani, M. (2009b). ChIP-on-chip analysis of DNA topoisomerases. Methods in molecular biology *582*, 103-118.

Bermejo, R., Kumar, A., and Foiani, M. (2012a). Preserving the genome by regulating chromatin association with the nuclear envelope. Trends Cell Biol *22*, 465-473.

Bermejo, R., Lai, M.S., and Foiani, M. (2012b). Preventing replication stress to maintain genome stability: resolving conflicts between replication and transcription. Molecular cell *45*, 710-718.

Bessler, J.B., Torres, J.Z., and Zakian, V.A. (2001). The Pif1p subfamily of helicases: region-specific DNA helicases? Trends Cell Biol *11*, 60-65.

Bessler, J.B., and Zakian, V.A. (2004). The amino terminus of the Saccharomyces cerevisiae DNA helicase Rrm3p modulates protein function altering replication and checkpoint activity. Genetics *168*, 1205-1218.

Bester, A.C., Roniger, M., Oren, Y.S., Im, M.M., Sarni, D., Chaoat, M., Bensimon, A., Zamir, G., Shewach, D.S., and Kerem, B. (2011). Nucleotide deficiency promotes genomic instability in early stages of cancer development. Cell *145*, 435-446.

Blow, J.J., and Dutta, A. (2005). Preventing re-replication of chromosomal DNA. Nat Rev Mol Cell Biol *6*, 476-486.

Bochman, M.L., Paeschke, K., and Zakian, V.A. (2012). DNA secondary structures: stability and function of G-quadruplex structures. Nat Rev Genet *13*, 770-780.

Bochman, M.L., Sabouri, N., and Zakian, V.A. (2010). Unwinding the functions of the Pif1 family helicases. DNA repair *9*, 237-249.

Boddy, M.N., Shanahan, P., McDonald, W.H., Lopez-Girona, A., Noguchi, E., Yates, I.J., and Russell, P. (2003). Replication checkpoint kinase Cds1 regulates recombinational repair protein Rad60. Molecular and cellular biology *23*, 5939-5946.

Boule, J.B., Vega, L.R., and Zakian, V.A. (2005). The yeast Pif1p helicase removes telomerase from telomeric DNA. Nature *438*, 57-61.

Boule, J.B., and Zakian, V.A. (2007). The yeast Pif1p DNA helicase preferentially unwinds RNA DNA substrates. Nucleic acids research *35*, 5809-5818.

Branzei, D., and Foiani, M. (2009). The checkpoint response to replication stress. DNA repair *8*, 1038-1046.

Branzei, D., and Foiani, M. (2010). Maintaining genome stability at the replication fork. Nat Rev Mol Cell Biol *11*, 208-219.

Brewer, B.J., and Fangman, W.L. (1987). The localization of replication origins on ARS plasmids in S. cerevisiae. Cell *51*, 463-471.

Brewer, B.J., and Fangman, W.L. (1988). A replication fork barrier at the 3' end of yeast ribosomal RNA genes. Cell *55*, 637-643.

Brewer, B.J., Lockshon, D., and Fangman, W.L. (1992). The arrest of replication forks in the rDNA of yeast occurs independently of transcription. Cell *71*, 267-276.

Brush, G.S., Morrow, D.M., Hieter, P., and Kelly, T.J. (1996). The ATM homologue MEC1 is required for phosphorylation of replication protein A in yeast. Proceedings of the National Academy of Sciences of the United States of America *93*, 15075-15080.

Budd, M.E., Antoshechkin, I.A., Reis, C., Wold, B.J., and Campbell, J.L. (2011). Inviability of a DNA2 deletion mutant is due to the DNA damage checkpoint. Cell Cycle *10*, 1690-1698.

Budd, M.E., and Campbell, J.L. (1995). A yeast gene required for DNA replication encodes a protein with homology to DNA helicases. Proceedings of the National Academy of Sciences of the United States of America *92*, 7642-7646.

Budd, M.E., and Campbell, J.L. (1997). A yeast replicative helicase, Dna2 helicase, interacts with yeast FEN-1 nuclease in carrying out its essential function. Molecular and cellular biology *17*, 2136-2142.

Budd, M.E., and Campbell, J.L. (2013). Dna2 is involved in CA strand resection and nascent lagging strand completion at native yeast telomeres. The Journal of biological chemistry *288*, 29414-29429.

Budd, M.E., Choe, W., and Campbell, J.L. (2000). The nuclease activity of the yeast DNA2 protein, which is related to the RecB-like nucleases, is essential in vivo. The Journal of biological chemistry *275*, 16518-16529.

Budd, M.E., Choe, W.C., and Campbell, J.L. (1995). DNA2 encodes a DNA helicase essential for replication of eukaryotic chromosomes. The Journal of biological chemistry *270*, 26766-26769.

Budd, M.E., Reis, C.C., Smith, S., Myung, K., and Campbell, J.L. (2006). Evidence suggesting that Pif1 helicase functions in DNA replication with the Dna2 helicase/nuclease and DNA polymerase delta. Molecular and cellular biology *26*, 2490-2500.

Byun, T.S., Pacek, M., Yee, M.C., Walter, J.C., and Cimprich, K.A. (2005). Functional uncoupling of MCM helicase and DNA polymerase activities activates the ATR-dependent checkpoint. Genes & development *19*, 1040-1052.

Cabal, G.G., Genovesio, A., Rodriguez-Navarro, S., Zimmer, C., Gadal, O., Lesne, A., Buc, H., Feuerbach-Fournier, F., Olivo-Marin, J.C., Hurt, E.C.*, et al.* (2006). SAGA interacting factors confine sub-diffusion of transcribed genes to the nuclear envelope. Nature *441*, 770-773.

Calzada, A., Hodgson, B., Kanemaki, M., Bueno, A., and Labib, K. (2005). Molecular anatomy and regulation of a stable replisome at a paused eukaryotic DNA replication fork. Genes & development *19*, 1905-1919.

Capra, J.A., Paeschke, K., Singh, M., and Zakian, V.A. (2010). G-quadruplex DNA sequences are evolutionarily conserved and associated with distinct genomic features in Saccharomyces cerevisiae. PLoS Comput Biol *6*, e1000861.

Casper, A.M., Nghiem, P., Arlt, M.F., and Glover, T.W. (2002). ATR regulates fragile site stability. Cell *111*, 779-789.

Cha, R.S., and Kleckner, N. (2002). ATR homolog Mec1 promotes fork progression, thus averting breaks in replication slow zones. Science *297*, 602-606.

Chabes, A., Domkin, V., and Thelander, L. (1999). Yeast Sml1, a protein inhibitor of ribonucleotide reductase. The Journal of biological chemistry *274*, 36679-36683.

Chabes, A., Georgieva, B., Domkin, V., Zhao, X., Rothstein, R., and Thelander, L. (2003). Survival of DNA damage in yeast directly depends on increased dNTP levels allowed by relaxed feedback inhibition of ribonucleotide reductase. Cell *112*, 391-401.

Chabes, A., and Stillman, B. (2007). Constitutively high dNTP concentration inhibits cell cycle progression and the DNA damage checkpoint in yeast Saccharomyces cerevisiae. Proceedings of the National Academy of Sciences of the United States of America *104*, 1183-1188.

Chen, X., Niu, H., Chung, W.H., Zhu, Z., Papusha, A., Shim, E.Y., Lee, S.E., Sung, P., and Ira, G. (2011). Cell cycle regulation of DNA double-strand break end resection by Cdk1-dependent Dna2 phosphorylation. Nature structural & molecular biology *18*, 1015-1019.

Cheng, X., Dunaway, S., and Ivessa, A.S. (2007). The role of Pif1p, a DNA helicase in Saccharomyces cerevisiae, in maintaining mitochondrial DNA. Mitochondrion *7*, 211-222.

Chilkova, O., Stenlund, P., Isoz, I., Stith, C.M., Grabowski, P., Lundstrom, E.B., Burgers, P.M., and Johansson, E. (2007). The eukaryotic leading and lagging strand DNA polymerases are loaded onto primer-ends via separate mechanisms but have comparable processivity in the presence of PCNA. Nucleic acids research *35*, 6588-6597.

Chisholm, K.M., Aubert, S.D., Freese, K.P., Zakian, V.A., King, M.C., and Welcsh, P.L. (2012). A genomewide screen for suppressors of Alu-mediated rearrangements reveals a role for PIF1. PloS one *7*, e30748.

Choe, W., Budd, M., Imamura, O., Hoopes, L., and Campbell, J.L. (2002). Dynamic localization of an Okazaki fragment processing protein suggests a novel role in telomere replication. Molecular and cellular biology *22*, 4202-4217.

Cobb, J.A., Bjergbaek, L., Shimada, K., Frei, C., and Gasser, S.M. (2003). DNA polymerase stabilization at stalled replication forks requires Mec1 and the RecQ helicase Sgs1. The EMBO journal *22*, 4325-4336.

Cobb, J.A., Schleker, T., Rojas, V., Bjergbaek, L., Tercero, J.A., and Gasser, S.M. (2005). Replisome instability, fork collapse, and gross chromosomal rearrangements arise synergistically from Mec1 kinase and RecQ helicase mutations. Genes & development *19*, 3055-3069.

Cohen-Fix, O., and Koshland, D. (1997). The anaphase inhibitor of Saccharomyces cerevisiae Pds1p is a target of the DNA damage checkpoint pathway. Proceedings of the National Academy of Sciences of the United States of America *94*, 14361-14366.

Cortez, D., Glick, G., and Elledge, S.J. (2004). Minichromosome maintenance proteins are direct targets of the ATM and ATR checkpoint kinases. Proceedings of the National Academy of Sciences of the United States of America *101*, 10078-10083.

Cotta-Ramusino, C., Fachinetti, D., Lucca, C., Doksani, Y., Lopes, M., Sogo, J., and Foiani, M. (2005). Exo1 processes stalled replication forks and counteracts fork reversal in checkpoint-defective cells. Molecular cell *17*, 153-159.

Couch, F.B., Bansbach, C.E., Driscoll, R., Luzwick, J.W., Glick, G.G., Betous, R., Carroll, C.M., Jung, S.Y., Qin, J., Cimprich, K.A*., et al.* (2013). ATR phosphorylates SMARCAL1 to prevent replication fork collapse. Genes & development *27*, 1610-1623.

Crabbe, L., Thomas, A., Pantesco, V., De Vos, J., Pasero, P., and Lengronne, A. (2010). Analysis of replication profiles reveals key role of RFC-Ctf18 in yeast replication stress response. Nature structural & molecular biology *17*, 1391-1397.

Dalgaard, J.Z., and Klar, A.J. (2000). swi1 and swi3 perform imprinting, pausing, and termination of DNA replication in S. pombe. Cell *102*, 745-751.

De Antoni, A., and Gallwitz, D. (2000). A novel multi-purpose cassette for repeated integrative epitope tagging of genes in Saccharomyces cerevisiae. Gene *246*, 179-185.

De Piccoli, G., Katou, Y., Itoh, T., Nakato, R., Shirahige, K., and Labib, K. (2012). Replisome stability at defective DNA replication forks is independent of S phase checkpoint kinases. Molecular cell *45*, 696-704.

Desany, B.A., Alcasabas, A.A., Bachant, J.B., and Elledge, S.J. (1998). Recovery from DNA replicational stress is the essential function of the S-phase checkpoint pathway. Genes & development *12*, 2956-2970.

Deshpande, A.M., and Newlon, C.S. (1996). DNA replication fork pause sites dependent on transcription. Science *272*, 1030-1033.

Dewar, J.M., and Lydall, D. (2010). Pif1- and Exo1-dependent nucleases coordinate checkpoint activation following telomere uncapping. The EMBO journal *29*, 4020-4034.

Di Micco, R., Fumagalli, M., Cicalese, A., Piccinin, S., Gasparini, P., Luise, C., Schurra, C., Garre, M., Nuciforo, P.G., Bensimon, A*., et al.* (2006). Oncogene-induced senescence is a DNA damage response triggered by DNA hyper-replication. Nature *444*, 638-642.

Doksani, Y., Bermejo, R., Fiorani, S., Haber, J.E., and Foiani, M. (2009). Replicon dynamics, dormant origin firing, and terminal fork integrity after double-strand break formation. Cell *137*, 247-258.

Dominguez-Sola, D., Ying, C.Y., Grandori, C., Ruggiero, L., Chen, B., Li, M., Galloway, D.A., Gu, W., Gautier, J., and Dalla-Favera, R. (2007). Non-transcriptional control of DNA replication by c-Myc. Nature *448*, 445-451.

Downs, J.A., Lowndes, N.F., and Jackson, S.P. (2000). A role for Saccharomyces cerevisiae histone H2A in DNA repair. Nature *408*, 1001-1004.

Duncker, B.P., Shimada, K., Tsai-Pflugfelder, M., Pasero, P., and Gasser, S.M. (2002). An N-terminal domain of Dbf4p mediates interaction with both origin recognition complex

(ORC) and Rad53p and can deregulate late origin firing. Proceedings of the National Academy of Sciences of the United States of America *99*, 16087-16092.

Durocher, D., Smerdon, S.J., Yaffe, M.B., and Jackson, S.P. (2000). The FHA domain in DNA repair and checkpoint signaling. Cold Spring Harb Symp Quant Biol *65*, 423-431.

Duxin, J.P., Dao, B., Martinsson, P., Rajala, N., Guittat, L., Campbell, J.L., Spelbrink, J.N., and Stewart, S.A. (2009). Human Dna2 is a nuclear and mitochondrial DNA maintenance protein. Molecular and cellular biology *29*, 4274-4282.

Elledge, S.J. (1996). Cell cycle checkpoints: preventing an identity crisis. Science *274*, 1664-1672.

Elledge, S.J., Zhou, Z., Allen, J.B., and Navas, T.A. (1993). DNA damage and cell cycle regulation of ribonucleotide reductase. Bioessays *15*, 333-339.

Engels, K., Giannattasio, M., Muzi-Falconi, M., Lopes, M., and Ferrari, S. (2011). 14-3-3 Proteins regulate exonuclease 1-dependent processing of stalled replication forks. PLoS genetics *7*, e1001367.

Fachinetti, D., Bermejo, R., Cocito, A., Minardi, S., Katou, Y., Kanoh, Y., Shirahige, K., Azvolinsky, A., Zakian, V.A., and Foiani, M. (2010). Replication termination at eukaryotic chromosomes is mediated by Top2 and occurs at genomic loci containing pausing elements. Molecular cell *39*, 595-605.

Fay, D.S., Sun, Z., and Stern, D.F. (1997). Mutations in SPK1/RAD53 that specifically abolish checkpoint but not growth-related functions. Curr Genet *31*, 97-105.

Fiorentino, D.F., and Crabtree, G.R. (1997). Characterization of Saccharomyces cerevisiae dna2 mutants suggests a role for the helicase late in S phase. Molecular biology of the cell *8*, 2519-2537.

Foiani, M., Liberi, G., Lucchini, G., and Plevani, P. (1995). Cell cycle-dependent phosphorylation and dephosphorylation of the yeast DNA polymerase alpha-primase B subunit. Molecular and cellular biology *15*, 883-891.

Forment, J.V., Blasius, M., Guerini, I., and Jackson, S.P. (2011). Structure-specific DNA endonuclease Mus81/Eme1 generates DNA damage caused by Chk1 inactivation. PloS one *6*, e23517.

Formosa, T., and Nittis, T. (1999). Dna2 mutants reveal interactions with Dna polymerase alpha and Ctf4, a Pol alpha accessory factor, and show that full Dna2 helicase activity is not essential for growth. Genetics *151*, 1459-1470.

Foury, F., and Dyck, E.V. (1985). A PIF-dependent recombinogenic signal in the mitochondrial DNA of yeast. The EMBO journal *4*, 3525-3530.

Foury, F., and Kolodynski, J. (1983). pif mutation blocks recombination between mitochondrial rho+ and rho- genomes having tandemly arrayed repeat units in

Saccharomyces cerevisiae. Proceedings of the National Academy of Sciences of the United States of America *80*, 5345-5349.

Froget, B., Blaisonneau, J., Lambert, S., and Baldacci, G. (2008). Cleavage of stalled forks by fission yeast Mus81/Eme1 in absence of DNA replication checkpoint. Molecular biology of the cell *19*, 445-456.

Fu, Y.V., Yardimci, H., Long, D.T., Ho, T.V., Guainazzi, A., Bermudez, V.P., Hurwitz, J., van Oijen, A., Scharer, O.D., and Walter, J.C. (2011). Selective bypass of a lagging strand roadblock by the eukaryotic replicative DNA helicase. Cell *146*, 931-941.

Ganley, A.R., and Kobayashi, T. (2014). Ribosomal DNA and cellular senescence: new evidence supporting the connection between rDNA and aging. FEMS yeast research *14*, 49-59.

Garg, P., Stith, C.M., Sabouri, N., Johansson, E., and Burgers, P.M. (2004). Idling by DNA polymerase delta maintains a ligatable nick during lagging-strand DNA replication. Genes & development *18*, 2764-2773.

George, T., Wen, Q., Griffiths, R., Ganesh, A., Meuth, M., and Sanders, C.M. (2009). Human Pif1 helicase unwinds synthetic DNA structures resembling stalled DNA replication forks. Nucleic acids research *37*, 6491-6502.

Greenfeder, S.A., and Newlon, C.S. (1992). Replication forks pause at yeast centromeres. Molecular and cellular biology *12*, 4056-4066.

Gruber, M., Wellinger, R.E., and Sogo, J.M. (2000). Architecture of the replication fork stalled at the 3' end of yeast ribosomal genes. Molecular and cellular biology *20*, 5777-5787.

Gu, Y., Masuda, Y., and Kamiya, K. (2008). Biochemical analysis of human PIF1 helicase and functions of its N-terminal domain. Nucleic acids research *36*, 6295-6308.

Harrison, J.C., and Haber, J.E. (2006). Surviving the breakup: the DNA damage checkpoint. Annu Rev Genet *40*, 209-235.

Hartwell, L.H., and Weinert, T.A. (1989). Checkpoints: controls that ensure the order of cell cycle events. Science *246*, 629-634.

Hashash, N., Johnson, A.L., and Cha, R.S. (2011). Regulation of fragile sites expression in budding yeast by MEC1, RRM3 and hydroxyurea. Journal of cell science *124*, 181-185.

Hashash, N., Johnson, A.L., and Cha, R.S. (2012). Topoisomerase II- and condensin-dependent breakage of MEC1ATR-sensitive fragile sites occurs independently of spindle tension, anaphase, or cytokinesis. PLoS genetics *8*, e1002978.

Hershman, S.G., Chen, Q., Lee, J.Y., Kozak, M.L., Yue, P., Wang, L.S., and Johnson, F.B. (2008). Genomic distribution and functional analyses of potential G-quadruplex-forming sequences in Saccharomyces cerevisiae. Nucleic acids research *36*, 144-156.

Homesley, L., Lei, M., Kawasaki, Y., Sawyer, S., Christensen, T., and Tye, B.K. (2000). Mcm10 and the MCM2-7 complex interact to initiate DNA synthesis and to release replication factors from origins. Genes & development *14*, 913-926.

Hoopes, L.L., Budd, M., Choe, W., Weitao, T., and Campbell, J.L. (2002). Mutations in DNA replication genes reduce yeast life span. Molecular and cellular biology *22*, 4136-4146.

Hu, J., Sun, L., Shen, F., Chen, Y., Hua, Y., Liu, Y., Zhang, M., Hu, Y., Wang, Q., Xu, W., *et al.* (2012). The intra-S phase checkpoint targets Dna2 to prevent stalled replication forks from reversing. Cell *149*, 1221-1232.

Huang, M., Zhou, Z., and Elledge, S.J. (1998). The DNA replication and damage checkpoint pathways induce transcription by inhibition of the Crt1 repressor. Cell *94*, 595-605.

Ivessa, A.S., Lenzmeier, B.A., Bessler, J.B., Goudsouzian, L.K., Schnakenberg, S.L., and Zakian, V.A. (2003). The Saccharomyces cerevisiae helicase Rrm3p facilitates replication past nonhistone protein-DNA complexes. Molecular cell *12*, 1525-1536.

Ivessa, A.S., Zhou, J.Q., Schulz, V.P., Monson, E.K., and Zakian, V.A. (2002). Saccharomyces Rrm3p, a 5' to 3' DNA helicase that promotes replication fork progression through telomeric and subtelomeric DNA. Genes & development *16*, 1383-1396.

Ivessa, A.S., Zhou, J.Q., and Zakian, V.A. (2000). The Saccharomyces Pif1p DNA helicase and the highly related Rrm3p have opposite effects on replication fork progression in ribosomal DNA. Cell *100*, 479-489.

Johansson, E., Garg, P., and Burgers, P.M. (2004). The Pol32 subunit of DNA polymerase delta contains separable domains for processive replication and proliferating cell nuclear antigen (PCNA) binding. The Journal of biological chemistry *279*, 1907-1915.

Johnson, R.E., Klassen, R., Prakash, L., and Prakash, S. (2015). A Major Role of DNA Polymerase delta in Replication of Both the Leading and Lagging DNA Strands. Molecular cell *59*, 163-175.

Kai, M., Boddy, M.N., Russell, P., and Wang, T.S. (2005). Replication checkpoint kinase Cds1 regulates Mus81 to preserve genome integrity during replication stress. Genes & development *19*, 919-932.

Kastan, M.B., and Bartek, J. (2004). Cell-cycle checkpoints and cancer. Nature *432*, 316-323.

Katou, Y., Kaneshiro, K., Aburatani, H., and Shirahige, K. (2006). Genomic approach for the understanding of dynamic aspect of chromosome behavior. Methods in enzymology *409*, 389-410.

Katou, Y., Kanoh, Y., Bando, M., Noguchi, H., Tanaka, H., Ashikari, T., Sugimoto, K., and Shirahige, K. (2003). S-phase checkpoint proteins Tof1 and Mrc1 form a stable replication-pausing complex. Nature *424*, 1078-1083.

Keil, R.L., and McWilliams, A.D. (1993). A gene with specific and global effects on recombination of sequences from tandemly repeated genes in Saccharomyces cerevisiae. Genetics *135*, 711-718.

Kim, E.M., and Burke, D.J. (2008). DNA damage activates the SAC in an ATM/ATR-dependent manner, independently of the kinetochore. PLoS genetics *4*, e1000015.

Kinoshita, E., Kinoshita-Kikuta, E., and Koike, T. (2009). Separation and detection of large phosphoproteins using Phos-tag SDS-PAGE. Nat Protoc *4*, 1513-1521.

Kinoshita, E., Kinoshita-Kikuta, E., Takiyama, K., and Koike, T. (2006). Phosphate-binding tag, a new tool to visualize phosphorylated proteins. Molecular & cellular proteomics : MCP *5*, 749-757.

Kobayashi, T. (2008). A new role of the rDNA and nucleolus in the nucleus--rDNA instability maintains genome integrity. Bioessays *30*, 267-272.

Kohler, A., and Hurt, E. (2007). Exporting RNA from the nucleus to the cytoplasm. Nat Rev Mol Cell Biol *8*, 761-773.

Kotter, P., Weigand, J.E., Meyer, B., Entian, K.D., and Suess, B. (2009). A fast and efficient translational control system for conditional expression of yeast genes. Nucleic acids research *37*, e120.

Krakoff, I.H., Brown, N.C., and Reichard, P. (1968). Inhibition of ribonucleoside diphosphate reductase by hydroxyurea. Cancer research *28*, 1559-1565.

Kumagai, A., and Dunphy, W.G. (2003). Repeated phosphopeptide motifs in Claspin mediate the regulated binding of Chk1. Nature cell biology *5*, 161-165.

Kumar, D., Abdulovic, A.L., Viberg, J., Nilsson, A.K., Kunkel, T.A., and Chabes, A. (2011). Mechanisms of mutagenesis in vivo due to imbalanced dNTP pools. Nucleic acids research *39*, 1360-1371.

Kumar, D., Viberg, J., Nilsson, A.K., and Chabes, A. (2010). Highly mutagenic and severely imbalanced dNTP pools can escape detection by the S-phase checkpoint. Nucleic acids research *38*, 3975-3983.

Kumar, S., and Burgers, P.M. (2013). Lagging strand maturation factor Dna2 is a component of the replication checkpoint initiation machinery. Genes & development *27*, 313-321.

Kunz, B.A., Kohalmi, S.E., Kunkel, T.A., Mathews, C.K., McIntosh, E.M., and Reidy, J.A. (1994). International Commission for Protection Against Environmental Mutagens and Carcinogens. Deoxyribonucleoside triphosphate levels: a critical factor in the maintenance of genetic stability. Mutat Res *318*, 1-64.

Labib, K., Tercero, J.A., and Diffley, J.F. (2000). Uninterrupted MCM2-7 function required for DNA replication fork progression. Science *288*, 1643-1647.

Lahaye, A., Leterme, S., and Foury, F. (1993). PIF1 DNA helicase from Saccharomyces cerevisiae. Biochemical characterization of the enzyme. The Journal of biological chemistry *268*, 26155-26161.

Lahaye, A., Stahl, H., Thines-Sempoux, D., and Foury, F. (1991). PIF1: a DNA helicase in yeast mitochondria. The EMBO journal *10*, 997-1007.

Langston, L.D., Zhang, D., Yurieva, O., Georgescu, R.E., Finkelstein, J., Yao, N.Y., Indiani, C., and O'Donnell, M.E. (2014). CMG helicase and DNA polymerase epsilon form a functional 15-subunit holoenzyme for eukaryotic leading-strand DNA replication. Proceedings of the National Academy of Sciences of the United States of America *111*, 15390-15395.

Lara-Gonzalez, P., Westhorpe, F.G., and Taylor, S.S. (2012). The spindle assembly checkpoint. Curr Biol *22*, R966-980.

Lee, K.H., Kim, D.W., Bae, S.H., Kim, J.A., Ryu, G.H., Kwon, Y.N., Kim, K.A., Koo, H.S., and Seo, Y.S. (2000). The endonuclease activity of the yeast Dna2 enzyme is essential in vivo. Nucleic acids research *28*, 2873-2881.

Lee, Y.D., and Elledge, S.J. (2006). Control of ribonucleotide reductase localization through an anchoring mechanism involving Wtm1. Genes & development *20*, 334-344.

Lee, Y.D., Wang, J., Stubbe, J., and Elledge, S.J. (2008). Dif1 is a DNA-damage-regulated facilitator of nuclear import for ribonucleotide reductase. Molecular cell *32*, 70-80.

Lengauer, C., Kinzler, K.W., and Vogelstein, B. (1998). Genetic instabilities in human cancers. Nature *396*, 643-649.

Leroy, C., Lee, S.E., Vaze, M.B., Ochsenbein, F., Guerois, R., Haber, J.E., and Marsolier-Kergoat, M.C. (2003). PP2C phosphatases Ptc2 and Ptc3 are required for DNA checkpoint inactivation after a double-strand break. Molecular cell *11*, 827-835.

Levikova, M., and Cejka, P. (2015). The Saccharomyces cerevisiae Dna2 can function as a sole nuclease in the processing of Okazaki fragments in DNA replication. Nucleic acids research *43*, 7888-7897.

Lew, D.J. (2003). The morphogenesis checkpoint: how yeast cells watch their figures. Curr Opin Cell Biol *15*, 648-653.

Liberi, G., Cotta-Ramusino, C., Lopes, M., Sogo, J., Conti, C., Bensimon, A., and Foiani, M. (2006). Methods to study replication fork collapse in budding yeast. Methods in enzymology *409*, 442-462.

Lin, W., Sampathi, S., Dai, H., Liu, C., Zhou, M., Hu, J., Huang, Q., Campbell, J., Shin-Ya, K., Zheng, L.*, et al.* (2013). Mammalian DNA2 helicase/nuclease cleaves G-quadruplex DNA and is required for telomere integrity. The EMBO journal *32*, 1425-1439.

Linskens, M.H., and Huberman, J.A. (1988). Organization of replication of ribosomal DNA in Saccharomyces cerevisiae. Molecular and cellular biology *8*, 4927-4935.

Lisby, M., and Rothstein, R. (2004). DNA damage checkpoint and repair centers. Curr Opin Cell Biol *16*, 328-334.

Liu, Y., Kao, H.I., and Bambara, R.A. (2004). Flap endonuclease 1: a central component of DNA metabolism. Annu Rev Biochem *73*, 589-615.

Longhese, M.P., Paciotti, V., Neecke, H., and Lucchini, G. (2000). Checkpoint proteins influence telomeric silencing and length maintenance in budding yeast. Genetics *155*, 1577-1591.

Longtine, M.S., McKenzie, A., 3rd, Demarini, D.J., Shah, N.G., Wach, A., Brachat, A., Philippsen, P., and Pringle, J.R. (1998). Additional modules for versatile and economical PCR-based gene deletion and modification in Saccharomyces cerevisiae. Yeast *14*, 953-961.

Lopes, J., Piazza, A., Bermejo, R., Kriegsman, B., Colosio, A., Teulade-Fichou, M.P., Foiani, M., and Nicolas, A. (2011). G-quadruplex-induced instability during leading-strand replication. The EMBO journal *30*, 4033-4046.

Lopes, M., Cotta-Ramusino, C., Liberi, G., and Foiani, M. (2003). Branch migrating sister chromatid junctions form at replication origins through Rad51/Rad52-independent mechanisms. Molecular cell *12*, 1499-1510.

Lopes, M., Cotta-Ramusino, C., Pellicioli, A., Liberi, G., Plevani, P., Muzi-Falconi, M., Newlon, C.S., and Foiani, M. (2001). The DNA replication checkpoint response stabilizes stalled replication forks. Nature *412*, 557-561.

Lopes, M., Foiani, M., and Sogo, J.M. (2006). Multiple mechanisms control chromosome integrity after replication fork uncoupling and restart at irreparable UV lesions. Molecular cell *21*, 15-27.

Lossaint, G., Larroque, M., Ribeyre, C., Bec, N., Larroque, C., Decaillet, C., Gari, K., and Constantinou, A. (2013). FANCD2 binds MCM proteins and controls replisome function upon activation of s phase checkpoint signaling. Molecular cell *51*, 678-690.

Lucca, C., Vanoli, F., Cotta-Ramusino, C., Pellicioli, A., Liberi, G., Haber, J., and Foiani, M. (2004). Checkpoint-mediated control of replisome-fork association and signalling in response to replication pausing. Oncogene *23*, 1206-1213.

Luna, R., Gaillard, H., Gonzalez-Aguilera, C., and Aguilera, A. (2008). Biogenesis of mRNPs: integrating different processes in the eukaryotic nucleus. Chromosoma *117*, 319-331.

Mailand, N., Falck, J., Lukas, C., Syljuasen, R.G., Welcker, M., Bartek, J., and Lukas, J. (2000). Rapid destruction of human Cdc25A in response to DNA damage. Science *288*, 1425-1429.

Majka, J., Niedziela-Majka, A., and Burgers, P.M. (2006). The checkpoint clamp activates Mec1 kinase during initiation of the DNA damage checkpoint. Molecular cell *24*, 891-901.

Makovets, S., and Blackburn, E.H. (2009). DNA damage signalling prevents deleterious telomere addition at DNA breaks. Nature cell biology *11*, 1383-1386.

Marini, F., Pellicioli, A., Paciotti, V., Lucchini, G., Plevani, P., Stern, D.F., and Foiani, M. (1997). A role for DNA primase in coupling DNA replication to DNA damage response. The EMBO journal *16*, 639-650.

Masai, H., Matsumoto, S., You, Z., Yoshizawa-Sugata, N., and Oda, M. (2010). Eukaryotic chromosome DNA replication: where, when, and how? Annu Rev Biochem *79*, 89-130.

Mateyak, M.K., and Zakian, V.A. (2006). Human PIF helicase is cell cycle regulated and associates with telomerase. Cell Cycle *5*, 2796-2804.

Matsuda, K., Makise, M., Sueyasu, Y., Takehara, M., Asano, T., and Mizushima, T. (2007). Yeast two-hybrid analysis of the origin recognition complex of Saccharomyces cerevisiae: interaction between subunits and identification of binding proteins. FEMS yeast research *7*, 1263-1269.

Mechali, M., Yoshida, K., Coulombe, P., and Pasero, P. (2013). Genetic and epigenetic determinants of DNA replication origins, position and activation. Curr Opin Genet Dev *23*, 124-131.

Menolfi, D., Delamarre, A., Lengronne, A., Pasero, P., and Branzei, D. (2015). Essential Roles of the Smc5/6 Complex in Replication through Natural Pausing Sites and Endogenous DNA Damage Tolerance. Molecular cell *60*, 835-846.

Mirkin, E.V., and Mirkin, S.M. (2007). Replication fork stalling at natural impediments. Microbiol Mol Biol Rev *71*, 13-35.

Mohanty, B.K., Bairwa, N.K., and Bastia, D. (2006). The Tof1p-Csm3p protein complex counteracts the Rrm3p helicase to control replication termination of Saccharomyces cerevisiae. Proceedings of the National Academy of Sciences of the United States of America *103*, 897-902.

Morawska, M., and Ulrich, H.D. (2013). An expanded tool kit for the auxin-inducible degron system in budding yeast. Yeast *30*, 341-351.

Mordes, D.A., Nam, E.A., and Cortez, D. (2008). Dpb11 activates the Mec1-Ddc2 complex. Proceedings of the National Academy of Sciences of the United States of America *105*, 18730-18734.

Musacchio, A. (2015). The Molecular Biology of Spindle Assembly Checkpoint Signaling Dynamics. Curr Biol *25*, R1002-1018.

Muzi-Falconi, M., Giannattasio, M., Foiani, M., and Plevani, P. (2003). The DNA polymerase alpha-primase complex: multiple functions and interactions. ScientificWorldJournal *3*, 21-33.

Myung, K., Datta, A., and Kolodner, R.D. (2001). Suppression of spontaneous chromosomal rearrangements by S phase checkpoint functions in Saccharomyces cerevisiae. Cell *104*, 397-408.

Navadgi-Patil, V.M., and Burgers, P.M. (2009). The unstructured C-terminal tail of the 9-1-1 clamp subunit Ddc1 activates Mec1/ATR via two distinct mechanisms. Molecular cell *36*, 743-753.

Navadgi-Patil, V.M., Kumar, S., and Burgers, P.M. (2011). The unstructured C-terminal tail of yeast Dpb11 (human TopBP1) protein is dispensable for DNA replication and the S phase checkpoint but required for the G2/M checkpoint. The Journal of biological chemistry *286*, 40999-41007.

Naylor, M.L., Li, J.M., Osborn, A.J., and Elledge, S.J. (2009). Mrc1 phosphorylation in response to DNA replication stress is required for Mec1 accumulation at the stalled fork. Proceedings of the National Academy of Sciences of the United States of America *106*, 12765-12770.

Nedelcheva, M.N., Roguev, A., Dolapchiev, L.B., Shevchenko, A., Taskov, H.B., Shevchenko, A., Stewart, A.F., and Stoynov, S.S. (2005). Uncoupling of unwinding from DNA synthesis implies regulation of MCM helicase by Tof1/Mrc1/Csm3 checkpoint complex. J Mol Biol *347*, 509-521.

Neelsen, K.J., Chaudhuri, A.R., Follonier, C., Herrador, R., and Lopes, M. (2014). Visualization and interpretation of eukaryotic DNA replication intermediates in vivo by electron microscopy. Methods in molecular biology *1094*, 177-208.

Nick McElhinny, S.A., Gordenin, D.A., Stith, C.M., Burgers, P.M., and Kunkel, T.A. (2008). Division of labor at the eukaryotic replication fork. Molecular cell *30*, 137-144.

Nishimura, K., Fukagawa, T., Takisawa, H., Kakimoto, T., and Kanemaki, M. (2009). An auxin-based degron system for the rapid depletion of proteins in nonplant cells. Nat Methods *6*, 917-922.

O'Neill, B.M., Szyjka, S.J., Lis, E.T., Bailey, A.O., Yates, J.R., 3rd, Aparicio, O.M., and Romesberg, F.E. (2007). Pph3-Psy2 is a phosphatase complex required for Rad53 dephosphorylation and replication fork restart during recovery from DNA damage. Proceedings of the National Academy of Sciences of the United States of America *104*, 9290-9295.

O'Rourke, T.W., Doudican, N.A., Mackereth, M.D., Doetsch, P.W., and Shadel, G.S. (2002). Mitochondrial dysfunction due to oxidative mitochondrial DNA damage is reduced through cooperative actions of diverse proteins. Molecular and cellular biology *22*, 4086-4093.

O'Rourke, T.W., Doudican, N.A., Zhang, H., Eaton, J.S., Doetsch, P.W., and Shadel, G.S. (2005). Differential involvement of the related DNA helicases Pif1p and Rrm3p in mtDNA point mutagenesis and stability. Gene *354*, 86-92.

Okazaki, R., Okazaki, T., Sakabe, K., Sugimoto, K., and Sugino, A. (1968). Mechanism of DNA chain growth. I. Possible discontinuity and unusual secondary structure of newly synthesized chains. Proceedings of the National Academy of Sciences of the United States of America *59*, 598-605.

Paciotti, V., Clerici, M., Scotti, M., Lucchini, G., and Longhese, M.P. (2001). Characterization of mec1 kinase-deficient mutants and of new hypomorphic mec1 alleles impairing subsets of the DNA damage response pathway. Molecular and cellular biology *21*, 3913-3925.

Paeschke, K., Bochman, M.L., Garcia, P.D., Cejka, P., Friedman, K.L., Kowalczykowski, S.C., and Zakian, V.A. (2013). Pif1 family helicases suppress genome instability at G-quadruplex motifs. Nature *497*, 458-462.

Paeschke, K., Capra, J.A., and Zakian, V.A. (2011). DNA replication through G-quadruplex motifs is promoted by the Saccharomyces cerevisiae Pif1 DNA helicase. Cell *145*, 678-691.

Palou, G., Palou, R., Zeng, F., Vashisht, A.A., Wohlschlegel, J.A., and Quintana, D.G. (2015). Three Different Pathways Prevent Chromosome Segregation in the Presence of DNA Damage or Replication Stress in Budding Yeast. PLoS genetics *11*, e1005468.

Pasero, P., Bensimon, A., and Schwob, E. (2002). Single-molecule analysis reveals clustering and epigenetic regulation of replication origins at the yeast rDNA locus. Genes & development *16*, 2479-2484.

Paulovich, A.G., and Hartwell, L.H. (1995). A checkpoint regulates the rate of progression through S phase in S. cerevisiae in response to DNA damage. Cell *82*, 841-847.

Pellicioli, A., and Foiani, M. (2005). Signal transduction: how rad53 kinase is activated. Curr Biol *15*, R769-771.

Pellicioli, A., Lucca, C., Liberi, G., Marini, F., Lopes, M., Plevani, P., Romano, A., Di Fiore, P.P., and Foiani, M. (1999). Activation of Rad53 kinase in response to DNA damage and its effect in modulating phosphorylation of the lagging strand DNA polymerase. The EMBO journal *18*, 6561-6572.

Pike, B.L., Yongkiettrakul, S., Tsai, M.D., and Heierhorst, J. (2003). Diverse but overlapping functions of the two forkhead-associated (FHA) domains in Rad53 checkpoint kinase activation. The Journal of biological chemistry *278*, 30421-30424.

Pike, J.E., Burgers, P.M., Campbell, J.L., and Bambara, R.A. (2009). Pif1 helicase lengthens some Okazaki fragment flaps necessitating Dna2 nuclease/helicase action in the two-nuclease processing pathway. The Journal of biological chemistry *284*, 25170-25180.

Pike, J.E., Henry, R.A., Burgers, P.M., Campbell, J.L., and Bambara, R.A. (2010). An alternative pathway for Okazaki fragment processing: resolution of fold-back flaps by Pif1 helicase. The Journal of biological chemistry *285*, 41712-41723.

Pinter, S.F., Aubert, S.D., and Zakian, V.A. (2008). The Schizosaccharomyces pombe Pfh1p DNA helicase is essential for the maintenance of nuclear and mitochondrial DNA. Molecular and cellular biology *28*, 6594-6608.

Poli, J., Tsaponina, O., Crabbe, L., Keszthelyi, A., Pantesco, V., Chabes, A., Lengronne, A., and Pasero, P. (2012). dNTP pools determine fork progression and origin usage under replication stress. The EMBO journal *31*, 883-894.

Postow, L., Crisona, N.J., Peter, B.J., Hardy, C.D., and Cozzarelli, N.R. (2001a). Topological challenges to DNA replication: conformations at the fork. Proceedings of the National Academy of Sciences of the United States of America *98*, 8219-8226.

Postow, L., Ullsperger, C., Keller, R.W., Bustamante, C., Vologodskii, A.V., and Cozzarelli, N.R. (2001b). Positive torsional strain causes the formation of a four-way junction at replication forks. The Journal of biological chemistry *276*, 2790-2796.

Prokisch, H., Scharfe, C., Camp, D.G., 2nd, Xiao, W., David, L., Andreoli, C., Monroe, M.E., Moore, R.J., Gritsenko, M.A., Kozany, C.*, et al.* (2004). Integrative analysis of the mitochondrial proteome in yeast. PLoS Biol *2*, e160.

Pursell, Z.F., Isoz, I., Lundstrom, E.B., Johansson, E., and Kunkel, T.A. (2007). Yeast DNA polymerase epsilon participates in leading-strand DNA replication. Science *317*, 127-130.

Putnam, C.D., Jaehnig, E.J., and Kolodner, R.D. (2009). Perspectives on the DNA damage and replication checkpoint responses in Saccharomyces cerevisiae. DNA repair *8*, 974-982.

Raghuraman, M.K., Winzeler, E.A., Collingwood, D., Hunt, S., Wodicka, L., Conway, A., Lockhart, D.J., Davis, R.W., Brewer, B.J., and Fangman, W.L. (2001). Replication dynamics of the yeast genome. Science *294*, 115-121.

Ragland, R.L., Patel, S., Rivard, R.S., Smith, K., Peters, A.A., Bielinsky, A.K., and Brown, E.J. (2013). RNF4 and PLK1 are required for replication fork collapse in ATR-deficient cells. Genes & development *27*, 2259-2273.

Raveendranathan, M., Chattopadhyay, S., Bolon, Y.T., Haworth, J., Clarke, D.J., and Bielinsky, A.K. (2006). Genome-wide replication profiles of S-phase checkpoint mutants reveal fragile sites in yeast. The EMBO journal *25*, 3627-3639.

Reichard, P. (1988). Interactions between deoxyribonucleotide and DNA synthesis. Annu Rev Biochem *57*, 349-374.

Reid, G.A., and Schatz, G. (1982). Import of proteins into mitochondria. Yeast cells grown in the presence of carbonyl cyanide m-chlorophenylhydrazone accumulate massive amounts of some mitochondrial precursor polypeptides. The Journal of biological chemistry *257*, 13056-13061.

Ribeyre, C., Lopes, J., Boule, J.B., Piazza, A., Guedin, A., Zakian, V.A., Mergny, J.L., and Nicolas, A. (2009). The yeast Pif1 helicase prevents genomic instability caused by G-quadruplex-forming CEB1 sequences in vivo. PLoS genetics *5*, e1000475.

Rossi, M.L., and Bambara, R.A. (2006). Reconstituted Okazaki fragment processing indicates two pathways of primer removal. The Journal of biological chemistry *281*, 26051-26061.

Rossi, M.L., Pike, J.E., Wang, W., Burgers, P.M., Campbell, J.L., and Bambara, R.A. (2008). Pif1 helicase directs eukaryotic Okazaki fragments toward the two-nuclease cleavage pathway for primer removal. The Journal of biological chemistry *283*, 27483-27493.

Rossi, S.E., Ajazi, A., Carotenuto, W., Foiani, M., and Giannattasio, M. (2015). Rad53-Mediated Regulation of Rrm3 and Pif1 DNA Helicases Contributes to Prevention of Aberrant Fork Transitions under Replication Stress. Cell Rep *13*, 80-92.

Rossi, S.E., Carotenuto, W., and Giannattasio, M. (2016). Genome-wide localization of Rrm3 and Pif1 DNA helicases at stalled active and inactive DNA replication forks of Saccharomyces cerevisiae. Genom Data *7*, 162-165.

Sabouri, N., McDonald, K.R., Webb, C.J., Cristea, I.M., and Zakian, V.A. (2012). DNA replication through hard-to-replicate sites, including both highly transcribed RNA Pol II and Pol III genes, requires the S. pombe Pfh1 helicase. Genes & development *26*, 581-593.

Saka, K., Takahashi, A., Sasaki, M., and Kobayashi, T. (2016). More than 10% of yeast genes are related to genome stability and influence cellular senescence via rDNA maintenance. Nucleic acids research *44*, 4211-4221.

Sanchez, Y., Bachant, J., Wang, H., Hu, F., Liu, D., Tetzlaff, M., and Elledge, S.J. (1999). Control of the DNA damage checkpoint by chk1 and rad53 protein kinases through distinct mechanisms. Science *286*, 1166-1171.

Sanders, C.M. (2010). Human Pif1 helicase is a G-quadruplex DNA-binding protein with G-quadruplex DNA-unwinding activity. Biochem J *430*, 119-128.

Santocanale, C., and Diffley, J.F. (1998). A Mec1- and Rad53-dependent checkpoint controls late-firing origins of DNA replication. Nature *395*, 615-618.

Schmidt, K.H., Derry, K.L., and Kolodner, R.D. (2002). Saccharomyces cerevisiae RRM3, a 5' to 3' DNA helicase, physically interacts with proliferating cell nuclear antigen. The Journal of biological chemistry *277*, 45331-45337.

Schulz, V.P., and Zakian, V.A. (1994). The saccharomyces PIF1 DNA helicase inhibits telomere elongation and de novo telomere formation. Cell *76*, 145-155.

Segurado, M., and Diffley, J.F. (2008). Separate roles for the DNA damage checkpoint protein kinases in stabilizing DNA replication forks. Genes & development *22*, 1816-1827.

Segurado, M., and Tercero, J.A. (2009). The S-phase checkpoint: targeting the replication fork. Biol Cell *101*, 617-627.

Shirahige, K., Hori, Y., Shiraishi, K., Yamashita, M., Takahashi, K., Obuse, C., Tsurimoto, T., and Yoshikawa, H. (1998). Regulation of DNA-replication origins during cell-cycle progression. Nature *395*, 618-621.

Siddiqui, K., On, K.F., and Diffley, J.F. (2013). Regulating DNA replication in eukarya. Cold Spring Harb Perspect Biol *5*.

Siede, W., Friedberg, A.S., and Friedberg, E.C. (1993). RAD9-dependent G1 arrest defines a second checkpoint for damaged DNA in the cell cycle of Saccharomyces cerevisiae. Proceedings of the National Academy of Sciences of the United States of America *90*, 7985-7989.

Sinclair, D.A., and Guarente, L. (1997). Extrachromosomal rDNA circles--a cause of aging in yeast. Cell *91*, 1033-1042.

Smolka, M.B., Albuquerque, C.P., Chen, S.H., and Zhou, H. (2007). Proteome-wide identification of in vivo targets of DNA damage checkpoint kinases. Proceedings of the National Academy of Sciences of the United States of America *104*, 10364-10369.

Sogo, J.M., Lopes, M., and Foiani, M. (2002). Fork reversal and ssDNA accumulation at stalled replication forks owing to checkpoint defects. Science *297*, 599-602.

Steinacher, R., Osman, F., Dalgaard, J.Z., Lorenz, A., and Whitby, M.C. (2012). The DNA helicase Pfh1 promotes fork merging at replication termination sites to ensure genome stability. Genes & development *26*, 594-602.

Stern, D.F., Zheng, P., Beidler, D.R., and Zerillo, C. (1991). Spk1, a new kinase from Saccharomyces cerevisiae, phosphorylates proteins on serine, threonine, and tyrosine. Molecular and cellular biology *11*, 987-1001.

Storici, F., and Resnick, M.A. (2006). The delitto perfetto approach to in vivo site-directed mutagenesis and chromosome rearrangements with synthetic oligonucleotides in yeast. Methods in enzymology *409*, 329-345.

Syljuasen, R.G., Sorensen, C.S., Hansen, L.T., Fugger, K., Lundin, C., Johansson, F., Helleday, T., Sehested, M., Lukas, J., and Bartek, J. (2005). Inhibition of human Chk1 causes increased initiation of DNA replication, phosphorylation of ATR targets, and DNA breakage. Molecular and cellular biology *25*, 3553-3562.

Szilard, R.K., Jacques, P.E., Laramee, L., Cheng, B., Galicia, S., Bataille, A.R., Yeung, M., Mendez, M., Bergeron, M., Robert, F.*, et al.* (2010). Systematic identification of fragile sites via genome-wide location analysis of gamma-H2AX. Nature structural & molecular biology *17*, 299-305.

Tanaka, H., Ryu, G.H., Seo, Y.S., Tanaka, K., Okayama, H., MacNeill, S.A., and Yuasa, Y. (2002). The fission yeast pfh1(+) gene encodes an essential 5' to 3' DNA helicase required for the completion of S-phase. Nucleic acids research *30*, 4728-4739.

Tercero, J.A., and Diffley, J.F. (2001). Regulation of DNA replication fork progression through damaged DNA by the Mec1/Rad53 checkpoint. Nature *412*, 553-557.

Tercero, J.A., Longhese, M.P., and Diffley, J.F. (2003). A central role for DNA replication forks in checkpoint activation and response. Molecular cell *11*, 1323-1336.

Thangavel, S., Berti, M., Levikova, M., Pinto, C., Gomathinayagam, S., Vujanovic, M., Zellweger, R., Moore, H., Lee, E.H., Hendrickson, E.A*., et al.* (2015). DNA2 drives processing and restart of reversed replication forks in human cells. The Journal of cell biology *208*, 545-562.

Tishkoff, D.X., Boerger, A.L., Bertrand, P., Filosi, N., Gaida, G.M., Kane, M.F., and Kolodner, R.D. (1997). Identification and characterization of Saccharomyces cerevisiae EXO1, a gene encoding an exonuclease that interacts with MSH2. Proceedings of the National Academy of Sciences of the United States of America *94*, 7487-7492.

Toledo, L.I., Altmeyer, M., Rask, M.B., Lukas, C., Larsen, D.H., Povlsen, L.K., Bekker-Jensen, S., Mailand, N., Bartek, J., and Lukas, J. (2013). ATR prohibits replication catastrophe by preventing global exhaustion of RPA. Cell *155*, 1088-1103.

Torres, J.Z., Bessler, J.B., and Zakian, V.A. (2004). Local chromatin structure at the ribosomal DNA causes replication fork pausing and genome instability in the absence of the S. cerevisiae DNA helicase Rrm3p. Genes & development *18*, 498-503.

Tourriere, H., Versini, G., Cordon-Preciado, V., Alabert, C., and Pasero, P. (2005). Mrc1 and Tof1 promote replication fork progression and recovery independently of Rad53. Molecular cell *19*, 699-706.

Travesa, A., Duch, A., and Quintana, D.G. (2008). Distinct phosphatases mediate the deactivation of the DNA damage checkpoint kinase Rad53. The Journal of biological chemistry *283*, 17123-17130.

Van Dyck, E., Foury, F., Stillman, B., and Brill, S.J. (1992). A single-stranded DNA binding protein required for mitochondrial DNA replication in S. cerevisiae is homologous to E. coli SSB. The EMBO journal *11*, 3421-3430.

Vas, A.C., Andrews, C.A., Kirkland Matesky, K., and Clarke, D.J. (2007). In vivo analysis of chromosome condensation in Saccharomyces cerevisiae. Molecular biology of the cell *18*, 557-568.

Vega, L.R., Phillips, J.A., Thornton, B.R., Benanti, J.A., Onigbanjo, M.T., Toczyski, D.P., and Zakian, V.A. (2007). Sensitivity of yeast strains with long G-tails to levels of telomere-bound telomerase. PLoS genetics *3*, e105.

Venema, J., and Tollervey, D. (1999). Ribosome synthesis in Saccharomyces cerevisiae. Annu Rev Genet *33*, 261-311.

Versini, G., Comet, I., Wu, M., Hoopes, L., Schwob, E., and Pasero, P. (2003). The yeast Sgs1 helicase is differentially required for genomic and ribosomal DNA replication. The EMBO journal *22*, 1939-1949.

Villa, F., Simon, A.C., Ortiz Bazan, M.A., Kilkenny, M.L., Wirthensohn, D., Wightman, M., Matak-Vinkovic, D., Pellegrini, L., and Labib, K. (2016). Ctf4 Is a Hub in the Eukaryotic Replisome that Links Multiple CIP-Box Proteins to the CMG Helicase. Molecular cell.

Vogelstein, B., and Kinzler, K.W. (2004). Cancer genes and the pathways they control. Nat Med *10*, 789-799.

Voineagu, I., Narayanan, V., Lobachev, K.S., and Mirkin, S.M. (2008). Replication stalling at unstable inverted repeats: interplay between DNA hairpins and fork stabilizing proteins. Proceedings of the National Academy of Sciences of the United States of America *105*, 9936-9941.

Wagner, M., Price, G., and Rothstein, R. (2006). The absence of Top3 reveals an interaction between the Sgs1 and Pif1 DNA helicases in Saccharomyces cerevisiae. Genetics *174*, 555-573.

Wang, J.C. (1996). DNA topoisomerases. Annu Rev Biochem *65*, 635-692.

Weinert, T. (1998). DNA damage and checkpoint pathways: molecular anatomy and interactions with repair. Cell *94*, 555-558.

Weinert, T.A., and Hartwell, L.H. (1988). The RAD9 gene controls the cell cycle response to DNA damage in Saccharomyces cerevisiae. Science *241*, 317-322.

Weinert, T.A., Kiser, G.L., and Hartwell, L.H. (1994). Mitotic checkpoint genes in budding yeast and the dependence of mitosis on DNA replication and repair. Genes & development *8*, 652-665.

Weitao, T., Budd, M., and Campbell, J.L. (2003a). Evidence that yeast SGS1, DNA2, SRS2, and FOB1 interact to maintain rDNA stability. Mutat Res *532*, 157-172.

Weitao, T., Budd, M., Hoopes, L.L., and Campbell, J.L. (2003b). Dna2 helicase/nuclease causes replicative fork stalling and double-strand breaks in the ribosomal DNA of Saccharomyces cerevisiae. The Journal of biological chemistry *278*, 22513-22522.

Wellinger, R.E., and Sogo, J.M. (1998). In vivo mapping of nucleosomes using psoralen-DNA crosslinking and primer extension. Nucleic Acids Res *26*, 1544-1545.

Wilson, M.A., Kwon, Y., Xu, Y., Chung, W.H., Chi, P., Niu, H., Mayle, R., Chen, X., Malkova, A., Sung, P.*, et al.* (2013). Pif1 helicase and Poldelta promote recombination-coupled DNA synthesis via bubble migration. Nature *502*, 393-396.

Wyrick, J.J., Aparicio, J.G., Chen, T., Barnett, J.D., Jennings, E.G., Young, R.A., Bell, S.P., and Aparicio, O.M. (2001). Genome-wide distribution of ORC and MCM proteins in S. cerevisiae: high-resolution mapping of replication origins. Science *294*, 2357-2360.

Yao, R., Zhang, Z., An, X., Bucci, B., Perlstein, D.L., Stubbe, J., and Huang, M. (2003). Subcellular localization of yeast ribonucleotide reductase regulated by the DNA replication

and damage checkpoint pathways. Proceedings of the National Academy of Sciences of the United States of America *100*, 6628-6633.

Yu, C., Gan, H., Han, J., Zhou, Z.X., Jia, S., Chabes, A., Farrugia, G., Ordog, T., and Zhang, Z. (2014). Strand-specific analysis shows protein binding at replication forks and PCNA unloading from lagging strands when forks stall. Molecular cell *56*, 551-563.

Zegerman, P., and Diffley, J.F. (2010). Checkpoint-dependent inhibition of DNA replication initiation by Sld3 and Dbf4 phosphorylation. Nature *467*, 474-478.

Zhang, D.H., Zhou, B., Huang, Y., Xu, L.X., and Zhou, J.Q. (2006). The human Pif1 helicase, a potential Escherichia coli RecD homologue, inhibits telomerase activity. Nucleic acids research *34*, 1393-1404.

Zhang, H., and Siede, W. (2004). Analysis of the budding yeast Saccharomyces cerevisiae cell cycle by morphological criteria and flow cytometry. Methods in molecular biology *241*, 77-91.

Zhao, X., Chabes, A., Domkin, V., Thelander, L., and Rothstein, R. (2001). The ribonucleotide reductase inhibitor Sml1 is a new target of the Mec1/Rad53 kinase cascade during growth and in response to DNA damage. The EMBO journal *20*, 3544-3553.

Zhao, X., Muller, E.G., and Rothstein, R. (1998). A suppressor of two essential checkpoint genes identifies a novel protein that negatively affects dNTP pools. Molecular cell *2*, 329-340.

Zhao, X., and Rothstein, R. (2002). The Dun1 checkpoint kinase phosphorylates and regulates the ribonucleotide reductase inhibitor Sml1. Proceedings of the National Academy of Sciences of the United States of America *99*, 3746-3751.

Zheng, L., and Shen, B. (2011). Okazaki fragment maturation: nucleases take centre stage. J Mol Cell Biol *3*, 23-30.

Zheng, P., Fay, D.S., Burton, J., Xiao, H., Pinkham, J.L., and Stern, D.F. (1993). SPK1 is an essential S-phase-specific gene of Saccharomyces cerevisiae that encodes a nuclear serine/threonine/tyrosine kinase. Molecular and cellular biology *13*, 5829-5842.

Zhou, J., Monson, E.K., Teng, S.C., Schulz, V.P., and Zakian, V.A. (2000). Pif1p helicase, a catalytic inhibitor of telomerase in yeast. Science *289*, 771-774.

Zhou, J.Q., Qi, H., Schulz, V.P., Mateyak, M.K., Monson, E.K., and Zakian, V.A. (2002). Schizosaccharomyces pombe pfh1+ encodes an essential 5' to 3' DNA helicase that is a member of the PIF1 subfamily of DNA helicases. Molecular biology of the cell *13*, 2180-2191.

Zhu, Z., Chung, W.H., Shim, E.Y., Lee, S.E., and Ira, G. (2008). Sgs1 helicase and two nucleases Dna2 and Exo1 resect DNA double-strand break ends. Cell *134*, 981-994.

Zou, L., and Elledge, S.J. (2003). Sensing DNA damage through ATRIP recognition of RPA-ssDNA complexes. Science *300*, 1542-1548.

7. Acknowledgments

First of all, I would like to thank my supervisor, Prof. Marco Foiani, for giving me the opportunity to join his team and to work in the amazing and stimulating scientific environment of IFOM.

I would like to express my sincere gratitude to my scientific guide during those years, Dr. Michele Giannattasio, for his continuous support, for his patience, for his wide scientific knowledge that he shared with me, with passion and enthusiasm, and for being an example of strong dedication to science.

Moreover, I want to express my gratitude to my internal supervisor, Dr. Dana Branzei, not only for the scientific support, but also for the encouragement she gave me and for her contagious scientific passion.

I thank my external supervisor Dr. Benoit Arcangioli for helpful advices, as well as my internal examiners, Dr. Ylli Doksani e Dr. Philippe Pasero, for the critical reading of this manuscript and for the insightful comments.

I thank Dr. Walter Carotenuto for the great help with microarray data analysis and Dr. Barnabas Szakal for sharing reagents with me.

I thank all the facilities of the campus, especially the Genomics Unit (Dr. Simone Minardi), for the precious technological support.

I thank all my colleagues for the everyday life in the lab; in particular I would like to thank Sophie Gay, Elisa Ferrari, Daniele Piccini and Demis Menolfi for the constant help, for the scientific discussions and for being great friends.

Above all, I want to thank my parents for their constant and unconditional support, encouragement and love. This milestone is dedicated to them.